

Reproduction spectrale de la couleur:
approches par modélisation d'imprimante et par halftoning
avec diffusion d'erreur vectorielle

Jérémie Gerhardt

Acknowledgment

I would like to thank my two directors Jon Yngve Hardeberg at HIG (Norway) and Francis Schmitt at ENST (France), to have selected me for this research work and for all the helpful discussions and feedback on my work during the last four years. I'm grateful to the Norwegian Research Council for the founding of my research on spectral color reproduction. I'm would like to thanks as well the jury of my thesis to have accepted to participate to evaluate my work.

I would like to thanks all my colleagues at the Norwegian Color Research Laboratory and in Gjøvik University College during the last four years of my thesis: Ali, Andrei, Arne Magnus, Øyvind, Ivar, Peter, Casper, David, Kristina, Eriko, Sven Erik, Ole,... and the PhD students from the NisLab.

Also my colleagues all over the world which I meet in random places for the color conferences: Lawrence, Garret, Philipp and others researchers from the RIT, Andreas at fogra, Nicolas, Damien and all the members of the French Color Expert Association group.

My other half Kati, now we have more time to spend together on the weekend and evening.

Ma famille, parents et grands-parents, frère et soeur, oncles et tante, cousin et cousines, toute la famille donc! Et ce même s'ils n'ont tout pas compris au gamut spectral.

Et les amis, ceux qui sont montés me voir dans le nord, ceux qui vont monter me voir ainsi que les nouveaux rencontrés lors de ces quatres dernières années.



Résumé

Dans ce travail de recherche nous posons le problème suivant: comment reproduire des données multispectrales avec un système d'impression jet d'encre multi-colorants? Deux approches sont comparées utilisant le même système d'impression: une première approche par modélisation d'imprimante et une seconde approche par halftoning avec diffusion d'erreur vectorielle.

Le domaine de recherche dans lequel nous évoluons est l'imagerie multispectrale et nous nous intéressons à la reproduction spectrale de la couleur, nous nous restreignons donc au spectre du visible. Les données que nous manipulons, réflectance spectrale d'une surface ou pixel d'une image spectrale sont typiquement représentées par un vecteur de 31 valeurs de 400nm à 700nm avec un pas de 10nm. Une image spectrale peut être décrite par 31 images en niveaux de gris. L'intérêt de la reproduction spectrale de la couleur est de pouvoir créer une copie parfaite et ainsi de résoudre les problèmes liés au phénomène de métamérisme: une scène originale et sa reproduction apparaissent identiques à un observateur humain lorsque observées dans les mêmes conditions d'illumination que lors de l'acquisition de la scène originale; si l'illumination change l'observateur humain percevra des différences entre les deux images.

Si le phénomène de métamérisme est un avantage en reproduction couleur (c.-à-d différentes combinaisons d'encre permettent de reproduire une même valeur colorimétrique, c'est un inconvénient pour la reproduction spectrale de la couleur. Pour contrôler spectralement notre système d'impression nous avons besoin de connaître la réponse spectrale de ce système. L'étape dite de caractérisation spectrale de l'imprimante permet d'établir la relation suivante: d'une combinaison de colorant envoyée à l'imprimante à la réflectance spectrale imprimée sur le papier. Nous utilisons les modèles d'imprimante de Murray-Davies (pour des impressions monocolorant), Neugebauer et Yules-Nielsen (pour des impressions multi-colorants) chacun dans leur forme spectrale. Tous ces modèles fonctionnent de façon similaire: ils disposent de réflectance spectrales décrivant les limites du gamut spectral de l'imprimante. Les limites correspondent à toutes les combinaisons binaires possibles entre les colorants du système d'impression et sont aussi appelées les primaires de Neugebauer (NPs). Ces modèles produisent une estimation de la réflectance spectrale d'une combinaison d'encre envoyée à l'imprimante en calculant la somme pondérée des NPs par la surface occupée par chacune d'elles pour une combinaison d'encre donnée. La précision de ces modèles est directement liée à la modélisation du phénomène de dot gain: une combinaison de colorant imprimée apparaîtra plus sombre que la combinaison souhaitée envoyée à l'imprimante. L'inversion du modèle de Murray-Davies permet de modéliser le dot gain mécanique qui est lié à la déformation de la goutte d'encre lorsqu'elle est éjectée sur le papier. Le facteur n du modèle de Yules-Nielsen permet de tenir compte du dot gain optique pour estimer la réflectance spectrale d'une combinaison d'encre. Ce second dot gain est dû aux multiples interactions entre les rayons lumineux arrivant sur le papier recouvert ou non de gouttes d'encre, se déplaçant dans le papier et émergeant par des zones recouvertes ou non de gouttes d'encre.

Pour reproduire des données spectrales avec notre imprimante nous sommes intéressés par la relation inverse du modèle spectral de l'imprimante: d'une réflectance spectrale à une combinaison d'encre pour contrôler l'imprimante. Cette transformation est appelée séparation spectrale des colorants et est réalisée en inversant le modèle spectral de Neugebauer. Cette inversion est un problème d'optimisation dans lequel un critère d'optimisation est minimisé: différence spectrale, différence colorimétrique ou combinaison de chacune d'elles. A chaque itération du processus d'optimisation une nouvelle combinaison de colorant est obtenue produisant une estimation de la réflectance spectrale désirée. Cette étape dans la chaîne d'opération menant à la reproduction spectrale de la couleur permet de comparer pour une réflectance spectrale donnée sa reproduction suivant un critère purement colorimétrique ou purement spectrale. Ceci permet d'illustrer la réduction du phénomène de métamérisme avec une reproduction spectrale. Parmi les méthodes testées pour l'inversion du modèle spectral de Neugebauer, l'inversion par minimisation d'une fonction de coût nous donne les meilleurs résultats pour ce problème. La méthode que nous avons développée permet d'obtenir la meilleure décomposition d'une réflectance spectrale par les NPs. Cette méthode est utilisée pour l'opération de gamut mapping spectrale

comme prétraitement avant l'étape de séparation spectrale des colorants. Une fois l'image spectrale transformée en image multi-canaux où chaque canal représente un colorant du système d'impression, l'opération appelée halftoning va transformer chaque pixel de chaque canal en donnée binaire pour déposer une goutte d'encre et pour ne pas en déposer à la position du pixel dans l'image. En variant la distribution spatiale des gouttes d'encre l'illusion d'un niveau de colorant sera créée. La séparation spectrale des colorants suivie par le halftoning pour chaque canal décrit notre première approche pour la reproduction spectrale de la couleur.

Notre seconde approche par halftoning avec diffusion d'erreur vectorielle permet de combiner en une seule opération les deux transformations présentent dans l'approche par modélisation de l'imprimante et halftoning. Cette technique de halftoning est une adaptation de l'algorithme pour des images couleurs à des images spectrales. Chaque pixel de l'image spectrale est remplacée par la NP la plus proche dans l'espace de dimension spectrale; la différence (c.-à-d. l'erreur) entre le pixel et la NP sélectionnée est pondérée et diffusée sur les pixels voisins avec un filtre de poids. Une NP correspond à une combinaison binaire des colorants et donc à une commande pour déposer ou non des gouttes d'encre. Cette technique de halftoning est relativement lente pour diffuser l'erreur accumulée et laisse des marques visibles dans l'image halftonée. Une fois ramenée au gamut de l'imprimante les erreurs créées sont plus faibles mais restent parfois visible. Nous avons cherché à limiter la diffusion d'erreur au pixel les plus proches de façon à éviter une trop grande accumulation d'erreur, pour cela la construction de filtre basée sur la distance de pixel à pixel voisin dans la région du filtre a été proposée. Cette génération de filtre a montré des améliorations dans l'image halftonée quant à la visibilité de l'erreur accumulée et la conservation des détails présents dans l'image originale. Enfin nous avons comparé les deux approches par la reproduction de données spectrales extraites de l'acquisition couleur spectrale d'une peinture. Une douzaine de réflectance spectrales mesurées ont été rapportées au gamut de l'imprimante en utilisant notre technique de gamut mapping spectrale. Ces données spectrales ont ensuite été reproduites en simulation et comparées en termes de différence spectrale et différences colorimétriques ainsi qu'en termes de distribution spatiale des NPs. Les performances des deux approches sont proches avec un avantage pour le halftoning par diffusion d'erreur vectorielle, cette technique produisant également des distributions de NPs stables et beaucoup moins bruitées que pour la première approche.

Abstract

In this research work we are addressing the problem of how to reproduce multi-spectral data with a multi-colorant inkjet printing system. Two approaches using the same printing system have been described and compared: a first approach by spectral printer modeling and a second approach using halftoning by spectral vector error diffusion (sVED).

The field of research is the field of multi-spectral imaging, we are interesting in spectral color reproduction, i.e. the data we are manipulating belong to the visible spectrum. The spectral reflectance of a surface or the pixel of a spectral image is typically represented by a vector of 31 values spanning the visible spectrum from 400nm to 700nm with a sampling interval of 10 nm. A spectral image can be represented by 31 grayscale images, one for each wavelength. Spectral color reproduction aims to produce a perfect, spectrally identical, copy of an original scene or document, and hence to solve the problem of metamerism. An original scene and its spectral color reproduction will thus appear identical under any viewing illuminant.

Metamerism can be an advantage in color reproduction, i.e. different colorant combinations can produce the same colorimetric value. But in spectral color reproduction we want to know the spectral response of the printing system. To control spectrally our printing system we need to characterize the printing system with a spectral printer model: for a given colorant combination the printer model will estimate the resulting spectral reflectance on the paper. We use the Murray-Davies model (for mono-colorant prints), the Neugebauer model and the Yule-Nielsen modified Neugebauer model (for multi-colorant prints) in their spectral form. All these models follow a similar approach to estimate the spectral reflectance of a colorant combination: a weighted sum of the spectral reflectances representing the printer gamuts limits. These limits correspond to all the binary combinations between the available colorants and are called the Neugebauer primaries (NPs). The accuracy of these models is directly related to how the dot gain phenomenon is taken into account in the estimation: the effective printed colorant combination will appear darker than the theoretical colorant combination sent to the printer. The inverse of the Murray-Davies model allows us to estimate the mechanical dot gain due to the deformation of the ejected drop of ink on the paper. The n factor introduced by the Yule-Nielsen modified Neugebauer model allows us to model the optical dot gain due to the multiple light and paper interaction: the ray of light penetrating the paper by an area covered by colorant or not, and leaving the paper by another area covered or not by colorant, this phenomenon increases the resulting dot size.

To reproduce spectral data we are interested in the inverse relation given by the spectral printer model: we want to know the colorant combination required to reproduce a spectral reflectance target and for controlling the printer. This transformation is called spectral colorant separation; it is obtained by inverting the spectral printer model. Since the model is not analytically invertible, we treat this as an optimization problem in which a criterion is minimized: spectral difference, color difference or combination of these differences. Each iteration of this optimization process provides a new colorant combination giving a closer estimation of the desired spectral reflectance target. The choice of criterion defines the type of reproduction and allows comparing color reproduction obtained by minimizing color difference, and spectral color reproduction by minimizing spectral difference. We can also illustrate the reduction of metamerism with spectral color reproduction. Among the tested methods for spectral colorant separation, the constrained minimization routine gave us the best results for inverting the spectral printer model. Our proposed method gives the best decomposition of a spectral reflectance into a sum of NPs. This method can be used as a spectral gamut mapping algorithm and is applied as a pre-processing before performing spectral colorant separation. Once a spectral image is transformed into a multi-colorant image the operation of halftoning will be performed on each colorant channel independently. This operation transforms each pixel into binary values which correspond to commands for the printer: 1 to lay down a drop of ink in a certain location and 0 not to. By varying the spatial distribution of the drops the halftoning operation can create the illusion of different color levels. Spectral colorant separation followed by independent halftoning of each colorant channel describes our first approach for spectral color reproduction.

Our second approach by spectral vector error diffusion combines both spectral colorant separation and halftoning in one operation. This is an adaptation of the vector error diffusion halftoning technique for color images to spectral images. Each pixel is replaced by the closest NP and the difference (i.e. the error) is weighted and diffused to the neighboring pixels. A filter weight is used to diffuse the error. A selected NP corresponds to a binary colorant combination and equivalently to a command for the printer to lay down or not drops of ink. The sVED halftoning technique is relatively slow to diffuse the error, meaning that a stable spatial dot distribution is reached after a large number of pixels. The spectral gamut mapping applied before sVED is shown to reduce this slowness effect but not completely. We have designed new filters to diffuse the error in order to avoid spreading error to already distant pixel in the area of the filter. This approach has shown good results in avoiding large error accumulation and good edge preservation comparing to the first approach.

Finally we have compared the two presented approaches by reproducing spectral reflectance data. These spectral targets came from a spectral color acquisition of a painting. A dozen measured spectral reflectances were first gamut mapped to the spectral printer gamut with our spectral gamut mapping technique. We have simulated the reproduction of these data by the two approaches. The second approach by sVED given better performances in term of spectral and color differences, but also provides a more uniform spatial dot distribution than the first approach.

Long Résumé

“Spectral Color Reproduction: Model based and vector error diffusion approaches”

Chapitre 1

Introduction

Motivation

Avec un système conventionnel de reproduction couleur il est possible faire l’acquisition couleur d’une scène et d’en imprimer une copie fidèle pour des conditions d’illumination données à l’acquisition et à la restitution. Si les conditions d’illumination changent un observateur humain percevra des différences entre l’originale et sa reproduction: phénomène dit de métamérisme. Pour résoudre les problèmes liés à ce phénomène nous devons utiliser un système de reproduction spectrale de la couleur.

Le concept de reproduction spectrale de la couleur a déjà été abordé dans le passé par Hunt (1975) lorsqu’il décrivait le procédé holographique couleur de Lippman comme étant le seul système capable d’enregistrer et de reproduire des données couleur spectrales. Depuis l’intérêt pour le multi-spectral n’a cessé de croître, pour la simple raison que toute l’information couleur est disponible quand on travaille avec des données spectrales. Là où un système classique d’acquisition couleur enregistre des informations liées aux interactions entre une surface et un illuminant spécifique, un système d’acquisition multi-spectral va permettre de simuler la couleur de cette surface pour différentes conditions d’illumination.

Un système de reproduction spectrale de la couleur suivra des étapes similaires à un système de reproduction couleur classique, mais rapportées à des données spectrales: acquisition spectrale de la couleur, stockage et reproduction spectrale de la couleur. Les parties acquisition et reproduction spectrale de la couleur utilisent des technologies similaires à l’acquisition et la reproduction couleur.

Des systèmes d’acquisition spectrale ont été construits à partir de caméras et de filtres (Hardenberg, 1999; Schmitt, 2005). Avec ce type d’installation il est possible de faire de l’archivage d’œuvres d’art de haute qualité: l’information est enregistrée sur des bandes de longueur d’onde plus réduites et plus nombreuses que les filtres traditionnels rouge, vert et bleu. Dans l’objectif de projeter des images multi-spectrales des filtres ont été ajoutés à des projecteurs couleur classique (Boosmann and Hill, 2003; Hill, 2007).

L’apparition de plus en plus courante d’imprimantes multi-colorant, avec comme premier but d’augmenter le gamut couleur de l’imprimante, a ouvert le chemin de la reproduction spectrale de la couleur. Les premières études scientifiques de ces systèmes d’impression ont porté sur la réduction du métamérisme (Kohler et Berns, 1993), la sélection des colorants (Kohler et Berns,

1993; Tzeng et Berns, 1999, 2000) et la caractérisation spectrale des imprimantes (Balasubramanian, 1999; Wyble et Berns, 2000, Hersch et al., 2004). Puis naturellement la reproduction spectrale de la couleur (Taplin et Berns, 2001; Berns et al., 2003; Kraushaar et Urban, 2006). Une chaîne complète d'opération pour la reproduction spectrale de la couleur existe donc et certains travaux de recherche tentent d'harmoniser cette chaîne en suivant un schéma similaire à la reproduction couleur (Rosen et al., 2003; Derhak et Rosen, 2006).

Dans ce travail de recherche nous avons étudié divers aspects de la reproduction spectrale de la couleur. Cela nécessite de comprendre certaines opérations pour le traitement des données spectrales comme la caractérisation spectrale des imprimantes, le *gamut mapping*, la séparation des colorants et l'opération de *halftoning*. Dans nos travaux nous avons caractérisé une imprimante jet d'encre multi-colorant avec un modèle spectral d'imprimante. Des méthodes pour inverser ce modèle et effectuer la séparation spectrale des colorants ont été proposées et discutées. Cette étape d'inversion est importante car elle permet de transformer une réflectance spectrale en une combinaison de colorants pour contrôler l'imprimante. Dans l'étape de halftoning nous avons utilisé une technique de diffusion d'erreur. Nous avons également proposé une seconde approche pour la reproduction d'images spectrales par halftoning par diffusion d'erreur vectorielle. Cette seconde approche utilise le même système d'impression multi-colorant et fournit de bons résultats.

Plan de la thèse

Dans le premier chapitre nous présentons en plus du problème posé les différentes publications scientifiques produites durant ce travail de thèse. Les notations mathématiques et abréviations sont regroupées à la fin de ce chapitre.

Dans le Chapitre 2 vous trouverez les bases de la colorimétrie, en particulier les relations entre source lumineuse, observateur standard et surface réfléchissant la lumière. Un système de reproduction métamérique de la couleur y est expliqué avec en parallèle un système de reproduction spectrale de la couleur. Si la technologie utilisée est la même les différences interviennent en terme de dimension des données à traiter: 3 dimensions pour la couleur et 31 dimensions pour une réflectance spectrale (31 valeurs décrivant un spectre de 400nm à 700nm avec un pas de 10nm).

Dans le Chapitre 3 nous parlons de modélisation spectrale des imprimantes, aussi appellée *forward printer model*. Nous cherchons à établir une relation entre une combinaison de colorant envoyée à l'imprimante et la réflectance spectrale imprimée. Les modèles de Murray-Davies, Neugebauer et Yules-Nielsen y sont exposés. Le phénomène de *dot gain* est également introduit.

Le Chapitre 4 présente nos résultats expérimentaux pour la caractérisation spectrale de notre imprimante jet d'encre multi-colorant.

Le Chapitre 5 concerne la relation inverse présentée dans les deux chapitres précédents, à savoir la transformation d'une réflectance spectrale à imprimer en une combinaison de colorants pour contrôler l'imprimante. Cette transformation dite de séparation spectrale des colorants permet d'illustrer la réduction de métamérisme dans la reproduction spectrale de la couleur. Cette opération est réalisée en inversant le modèle spectral de l'imprimante, c'est un problème d'optimisation.

Au Chapitre 6 nous présentons l'opération de halftoning qui est la dernière transformation appliquée à l'image avant son impression. Cette opération intervient donc après la séparation spectrale des colorants et l'image spectrale est alors représentée sous la forme d'une image multi-canal, un canal par colorant. Le halftoning va binariser ces canaux indépendamment les uns des autres, chaque valeur de pixel devenant une commande pour l'imprimante de déposer ou non une goutte d'encre à la position du pixel. Dans ce chapitre nous présentons également une seconde approche pour la reproduction spectrale de la couleur par diffusion vectorielle de l'erreur. Cette technique de halftoning combine en une opération la séparation spectrale des colorants et le halftoning pour chaque canal. Nous parlerons également dans ce chapitre de gamut mapping spectral par l'inversion du modèle spectral de l'imprimante.

Enfin dans le Chapitre 7 nous comparons expérimentalement les deux approches présentées pour la reproduction spectrale de la couleur.

Chapitre 2

Bases de colorimétrie et chaîne d'opérations pour la reproduction d'image couleur

Ce chapitre décrit les bases de la colorimétrie pour la reproduction couleur, le phénomène de métamérisme et la chaîne typique des opérations appliquées à une image pour sa reproduction couleur y sont également expliqués.

Colorimétrie

Nous nous restreignons à la configuration suivante pour le calcul de la valeur colorimétrique d'un signal lumineux: une source lumineuse est réfléchie sur une surface dont les propriétés sont connues (e.g. la réflectance spectrale d'une surface de papier recouverte d'encre jaune). L'observateur standard CIE 1931 et les courbes décrivant sa sensibilité spectrale (voir CMFs Figure 2.1 (a)) sont utilisés pour déduire les valeurs des tristimulus X, Y et Z correspondant à ce signal (voir Equation 2.1).

Le calcul des tristimulus X, Y et Z révèle que deux surfaces de réflectance spectrale différente observées sous une condition d'illumination définie peuvent donner la même réponse colorimétrique: c'est le phénomène de métamérisme, voir Equation 2.8. Si les conditions d'illumination changent l'observateur humain percevra des différences, voir Equation 2.9.

Différences spectrale et colorimétriques

Pour comparer des réflectances spectrales entre elles, la première différence est obtenue en calculant la distance Euclidienne entre deux réflectances spectrales (voir Equation 2.12). En plus de cette information la différence CIE 1976 dans l'espace CIELAB est calculée également pour plusieurs conditions d'illuminations (voir Equation 2.13), cette différence renseigne sur l'erreur perçue par un observateur humain. La différence CIE 1994 est également utilisée avec les coefficients recommandés pour les arts graphiques (voir Equation 2.15).

Chaîne de traitement de l'image pour sa reproduction couleur

La chaîne de traitement de l'image pour sa reproduction couleur est présentée Figure 2.5. Avant d'être reproductible, une image RVB (Rouge, Vert, Bleu) va subir plusieurs transformations:

1. l'opération de gamut mapping: toutes les couleurs d'une image ne sont peut-être pas reproductibles dans le volume de couleur (c.-à-d. le gamut couleur) de l'imprimante: cette opération va rapporter les données de l'image vers le gamut de l'imprimante (ou d'un écran si on utilise ce média) tout en minimisant la perte d'information.
2. la séparation des colorants consiste à exprimer une valeur colorimétrique d'une image en une combinaison de colorant qui sera utilisée pour contrôler l'imprimante.
3. le scaling adapte la résolution de l'image à celle de l'imprimante. C'est généralement une opération de suréchantillonnage de l'image.
4. le halftoning est la dernière opération qui rend l'image imprimable en transformant chaque pixel de l'image en une commande pour l'imprimante de déposer ou non une goutte d'encre à telle ou telle position.

Pour la reproduction couleur d'image spectrale la même chaîne de traitement est suivie, la différence venant de la dimension des données à traiter: de 3 dimensions pour une image RGB à 31 dimensions pour une image spectrale lorsque chaque pixel de l'image (c.-à-d. une réflectance spectrale) est décrit par un vecteur de 31 valeurs couvrant le spectre du visible de 400nm à 700nm.

Halftoning

Nous utilisons une imprimante jet d'encre multi-colorant pour reproduire nos images. Ce type d'imprimante ne peut générer que deux niveaux par colorant: 0 ou 1. Cette valeur binaire correspond à une commande pour déposer ou non une goutte d'encre. L'opération de halftoning devient nécessaire quand le média utilisé pour reproduire un niveau de couleur ne peut que générer un nombre limité de niveau (Hains et al., 2003; Ulichney, 1987a; Lau et Arce, 2001). En variant la distribution spatiale de points (c.-à-d. des gouttes d'encre) l'illusion de niveaux de couleur peut être créée.

Il existe deux familles de halftoning: la première va chercher à grossir la taille d'un point sur une grille (c.-à-d. le pas entre deux centres de point restant constant) pour créer l'illusion d'un niveau de colorant, technique dite de halftoning par modulation d'amplitude ou *amplitude modulated halftoning* (AM). La seconde famille va varier la distribution spatiale de points de taille constante pour créer l'illusion de niveaux de couleur, technique dite de halftoning par modulation de fréquence ou *frequency modulated halftoning* (FM). Nous utilisons une technique de diffusion d'erreur (technique dite *scalar error diffusion* (SED)) avec filtre pour pondérer l'erreur à distribuer. La Figure 2.9 illustre la technique de halftoning par SED. Différents filtres existent: Floyd-Steinberg (Floyd et Steinberg, 1976), Jarvis-Judice-Ninke (Jarvis et al., 1976), pour diffuser l'erreur au cours de l'opération de halftoning. Cette technique halftone une image pixel par pixel (voir Equation 2.19) en suivant un chemin de parcours d'image défini comme montré à la Figure 2.8. Deux exemples, un pour chaque famille de halftoning sont présentés Figure 2.11 pour l'halftoning AM et Figure 2.12 pour l'halftoning FM.

Chapitre 3

Caractérisation spectrale des imprimantes: théorie

La caractérisation spectrale de notre système d'impression permet d'établir la transformation d'une combinaison de m colorants à la réflectance spectrale imprimée sur le papier. Cette transformation est aussi appelée le modèle de l'imprimante (ou *forward printer model*). Le modèle inverse de l'imprimante permet de transformer une réflectance spectrale en une combinaison de m colorants.

Un modèle d'imprimante permet d'estimer la couleur imprimée pour une combinaison de colorant envoyée à l'imprimante. Pour cela quelques paramètres décrivant le système d'impression sont nécessaires: réflectances spectrales décrivant les limites du gamut de l'imprimante ainsi que des rampes mono-colorant pour décrire le recouvrement du papier de 0% à 100%.

Nous utilisons des modèles d'imprimante de type regression based (Wyble et Berns, 2000) pour caractériser notre système d'impression: modèle de Murray-Davies (Murray, 1936) pour les impressions mono-colorant et le phénomène de dot gain, les modèles de Neugebauer (1937) et Yules-Nielsen (Yules et Nielsen, 1951) pour les impressions multi-colorant.

Modèle de Murray-Davies et *dot gain*

Le modèle de Murray-Davies (MD) produit une estimation de la réflectance spectrale d'un niveau de colorant en calculant la somme pondérée de la réflectance du papier vierge d'encre et celle du papier complètement recouvert par le colorant employé (voir Equation 3.1).

Ce modèle permet d'illustrer le phénomène de dot gain. Les Figure 3.1 (a) et Figure 3.1 (b) permettent de comparer les réflectances spectrales imprimées et mesurées d'une rampe de cyan avec celles simulées par le modèle de MD. La simulation par MD présente une évolution linéaire des réflectances spectrales de la rampe de colorant alors que la mesure de cette rampe montre une relation différente entre les niveaux de la rampe. Le rendu colorimétrique de la rampe mesurée et simulée illustre clairement le dot gain, les valeurs imprimées de la rampe sont plus sombres que les valeurs souhaitées.

Il y a deux types de dot gain (Viggiano, 1983): un dot gain mécanique lié à la déformation de la goutte d'encre éjectée sur le papier et un dot gain optique liée aux multiples interactions entre les rayons lumineux arrivant sur le papier et se propageant entre le papier et les couches d'encre imprimées.

L'inversion du modèle de MD permet d'établir la relation entre la valeur théorique et la valeur effective d'un niveau de la rampe imprimée. Suivant l'Equation 3.2 une table de correction (LUT) peut ainsi être établie. L'utilisation de cette LUT dans le modèle de MD permet d'affiner l'estimation des réflectances spectrales. Les différences entre les réflectances spectrales dans la Figure 3.1 (a) et la Figure 3.1 (c) sont réduites, la valeur effective utilisée à la place de la valeur théorique a permis de corriger le modèle de MD en intensité, en revanche le rendu colorimétrique montre toujours une légère différence colorimétrique entre les mesures et les estimations.

Le dot gain optique peut être ajouté au modèle de MD avec l'utilisation du facteur n de Yules-Nielsen (1951). La valeur de ce facteur n dans l'Equation 3.9 est obtenue par optimisation: plusieurs estimations des réflectances spectrales d'une rampe sont réalisées à partir du modèle de MD et de différentes valeurs pour n . Les réflectances simulées sont comparées à celles imprimées en calculant les différences colorimétriques et spectrales, voir les Figures 3.3 (a), 3.3 (b), 3.4 (a) et 3.4 (b) ainsi que les Tableaux 3.2 et 3.3.

Modèle de Neugebauer et équations de Demichel

Pour des impressions multi-colorant le modèle de Murray-Davies n'est plus suffisant et est remplacé par le modèle de Neugebauer (NG). Le modèle de NG va estimer la réflectance spectrale d'une combinaison de colorants en calculant la somme pondérée des primaires de Neugebauer (NPs) pour cette combinaison donnée. Le poids des NPs représentent les surfaces occupées par chacune des NPs. Les NPs représentent toutes les couleurs solides que peut produire un système d'impression. Une imprimante m encres disposera de 2^m NPs, voir Equation 3.32 pour le modèle spectral de NG.

La communication avec une imprimante se faisant par des combinaisons de colorants, une estimation du niveau (c.-à-d. surface occupée) de chaque NP pour une combinaison de colorants donnée est nécessaire: le modèle statistique de Demichel (1924) nous permet de réaliser cette estimation. Voir Equation 3.21 pour une combinaison de deux colorants, Equation 3.25 pour une combinaison de trois colorants et Equation 3.30 pour généralisation à m colorants.

Modèle de Yules-Nielsen et facteur n

Le dot gain optique peut aussi être pris en compte dans l'estimation de la réflectance spectrale d'une combinaison de colorants, et ce toujours sous la forme du facteur n , voir Equation 3.36 pour le modèle spectral de Neugebauer modifié par Yules-Nielsen.

La valeur du facteur n est calculée pour chaque système d'impression. La déduction d'un facteur n à partir des différentes valeurs pour chaque impression mono-colorant ne donne pas forcément les meilleurs résultats pour modéliser le dot gain optique de combinaisons multi-colorant. Un facteur n obtenu par optimisation sur un échantillon de combinaisons multi-colorant permettra d'améliorer les performances du modèle de l'imprimante.

Le diagramme présenté Figure 3.5 regroupe les différentes étapes de la caractérisation spectrale de l'imprimante: de la transformation valeur théorique à la valeur effective pour chaque colorant d'une combinaison, estimation des poids pour chaque NP à partir des valeurs effectives des colorants, puis estimation de la réflectance spectrale par Neugebauer ou Yules-Nielsen.

Conclusion

Les modèles d'imprimante présentés pour la caractérisation de notre système d'impression sont relativement simples et présentent la caractéristique d'être facilement inversible. Cette information est importante car c'est le modèle inverse de l'imprimante qui permettra de communiquer avec l'imprimante et d'obtenir une combinaison de colorant pour reproduire une réflectance spectrale donnée.

Chapitre 4

Caractérisation spectrale des imprimantes: expérimentation

Ce chapitre présente les résultats expérimentaux pour la caractérisation spectrale de notre système d'impression. Notre système est constitué d'une imprimante jet d'encre Epson Photo Stylus 2100 avec 7 colorants. Le jeu de colorant fournit avec l'imprimante a été remplacé par un jeu comprenant les colorants cyan, magenta, jaune, noir, rouge, vert et bleu (voir à la Figure 4.1 les $2^7 = 128$ primaires de Neugebauer de notre système d'impression). Du papier photo Epson 194g/m² a été sélectionné après une rapide comparaison de différents types de papier. Pour communiquer avec l'imprimante nous utilisons un pilote d'imprimante dédié. Les données prêtes à l'impression doivent être présentées au pilote sous la forme d'une image TIFF CMYK + canaux spots. Chaque canal de l'image TIFF doit aussi être binarisé de façon à commander qu'une goutte d'encre soit déposée ou non, la résolution de l'image devant correspondre à celle de l'imprimante.

Pour construire le modèle de l'imprimante nous avons suivi les étapes décrites dans la caractérisation spectrale de l'imprimante avec le modèle spectral de Neugebauer. Les rampes monocolorants pour les 7 colorants ont été imprimées et mesurées et, par l'inversion du modèle de Murray-Davies, autant de LUTs ont été créées.

Une mire constituée de 4175 combinaisons de colorant est imprimée et mesurée. Environ 10% de ces combinaisons sont utilisées pour calculer le meilleur facteur n pour ce système. Les graphes présentés Figure 4.4 décrivent les performances de notre modèle par rapport à la valeur du facteur n choisie. Le Tableau 4.3 récapitule les performances pour le modèle spectral de Neugebauer et le modèle spectral de Yules-Nielsen appliqués à notre système d'impression. Le modèle de Yules-Nielsen donne les meilleurs résultats, le dot gain mécanique et le dot gain optique étant pris en compte dans les estimations par ce modèle.

Pour améliorer les performances du modèle de l'imprimante, le choix d'un modèle comme le modèle cellulaire de Neugebauer devrait répondre à nos attentes. En utilisant des primaires de Neugebauer intermédiaires (et non uniquement les NPs décrivant les limites du gamut de l'imprimante) le phénomène de dot gain est mieux modélisé.

Chapitre 5

Inversion du modèle spectrale de l'imprimante

Ce chapitre traite de l'inversion du modèle spectral de l'imprimante utilisé dans le chapitre précédent: l'inversion du modèle spectral de Neugebauer. Cette étape dans la chaîne d'opération pour la reproduction d'image spectrale couleur est appelée séparation des colorants. Pour chaque réflectance spectrale à imprimer la séparation des colorants fournit une combinaison de colorants pour contrôler l'imprimante et reproduire cette réflectance spectrale. L'inversion du modèle spectral de l'imprimante est rendue possible par la résolution d'un problème d'optimisation. La solution du problème une fois réinjectée dans le modèle spectral de l'imprimante doit produire une estimation de la réflectance spectrale pour la combinaison de colorants obtenue. La différence

entre la réflectance spectrale estimée et la réflectance spectral désirée est minimale pour les paramètres du problème d'optimisation (Equation 5.1).

Cette opération de séparation de colorants permet de comparer en simulation la reproduction couleur et la reproduction spectrale d'une donnée spectrale. Le processus d'optimisation compare à chaque itération une réflectance spectrale estimée avec la réflectance spectrale désirée (Equation 5.3). Le choix du critère pour comparer ces deux réflectances spectrales permet de définir une reproduction spectrale ou une reproduction colorimétrique pour la reproduction de données spectrales.

Comparaison des méthodes d'inversion

La méthode que nous avons développée pour l'inversion du modèle spectral de l'imprimante a été comparée à plusieurs méthodes d'inversion existantes. Les trois méthodes comparées sont: l'inversion par régression linéaire itérative (LRI, voir Section 5.2.1), l'inversion avec minimisation d'une fonction de coût avec contraintes (CMR, voir Section 5.2.2) et notre méthode dite d'inversion optimale pour les poids (WI, voir Section 5.2.3). Notre méthode suit le processus inverse des étapes constituant le modèle spectral de Neugebauer: inversion optimale pour les poids des primaires de Neugebauer. La solution de ce premier problème répond aux contraintes du modèle de Demichel (voir Equation 5.15). Ensuite utilisant la formulation du modèle de Neugebauer défini par l'Equation 5.20 un jeu de colorants est extrait du jeu de poids obtenu après inversion du premier problème.

La comparaison des méthodes d'inversion existantes avec notre méthode a montré que la méthode CMR fournissait les meilleurs résultats pour l'inversion du modèle spectral de Neugebauer (voir Tableaux 5.1 à 5.3). Malgré cela notre méthode d'inversion WI a montré que sa première étape pouvait être utilisée comme technique de *gamut mapping* spectral: le produit des poids des primaires de Neugebauer par leur réflectance spectrale nous donne la meilleure estimation dans le gamut spectral de l'imprimante de la réflectance spectrale désirée. Une étude des performances de cette technique de *gamut mapping* spectral est présentée dans l'Appendix B.

Comparaison entre reproduction couleur et reproduction spectrale de donnée spectrales

Pour cette étude la méthode d'inversion CMR a été utilisée. Cette méthode permet facilement de changer le critère d'optimisation et ainsi de sélectionner le type de reproduction désiré: différence colorimétrique CIE 1976 pour une reproduction couleur sous un illuminant donné (voir Equation 5.22), différence spectrale sRMS pour reproduction spectrale (voir Equation 5.24). Nous avons aussi testé un critère colorimétrique intégrant quatre illuminants (voir Equation 5.22) et un dernier critère combinant une différence colorimétrique CIE 1976 sous un illuminant et une différence spectrale. L'importance accordée à la différence colorimétrique ou spectrale dans le dernier critère présenté peut être ajustée avec un paramètre alpha (voir Equation 5.25).

L'étude des résultats de l'expérience conduite pour comparer ces différents critères a montré que le critère purement colorimétrique donnait les meilleurs résultats pour chaque illuminant testé. Le critère purement spectral a montré la meilleure performance en termes de différence spectrale mais aussi des différences colorimétriques plus homogènes pour les illuminants testés par comparaison à l'approche purement colorimétrique (voir Tableaux 5.4 à 5.0). Le troisième critère testé qui moyenne quatre différences colorimétriques pour quatre illuminants donnés se situait en terme de performance entre le purement colorimétrique et le purement spectral. Enfin, le quatrième critère testé a permis d'évaluer l'évolution des différences colorimétriques et spectrales en fonction de la valeur du paramètre alpha. On peut observer que certaines combinaisons de colorants satisfont chacune des deux approches simultanément: voir Figure 5.6 où un alpha diminuant l'importance de la différence spectral sRMS garde cette différence presque constante tout en diminuant les différences colorimétriques. Sur ces résultats on peut donc observer une amélioration de la reproduction spectrale par rapport à une reproduction purement

colorimétrique, plusieurs conditions d'illumination pouvant être prises en compte simultanément. Ajouter plus d'illuminants au critère défini par l'Equation 5.22 devrait permettre de trouver une combinaison de colorants satisfaisant un très grand nombre de conditions d'illumination. Mais cela ne devrait aussi optimiser que seulement pour l'observateur de référence, le critère d'optimisation avec le paramètre alpha semble être un bon compromis entre une reproduction purement spectrale et purement colorimétrique.

Chapitre 6

Halftoning par diffusion d'erreur vectorielle spectrale (sVED)

Dans les chapitres précédents nous avons présenté la chaîne d'opérations à appliquer à une image spectrale pour sa reproduction. Cette chaîne d'opérations est une adaptation de celle utilisée pour la reproduction d'images couleurs à la reproduction d'images spectrales: caractérisation spectrale du système d'impression, séparation des colorants puis halftoning des canaux colorants. La dernière opération de halftoning traite chaque canal colorant indépendamment les uns des autres, après cette transformation chaque pixel de chaque canal a une valeur binaire qui correspond à une commande pour l'imprimante de déposer ou non une goutte d'encre à la position du pixel. Le halftoning par diffusion d'erreur vectorielle (VED) permet de combiner en une seule opération l'étape de séparation des colorants et de halftoning (voir en Figure 6.1 la mise en parallèle des deux chaînes d'opérations).

Le halftoning par VED pour image spectrale (sVED) est une adaptation de la technique de halftoning par VED pour image couleur (Haneishi et al., 1996; Kouzaki et al., 1999; Kawaguchi et al., 1999). Le halftoning par VED est lui même basé sur la technique de diffusion d'erreur scalaire (Ulichney, 1987a) (voir Section 2.6.2). Avec le halftoning par sVED tous les canaux colorants sont halftonés simultanément. Successivement chaque pixel est remplacé par sa primaire de Neugebauer (NP) la plus proche en distance Euclidienne (voir Figure 6.2). Une primaire de Neugebauer correspond à une combinaison binaire des colorants du système d'impression et donc à une commande pour l'imprimante. La différence entre la NP sélectionnée et le pixel halftonné (c.-à-d. l'erreur) est diffusée à l'aide d'un filtre de poids, suivant le chemin de parcours dans l'image, allant de gauche à droite et de bas en haut.

Evaluation du halftoning par sVED

Une première évaluation du halftoning par sVED sur des images spectrales a montré un comportement de l'algorithme similaire à celui des images couleurs: la distribution spatiale des points est visuellement agréable, le halftoning par VED étant connu pour améliorer la qualité des images halftonées par rapport au halftoning par diffusion d'erreur scalaire, et ce en utilisant les mêmes filtres de poids pour diffuser l'erreur dans l'image (Floyd et Steinberg, 1976; Jarvis, Judice et Ninke, 1976). Mais le halftoning par VED (et par sVED) est également très lent à diffuser l'erreur, ceci étant dû à une trop grande accumulation de l'erreur durant le halftoning. Cette accumulation d'erreur apparaît sous la forme de trainée dans l'image et résulte souvent en une perte de détails, voir Figures 6.3 (a) à 6.3 (f). L'image spectrale de la mire ColorChecker MacBeth (*CC*) permet d'observer clairement le débordement de l'erreur d'une zone de l'image aux autres suivant le chemin parcouru par le filtre.

Amélioration du halftoning par sVED

La dernière transformation appliquée à une image avant son impression est le *scaling*. Il consiste en un suréchantillonnage de l'image afin d'adapter sa résolution à celle de l'imprimante. Une simulation de cette opération est réalisée Figure 6.7 où la résolution est augmentée trois fois: on peut observer que l'augmentation de la résolution va permettre de réduire la visibilité de la lenteur de l'algorithme. Les Figures 6.9 (a) et 6.9 (b) présentent deux images halftonées de

l'image spectrale de la mire *CC* pour une imprimante 6 colorants en (a) et 7 colorants en (b). Pour chacune des images halftonées l'image originale a été agrandie d'un facteur deux de façon à simuler le changement de résolution. Les débordements de l'erreur en Figure 6.3 (f) sont maintenant moins visibles dans la Figure 6.9 (b).

Spectral gamut mapping

Le suréchantillonnage de l'image ne résout pas tous les problèmes du sVED, le halfoning des pixels de l'image en partie situés en dehors du gamut de l'imprimante va générer des erreurs à diffuser trop importantes. Pour éviter de diffuser des erreurs trop importante dès le départ de l'algorithme les images spectrales sont mappées vers le gamut spectral de l'imprimante en utilisant la technique de gamut mapping spectral décrite dans l'Appendix B.

Les Figure 6.10 (a) et (b) présentent les rendus colorimétriques de l'image spectrale de la mire *CC* pour l'imprimante 6 colorants et 7 colorants respectivement. Les images halftonées de ces images rapportés au gamut spectral de chacune des imprimantes sont présentées Figure 6.12 (a) et (b) respectivement. On peut observer pour chacune des imprimantes une nette amélioration de la qualité de l'image halftonée: conservation des détails dans l'image, très faible débordement de l'erreur.

Contrôle de l'erreur

Malgré l'opération de gamut mapping comme pré-traitement avant le sVED nous pouvons toujours observer un léger effet de bord. Même rapportée au gamut spectral de l'imprimante les erreurs générées par le sVED modifient grandement les réflectances spectrales dans l'image spectrale, voir Figures 6.14 (a) et (b) et Figures 6.18 (a) et (b) pour des exemples de réflectances spectrales extraits de l'image spectrale de la mire *CC*. Pour continuer à réduire la visibilité de l'erreur diffusée nous avons cherché à contrôler l'erreur en agissant directement sur la forme des réflectances spectrales avant la sélection de la NP (voir les diagrammes Figure 6.13 et Figure 6.17).

Cette approche pour contrôler la diffusion d'erreur a montré de bon comportement lors de changement de région dans l'image, mais elle a aussi parfois détérioré la qualité de l'image halftonée (en particulier lors du contrôle de l'erreur par *clipping*). Cela a indiqué la difficulté à trouver une valeur de seuillage unique pour une image entière. Une adaptation de la condition et/ou de la valeur de seuillage à l'information locale de l'image devrait améliorer le contrôle de l'erreur dans le sVED.

Design de nouveaux filtres

Une dernière approche a été étudiée en travaillant directement sur le design des filtres pour diffuser l'erreur. Une approche par perturbation d'un filtre existant ou création d'un nouveau filtre en accord avec l'information locale de l'image n'est pas nouvelle (Ulichney, 1987b). La règle principale suivie est que la somme des poids d'un filtre doit rester égale à 1 (voir Equation 6.7). Pour chaque pixel halftonné un nouveau filtre est donc créé (voir diagramme Figure 6.21).

Nous avons d'abord testé une simple permutation des poids d'un filtre existant, voir Figure 6.23 (a) et (b). Comparées aux images halftonées avec le filtre original sans permutation (voir Figure 6.12 (a) et (b)) les images obtenues sont un peu plus bruitées et les effets de bord un peu moins visible.

Enfin nous avons cherché à utiliser l'information présente dans l'image pour créer de nouveaux filtres en diffusant une plus grande quantité d'erreur aux pixels proches du pixel halftonné et en évitant d'accumuler trop d'erreur aux pixels plus éloignés du pixel halftonné. La valeur des poids des filtres est calculée en fonction de la distance du pixel halftonné à ses voisins dans la région du filtre. Les images obtenues (voir Figures 6.25 (a) et (b)) n'ont quasiment plus d'effets de bord visibles mais sont légèrement bruitées. Cette dernière approche une fois combinée à une remise à zéro de l'erreur devrait permettre d'améliorer encore la qualité de l'image halftonée.

Chapitre 7

Comparaison des deux approches proposées pour la reproduction spectrale couleur

Dans ce dernier chapitre nous avons comparé expérimentalement les deux approches pour la reproduction de données spectrales. Les données spectrales à reproduire proviennent de l'acquisition spectrale d'une peinture (Dupraz, Ben Chouikha et Alquié, 2007). A partir de cette acquisition une douzaine de réflectances spectrales ont été utilisées pour créer des patches à valeur spectrale unique, voir Figure 7.1 et Figure 7.2.

Les réflectances spectrales ont été reproduites en simulation pour notre imprimante 7 colorants. Dans la première étape nous avons mappé les données spectrales au gamut spectral de l'imprimante avec notre technique de gamut mapping spectral (voir Appendix B). Chaque patch est de taille 256×256 pixels.

La comparaison des deux approches peut se faire du point de vue des différences colorimétriques et/ou spectrales (voir Tableau 7.2) et du point de vue des patches halftonés (c.-à-d. comparaison des distributions spatiales des NPs). La valeur de la réflectance spectrale de chaque patch halftonné est estimée en calculant la moyenne des NPs présentes dans chaque patch. La première conclusion est que la reproduction par sVED est plus performante, les plus petites différences colorimétriques et spectrales étant obtenues pour cette approche. Les performances des deux approches restant proches il est nécessaire de comparer également les distributions spatiales de NPs (voir Figures 7.4 à 7.9). Des filtres identiques ont été utilisés (Jarvie, Judice et Ninke, 1976) pour le halftoning par diffusion d'erreur après la séparation des colorants et pour le halftoning par diffusion d'erreur spectrale vectorielle. La seconde approche a produit des distributions beaucoup moins bruitées et plus agréables visuellement. Cependant des expérimentations sur d'autres images spectrales doivent encore être conduites pour comparer pleinement ces approches pour la reproduction de données spectrales.

Chapitre 8

Conclusions et Perspectives

La Figure 6.1 présente les deux chaînes d'opérations pour la reproduction qui ont été testées dans ce travail de recherche, chacune utilisant le même système d'impression. L'approche par diffusion vectorielle de l'erreur spectrale (sVED) offre l'avantage de ne nécessiter que peu de paramètres: les réflectances spectrales primaires de Neugebauer (NPs). Cette approche ne résout pas tous les problèmes et en introduit de nouveaux. Cette approche étant purement une approche par halftoning les améliorations ne peuvent venir que de l'algorithme lui-même. L'opération de gamut mapping spectral proposée permet de limiter la visibilité de l'erreur dans l'image halftonnée et le design de nouveaux filtres pour diffuser l'erreur en fonction de l'information locale contribue aussi à l'amélioration de l'algorithme.

L'étape de gamut mapping spectral est importante car elle permet de simuler la reproduction ou d'évaluer la possibilité de la reproduction spectrale de la couleur pour différents systèmes d'impression. La séparation des colorants est effectuée dans notre cas par l'inversion du modèle spectral de NG. Une inversion d'un modèle plus physique comme le modèle de Clapper-Yule pourra être également testée.

Le halftoning par sVED peut encore être amélioré en continuant l'adaptation des filtres avec l'information locale dans l'image. Le plus intéressant avec cette approche est qu'elle permet de manipuler les données spectrales plus longtemps dans la chaîne d'opération de la reproduction spectrale et qu'aucune différence colorimétrique n'est impliquée. D'autres techniques de halftoning pour des images couleur font varier le parcours dans l'image et diffusent l'erreur dans

toutes les directions. Une approche similaire pour des images spectrales devrait aussi réduire les marques laissées par le halftoning par sVED.

Enfin la technologie par jet d'encre a été utilisée pour nos expérimentations: la comparer à d'autres techniques d'impression serait intéressant. Une recherche des meilleurs colorants pour une image spectrale devrait aussi améliorer la reproduction: la reproduction d'une peinture avec des propriétés spectrales très différentes de celles des colorants du système d'impression est une sérieuse limitation à une parfaite reproduction spectrale de la couleur. La reproduction spectrale de la couleur doit être vue comme une amélioration de la reproduction couleur classique avec la réduction du phénomène de métamérisme.

Contents

1	Introduction	31
1.1	Motivation	31
1.2	Thesis outline	32
1.3	Publications	32
1.4	Notation in this document	33
1.5	Abbreviations	35
2	Basics and Fundamentals	37
2.1	Introduction	37
2.2	Colorimetry for reflective objects	37
2.2.1	Calculation of the CIEXYZ tristimulus values	39
2.2.2	Calculation of the CIELAB values	41
2.2.3	Metamerism	41
2.3	Color and spectral differences	42
2.3.1	Spectral RMS	42
2.3.2	CIE 1976 color difference	42
2.3.3	CIE 1994 color difference	43
2.4	Spectral reflectance measurement	43
2.4.1	Spectral reflectance measurement of test charts	43
2.4.2	Spectral reflectance measurement of images	43
2.5	Color reproduction workflow	44
2.5.1	Additive color process	44
2.5.2	Subtractive color process	44
2.5.3	Colorant separation process for CMY printer	45
2.5.4	Black ink generation	45
2.5.5	Gamut mapping	46
2.5.6	Multi-colorant printing system	46
2.5.7	Scaling process	47
2.6	Halftoning process	47
2.6.1	Amplitude modulated halftoning	47
2.6.2	Frequency modulated halftoning	47
2.7	Conclusion	52
3	Spectral printer characterization: theory	53
3.1	Introduction	53
3.2	Single colorant print	54
3.2.1	Murray-Davies	54
3.2.2	Dot gain effect	54
3.2.3	Inverse Murray-Davies	56
3.2.4	Murray-Davies and the Yule-Nielsen n factor	57
3.3	Multi-colorant print	58
3.3.1	The Demichel model	61

3.3.2	The spectral Neugebauer model	63
3.3.3	The spectral cellular Neugebauer model	64
3.3.4	The Yule-Nielsen modified spectral Neugebauer model	64
3.4	Discussion and conclusion	65
4	Spectral printer characterization: experimentation	67
4.1	Introduction	67
4.2	Experiment	67
4.2.1	Spectral modeling	68
4.2.2	Experimental setups	69
4.2.3	Results and Discussion	69
4.3	Conclusion	73
5	Inversion of the spectral printer model	75
5.1	Introduction	75
5.2	Method of inversion for the spectral Neugebauer equations	76
5.2.1	Inversion by linear regression iteration (LRI)	77
5.2.2	Inversion with a constraint minimization routine (CMR)	77
5.2.3	Optimal inversion of the weights (WI)	78
5.3	Comparison of inversion methods	79
5.3.1	Experiment	79
5.3.2	Results and discussion	79
5.4	Comparison of color reproduction and spectral color reproduction	82
5.4.1	Color reproduction by single color difference	82
5.4.2	Color reproduction by average color difference	82
5.4.3	Spectral color reproduction	82
5.4.4	Combining color reproduction and spectral color reproduction	83
5.4.5	Experiment	83
5.4.6	Results and discussion	84
5.5	Conclusion	94
6	Spectral vector error diffusion	97
6.1	Introduction	97
6.2	Spectral vector error diffusion	100
6.3	Evaluation of sVED	101
6.3.1	sVED of spectral patches	103
6.3.2	sVED of spectral images	109
6.4	Preprocessing by spectral gamut mapping	112
6.4.1	Spectral gamut mapping by inverting the spectral printer model	112
6.4.2	Experiments	112
6.5	Controlling the error	117
6.5.1	Reflectance clipping	117
6.5.2	Experiments	117
6.5.3	Reflectance scaling	122
6.5.4	Experiments	122
6.6	Designing new filters	127
6.6.1	Design filter by random placement of existing weights	128
6.6.2	Experiments	128
6.6.3	Design filter by distance	132
6.6.4	Experiments	132
6.7	Conclusion	136

7 Comparison of the spectral color reproduction workflows	139
7.1 Introduction	139
7.2 Experiment	139
7.2.1 Spectral gamut mapping	139
7.2.2 Colorant separation and halftoning by colorant channel	139
7.2.3 Spectral vector error diffusion	142
7.3 Comparison of the dot distribution	142
7.4 Conclusion	150
8 Conclusions and Perspective	151
8.1 Thesis work overview	151
8.2 Perspective and future works	152
A Printer characterization	155
A.1 Magenta	156
A.2 Yellow	159
A.3 Black	162
A.4 Blue	165
A.5 Red	168
A.6 Green	171
B Spectral gamut mapping	175
B.1 Introduction	175
B.2 Spectral gamut mapping by inverting the spectral printer model	175
B.3 Experiment	176
B.3.1 Spectral gamut mapping on single spectral reflectance	176
B.3.2 Spectral gamut mapping on spectral image	182
C Spectral Vector error diffusion	183
C.1 Evaluation of sVED	183
C.2 Preprocessing	188
C.3 Evaluation of sVED with clipping	193
C.4 Evaluation of sVED with scaling	196
C.5 Evaluation of sVED with new filter design by distance	199
C.6 Evaluation of sVED with new filter design by random placement of existing weights	202

List of Tables

1.1	Abbreviations used in this document	35
3.1	MD model performance for the ramp of cyan and $n = 1$	57
3.2	Best n factors for the ramp of cyan	59
3.3	Best n factors for the ramp of cyan	60
4.1	n factor versus single colorant ramps and various color and spectral difference . .	70
4.2	Performance of the YNSN model for the best n factor values obtained by optimization on the single colorant ramps	71
4.3	Performance of the YNSN model for the best n factor values obtained by optimization on approximatively 10% of the printed test chart.	73
5.1	Inversion performance the grid with LRI, CMR and WI methods	81
5.2	Inversion performance for the ColorChercker with the LRI, CMR and WI methods	81
5.3	Inversion performance for the gamut mapped ColorChercker with the LRI, CMR and WI methods	81
5.4	Performance of color reproduction and spectral reproduction for the grid with the six colorants printer	85
5.5	Performance of color reproduction and spectral reproduction for the Esser test chart with the six colorants printer	85
5.6	Performance of color reproduction and spectral reproduction for the ColorChecker test chart with the six colorants printer	86
5.7	Performance of color reproduction and spectral reproduction for the grid with the seven colorants printer	86
5.8	Performance of color reproduction and spectral reproduction for the Esser test chart grid with the seven colorants printer	87
5.9	Performance of color reproduction and spectral reproduction for the ColorChecker test chart with the seven colorants printer	87
6.1	Differences between the simulated reflectances of our randomly 100 created patches and their reproduction by sVED for our 6 colorants printer.	103
6.2	Differences between the simulated reflectances of our randomly 100 created patches and their reproduction by sVED for our 7 colorants printer.	104
6.3	Differences between single patches of the ColorChecker and their simulated reproduction by sVED for the 6 colorants printer and the 7 colorants printer	107
6.4	Differences between single patches of the gamut mapped ColorChecker and their simulated reproduction by sVED for the 6 colorants printer and the 7 colorants printer	115
6.5	Differences between single patches of the gamut mapped ColorChecker and their simulated reproduction by sVED and clipping for the 6 colorants printer and the 7 colorants printer	120

6.6	Differences between single patches of the gamut mapped ColorChecker and their simulated reproduction by sVED and scaling for the 6 colorants printer and the 7 colorants printer	125
6.7	Differences between single patches of the gamut mapped ColorChecker and their simulated reproduction by sVED and new filters by random placement of existing weights for the 6 colorants printer and the 7 colorants printer	130
6.8	Differences between single patches of the gamut mapped ColorChecker and their simulated reproduction by sVED and new filter by distance for the 6 colorants printer and the 7 colorants printer	134
7.1	Differences between spectral reflectances measurements and their gamut mapped version	143
7.2	Differences between the 12 gamut mapped spectral reflectances and their reproduction by CS + SED and reproduction by sVED	143
A.1	Differences between ramp of Magenta measurements and estimated spectral reflectances by MD	156
A.2	Differences between ramp of Yellow measurements and estimated spectral reflectances by MD	159
A.3	Differences between ramp of Black measurements and estimated spectral reflectances by MD	162
A.4	Differences between ramp of Red measurements and estimated spectral reflectances by MD	165
A.5	Differences between ramp of Green measurements and estimated spectral reflectances by MD	168
A.6	Differences between ramp of Blue measurements and estimated spectral reflectances by MD	171
B.1	Differences between the ColorChecker spectral reflectances and their spectral gamut mapped version for the 6 and 7 colorants printer	177

List of Figures

2.1	CIE CMFs 1931 and CIE CMFs 1964	38
2.2	SPDs of some CIE standard illuminants	38
2.3	Human observer and daylight illuminant	39
2.4	Human observer and fluorescent illuminant	40
2.5	Color reproduction workflow	44
2.6	Additive color mixing	44
2.7	Subtractive color mixing	45
2.8	Raster scan path	48
2.9	The process of scalar error diffusion	49
2.10	Original grayscale image	49
2.11	Example of AM halftoning	50
2.12	Example of FM halftoning by SED	51
3.1	Spectral reflectance measurements and estimations by MD of the cyan ramp and their correspondings RGB color renderings	55
3.2	LUTs for the ramp of cyan	57
3.3	Color and spectral differences versus n factor values for the ramp of cyan	59
3.4	Color and spectral differences versus n factor values for the ramp of cyan	60
3.5	NG diagram	64
4.1	The 128 NP of the Epson Stylus 2100 inkjet printer	68
4.2	The seven LUTs of the Epson Stylus 2100 printer	69
4.3	Test chart for the Epson stylus 2100 printer	70
4.4	Best n factor value versus color differences and spectral differences between the measured test chart and its simulation by the YNSN model.	72
5.1	Difference between original ColorChecker and its gamut mapped version	80
5.2	Inversion performance for the ColorChecker with CMR, LRI and WI methods	80
5.3	NP spectral reflectance for our six and seven printer	83
5.4	Differences between the grid spectral reflectances and their simulated reproductions for the 6 colorants printer	88
5.5	Differences between the gamut mapped Esser test chart spectral reflectances and their simulated reproductions for the 6 colorants printer	89
5.6	Differences between the gamut mapped ColorChecker test chart spectral reflectances and their simulated reproductions for the 6 colorants printer	90
5.7	Differences between the grid spectral reflectances and their simulated reproductions for the 7 colorants printer	91
5.8	Differences between the gamut mapped Esser test chart spectral reflectances and their simulated reproductions for the 7 colorants printer	92
5.9	Differences between the gamut mapped ColorChecker test chart spectral reflectances and their simulated reproductions for the 7 colorants printer	93

6.1	Comparison of spectral color reproduction workflow	99
6.2	The process of spectral vector error diffusion halftoning	100
6.3	Example of halftoning by sVED	102
6.4	Example of spectral reflectances during the sVED process	103
6.5	The NPs spectral reflectances of our 6 colorants and 7 colorants printers	104
6.6	Halftoning by sVED of the ColorChercher spectral patches for the 6 and 7 colorants printer	106
6.7	Visibility of the border effect in sVED versus printer resolution	108
6.8	the original ColorChecker spectral image	109
6.9	sVED of the <i>CC</i> spectral image for the 6 and 7 colorants printer	110
6.10	Gamut mapped <i>CC</i> spectral image for both 6 and 7 colorants printers	113
6.11	Halftoning by sVED of the gamut mapped ColorChercher spectral patches for the 6 and 7 colorants printer	114
6.12	sVED of the gamut mapped <i>CC</i> spectral image for the 6 and 7 colorants printer	116
6.13	The process of spectral vector error diffusion halftoning with clipping	117
6.14	Example of clipping to control the error in sVED	117
6.15	Halftoning by sVED with clipping of the gamut mapped ColorChecker spectral patches for the 6 and 7 colorants printer	119
6.16	sVED with clipping of the gamut mapped <i>CC</i> spectral image the 6 and 7 colorants printer	121
6.17	The process of spectral vector error diffusion halftoning with scaling	122
6.18	Example of scaling to control the error in sVED	122
6.19	Halftoning by sVED with scaling of the gamut mapped ColorChercher spectral patches for the 6 and 7 colorants printer	124
6.20	sVED with scaling of the gamut mapped <i>CC</i> spectral image the 6 and 7 colorants printer	126
6.21	The process of spectral vector error diffusion halftoning with new filter design	127
6.22	Halftoning by sVED with new filter by random placement of existing weights of the gamut mapped ColorChercher spectral patches for the 6 and 7 colorants printer	129
6.23	sVED with new filter by random placement of existing weights of the gamut mapped <i>CC</i> spectral image for the 6 and 7 colorants printer	131
6.24	Halftoning by sVED with new filter by distance of the gamut mapped ColorChercher spectral patches for the 6 and 7 colorants printer	133
6.25	sVED with new filter by distance of the gamut mapped <i>CC</i> spectral image the 6 and 7 colorants printer	135
7.1	Illustration of sample measurements for the paint <i>La Madeleine</i>	140
7.2	Paint of <i>La Madeleine</i>	141
7.3	Spectral reflectances of the measured and gamut mapped samples of the paint <i>La Madeleine</i>	142
7.4	Halftoned patches of samples 1 and 2 of <i>La Madeleine</i> paint	144
7.5	Halftoned patches of samples 3 and 4 of <i>La Madeleine</i> paint	145
7.6	Halftoned patches of samples 5 and 6 of <i>La Madeleine</i> paint	146
7.7	Halftoned patches of samples 7 and 8 of <i>La Madeleine</i> paint	147
7.8	Halftoned patches of samples 9 and 10 of <i>La Madeleine</i> paint	148
7.9	Halftoned patches of samples 11 and 12 of <i>La Madeleine</i> paint	149
A.1	Measured ramps and MD estimation in sRGB for illuminant D50	156
A.2	Measurement of Magenta ramp versus MurrayDavis estimation	157
A.3	Monochromatic ramps of Magenta and simulation by various Murray Davis model	158
A.4	Measured ramps and MD estimation in sRGB for illuminant D50	159
A.5	Measurement of Yellow ramp versus MurrayDavis estimation	160
A.6	Monochromatic ramps of Yellow and simulation by various Murray Davis model	161
A.7	Measured ramps and MD estimation in sRGB for illuminant D50	162

A.8 Measurement of Black ramp versus MurrayDavis estimation	163
A.9 Monochromatic ramps of Black and simulation by various Murray Davis model	164
A.10 Measured ramps and MD estimation in sRGB for illuminant D50	165
A.11 Measurement of Red ramp versus MurrayDavis estimation	166
A.12 Monochromatic ramps of Red and simulation by various Murray Davis model	167
A.13 Measured ramps and MD estimation in sRGB for illuminant D50	168
A.14 Measurement of Green ramp versus MurrayDavis estimation	169
A.15 Monochromatic ramps of Green and simulation by various Murray Davis model	170
A.16 Measured ramps and MD estimation in sRGB for illuminant D50	171
A.17 Measurement of Blue ramp versus MurrayDavis estimation	172
A.18 Monochromatic ramps of Blue and simulation by various Murray Davis model	173
B.1 ColorChecker patches 1 to 6	178
B.2 ColorChecker patches 7 to 12	179
B.3 ColorChecker patches 13 to 18	180
B.4 ColorChecker patches 19 to 24	181
B.5 Color rendering of the gamut mapped ColorChecker spectral image for a CMYK printer and a 7 colorants printer	182
C.1 The original <i>YarnPalette</i> spectral image	183
C.2 The original <i>WomanReading</i> spectral image	184
C.3 sVED of the <i>YP</i> spectral image for the 6 and 7 colorant printers	185
C.4 sVED of the <i>WR</i> spectral image for the 6 inks printer	186
C.5 sVED of the <i>WR</i> spectral image for the 7 inks printer	187
C.6 Gamut mapped <i>YP</i> spectral image for the 6 and 7 colorant printers	189
C.7 Gamut mapped <i>WR</i> spectral image for 6 and 7 colorant printers	190
C.8 sVED of the gamut mapped <i>YP</i> spectral image for the 6 and 7 colorant printers	191
C.9 sVED of the gamut mapped <i>WR</i> spectral image for 6 and 7 colorant printers	192
C.10 sVED with clipping of the gamut mapped <i>YP</i> spectral image for the 6 and 7 colorant printers	194
C.11 sVED with clipping of the gamut mapped <i>WR</i> spectral image 6 and 7 colorant printers	195
C.12 sVED with scaling of the gamut mapped <i>YP</i> spectral image for the 6 and 7 colorant printers	197
C.13 sVED with scaling of the gamut mapped <i>WR</i> spectral image for the 6 and 7 colorant printers	198
C.14 sVED with filter by distance of the gamut mapped <i>YP</i> spectral image for the 6 and 7 colorants printer	200
C.15 sVED with new filter by distance of the gamut mapped <i>WR</i> spectral image for the 6 and 7 colorants printer	201
C.16 sVED with new filter by random placement of existing weights of the gamut mapped <i>YP</i> spectral image for 6 and 7 colorant printers	203
C.17 SVED with new filter by random filter weight position of the WR spectral image with and without gamut mapping for the 6 and 7 inks printer	204

Chapter 1

Introduction

1.1 Motivation

With a conventional color reproduction system it is possible to make a color acquisition of a scene under a given illuminant and to print a faithful color reproduction of it. For instance a painting and its color reproduction viewed side by side under the illuminant used for the acquisition will appear identical even if the spectral properties of the painting pigments are different from those of the inks. This phenomenon is called metamerism. However the human observer will distinguish differences between the two color images if the illumination changes, due to the loss of metamerism. This problem can be solved with a spectral color reproduction system.

The concept of spectral color reproduction is not new, Hunt (1975) reviewed the Lippman color holographic process as the only system able to record spectral color information. But due to complex implementation it was not used. Since a few decades the interest for spectral color reproduction system has increased with the growing field of multispectral imaging. Indeed multispectral imaging offers the great advantage to dispose of the full spectral color information of a surface. When a color acquisition system records the color of a surface under a given illuminant, a multispectral acquisition system can record the spectral reflectance of a surface and allows us to simulate its color under any illuminants.

A spectral color reproduction workflow is made of several steps: a spectral color acquisition, a spectral data storage and a spectral color reproduction. Both spectral color acquisition and spectral color reproduction systems use similar technologies as for color acquisition and color reproduction.

Spectral color acquisition system have been built based on digital cameras and filters (Hardeberg, 1999; Schmitt, 2005). Such systems allow to make high quality archives of scenes or paintings by recording information for a larger set of wavelengths than the traditional red, green and blue filters. With a similar approach of using filters and regular projector spectral display system have been built using 6-primary display (Boosmann and Hill, 2003; Hill, 2007).

The introduction of multi-colorant printers in color printing, for a primary goal of increasing printer color gamut, has offered new possibilities in spectral color reproduction. The first works with a spectral use of multi-colorant printer were focused on reducing metamerism (Kohler and Berns, 1993), on colorant selection (Kohler and Berns, 1993; Tzeng and Berns, 1999, 2000) and spectral printer modeling (Balasubramanian, 1999; Wyble and Berns, 2000; Hersch et al., 2004). Then spectral color reproduction of spectral images was introduced (Taplin and Berns, 2001; Berns et al., 2003; Kraushaar and Urban, 2006). A complete workflow for spectral color reproduction is existing and research works are being carried out to connect acquisition and reproduction of spectral image (Rosen et al., 2003; Derhak and Rosen, 2006) as it could be done in a color reproduction system.

In this research we have investigated the various aspects of spectral color reproduction. It requires us to understand the processes involved in a multispectral color reproduction system

such as spectral printer modeling, gamut mapping, colorant separation and halftoning. In our work a multi-colorant inkjet printer have been characterized with a spectral printer model. Methods for inverting this model have been proposed and discussed. The inverse model is important because it establishes the transformation from spectral reflectances to colorant values for controlling the printer. In our spectral color reproduction workflow error diffusion halftoning technique has been used. Also we proposed an alternative halftoning technique called spectral vector error diffusion to print spectral image with the same multi-colorant printing system. This second approach offers advantages since it requires less data to characterize the printing system and offer good results.

1.2 Thesis outline

This thesis is organized as follows. In Chapter 2 you will find basis of colorimetry, in particularly the relationship between light source, observers and reflective objects. The metameric color reproduction system is there described in parallel to the spectral color reproduction system. Such systems use the same technology to reproduce or to record images but they differ on the dimension of the data they manipulate. A color can be expressed by three values when spectral reflectance could need up to 31 values and more (here 31 values means a spectral reflectance covering the visible spectra from 400nm to 700nm with 10nm steps). The terminology for the printing workflow is listed and explained, finally the halftoning techniques will be introduced.

In Chapter 3 we talk about spectral printer characterization, we are interested in finding the relationship between a colorant combination and the resulting spectral reflectance printed on the paper. This transformation is called the forward printed model. Starting with a monochromatic print up to multi-colorant print we introduce the following printer models in their spectral form: the spectral Murray-Davies model, the spectral Neugebauer model and the spectral Yule-Nielsen modified Neugebauer model. By describing these models we will point on the non-stability of a printer device, the dot gain phenomena, its non-linearity and how to take this in account in the characterization.

In the following Chapter 4 we experiment and evaluate the spectral Neugebauer model and the spectral Yule-Nielsen modified Neugebauer (YNSN) model. This chapter allows to introduce our experimental setup based on a multi-colorant printing system.

The two previous chapters were focusing on controlling the spectral response of a printing system, we were establishing the forward printer model of the printer. In Chapter 5 we are interested by the inverse transformation: the inverse printer model. This operation allows to perform the colorant separation and to find the colorant combination to command the printer to reproduce spectral reflectance data. Also in this chapter will be discussed the differences between colorimetric and spectral reproduction and how metamerism can be reduced with spectral color reproduction. This will be evaluated during the inversion of the printer model.

Halftoning is the last transformation applied in the spectral color reproduction system before printing the image. After the colorant separation with the inverse spectral printer model the spectral image is transformed in a colorant image, this image is halftoned channel independently before printing. In Chapter 6 we proposed an alternative to the spectral color reproduction workflow by halftoning directly the spectral image before printing. An evaluation and discussion of this halftoning technique called spectral vector error diffusion is done in this chapter. Also a spectral gamut mapping technique based on the inverse printer model.

Finally a comparison between the two described spectral color reproduction workflow is done. One following the similar steps as in a metameric color reproduction workflow and a second using spectral vector diffusion as workflow.

1.3 Publications

- In *Characterization of an eight colorant inkjet system for spectral color reproduction* (Hardeberg and Gerhardt, 2004) presented at the CGIV conference in Aachen, we tested and evaluated the spectral Neugebauer model for an eight ink printing system.
- In *Caractérisation spectrale d'un système d'impression jet d'encre huit encre* (Hardeberg and Gerhardt, 2005) for journal *Revue traitement du signal* we continued to investigate properties of the spectral Neugebauer model.
- In *Inversion of the Spectral Neugebauer Printer Model* (Alsam, Gerhardt, and Hardeberg, 2005) at the AIC conference in Granada we have inverted the spectral Neugebauer equation. The problem is solved by optimization technique.
- In *Spectral Colour Reproduction by Vector Error Diffusion* (Gerhardt and Hardeberg, 2006) at the CGIV conference in Leeds we presented a technique for halftoning spectral images and asked the question if this techniques can be used to reproduce spectral data.
- In *Controlling the error in Spectral Vector Error Diffusion* (Gerhardt and Hardeberg, 2007a) at the EI conference in San Jose we showed the problem of error accumulation in spectral vector error diffusion and proposed techniques for reducing the error spread during the halftoning process. Techniques based on preprocessing of the spectral image before halftoning and error thresholding during the halftoning process were used.
- In *Spectral color reproduction versus color reproduction* (Gerhardt and Hardeberg, 2007b) at the Iarigai conference in Grenoble we compare the reproduction of spectral data based on different approaches for the colorant separation process. This transformation is an optimization operation in which a criterion is minimized: a CIELAB difference for colorimetric print and spectral difference for spectral print.
- In *Towards spectral color reproduction* (Hardeberg and Gerhardt, 2007) presented at Ninth International Symposium on Multispectral Colour Science and Application, we gave an overview of the multispectral imaging field and some recent advances in spectral color reproduction.

1.4 Notation in this document

- Vectors are represented in lowercase boldface letters, e.g. \mathbf{a} , and they are written as column vectors, \mathbf{a}^T is the transposed vector of \mathbf{a} , the term a_j describes the j th element of an N element vector,

$$\mathbf{a} = \begin{bmatrix} a_1 \\ a_2 \\ \vdots \\ a_N \end{bmatrix}$$

- An $(N \times M)$ matrix constitutes of N rows and M columns, an element at the i th line and j th column will be written a_{ij}

$$\mathbf{A} = \begin{bmatrix} a_{11} & a_{12} & \cdots & a_{1M} \\ a_{21} & a_{12} & \cdots & a_{2M} \\ \vdots & \vdots & \ddots & \vdots \\ a_{N1} & a_{N2} & \cdots & a_{MN} \end{bmatrix}$$

- The diagonal matrix $\mathbf{L}_a = \text{diag}(\mathbf{a})$ describes a square matrix of size $(N \times N)$ full of 0 where the diagonal values are filled with the vector \mathbf{a} of size $(N \times 1)$:

$$\mathbf{L}_a = \begin{bmatrix} a_1 & 0 & 0 & \cdots & 0 \\ 0 & a_2 & 0 & \cdots & 0 \\ 0 & 0 & a_3 & \cdots & 0 \\ \vdots & \vdots & \vdots & \ddots & \vdots \\ 0 & 0 & 0 & \cdots & a_N \end{bmatrix}$$

- The discrete integral is defined by:

$$\int_{x_1}^{x_2} f(x)dx = \sum_{i=1}^{i=N} f(x_i)$$

- The product of matrix \mathbf{A} of size $(M \times N)$ by a vector \mathbf{b} of size $(N \times 1)$ is defined by:

$$\mathbf{Ab} = \mathbf{c}$$

where \mathbf{c} is a vector of size $(M \times 1)$ and each element of this vector is defined by:

$$c_i = \sum_{r=1}^n a_{ir} b_r = a_{i1} b_1 + \cdots + a_{in} b_n$$

for i and with $1 \leq i \leq M$.

- The product of two matrices \mathbf{A} of size $(M \times N)$ and a \mathbf{B} of size $(N \times P)$ is defined by:

$$\mathbf{AB} = \mathbf{C}$$

where \mathbf{C} is a matrix of size $(M \times P)$ and each element of this matrix is defined by:

$$\mathbf{C}_{ij} = \sum_{r=1}^n a_{ir} b_{rj} = a_{i1} b_{1j} + a_{i1} b_{2j} + \cdots + a_{in} b_{nj}$$

for each pair i and j with $1 \leq i \leq M$ and $1 \leq j \leq P$.

1.5 Abbreviations

The abbreviations used in this document are listed in Table 1.1.

Abbreviation	
AM	amplitude modulated
CIE	Commission Internationale de l'Eclairage
CMFs	Color Matching Functions
CMR	Constraint Minimization Routine
FM	frequency modulated
GM	gamut mapping
LRI	Linear Regression Iteration
MD	Murray-Davies
NG	Neugebauer
NP	Neugebauer primary
NPs	Neugebauer primaries
RGB	Red Green Blue
SED	scalar error diffusion
VED	vector error diffusion
WI	Weight Inversion
YNSN	Yules-Nielsen modified Neugebauer model
SGM	spectral gamut mapping
SRMS	spectral root mean square
SVED	spectral vector error diffusion

Table 1.1: Abbreviations used in this document

Chapter 2

Basics and Fundamentals

2.1 Introduction

In this chapter we recall some of the basic concepts of colorimetry, particularly the relationship between light sources, observers and reflective objects. For instance how to compute the tristimuluss CIEXYZ and CIELAB of an object knowing its spectral reflectance property, illuminant and observer conditions. The problem of metamerism will be introduced as well as the metrics used in this thesis work. The metrics allow to evaluate the difference between two spectral reflectances or two tristimuluss. Further and complete information on colorimetry can be found for instance in the books of Hunt (1975); Wyszecki and Stiles (1982a); Sharma (2003).

The spectral reflectance of an image, a painting, or a test chart have to be measured. In case of a test chart its grid structure make it easy to measure with measuring device such as Gretag Macbeth Spectrolino. Spectral image measurement of painting requires other measurement devices. These devices are often made of digital camera and acquisition are performed for different wavelengths (Hardeberg, 1999; Schmitt, 2005).

Once colorimetric data or spectral data have been recorded we would like to reproduce them. The color reproduction workflow describes the processes involve in the reproduction of a color image. The metamerism phenomenon is used in color reproduction (Kohler and Berns, 1993; Ostromoukhov, 1993) and the description of color reproduction by a cmyk and a multi-colorant printer will illustrate how metamerism is an advantage in color reproduction. In Section 2.5 of this chapter will also introduce the spectral color reproduction workflow we are using in our work. It is based on a multi-colorant printer system but with spectral colorant separation instead of a colorant separation process.

We use a multi-colorant inkjet printer to reproduce spectral images. Such printer can produce binary levels per colorant (i.e. a drop of colorant is laid down or not) and this means that an n colorant printer can produce only 2^n levels per pixel. To create the illusion of printed color levels a transformation will be applied to the image, operation called halftoning. This is the last transformation applied to an image before printing and it converts the colorant value of each pixel into a binary value, various techniques exist for halftoning (Ulichney, 1987a; Lau and Arce, 2001; Hains et al., 2003). In Section 2.6 of this chapter we briefly explain the amplitude modulated and frequency modulated halftoning techniques. A particular attention will be given on the second technique such as error diffusion halftoning and vector error diffusion halftoning.

2.2 Colorimetry for reflective objects

We know that the human eye has three cones, each of them behaves like a narrow band filter on the visible spectrum. The CIE (Commission Internationale de l'Eclairage) has defined official Standard Observers with the color matching functions (CMFs). The CMFs describe average observer sensitivity, they have been obtained after experiment in 1931 and 1964 (Wyszecki and

Stiles, 1982b). The color matching functions of both Standard Observer are shown in Figure 2.1 (a) and (b). CMFs 1931 $\bar{x}(\lambda)$, $\bar{y}(\lambda)$ and $\bar{z}(\lambda)$ consider an angle of 2° when looking at a colored surface and CMFs 1964 $\bar{x}_{10}(\lambda)$, $\bar{y}_{10}(\lambda)$ and $\bar{z}_{10}(\lambda)$ an angle of 10° .

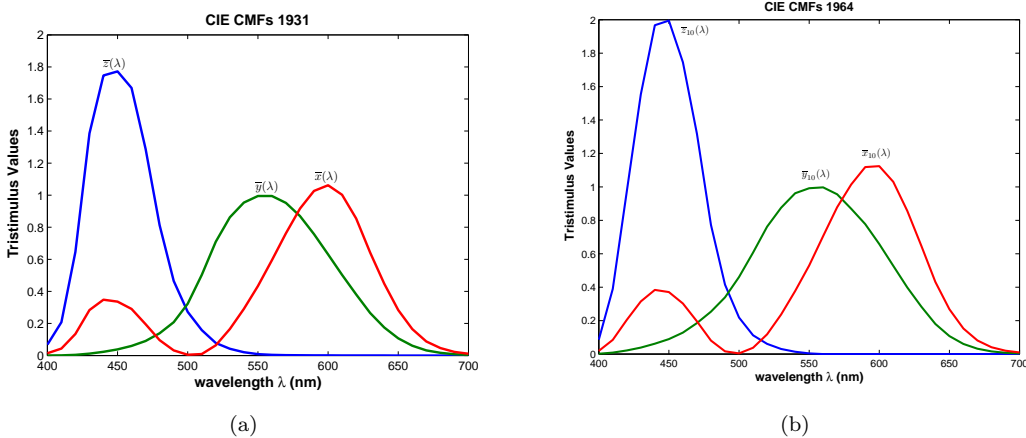


Figure 2.1: CIE color matching functions $\bar{x}(\lambda)$, $\bar{y}(\lambda)$ and $\bar{z}(\lambda)$ for the 2° 1931 standard observer in (a) and CIE color matching functions $\bar{x}_{10}(\lambda)$, $\bar{y}_{10}(\lambda)$ and $\bar{z}_{10}(\lambda)$ for the 10° 1964 standard observer in (b).

The color perceived by a human observer is the result of the interaction between an observer, the spectral properties of a surface and an illuminant defined by its spectral power distribution (SPD). Colorimetry has defined official standard SPDs (CIE, 2004) that describe common illuminant such as daylight illuminant, artificial illuminant (used in museum or in shop for example). In Figure 2.2 the SPDs of various standard illuminants are displayed for both daylighth illuminant (a) and fluorescent illuminant (b).

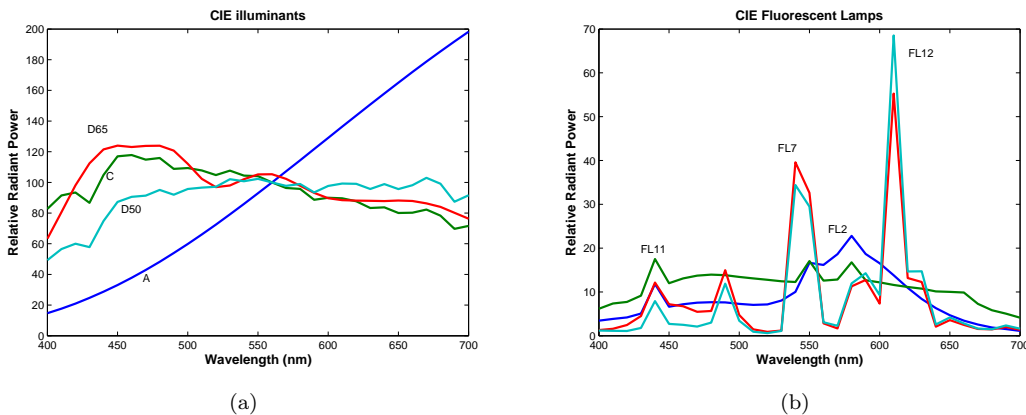


Figure 2.2: Spectral power distribution of the standard daylight illuminants A, D65, C and D50 in (a) and the standard fluorescent illuminants FL2, FL7, FL11 and FL12 in (b).

Based on CMFs, a SPD and a spectral reflectance, it is possible to estimate the color perceived by a human observer. This color is represented by a tristimulus CIEXYZ, RGB depending of the color space chosen. CMFs, SPDs and spectral reflectances are represented by vectors of data covering uniformly the visible spectrum space. Typically in this thesis work these vectors will represent data between 400nm and 700nm with 10nm step, $N = 31$ values will then describe a spectral reflectance, SPD or CMF. Figure 2.3 and Figure 2.4 illustrate the observation by

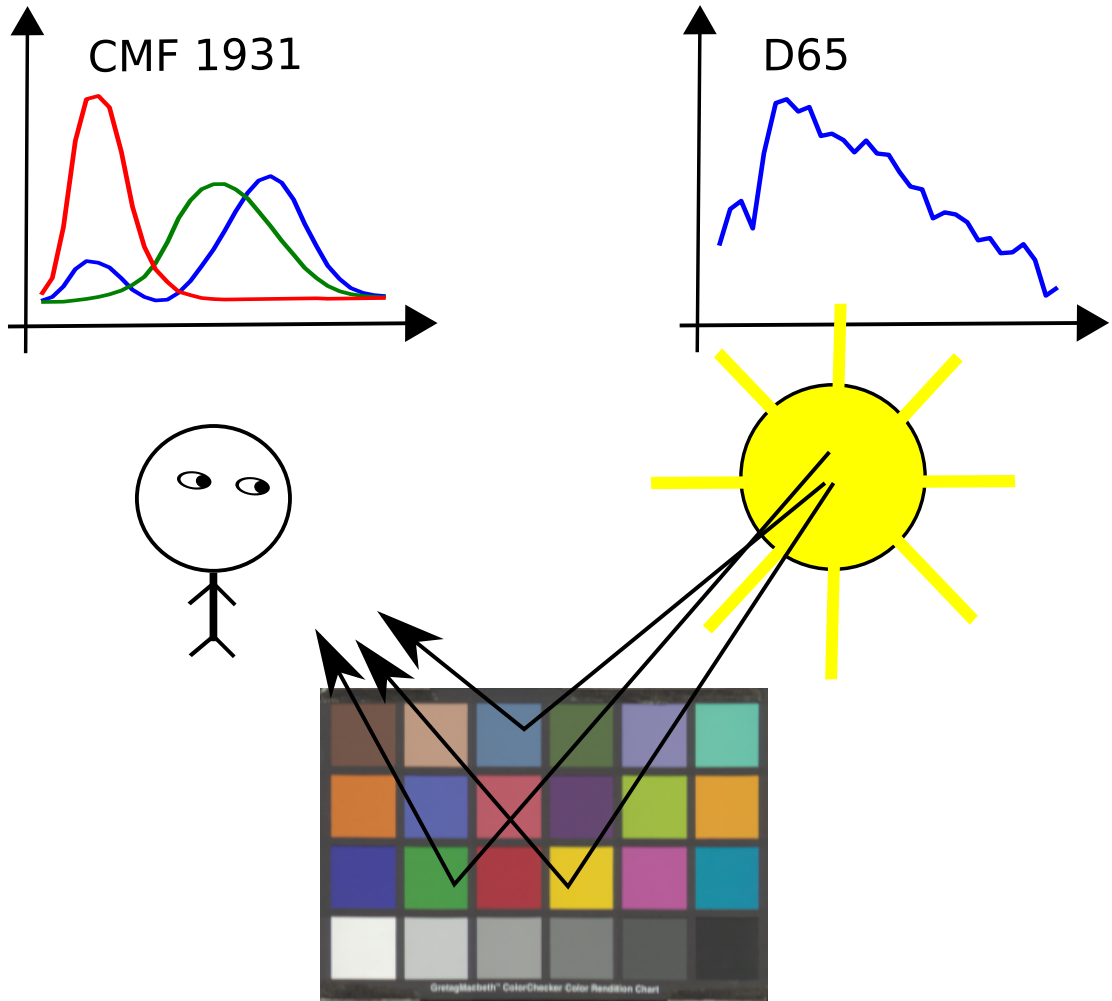


Figure 2.3: Illustration of the color perception by a human observer. The observer is looking toward the ColorChecker testchart, each patch is characterized by a spectral reflectance. The scene (i.e. the testchart) is under daylight D65. The colors used to display the testchart have been calculated for the illumination and observer specifications.

the CIE 1931 standard observer of the ColorChecker testchart for two different illumination conditions: daylight (D65) and fluorescent light (FL11).

2.2.1 Calculation of the CIEXYZ tristimulus values

The tristimulus values X, Y and Z of the reflective surface of an object is dependent on the interaction between an illuminant, an observer and its spectral properties. They are defined

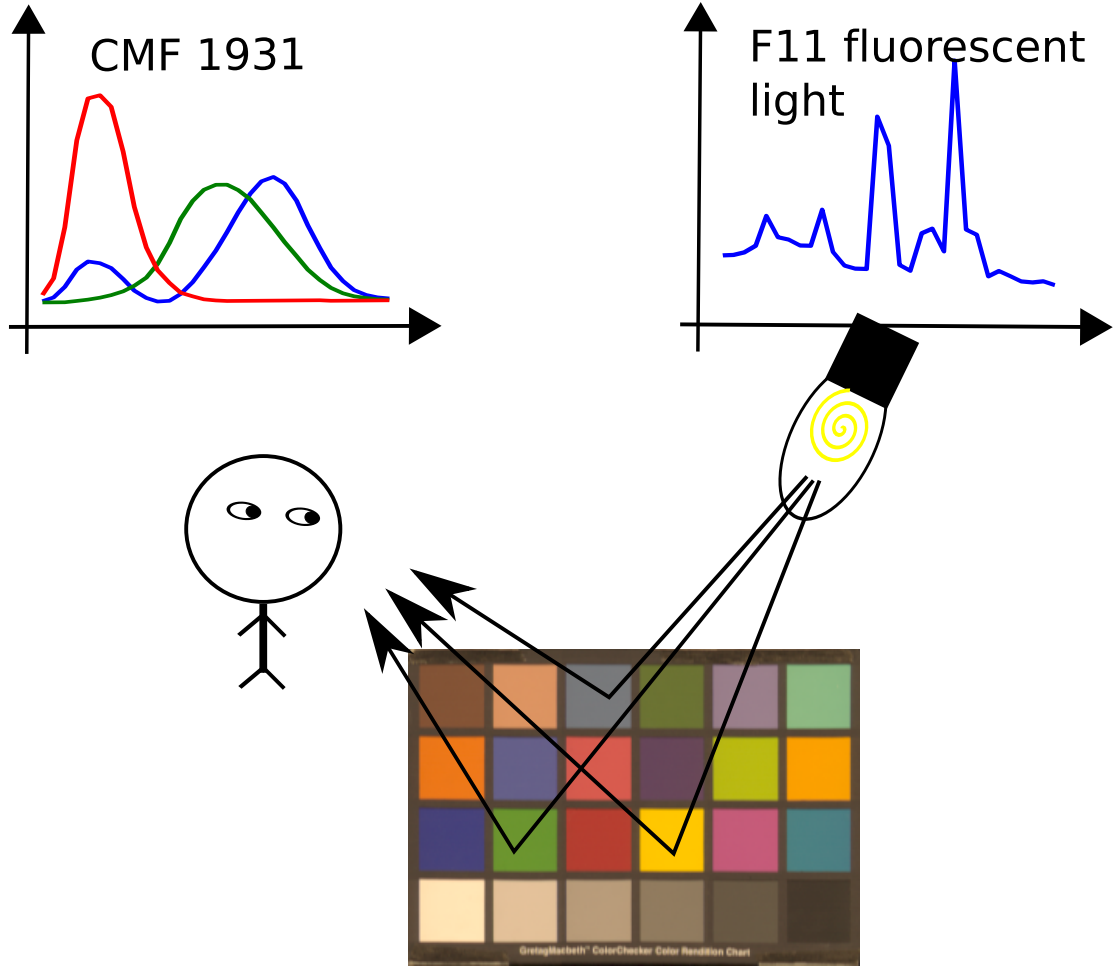


Figure 2.4: Illustration of the color perception by a human observer. The observer is looking toward the ColorChecker testchart, each patch is characterized by a spectral reflectance. The scene (i.e. the testchart) is under fluorescent lighting condition FL11. The colors used to display the testchart have been calculated for the illumination and observer specifications.

with:

$$\begin{aligned} X &= k \int_{\lambda_{min}}^{\lambda_{max}} \bar{x}(\lambda) l(\lambda) r(\lambda) d\lambda, \\ Y &= k \int_{\lambda_{min}}^{\lambda_{max}} \bar{y}(\lambda) l(\lambda) r(\lambda) d\lambda, \\ Z &= k \int_{\lambda_{min}}^{\lambda_{max}} \bar{z}(\lambda) l(\lambda) r(\lambda) d\lambda, \end{aligned} \quad (2.1)$$

where the normalization factor k is defined by the equation:

$$k = \frac{100}{\int_{\lambda_{min}}^{\lambda_{max}} \bar{y}(\lambda) l(\lambda) d\lambda}, \quad (2.2)$$

and $l(\lambda)$ is the light source SPD, $\bar{x}(\lambda)$, $\bar{y}(\lambda)$ and $\bar{z}(\lambda)$ are the CIE 1931 CMFs and $r(\lambda)$ the spectral reflectance of the surface. The calculation is performed for wavelength interval λ_{min} to

λ_{max} in the range of the visible spectrum. Each one of these spectral quantities are commonly represented as a set of N samples uniformly spaced over the visible spectrum.

The representation of both CIE CMFs and CIE SPDs as samples allows to write the previous integrals in Equation 2.2 in a discrete notation form as:

$$\begin{aligned} X &= k \sum_{i=1}^N \bar{x}(\lambda_i) l(\lambda_i) r(\lambda_i) \\ Y &= k \sum_{i=1}^N \bar{y}(\lambda_i) l(\lambda_i) r(\lambda_i) \\ Z &= k \sum_{i=1}^N \bar{z}(\lambda_i) l(\lambda_i) r(\lambda_i) \end{aligned} \quad (2.3)$$

and the k factor in Equation 2.2 as:

$$k = \frac{100}{\sum_{i=1}^N \bar{y}(\lambda_i) l(\lambda_i)} \quad (2.4)$$

and the tristimuluss X , Y and Z : in Equation 2.4 can be grouped in one equation while rewritten in a matrix notation such that:

$$\mathbf{t} = \mathbf{A}^T \mathbf{L} \mathbf{r} \quad (2.5)$$

where $t = [X, Y, Z]^T$ is the vector containing the calculated tristimulus values CIEXYZ, \mathbf{A} is the matrix containing the CIE CMFs $\bar{x}(\lambda)$, $\bar{y}(\lambda)$ and $\bar{z}(\lambda)$ as follows $[\bar{\mathbf{x}} \ \bar{\mathbf{y}} \ \bar{\mathbf{z}}]$, \mathbf{L} a square matrix with the \mathbf{I} as diagonal values the vector notation of the illuminant SPD $l(\lambda)$ and the rest of 0, ($\mathbf{L} = \text{diag}(\mathbf{I})$) and \mathbf{r} a vector containing the spectral reflectance values $r(\lambda)$.

2.2.2 Calculation of the CIELAB values

The CIELAB color space is a good approximation of how a human observer perceives the difference between two colors (Hunt, 1975). To calculate the CIELAB values of a spectral reflectance we first compute its CIEXYZ tristimulus values as in Equation 2.4, then then with the following equations:

$$\begin{aligned} L^* &= 116f(Y/Y_W) - 16 \\ a^* &= 500(f(X/X_W) - f(Y/Y_W)) \\ b^* &= 200(f(Y/Y_W) - f(Z/Z_W)) \end{aligned} \quad (2.6)$$

we obtain the L^* , a^* and b^* values where the function $f(\alpha)$ is defined by:

$$f(\alpha) = \begin{cases} 7.787\alpha + \frac{16}{116}; & \text{if } \alpha \leq 0.008856 \\ \alpha^{1/3}; & \text{otherwise} \end{cases} \quad (2.7)$$

and X_W , Y_W and Z_W are the white point CIEXYZ tristimulus values of the illuminant used for the CIEXYZ tristimulus calculation (CIE, 2004).

2.2.3 Metamerism

Looking at Equation 2.5 shows that two surfaces with different spectral reflectances \mathbf{r}_1 and \mathbf{r}_2 can have the same CIEXYZ tristimulus values response \mathbf{t} :

$$\mathbf{A}^T \mathbf{L}_1 \mathbf{r}_1 = \mathbf{A}^T \mathbf{L}_1 \mathbf{r}_2 \quad (2.8)$$

where $\mathbf{L}_1 = \text{diag}(\mathbf{l}_1)$. This is the definition of metameric match, the reflectances \mathbf{r}_1 and \mathbf{r}_2 being metamers under the illuminant with the spectral power distribution $\mathbf{l}_1(\lambda)$. The consequences of this phenomenon are in matching two reflective objects, a metameric match under one viewing illuminant is destroyed under other viewing illuminants:

$$\mathbf{A}^T \mathbf{L}_1 \mathbf{r}_1 \neq \mathbf{A}^T \mathbf{L}_2 \mathbf{r}_2 \quad (2.9)$$

for $\mathbf{L}_2 = \text{diag}(\mathbf{l}_2)$ and

$$\mathbf{l}_1(\lambda) \neq \mathbf{l}_2(\lambda). \quad (2.10)$$

This problem is called metamericism mismatch. In color reproduction metamericism is an advantage to reproduce given tristimulus, it does not need to know the spectral reflectance of the original surface.

In order to compare conventional color reproduction and spectral reproduction we need to estimate the amount of metamericism mismatch which can appear between two color samples. In the next section we present different measures to address this problem.

2.3 Color and spectral differences

To calculate the difference between two spectral reflectances or between two colors, the Euclidean distance between them is usually computed. But for spectral reflectance the spectral root mean square (sRMS) difference is often chosen instead. sRMS difference is proportional to the Euclidean distance. sRMS difference is purely spectral and does say nothing about the perception of the difference by a human observer.

2.3.1 Spectral RMS

In the following we will calculate spectral root mean square is defined as:

$$\text{sRMS} = \sqrt{\frac{1}{N} \sum_{i=1}^N (r_1(\lambda_i) - r_2(\lambda_i))^2} \quad (2.11)$$

where N is the number of samples describing $r_1(\lambda)$ and $r_2(\lambda)$ and rewritten in a matrix notation:

$$\text{sRMS} = \sqrt{\frac{1}{N} (\mathbf{r}_1 - \mathbf{r}_2)^T (\mathbf{r}_1 - \mathbf{r}_2)} \quad (2.12)$$

2.3.2 CIE 1976 color difference

The calculation of the difference between two CIELAB values is preferred to the difference between the corresponding two CIEXYZ tristimulus values. The CIEXYZ color space does not take into account the non-linearity of color difference perception by a human observer and the CIELAB color space does.

The CIE1976 or ΔE_{ab}^* (CIE, 2006) difference is the standard CIE color difference, which is the Euclidean distance between two colors calculated in the three-dimensional CIELAB color space:

$$\Delta E_{ab}^* = \sqrt{(\Delta L^*)^2 + (\Delta a^*)^2 + (\Delta b^*)^2} \quad (2.13)$$

where

$$\begin{aligned} \Delta L^* &= L_2^* - L_1^* \\ \Delta a^* &= a_2^* - a_1^* \\ \Delta b^* &= b_2^* - b_1^* \end{aligned} \quad (2.14)$$

and $[L_1 \ a_1 \ b_1]^T$ and $[L_2 \ a_2 \ b_2]^T$ are the CIELAB values of the spectral reflectances \mathbf{r}_1 and \mathbf{r}_2 for a given illuminant and observer.

2.3.3 CIE 1994 color difference

This is a more recent modification which has been recommended by CIE TC1-29 as the CIE94 color difference formula.

$$\Delta E_{94}^* = \sqrt{\left(\frac{\Delta L^*}{k_L S_L}\right)^2 + \left(\frac{\Delta C^*}{k_C S_C}\right)^2 + \left(\frac{\Delta H^*}{k_H S_H}\right)^2} \quad (2.15)$$

where the parameters are defined by:

$$\begin{aligned} \Delta C^* &= C_2^* - C_1^* \\ \Delta H^* &= \sqrt{(\Delta a^*)^2 + (\Delta b^*)^2 - (\Delta C^*)^2} \\ C_1^* &= \sqrt{(a_1^*)^2 + (b_1^*)^2} \\ C_2^* &= \sqrt{(a_2^*)^2 + (b_2^*)^2} \\ k_L = k_C = k_H &= 1 \\ S_L &= 1 \\ S_C &= 1 + k_1 C_1^* \\ S_H &= 1 + k_2 C_1^* \\ k_1 &= 0.0045 \\ k_2 &= 0.0015 \end{aligned} \quad (2.16)$$

where the coefficients k have been set for graphic arts application, changes should be applied to those coefficients when color ΔE_{94}^* is applied to textiles.

Also it is important to notice that this metric establishes the difference between a reference color and a modified color. If we had a function called $\text{CIE94}(\mathbf{r}_1, \mathbf{r}_2)$ taking as input argument two spectral reflectances \mathbf{r}_1 and \mathbf{r}_2 then calling $\text{CIE94}(\mathbf{r}_1, \mathbf{r}_2)$ will be different than $\text{CIE94}(\mathbf{r}_2, \mathbf{r}_1)$.

In order to get an idea of the values obtained after calculation of ΔE_{ab}^* for various illuminant, ΔE_{94}^* and spectral RMS refer to in Table B.1 in Appendix B.3.1. The spectral reflectances used to calculate the various color differences in Table B.1 are displayed in Figure B.1 to Figure B.4.

2.4 Spectral reflectance measurement

In both measurement system, Spectrolino or multispectral acquisition system, the unknowns are the spectral properties of a surface. Illuminant condition and spectral response of device are known.

2.4.1 Spectral reflectance measurement of test charts

In this thesis we measure test chart with dedicated devices. To measure the spectral reflectance of a test chart we have used the Gretag MacBeth spectrolino, it measures the reflected light at the surface normal for an emitted and controlled light at 45° .

2.4.2 Spectral reflectance measurement of images

I refer here to work on system using digital camera and filters to perform spectral acquisition of images, paintings (Hardeberg, 1999). Such system does not measure directly the spectral properties of a surface but record the camera sensor response at different wavelength set by the filters. Based on the response, the camera sensitivity and filters properties the spectral reflectance of each pixel in the image is reconstructed.

2.5 Color reproduction workflow

The color reproduction workflow describes the different transformations applied to an RGB image before to be printed by a digital printer, this for a CMY printer (i.e. Cyan,Magenta and Yellow printer) or a multi-ink printer, see Figure 2.5. The first observation is a device such as computer screen (CRT or LCD) and printer do not produce color identically: one use the additive color process and the second the subtractive color process.

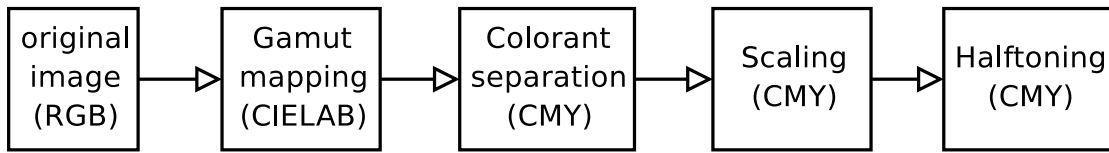


Figure 2.5: The color reproduction workflow for the reproduction of an RGB image. Before printing several transformations are applied to the image: gamut mapping, colorant separation, scaling and halftoning. Similar workflow is used for a CMY or multi-ink printer.

2.5.1 Additive color process

Let assume that the image to print is a digital RGB image. The pixels of three separate color channels red (R), green (G) and blue (B) are usually coded on 8 bits values between 0 and 255. The three channels are usually multiplexed in a same file to build a color image with 24 bits per pixel. When a continuous tone image is visualized on a computer screen such as a CRT monitor, the pixel values of each color channel are used to control to amount of light to emit to display the colors, it is the additive color process. In Figure 2.6 is shown an illustration of the additive color process to display colors on a computer screen.

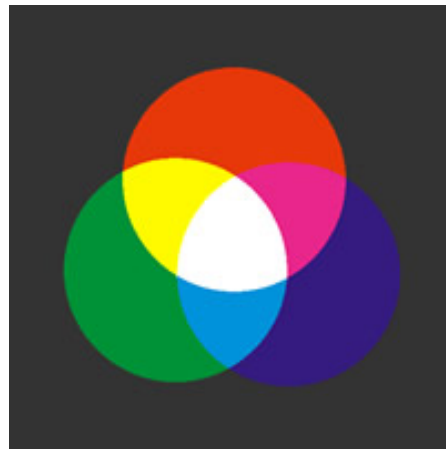


Figure 2.6: The additive color process. We can see in this example that the projection of the equal amount of the three primary colors red, green and blue produces white.

2.5.2 Subtractive color process

As opposed to the additive color process a printer follows the subtractive color process. The subtractive color process is based on the three primary subtractive colors cyan, magenta and yellow. They absorb certain wavelengths and transmit the others which are then reflected by the white paper. In Figure 2.7 is shown a example of the subtractive color process to display colors on a white surface such as a paper sheet.

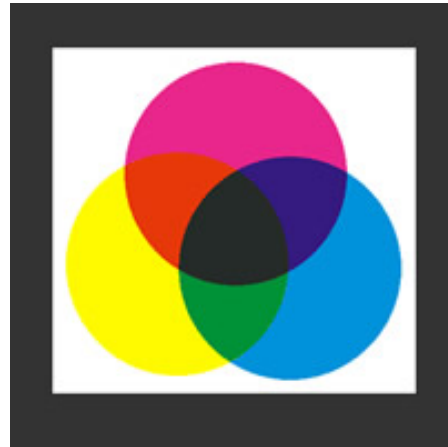


Figure 2.7: The subtractive color process. We can see in this example that the mixing of the three primaries will produce black.

2.5.3 Colorant separation process for CMY printer

Colorant separation process will convert a color expressed as a set of RGB values to a set of CMY values. In an ideal case where RGB and CMY are complementary the colorant separation is simply performed as:

$$\begin{aligned} c &= 1 - r \\ m &= 1 - g \\ y &= 1 - b \end{aligned} \tag{2.17}$$

and we assume here that the digital signals R, G and B have been normalized within [0,1], such that $[r\ g\ b] = [1\ 1\ 1]$ equals white and $[c\ m\ y] = [1\ 1\ 1]$ equals black. Also this equation tells us that the volume of color of the RGB device is equivalent to the CMY device. This unfortunately not always the case.

In printing the best white we can obtain is the whiteness of the paper substrate. Identically the best black a printer can produce is the superposition of the three colorants CMY and it often provide only dark grey where we would like pure black. To compensate this problem black ink (K) have been added to CMY printer to form CMYK printer.

2.5.4 Black ink generation

The generation of the black channel is made after colorant separation RGB to CMY. Different techniques exist for the control of the black channel. The process of under color removal (UCR) will eliminate the amounts of cyan, magenta and yellow that would have been added to the neutral gray and replace them with black ink as follow:

$$\begin{aligned} k &= \min(c, m, y) \\ c' &= c - k \\ m' &= m - k \\ y' &= y - k \end{aligned} \tag{2.18}$$

where c' , m' and y' are the new CMY values.

Add of black ink to CMY printer has several advantages: it allows to reduce the ink consumption (regarding of which black ink generation is chosen), it increases the color gamut of the printer (from dark grey to pure black).

Black ink generation is a first example of metameric printing: a tristimulus can now be printed by various colorant combinations. A grey level can for example be printed by the same quantity of cyan, magenta and yellow, or only black or a variety of cyan, magenta, yellow and black colorant combination.

2.5.5 Gamut mapping

The number of available colorant for printer has increased which makes the colorant separation in Equation 2.18 obsolete for multi-colorant¹ printer. Both color gamut of our RGB device and printer have different shape and size. There is a need of gamut mapping in order to not loose information when going from RGB device color gamut to printer color gamut for example.

Concretely the operation is performed in another color space such as CIELAB. Computer screen, projector, printer do not cover the same color gamut, they are defined by an ICC profile which describes their color gamut and all transformation are performed in a profile connection space (PCS) (ICC.1:2004-10).

Gamut mapping has to answer the questions of defining a color gamut and especially to described the boundary of such color volume: gamut boundary descriptor, and providing strategy to map color data from one gamut to the other: gamut mapping algorithm. More information about gamut mapping can be found in Morovič and Luo (2001) work. This is of course one of a key transformation in the color reproduction workflow because you want your picture displayed on a computer screen as identical as possible on the paper after printing.

2.5.6 Multi-colorant printing system

A multi-colorant printing system typically includes the four colorants CMYK plus 2, 3 or more colorants. We can find either colorants with new colors such as red (R), green (G) or blue (B) or lighter version of cyan (c) and magenta (m) (to reduce the perception of isolated dark dots on a clear background as we will see in section 2.6). One system will increase its gamut with CMYKRGB (Ostromoukhov, 1993) when another will decrease the graininess aspect of the print in the light color with CMYKcm (Agar, 2001). A light color can be reproduced with more drop of inks of c and m than C and M.

To print color images, a multi-colorant printing system follows the similar operation as for CMYK printing system. However the availability of a larger number of colorants opens the possibility of metameric print: an RGB pixel in the color image can be represented by different colorant combinations as we already saw it with CMYK printing.

The generation of the black channel in multi-colorant printing system performed with a similar operation as for CMYK printing: by using the black ink K to represent the neutral component of a color by black. Also it allows to reduce the ink consumption and increase the color gamut in the dark area (Jang et al., 2006).

From the RGB to the CMYK version of the same color image, we needed three to four color channels to describe the color image. When we work with multi-colorant printing system the color image is after the colorant separation a multi-channel continuous tone image. The term continuous tone means each pixel get a continuous value for each channel. But the printer being a digital printer, only a binary level per pixel and colorant can be printed. Transformation called halftoning will convert a multi-channel continuous tone image in a multi-channels binary image.

A practical remark, ink limitation or colorant coverage limitation are describing the maximum amount of colorant a printer can use when printing a color. This limit is traditionally fixed to 300%: with a color printer working with CMY, the maximum darkest color reachable is black and is obtained with the maximum quantity of the three available colorant CMY (i.e. 300% of ink coverage on the white paper). So In a multi-channel image, the summation of the colorant value by channel should end up too with a maximum of 300%. This practical consideration will be investigated in the next chapter for the spectral printer characterization.

¹The terms multi-ink or hifi printing can be found for multi-colorant printing system, in this thesis we will use the term multi-colorant

The colorant separation will be performed after gamut mapping. A printer model establishes a transformation control value to colorimetric printed value. It is the inverse printer model that will be used to go from the PCS to colorant combination that will control the printer.

2.5.7 Scaling process

Computer screen and printer do not have exactly the same resolution. Printers are often higher resolution and scaling of the image is necessary to match the two devices resolutions. Scaling process is a resampling transformation applied to the image. This operation is generally performed after the command print has been sent to the printer. It has to be noted that this step in the color reproduction workflow is not taken into account in the printer model.

2.6 Halftoning process

Halftoning is needed when the media which is used to reproduce an image cannot reproduce a large number of levels (Hains et al., 2003; Ulichney, 1987a; Lau and Arce, 2001). A digital printer is typically able to create two levels per colorant, meaning a drop of ink is laid down or not laid down on the paper.

The operation of reducing the number of gray levels or color levels in continuous tone image while maintaining the illusion of a continuous tone image is called halftoning. By varying the dot distribution and the dot density the halftoning process creates the illusion of a continuous tone image. A dot is not necessarily a single pixel in the scaled multi-colorant image. Regarding of the halftoning technique this dot will vary in density (its size). Typically a dot or halftone-cell is referred to a cell (usually squared shape) of $c \times n$ pixels. The halftoning process converts a pixel value, typically a 8 bits value in the range [0, 255] to a binary level {0, 1}.

After this step the image is made of binary colorant channels or binary ink-screens, each pixel of the colorant channels has binary level {0, 1}. Finally the halftone image values controls the printhead of the printer. A pixel set to 1 will allows to lay down a drop of ink at the pixel position on the paper.

In the next section we describe the two main families of halftoning process: amplitude modulated halftoning (AM halftoning) and frequency modulated halftoning (FM halftoning). The color channels of the image are then called screens.

2.6.1 Amplitude modulated halftoning

This technique varies the size of a dot to create the illusion of a color level. The dots are equally spaced. The halftoning operation which converts the continuous tone pixel value to the binary pixel value is a pixel to pixel operation performed by a threshold mask.

A dot or halftone cell of size 8×8 can create 64 levels for example. Applying such mask on an image of 256 levels will require to quantify the image values before halftoning it. In Figure 2.11 is presented an example of color image halftoned by AM technique with 8×8 mask which grows a circular dot, concretely the cell is filled from the center following a spiral path.

The dot shape is directly connected to the mask. The result of the thresholding mask versus the current halftone-cell will let the halftone cell full of 0 and 1. The order of filling an halftone-cell will reveal the dot shape and bigger the dot darker the level. Attention has to be made on the halftone-cell versus the resolution of the printer because to be able to see the dot shape is unpleasant visually.

2.6.2 Frequency modulated halftoning

In scalar error diffusion (SED) technique the output pixel value (0 or 1) of an ink channel is calculated independently of the other ink channels as in AM halftoning. An output pixel is set by a thresholding condition. Then the difference (i.e. the error) between the input pixel

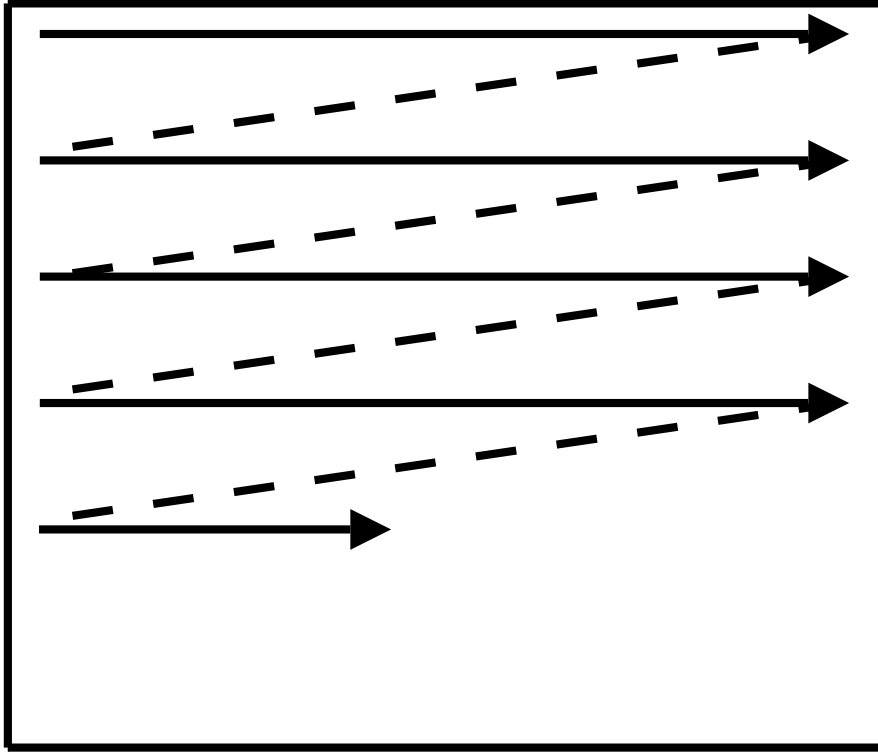


Figure 2.8: Illustration of the raster scan path for error diffusion and spectral vector error diffusion. Starting from the top left of the image the halftoning is performed line by line from the top to the bottom.

value and output pixel value is diffused to the neighboring pixels with a weight filter. Several propositions exist for the choice of the weight filter: Floyd-Steinberg (Floyd and Steinberg, 1976) and Jarvis-Judice-Ninke (Jarvis et al., 1976), aiming to break up the worm patterns typically found in SED. This operation is performed for each colorant channel in a raster scan mode, see Figure 2.8.

Figure 6.2 illustrates the SED diagram and how the error is spread in the image during the filtering. $in(x, y)$ is the original pixel value at position (x, y) in the image, $out(x, y)$ is thresholded pixel value such that:

$$out(x, y) = \begin{cases} \text{if } m(x, y) \geq 0.5 \\ \quad out(x, y) = 1, \\ \text{else} \\ \quad out(x, y) = 0, \end{cases} \quad (2.19)$$

for $m(x, y)$ being the modified pixel at position (x, y) , the error is calculated as follows:

$$err(x, y) = m(x, y) - out(x, y) \quad (2.20)$$

and is diffused to the neighboring pixels as follows:

$$m(x + i, y + j) = m(x + i, y + j) + w(i, j) * err(x, y) \quad (2.21)$$

according to the size of the weight filter.

In Figure 2.12, an example is presented of a grayscale image halftoned by SED with Floyd-

Steinberg's filter, see the following equations for the filter weight values:

$$\begin{bmatrix} & \bullet & w_{1,3} \\ w_{2,1} & w_{2,2} & w_{2,3} \end{bmatrix} = \left(\frac{1}{16}\right) \times \begin{bmatrix} & \bullet & 7 \\ 3 & 5 & 1 \end{bmatrix} \quad (2.22)$$

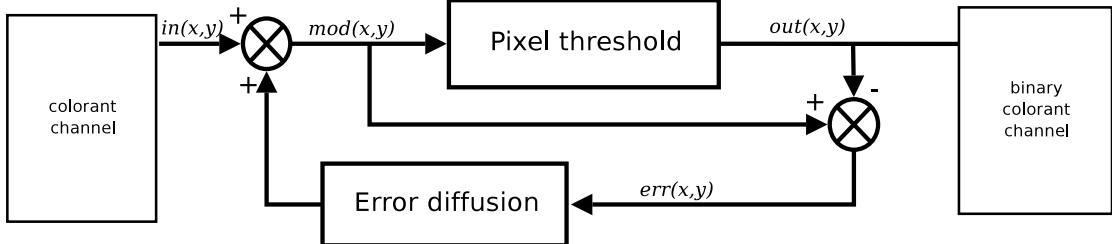


Figure 2.9: The process of scalar error diffusion. Each colorant channel of a continuous tone colorant image is halftoned following the same process independently spectral vector error diffusion halftoning.



Figure 2.10: Original continuous tone grayscale image. Each pixel value is coded in 8 bits.



Figure 2.11: Halftoned image by AM halftoning technique. In this example a 8×8 mask and circular dot shape have been used. The dot is created by filling the mask from the center in a spiral path.



Figure 2.12: Halftoned image by FM halftoning technique. In this example SED with Floyd-Steinberg filter have been used. Filter weights are displayed in Equation 2.22

2.7 Conclusion

The different sections of this chapter have introduced the basis of colorimetry to understand this research. The color printing workflow have been shortly described as well as the transformations applied to color image to be printed, from a continuous tone image to a multi-colorant binary image. For our experiments we will use a multi-colorant printing system, it provides a bigger gamut with a wider variety of spectral reflectances.

In the two following chapters we expose a technique to model spectrally a multi-colorant printing system. The idea is to characterize a printer in order to achieve spectral printing, which allows us to avoid metameric matches under only a given illuminant but, ideally, allows us to obtain perfect color matches under any given illuminants.

But we should not forget the complexity of a printing system and its constraints when characterizing it. In particular different sets of colorants can be used for a given multi-colorant printer, and different halftoning techniques can be used.

Chapter 3

Spectral printer characterization: theory

3.1 Introduction

A printer model establishes the transformation between a combination of the m colorants used to print a color patch and the spectral reflectance of the resulting printed patch. A model predicting the spectral reflectance of a colorant combination is called a forward model and a model performing the inverse transformation from a spectral reflectance to a colorant combination is called an inverse printer model.

A printer model simulates the behavior of the printing device with a few parameters such as the known spectral responses of the printer for a set of given colorant combinations. Typically these colorant combinations describe the spectral gamut boundaries of the printing device: single colorant ramps for all colorants and all the combination between the colorants at maximum level. A colorant level is expressed as a coverage value from 0% to 100% for a single colorant. The colorant coverage limitation of a colorant combination is typically fixed to 300%, where the total coverage of a colorant combination is the sum of the coverages of each colorant for a given combination.

We can distinguish between two kinds of printer models, the computational and the physical ones. Typically the computational consists in building a grid in m dimensions for an m -colorants printer, this to create a m dimensions lookup-table or m LUT (Heuberger et al., 1992). The estimation of a colorant combination will be calculated by interpolation in the dimension of the LUT. There is a trade-off between the size of the grid and the accuracy of the interpolation. A m LUT with 5 levels per colorant for a 7 colorants printer will need to print and measure $5^7 = 78125$ colorant combinations; this being too much for most practical application.

The physical models attempt to imitate the physics involved in the printing device. Here also these models can be classified in two subtypes with regards of the assumptions they make and their complexity (Wyble and Berns, 2000): regression based and first-principals models. Regression based models are rather simple and works with a few parameters to predict a printer output while first-principals model will closely imitate the physics of the printing process by taking into account multiple light interactions between the paper and the ink layers, for instance. Regression based models are commonly used to model the behavior of digital printing devices.

During the last 70 years printing technology has evolved and the printer models as well. Starting from single colorant printing device the Murray-Davies model (Murray, 1936) predicts the output spectral reflectances of a single colorant coverage value knowing the spectral reflectance of the paper and maximum colorant coverage value. This model was extended to color by Neugebauer (1937), see Wyble and Kraushaar (2005) for a translated and commented version of the original document. The prediction of a colorant combination is the summation of all the colorants involved in the printing process weighted by their coverage on the paper. All the

colorants are referring to all the primaries (cyan, magenta and yellow in case of a CMY printer) plus all the combination between them plus the paper, these colors are called the Neugebauer primaries (NP). Later the interaction of light penetrating and scattering into the paper was added to these models by Yules and Nielsen (1951) as form of an exponent known as the n factor.

In this chapter we will investigate the Murray-Davies model, the Neugebauer model and the Yule-Nielsen modified spectral Neugebauer model. To illustrate the performance of the tested forward models we will use real measurement. We use the Epson Photo Stylus 2100 inkjet printer with seven inks.

3.2 Single colorant print

3.2.1 Murray-Davies

The Murray-Davies (MD) model predicts the reflectance of a single colorant coverage. The estimation of the spectral reflectance of a colorant coverage c is calculated as follows:

$$\hat{r}(\lambda) = (1 - c) \times r_{\text{paper}}(\lambda) + c \times r_{\text{col, max}}(\lambda) \quad (3.1)$$

where $r_{\text{paper}}(\lambda)$ is the paper measured spectral reflectance, $r_{\text{col, max}}(\lambda)$ is the measured spectral reflectance of the paper covered by the colorant at maximum coverage, typically $r_{\text{col, max}}(\lambda) = r_{\text{col, 100\%}}(\lambda)$ and $\hat{r}(\lambda)$ is the predicted spectral reflectance.

To evaluate the spectral MD model we print a pure cyan ramp. A ramp of single colorant is a series of patches with coverage values from 0% to 100% with linear spacing between the steps. After printing the spectral reflectances of the patches are measured with a Spectrolino. The measurements are then compared with the estimation by the MD model. The colorant values c used for controlling the printer and performing the MD estimation are called the theoretical colorant value.

In Figure 3.1 (a) and 3.1 (b) we display the measured and estimated spectral reflectances of a cyan ramp. The ramp is constituted of 16 levels equally spaced from 0% to 100%. We can observe in this figures the differences between the simulated and measured spectral reflectances. The measured spectral reflectances being not equally spaced as the estimated, i.e. the effective coverage of the paper for a single colorant value is different than the theoretical colorant value sent to the printer. The measured spectral reflectances are darker than their estimations, this is due to the dot gain effect. To illustrate visually the dot gain we can see in Figure 3.1 (e) the first two ramps displayed in rgb colors under illuminant D50. The simulated ramp presents a real (first ramp) gradient of cyan color while the measured ramp (second ramp) reaches too fast the maximum cyan level.

3.2.2 Dot gain effect

There are two types of dot gain, mechanical dot gain and optical dot gain (Viggiano, 1983). The first one is due to the impact of the drop of ink on the paper. The drop of ink on the paper is not perfectly round. The second is due to ink and paper interaction, light penetrating into the paper covered by ink or not and going out by area covered by ink or not increases the size of the drops. This gain of dot size increases the theoretical colorant coverage c , this theoretical value is referred to as the desired colorant coverage value as opposed to the effective colorant coverage value obtained with the dot gain effect.

The prediction made by the MD model is too bright compared to the measurement. A relation between theoretical colorant coverage and effective colorant coverage is needed. The inverse of the Murray Davies model establishes the transformation from theoretical to effective colorant coverage.

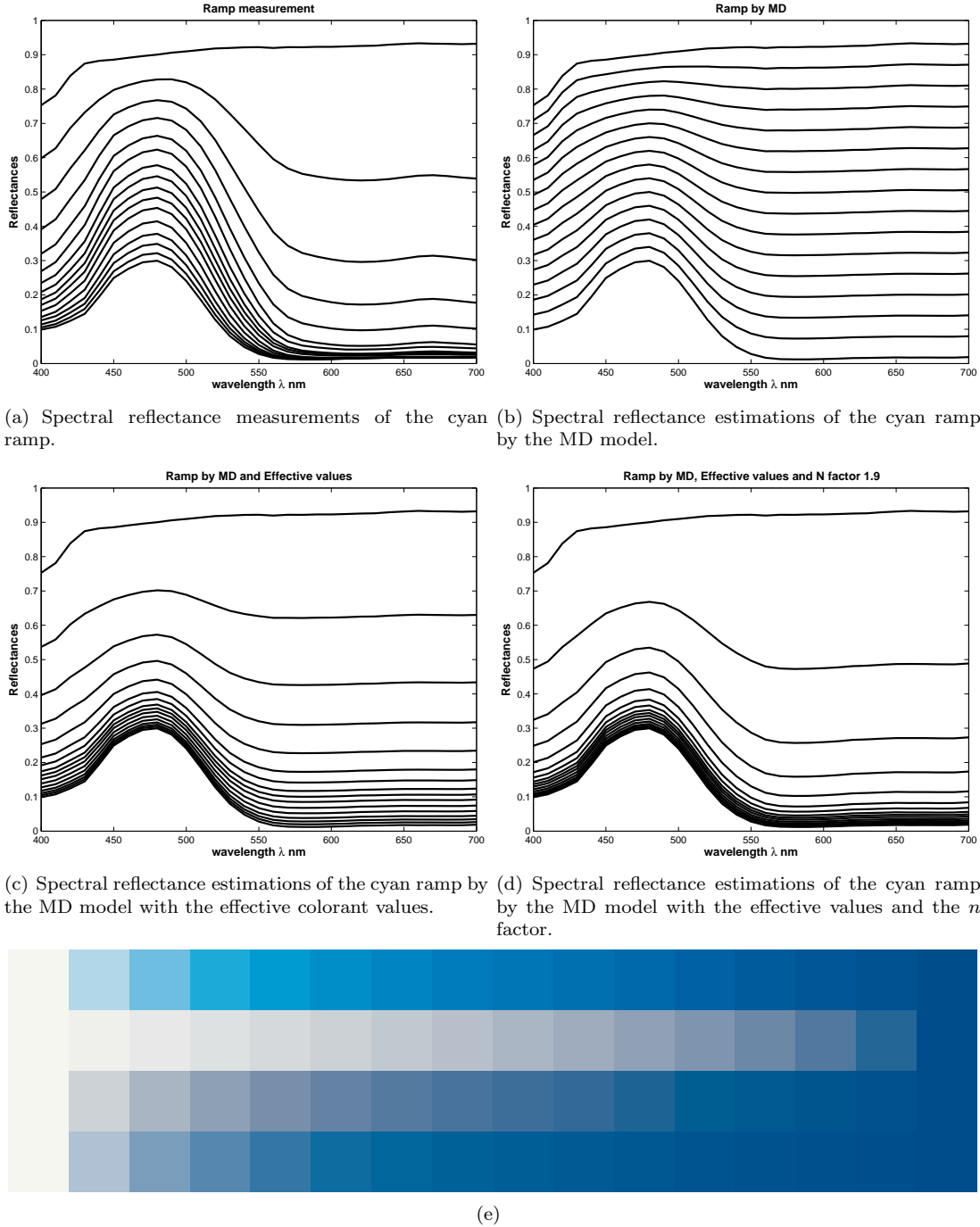


Figure 3.1: Spectral reflectances of the cyan ramp, the ramp is made of 16 levels equally spaced from 0% to 100% coverage. In Figure (a) the spectral reflectance measurement of the printed ramp, in (b) the estimated spectral reflectances of the ramp by the Murray-Davies (MD) model, in (c) the estimated spectral reflectances by the MD model with effective values and in (d) the estimated spectral reflectances with the effective values and the n factor. In Figure (e) is displayed a RGB color rendering for illuminant CIE D50 of the above spectral reflectances. The first row represents the measured ramp as in Figure (a) and the three following its estimation by the MD model as in Figure (b), (c) and (d).

3.2.3 Inverse Murray-Davies

The inverse of the Murray Davies equation allows to estimate the effective area covered by the colorant of a known input value, value called theoretical value. The effective dot area is found by rewriting the Equation 3.1 as follow:

$$r_{\text{meas}}(\lambda) = (1 - a_{\text{eff}}) \times r_{\text{paper}}(\lambda) + a_{\text{eff}} \times r_{\text{col, max}}(\lambda) \quad (3.2)$$

where c the theoretical colorant coverage value is replaced by a_{eff} the effective colorant coverage value we are looking for, and the previously estimated spectral reflectance $\hat{r}(\lambda)$ in Equation 3.1 is replaced by the measured spectral reflectance $r_{\text{meas}}(\lambda)$,

$$r_{\text{meas}}(\lambda) = r_{\text{paper}}(\lambda) - a_{\text{eff}}r_{\text{paper}}(\lambda) + a_{\text{eff}}r_{\text{col, max}}(\lambda) \quad (3.3)$$

and continuing to isolate the a_{eff} term:

$$r_{\text{meas}}(\lambda) - r_{\text{paper}}(\lambda) = a_{\text{eff}}(r_{\text{col, max}}(\lambda) - r_{\text{paper}}(\lambda)) \quad (3.4)$$

we obtain a relation between the spectral reflectance of the paper, the spectral reflectance at full colorant coverage and the spectral reflectance for a known theoretical coverage value:

$$a_{\text{eff}} = \frac{r_{\text{meas}}(\lambda) - r_{\text{paper}}(\lambda)}{r_{\text{col, max}}(\lambda) - r_{\text{paper}}(\lambda)} \quad (3.5)$$

and this gives us the effective colorant colorant coverage by wavelength $a_{\text{eff}}(\lambda)$ for a theoretical colorant value. In Figure 3.2 (a) are displayed the relations from theoretical values to effective values by wavelength obtained from Equation 3.5 for the ramp of cyan. From this figure we can see that very different relations can be obtained regarding of the wavelength.

In order to obtain a transformation from theoretical colorant value to effective colorant value for all wavelength we calculate the average difference $r_{\text{meas}}(\lambda) - r_{\text{paper}}(\lambda)$ normalized by the difference $r_{\text{col, max}}(\lambda) - r_{\text{paper}}(\lambda)$. To do so we rewrite these differences in a vector notation form as follow:

$$\mathbf{r}_{m,p} = \mathbf{r}_{\text{meas}} - \mathbf{r}_{\text{paper}} \quad (3.6)$$

for the upper term of Equation 3.5 and the lower term as follow:

$$\mathbf{r}_{c,p} = \mathbf{r}_{\text{col, max}} - \mathbf{r}_{\text{paper}} \quad (3.7)$$

and then we can write:

$$a_{\text{eff}} = \frac{\mathbf{r}_{c,p}^T \mathbf{r}_{m,p}}{\mathbf{r}_{c,p}^T \mathbf{r}_{c,p}}. \quad (3.8)$$

By calculating a_{eff} for each spectral reflectance measurement corresponding to a known theoretical colorant value sent to the printer we can establish a desired relation theoretical to effective value under the form of a look-up table (LUT) for single colorant printing. This operation can be performed for all the available colorants of a printing system.

The obtained LUTs for the cyan ramp shows that the effective coverage of the cyan rapidly reaches a maximum, see Figure 3.2 (b). Cyan ramp estimation by MD and the effective coverage from the LUT provides better spectral reflectance estimation, see Figure 3.1 (c). A color rendering for illuminant D50 is displayed in Figure 3.1 (e), see the third ramp. We can observe in the color rendering of the ramp that the simulated ramp spectral reflectances with MD and effective colorant values are closer in intensity to the measured spectral reflectances, but we can also observe a small color shift. This shift can be explained by the correction itself brought with the effective values: we use the same effective value for all wavelengths and we have seen that the relation theoretical to effective values by wavelength creates very different LUTs, see Figure 3.2 (a). The effective maximum coverage value is not fixed, it could vary for others colorants or print on different paper media such as copy paper or photo paper for example.

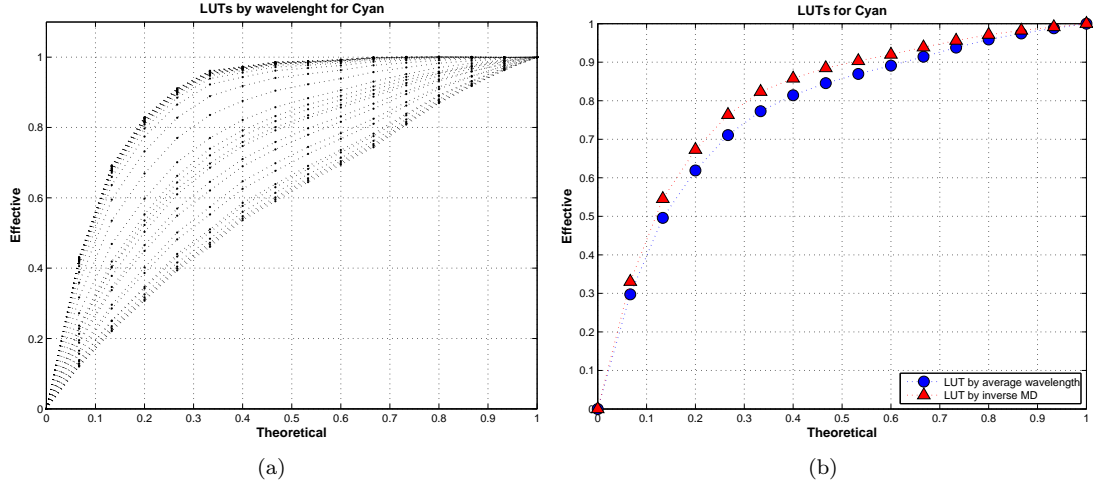


Figure 3.2: Calculated LUTs for the ramp of single colorant cyan, in (a) are shown the LUTs by wavelength obtained from Equation 3.5 and in (b) the LUTs obtained from Equation 3.8 and LUT by averaging all LUTs in (a) by wavelength.

3.2.4 Murray-Davies and the Yule-Nielsen n factor

The inversion of the MD equation (see Equation 3.1) takes care only of the mechanical dot gain, the optical dot gain can be added to the MD equation using an exponent $1/n$ called n factor. This factor was introduced by Yules and Nielsen (1951) in their works on light penetration and scattering between the inks and the paper. The introduction of this n factor should correct the non-linearity in the transformation theoretical colorant value to effective colorant value. The MD equation becomes:

$$\hat{r}^{1/n}(\lambda) = (1 - c) \times r_{\text{paper}}^{1/n}(\lambda) + c \times r_{\text{col, max}}^{1/n}(\lambda) \quad (3.9)$$

and rewriting Equation 3.5 with the $1/n$ exponent we obtain:

$$a_{\text{eff}} = \frac{r_{\text{meas}}^{1/n}(\lambda) - r_{\text{paper}}^{1/n}(\lambda)}{r_{\text{col, max}}^{1/n}(\lambda) - r_{\text{paper}}^{1/n}(\lambda)}. \quad (3.10)$$

In case of $n = 1$ we can see that Equation 3.9 is equivalent to Equation 3.2 and then performance the MD model with effective coverage values for these two equations will be similar. In Table 3.1 are presented the average colorimetric and spectral differences between the simulated ramp by the MD model with effective coverage values and $n = 1$ and the measured ramp for the ramp of cyan.

Table 3.1: Performance of the MD model with effective coverage values and $n = 1$ for the ramp of cyan.

		ΔE_{ab}^*					ΔE_{94}^*	sRMS
		A	D65	D50	F11	F31	D50	
n=1	Av.	26.78	16.82	19.85	20.31	23.09	7.47	0.078
	Std.	15.79	10.36	12.10	12.21	13.42	4.27	0.054
	Max.	46.61	30.22	35.52	36.12	39.37	12.20	0.151

We can distinguish between two methods to find the n factor, both using an iterative process which estimates the spectral reflectances of ramp by the MD model for various n factor values. Then comparing the estimated spectral reflectances with the measured spectral reflectances

a n value is selected, value bringing the smallest colorimetric differences or smallest spectral difference.

Method 1

The first method will calculate a LUT including an n value. In this method mechanical and optical dot gain are evaluated together. After using the vector notation as in Equation 3.8 where:

$$\mathbf{r}_{m,p} = \mathbf{r}_{\text{meas}}^{1/n} - \mathbf{r}_{\text{paper}}^{1/n}, \quad (3.11)$$

and

$$\mathbf{r}_{c,p} = \mathbf{r}_{\text{col, max}}^{1/n} - \mathbf{r}_{\text{paper}}^{1/n}, \quad (3.12)$$

we raise a_{eff} to the power n :

$$a_{\text{eff}} = \left(\frac{\mathbf{r}_{c,p}^T \mathbf{r}_{m,p}}{\mathbf{r}_{c,p}^T \mathbf{r}_{c,p}} \right)^n. \quad (3.13)$$

Method 2

The second method will start by calculating a LUT for $n = 1$, see Table 3.1. Then the spectral MD model is run for several n values as in Equations 3.9 with the effective colorant values obtained with the previous calculated LUT. The n value given the smallest sRMS difference between measurements and estimated spectral reflectances for the ramp is chosen. During this selection process one can see that different metrics can be used to select the best n factor. Ideally we are looking for the n value which minimizes the spectral difference between the ramp spectral reflectances and their estimation.

In Table 3.2 and Table 3.3 are presented the performances of the MD model with effective coverage values for Method 1 and Method 2 respectively. Figure 3.3 and Figure 3.4 illustrate how the performance of the MD model evolves with the n factor as parameter for Method 1 and Method 2. We can see that the introduction of the n factor brings improvement in term of color and spectral differences between the simulated and measured ramp. The Method 2 is giving better results than Method 1. Also it shows the difficulty to choose a good n factor value, regarding of what we want to minimize: color difference for a given illuminant, spectral difference.

3.3 Multi-colorant print

When working with more than one ink, the Murray Davies model itself is no longer sufficient. The estimation of the areas covered or not covered by colorants is not straightforward anymore. During the printing process the drops of inks of different colorants may overlap, this due to misplacement of the ink drops.

Let us consider a two inks print with cyan and magenta. Such printing system can produce four different colors resulting from the print of cyan, magenta, paper and the combination of cyan and magenta when a layer of cyan is covered by a layer of magenta: that is the subtractive color mixing process, see Section 2.5.2.

When a colorant combination is printed, only colorant values are sent to the printer which will result in various colorant overlaps regarding of the colorant values in the colorant combination. If we were printing a colorant combination made of 20% of cyan and 30% of magenta the following equation will not be accurate enough:

$$\hat{r}(\lambda) = 0.2r_c(\lambda) + 0.3r_m(\lambda) + 0.5r_{\text{paper}}(\lambda), \quad (3.14)$$

where $r_c(\lambda)$, $r_m(\lambda)$ are the spectral reflectances of cyan and magenta at full coverage and $r_{\text{paper}}(\lambda)$ the spectral reflectance of the paper. It will not be accurate enough because the spectral reflectance of magenta overlapping cyan is not taken into account in the estimation.

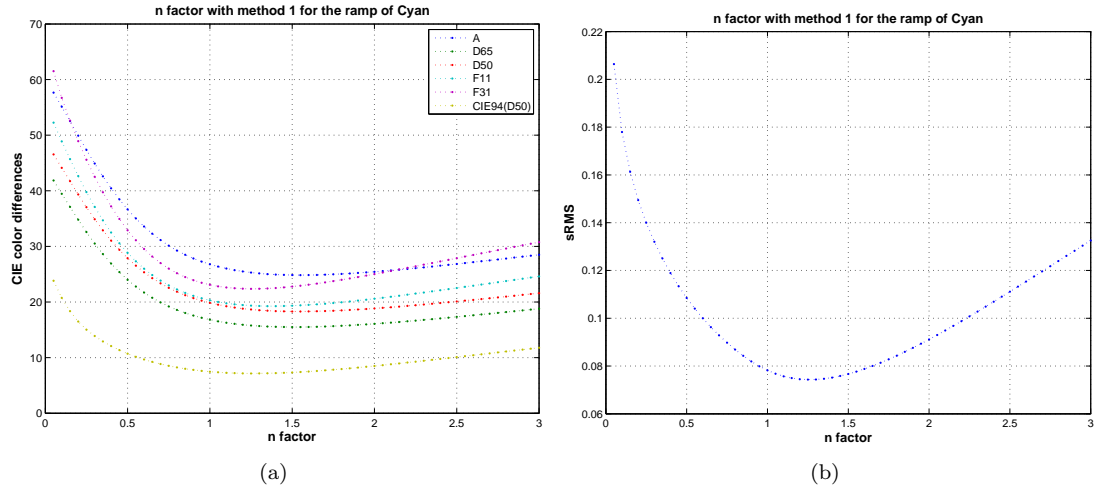


Figure 3.3: Performances of the MD model with effective values and various n factor values using Method 1 to calculate the best n factor. In (a) are displayed the performances of the MD in term of CIE76 and CIE94 color differences, in (b) in term of sRMS spectral difference.

Table 3.2: Best n factor selected by the Method 1 for the simulated ramp of cyan by the MD model. The first three raws show the n factor which gives the smallest average CIE1976 color difference for illuminant A and 1931 standard observer, and so for the others illuminant and spectral sRMS. Each Av. line correspond to the minimum value of each curve in Figure 3.3 (a) and 3.3 (b).

Best n factor for		A	ΔE_{ab}^*	D65	D50	F11	F31	ΔE_{94}^*	D50	sRMS
$\Delta E_{ab}^*(A)$	Av.	24.84	15.52	18.30	19.48	23.11	7.50	0.079		
	n=1.6 Std.	15.12	10.09	11.70	12.43	13.99	4.88	0.063		
	Max.	44.16	28.05	33.15	35.11	40.19	13.74	0.186		
$\Delta E_{ab}^*(D65)$	Av.	24.84	15.49	18.30	19.33	22.77	7.33	0.077		
	n=1.5 Std.	15.04	9.98	11.60	12.20	13.62	4.63	0.059		
	Max.	44.12	28.05	33.16	34.86	39.53	12.95	0.170		
$\Delta E_{ab}^*(D50)$	Av.	24.84	15.49	18.30	19.33	22.77	7.33	0.077		
	n=1.5 Std.	15.04	9.98	11.60	12.20	13.62	4.63	0.059		
	Max.	44.12	28.05	33.16	34.86	39.53	12.95	0.170		
$\Delta E_{ab}^*(F11)$	Av.	24.93	15.54	18.36	19.26	22.52	7.22	0.075		
	n=1.4 Std.	15.04	9.92	11.56	12.04	13.33	4.44	0.055		
	Max.	44.23	28.18	33.30	34.74	39.03	12.28	0.156		
$\Delta E_{ab}^*(F31)$	Av.	25.14	15.67	18.53	19.29	22.38	7.16	0.074		
	n=1.3 Std.	15.10	9.93	11.58	11.95	13.14	4.30	0.053		
	Max.	44.50	28.45	33.59	34.78	38.72	11.77	0.146		
$\Delta E_{94}^*(D50)$	Av.	25.14	15.67	18.53	19.29	22.38	7.16	0.074		
	n=1.3 Std.	15.10	9.93	11.58	11.95	13.14	4.30	0.053		
	Max.	44.50	28.45	33.59	34.78	38.72	11.77	0.146		
sRMS	Av.	25.14	15.67	18.53	19.29	22.38	7.16	0.074		
	n=1.3 Std.	15.10	9.93	11.58	11.95	13.14	4.30	0.053		
	Max.	44.50	28.45	33.59	34.78	38.72	11.77	0.146		

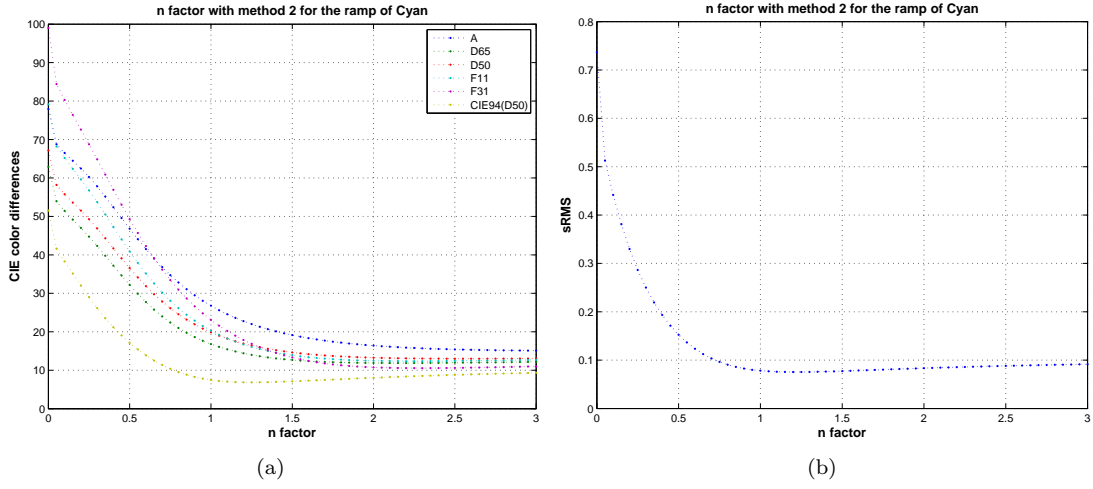


Figure 3.4: Performances of the MD model with effective values and various n factor values using Method 2 to calculate the best n factor. In (a) are displayed the performances of the MD in term of CIE76 and CIE94 color differences, in (b) in term of sRMS spectral difference.

Table 3.3: Best n factor selected by the Method 2 for the simulated ramp of cyan by the MD model. The first three raws show the n factor which gives the smallest average CIE1976 color difference for illuminant A and 1931 standard observer, and so for the others illuminant and spectral sRMS. Each Av. line correspond to the minimum value of each curve in Figure 3.4 (a) and 3.4 (b).

Best n factor for		ΔE_{ab}^*					ΔE_{94}^* D50	sRMS
		A	D65	D50	F11	F31		
$\Delta E_{ab}^*(A)$	Av.	14.99	12.50	13.27	13.15	11.61	9.87	0.095
	Std.	8.72	7.82	8.11	8.31	7.25	6.59	0.073
	Max.	26.06	21.82	23.28	23.06	21.77	18.67	0.209
$\Delta E_{ab}^*(D65)$	Av.	15.88	11.88	13.08	12.37	10.57	8.37	0.085
	Std.	9.75	7.47	8.17	7.79	6.11	5.35	0.062
	Max.	29.23	21.73	24.14	23.15	18.36	14.97	0.174
$\Delta E_{ab}^*(D50)$	Av.	15.32	11.99	13.00	12.47	10.67	8.92	0.089
	Std.	9.23	7.51	8.04	7.81	6.10	5.79	0.066
	Max.	27.78	21.61	23.62	22.86	17.56	16.33	0.186
$\Delta E_{ab}^*(F11)$	Av.	15.88	11.88	13.08	12.37	10.57	8.37	0.085
	Std.	9.75	7.47	8.17	7.79	6.11	5.35	0.062
	Max.	29.23	21.73	24.14	23.15	18.36	14.97	0.174
$\Delta E_{ab}^*(F31)$	Av.	15.69	11.89	13.04	12.37	10.55	8.52	0.086
	Std.	9.59	7.47	8.12	7.78	6.05	5.47	0.063
	Max.	28.79	21.67	23.96	23.03	18.06	15.34	0.177
$\Delta E_{94}^*(D50)$	Av.	21.31	13.64	15.98	15.51	16.00	6.86	0.076
	Std.	13.08	8.68	10.08	9.79	9.83	4.15	0.052
	Max.	38.71	25.29	29.62	29.04	28.94	11.73	0.147
sRMS	Av.	22.77	14.41	16.96	16.71	17.88	6.87	0.075
	Std.	13.85	9.12	10.63	10.44	10.82	4.10	0.052
	Max.	40.93	26.55	31.20	30.92	31.83	11.64	0.146

When the colorant coverages increase, e.g. values bigger than 50% it is important to estimate all the different colorant overlaps.

The spectral reflectance estimation of a colorant combination should include all possible overlaps between the colorant as follows:

$$\hat{r}(\lambda) = a_1 r_{paper}(\lambda) + a_2 r_c(\lambda) + a_3 r_m(\lambda) + a_4 r_{c+m}(\lambda), \quad (3.15)$$

where the $r_{c+m}(\lambda)$ is the spectral reflectance of magenta overlapping cyan and the a_i for $i = 1$ to 4 the areas covered by the spectral reflectances in Equation 3.15.

A good estimation of a colorant combination should take into account all the primaries (i.e. the colorants) of the printer plus the all the possible overlaps between these primaries plus the paper. This set of primaries is called the Neugebauer primaries (NP). We can observe that a m colorants printer can produce:

$$N = 2^m \text{ NP}. \quad (3.16)$$

The Neugebauer model (Neugebauer, 1937) is an extension of the Murray-Davis model, on a unit area the Neugebauer model will sum and weight the NP according to their coverage on the paper. The NP coverage is estimated with the statistical Demichel model (Demichel, 1924).

3.3.1 The Demichel model

The Demichel model is a statistical model which estimates the NP coverage for a given colorant combination. Theoretically, it assumes that the colorant coverage is statistically independent, i.e. independence between the ink-screens, independence between the dot placement.

For a given colorant combination of $m > 1$ colorants we have :

$$c_j \in [0, 1] \text{ for } j \in \{1, \dots, m\}, \quad (3.17)$$

where $c_j = 0$ for no inks laid down for the j th colorant and $c_j = 1$ for full coverage of the j th colorant and we called w_i the weights for the of the NP with the following properties:

$$\sum_{i=0}^{2^m-1} w_i = 1 \text{ and } 0 < w_i < 1. \quad (3.18)$$

The independence between the colorant screens and random distribution of the dot are two assumptions made by the Demichel model. These assumptions have been studied at different levels by Viggiano (1990), Chang et al. (1995) by imposing different shapes for unit area, Hersch et al. (2005) by looking at the dot gain in colorant overlapping or for the screens independence by Rogers (1998).

Demichel weights for two inks (m=2)

The Demichel equations for a two colorants combination are:

$$\begin{aligned} w_0 &= (1 - c_1)(1 - c_2), \\ w_1 &= c_1(1 - c_2), \\ w_2 &= (1 - c_1)c_2, \\ w_{12} &= c_1c_2, \end{aligned} \quad (3.19)$$

and

$$\mathbf{w}_{(2)} = [w_0 \ w_1 \ w_2 \ w_{12}]^T \quad (3.20)$$

where $\mathbf{w}_{(2)}$ is a vector weights for a two colorant combination, w_0 is the weight accounting for the paper, w_1 the weight for the first colorant c_1 , w_2 for colorant c_2 and w_{12} for the overlap between colorant c_1 and colorant c_2 . We can also see that two colorants gives $2^2 = 4$ weights.

In order to rewrite in a matrix form the calculation of the Demichel weights, we first expand the previous equation:

$$\begin{aligned} w_0 &= 1 - c_1 - c_2 + c_1c_2, \\ w_1 &= c_1 - c_1c_2, \\ w_2 &= c_2 - c_1c_2, \\ w_{12} &= c_1c_2. \end{aligned} \quad (3.21)$$

By defining a matrix of coefficient $\mathbf{M}_{(2)}$:

$$\mathbf{M}_{(2)} = \begin{bmatrix} 1 & -1 & -1 & 1 \\ 0 & 1 & 0 & -1 \\ 0 & 0 & 1 & -1 \\ 0 & 0 & 0 & 1 \end{bmatrix} \quad (3.22)$$

such that multiplying $\mathbf{M}_{(2)}$ by a vector of coefficient $\mathbf{c}_{(2)}$ for a colorant combination of two colorants:

$$\mathbf{c}_{(2)} = [1 \ c_1 \ c_1 \ c_1c_2]^T \quad (3.23)$$

we obtain the calculation of the weights for a colorant combinations of two colorants in a matrix form:

$$\mathbf{w}_{(2)} = \mathbf{M}_{(2)}\mathbf{c}_{(2)}. \quad (3.24)$$

Demichel weights for three inks (m=3)

The Demichel equations for a three colorants combination will be:

$$\begin{aligned} w_0 &= (1 - c_1)(1 - c_2)(1 - c_3), \\ w_1 &= c_1(1 - c_2)(1 - c_3), \\ w_2 &= (1 - c_1)c_2(1 - c_3), \\ w_3 &= (1 - c_1)(1 - c_2)c_3, \\ w_{12} &= c_1c_2(1 - c_3), \\ w_{13} &= c_1(1 - c_2)c_3, \\ w_{23} &= (1 - c_1)c_2c_3, \\ w_{123} &= c_1c_2c_3, \end{aligned} \quad (3.25)$$

where w_0 is the weight accounting for the paper, w_1 , w_2 and w_3 the weights for the single colorant c_1 , c_2 and c_3 . w_{12} , w_{13} and w_{23} the weights accounting for the overlaps between two colorants and w_{123} the weight for overlap between the three colorants. We can also see that three colorants gives $2^3 = 8$ weights.

In order to re-write in a matrix form the calculation of the Demichel weights, we first expand the previous equation:

$$\begin{aligned} w_0 &= 1 - c_1 - c_2 - c_3 + c_1c_2 + c_1c_3 + c_2c_3 - c_1c_2c_3, \\ w_1 &= c_1 - c_1c_2 - c_1c_3 + c_1c_2c_3, \\ w_2 &= c_2 - c_1c_2 - c_2c_3 + c_1c_2c_3, \\ w_3 &= c_3 - c_1c_3 - c_2c_3 + c_1c_2c_3, \\ w_{12} &= c_1c_2 - c_1c_2c_3, \\ w_{13} &= c_1c_3 - c_1c_2c_3, \\ w_{23} &= c_2c_3 - c_1c_2c_3, \\ w_{123} &= c_1c_2c_3. \end{aligned} \quad (3.26)$$

By defining a matrix of coefficient $\mathbf{M}_{(3)}$:

$$\mathbf{M}_{(3)} = \begin{bmatrix} 1 & -1 & -1 & -1 & 1 & 1 & 1 & -1 \\ 0 & 1 & 0 & 0 & -1 & -1 & 0 & 1 \\ 0 & 0 & 1 & 0 & -1 & 0 & -1 & 1 \\ 0 & 0 & 0 & 1 & 0 & -1 & -1 & 1 \\ 0 & 0 & 0 & 0 & 1 & 0 & 0 & -1 \\ 0 & 0 & 0 & 0 & 0 & 1 & 0 & -1 \\ 0 & 0 & 0 & 0 & 0 & 0 & 1 & -1 \\ 0 & 0 & 0 & 0 & 0 & 0 & 0 & 1 \end{bmatrix} \quad (3.27)$$

such that multiplying $\mathbf{M}_{(3)}$ by a vector of coefficient $\mathbf{c}_{(3)}$ for a colorant combination of three colorants:

$$\mathbf{c}_{(3)} = [1 \ c_1 \ c_2 \ c_3 \ c_1c_2 \ c_2c_3 \ c_1c_3 \ c_1c_2c_3]^T \quad (3.28)$$

we obtain the calculation of weights for colorant combination of three colorants in a matrix form:

$$\mathbf{w}_{(3)} = \mathbf{M}_{(3)}\mathbf{c}_{(3)}. \quad (3.29)$$

Demichel for m inks

The extension to m colorants is straightforward following the examples for 2, 3 inks and the formulation:

$$w_i = \prod_{j=1 \rightarrow m} \begin{cases} c_j; & \text{if colorant } j \text{ is part of the } i\text{th NP} \\ (1 - c_j); & \text{else} \end{cases} \quad (3.30)$$

with the matrix notation:

$$\mathbf{w}_{(m)} = \mathbf{M}_{(m)}\mathbf{c}_{(m)}. \quad (3.31)$$

3.3.2 The spectral Neugebauer model

The spectral Neugebauer model says that the spectral reflectance of a printed colorant combination is the weighted summation of the Neugebauer primaries (NP) spectral reflectances. The weights are the areas covered by these NP for a given colorant combination. The areas are estimated by the Demichel model. For a m colorants printer, the spectral reflectance of a colorant combination is given by:

$$\hat{r}(\lambda) = \sum_{i=0}^{2^m-1} w_i r_{i,\max}(\lambda), \quad (3.32)$$

where w_i and $r_{i,\max}(\lambda)$ are the weight and spectral reflectance of the i th NP and $\hat{r}(\lambda)$ is the estimated spectral reflectance.

In a matrix notation, the estimated spectral reflectance \mathbf{r} of an m colorants combination will be defined by:

$$\hat{\mathbf{r}} = \mathbf{w}_{(m)}\mathbf{P}_{(m)}, \quad (3.33)$$

with $\mathbf{P}_{(m)}$ being the matrix of NP. Each column of $\mathbf{P}_{(m)}$ is a spectral reflectance of a NP, the NP are stored in a similar order as for the weights, e.g. with a two inks print we will have:

$$\mathbf{P}_{(2)} = [\mathbf{p}_0 \ \mathbf{p}_1 \ \mathbf{p}_2 \ \mathbf{p}_{12}], \quad (3.34)$$

Using the full notation of $\mathbf{w}_{(m)}$ as in Equation 3.31 we can write the spectral reflectance estimation of a colorant combination of m colorants as follow:

$$\hat{\mathbf{r}} = \mathbf{M}_{(m)}\mathbf{c}_{(m)}\mathbf{P}_{(m)}. \quad (3.35)$$

In a similar way as for the spectral Murray-Davis (MD) model, the NPs have to be printed and measured before making estimation of any colorant combination. Also the effective colorant values have to be used instead of the theoretical colorant values describing a colorant combination. As for single colorant print the printer is subject to dot gain. The transformation theoretical c_j to effective c'_j is performed using looking table (LUT) as described in Section 3.2.3 on MD inversion.

In this thesis we have used single colorant ramps to estimate the dot gain colorant combination for $m > 1$ colorants in a first approach, a second approach using optimization on measured spectral reflectance of colorant combinations has been tested in Section 4.2.1. It is possible to add a dot gain by NP for example as Tzeng (1999) or Hersch and Crêté (2005) did in their works. In Figure 3.5 is grouped the steps involved in the spectral Neugebauer model: effective colorant values calculation, Demichel equations and spectral Neugebauer equations.

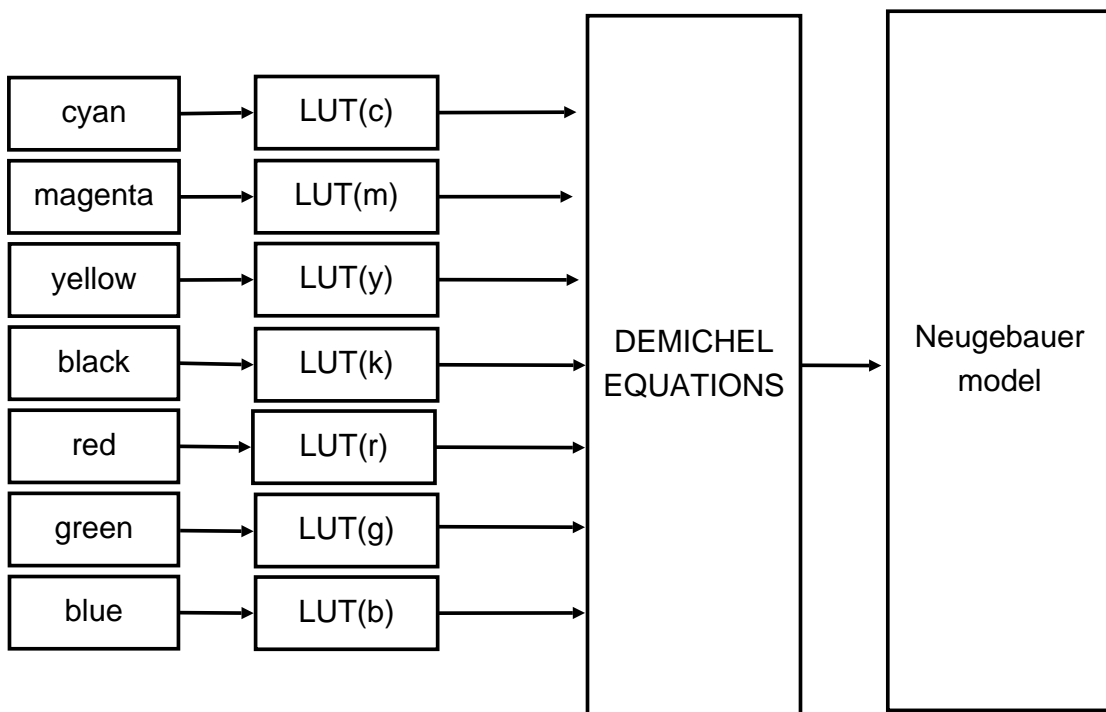


Figure 3.5: Diagram of the spectral Neugebauer model, from theoretical colorant values to its effective colorant values, Demichel equations and Negebauer model for a 7 colorants combination.

3.3.3 The spectral cellular Neugebauer model

The spectral cellular Neugebauer model uses the same equations as for the spectral Neugebauer model (Heuberger et al., 1992; Rolleston and Balasubramanian, 1993). The difference comes from the available NP, the idea is to dispose of intermediate NP values in order to affine the estimation.

There is trade-off between the number of NP to print and measure and the accuracy of the model. For example a 4 colorants printer with three level per colorant [0 50% 100%] will require the print of $3^4 = 81$ NP.

3.3.4 The Yule-Nielsen modified spectral Neugebauer model

As for the Murray-Davies model, the Yules-Nielsen n factor can be added to the Neugebauer equation, this to include the light and paper interaction in the reflectance estimation of a colorant combination.

The NG Equation 3.32 is modified as follows:

$$\hat{r}^{1/n}(\lambda) = \sum_{i=0}^{2^m-1} w_i r_{i,\max}^{1/n}(\lambda). \quad (3.36)$$

where the n factor is calculated from the single colorant ramps as described in Section 3.2.4. Tuning can be performed on the selection of the n factor and value(s) can be selected by colorant, by wavelength (Wyble and Berns, 2000) or even by halftoning technique.

3.4 Discussion and conclusion

In this chapter we have presented the spectral printer characterization. Just as in color printer characterization this operation is required to obtain the transformation from a control value sent to the printer to the spectral (or colorimetric) value printed on paper.

We have used the spectral Neugebauer (NG) model which is an extension to multi-colorant print of the Murray-Davies (MD) model. The NG model says that the spectral reflectance estimation of a printed colorant combination is the weighted sum of the Neugebauer primaries (NP). The weights correspond to the surfaces covered by the NP. The NP are all the primaries of the printer plus all combinations between them plus the paper. We choose this approach for its simplicity, it does not require much information from the printing system: a ramp for each colorant and the NP. In case of a 7 colorants printer we have to print and measure $7 \times 16 + 2^7 = 240$ patches when each ramp of single colorant is made of 16 patches and 2^7 being the number of NP. Comparing to a look-up table (LUT) approach less prints and measurements are needed. Also the printer characterization is independent of the halftoning technique used to print the colorant combination. The Demichel model will estimate the NP coverage on the paper and this with the only assumption of independence between the colorant channels: the placement of the drops of ink of the colorant 1 is independent of the placement of drops of ink of colorant 2 and so for all the colorants available in a printing system.

The printer is a known unstable system, proof is the dot gain phenomenon. It increases the theoretical dot size and it results brighter spectral reflectance (or color) prediction by the printer model than the desired printed colorant combination. Both mechanical and optical dot gain can be encompassed in the printer characterization by using the inverse MD model: a relationship between the theoretical colorant value and the effective colorant value can be then established. This transformation is used as LUT for each colorant channel before performing color or spectral prediction with the NG model. But it is the add of the n factor from the Yules-Nielsen to the MD and NG equations which allows to include the optical dot gain in these printer models. The mechanical dot gain being estimated for $n = 1$. Attention has to be put on the creation of these LUTs because the transformation can be established for different criteria from the ramp of single colorant: comparison of prediction and measure of ramp level can be performed under spectral difference, color difference (CIEXYZ, CIELAB) (Kraushaar and Urban, 2006) or even by wavelength. The manner the LUT is created has to be remained for the colorant separation (see Chapter 5).

The dot gain is a big source of error in the NG printer model estimation and especially the optical dot gain. Usually one n factor is chosen for all colorants and it is often assumed that a study of the dot gain by colorant is accurate enough: basically the mechanical dot gain is described for each colorant but only an average optical dot gain is finally considered. By doing so we simplify drastically the printing system and it is getting worse for a multi-colorant printer due to the very different available colorants.

The NG model assumes that each screen of colorant channel is perfectly bi-level after halftoning and each drop of colorant has a constant spectral reflectance, meaning all NP have a fixed value. If this consideration was true only the mechanical dot gain should be corrected to characterize a printer. The cellular NG model (Rolleston and Balasubramanian, 1993) have shown improvement in disposing of more intermediate NP: to divide the colorant space combines interpolation and NG model. Another solution which is still considering fixed NP is to optimize the parameters directly: from the measurement of the NP and some sample printed and measured the optimal NP can be extracted (Xia et al., 1999; Balasubramanian, 1999; Lana et al., 2005). All these approaches also shows that different n factor values can be used. To continue on the optical dot gain, improvement have been shown while considering different dot gains in case of ink printed in superposition of others ink layers (Hersch and Crête, 2005).

The cellular NG model, the n factor or multiple dot gain are all increasing the printer model accuracy. But they do not integrate completely the multiple light, air and paper interaction. The Clapper-Yule spectral color prediction model and all its modification proposed by Hersch et al. (2005) gives very good results. The model is similar on the steps involves in the prediction of a colorant combination with the NG or YNSN model: theoretical to effective colorant value, NP coverage calculation with the Demichel equations and sum of the NP. The difference comes from the data needed to characterize the printing system such internal reflection factor or specular reflection factor.

In the perspective of controlling spectrally our printing system it is important to dispose of an easily invertible printer model. In the next chapter we will present our experimental results for the spectral characterization of our multi-colorant printing system. We use the spectral NG model and the YNSN model.

Chapter 4

Spectral printer characterization: experimentation

4.1 Introduction

In this chapter you will find the description of our experiments and results for the spectral printer characterization of our spectral printing system. Our system is based on a multi-colorant inkjet printer with seven inks. We use the Epson 2100 Photo Stylus inkjet printer where the original set of inks have been replaced by a cyan, magenta, yellow, black, red, green and blue (CMYKRGB) set of inks. we use the spectral Neugebauer (NG) printer model and the spectral Yule-Nielsen modified Neugebauer (YNSN) to characterize our system (Hardeberg and Gerhardt, 2004, 2005).

We are interested in the transformation from digital control value to colorimetric value or spectral reflectance on the paper, digital control value being a colorant combination. We want a clear description of each colorant channel response before to start making spectral reflectance estimation. We want for example to know the response of the printer for each monochromatic ramp. A ramp is a series of digital control value from 0 to maximum level with a linear step increment. This first part of the characterization will be used to build lookup-table to establish the transformation theoretical colorant value to effective colorant value. This step helps to set the maximum colorant value or coverage per colorant channel.

The biggest problem while characterizing the printer is to be able to override the color management embedded in the printer. We know that when a picture is sent to the printer several transformations will applied be to it: gamut mapping, colorant separation, scaling and halftoning. If we think of grey scale ramp, a metameric print of it allows to print several different colorant combinations for the same colorimetric printed values.

To override the color management means to be able to control the printhead of the printer. It also means we have to adapt the test chart or image to be printed with the resolution of the printer: this result in scaling the image by a large factor. And finally the image has to be halftoned, each pixel value of an image is set to 0 or 1 and this is a command for the printhead to lay down or not a drop of ink at the pixel position.

We use a dedicated software to drive the printer. This software requires an TIFF image set to the printer resolution, the image has to be halftoned. Halftoning is performed by channel independently by error diffusion.

4.2 Experiment

In this experiment we have used the Epson Stylus Photo 2100 inkjet printer. This printer is a 7 channel printer where the original set of inks has been replaced by a set of CMYKRGB colorants from Epson. The original set of ink from Epson was CMYKcmk, the traditional CMYK

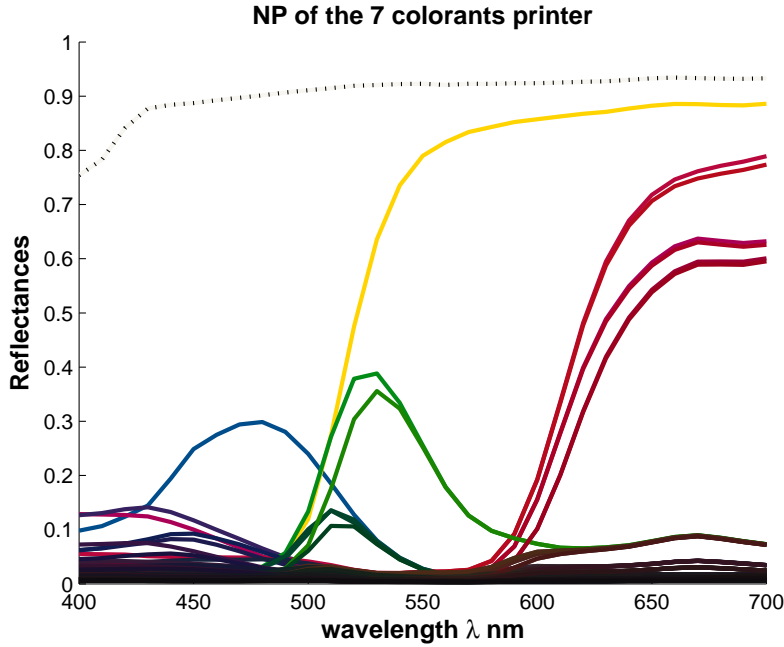


Figure 4.1: Spectral reflectances of the 2^7 NP for the Epson Stylus 2100 printer plus the spectral reflectance of the paper on which the primaries have been printed.

colorants plus a lighter cyan, magenta and black, see Figure 4.1 for the spectral reflectances of the 2^7 Neugebauer primaries (NP) at full coverage. The colorant combinations have been printed on Epson photo paper.

To communicate with the printer we use a modified driver. This driver take TIFF image as input. In case of printing a test chart, we store in a text file the description of each patch. In the text file the colorant values are stored as follow: one line per patch and seven columns per line, one for each colorant coverage value.

Then with a function wrote in Matlab we convert our text file in a TIFF image. This image is a colorant image where each pixel corresponds to colorant combination (i.e. a line in the text file). The image is saved under TIFF cmyk plus spot channels format, this format allowed to save m channels images for $m > 4$. A scaling is performed on the TIFF image to fit with the printer resolution and the scaled image is finally halftoned.

Halftoning is performed by error diffusion for each channel independently. The TIFF image has now binary value for each pixel of each channel and with the help of the modified driver the image is printed without any more transformation. A binary value at a pixel position of a colorant channel corresponds to control command to the printer: to lay down a drop of ink for 1 or no drop to lay down for 0.

A short comparison of the color gamut versus the paper has been performed. We have tested different papers with this printer. The best results being obtained for Epson photo paper $194g/m^2$. With this paper we got best interaction ink/paper: drying fast, less soaking of the inks, bigger gamut.

4.2.1 Spectral modeling

To build the spectral Neugebauer model we need the spectral reflectances of the NPs and the spectral reflectances of each single colorant ramp. Each ramp is made of 16 linearly spaced steps from 0% to 100%. The ramp measurements allow to create look-up tables (LUTs) for each colorant (see Figure 4.2) and to find the n factor (see Section 3.2.4) for this printing system.

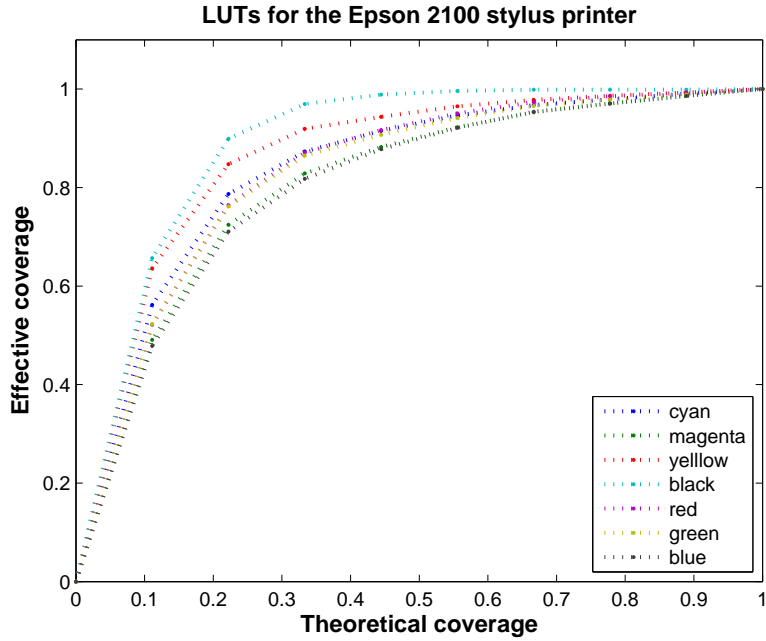


Figure 4.2: The seven LUTs of the Epson Stylus 2100 printer, these LUTs were obtained from prints on photo paper. We can observe a slight difference for the maximum coverage value reached by the different colorants. But around 60% of theoretical coverage all the colorants have almost reached 90% of effective coverage of the paper.

The estimation of the spectral reflectance from the colorant combination of each patch is performed using Equation 3.32 and Equation 3.36, see Figure 3.5 in Section 3.3.2 for the diagram of the NG model workflow. The weights in these equations are calculated with the Demichel equations for seven inks for the effective colorant values. The effective values are obtained by interpolation using the LUTs and the theoretical values of each patch.

4.2.2 Experimental setups

A test chart has been designed to evaluate the performance of the spectral model of this printer. A regular grid in 7 dimensions in the colorant space has been created, each colorant could get 4 defined values in [0% 33% 66% 100%] for a total of $4^7 = 16384$ patches. The values describing our grid are the effective coverage values. To calculate the corresponding theoretical coverage value each LUT has been inverted. To take into account the printer coverage limitation in our experiment we have printed only the patches for a colorant coverage summation below 280% (this based on LUTs observation). We avoid then to include in the evaluation patches with too much ink. Our grid is finally made of 4175 patches. For practical reason the grid (i.e. our test target) have been divided in several smaller grids to fit on A4 paper, then the grids have been printed successively. You can see in Figure 4.3 the first subgrid printed.

4.2.3 Results and Discussion

The test chart measurements are compared with their estimation by the spectral printer model. Colorimetric and spectral differences between the estimated spectral reflectances and the measured spectral reflectances are displayed in Table 4.2. Various n factor values are tested in this experiment.

We have seen in the previous chapter (see Section 3.2.4) that different n factor values can

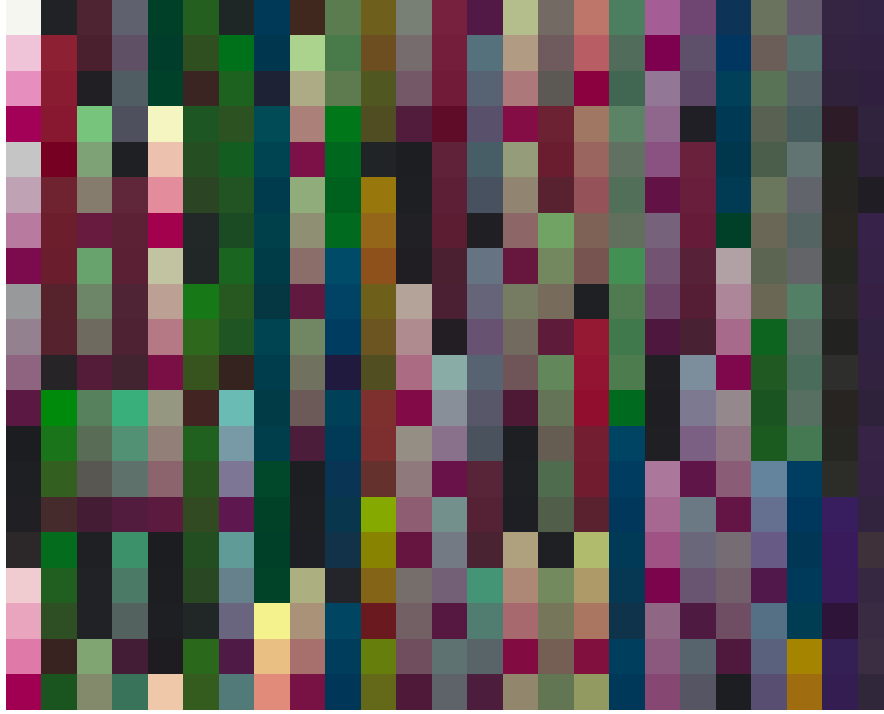


Figure 4.3: The 500 first patches of the designed testchart for the Epson stylus 2100 printer.

be chosen, e.g. one value will minimize a color difference for one given illuminant and another n value will minimize a spectral difference, see Figure 3.4 for the n factor versus the ramp of single colorant cyan. In Table 4.1 are displayed the best n values obtained by colorant for the Method 2.

Table 4.1: n factor versus single colorant ramp and various color and spectral difference. This results illustrate the difficulty to select one n factor value for all the colorants.

	cyan	magenta	yellow	black	red	green	blue
$\Delta E_{ab}^*(A)$	2.3	2.2	1.3	1.1	1.7	1.6	3.4
$\Delta E_{ab}^*(D65)$	1.9	2.5	1.6	1.1	1.9	1.7	3.8
$\Delta E_{ab}^*(D50)$	1.8	2.5	1.6	1.1	1.9	1.6	3.9
$\Delta E_{ab}^*(F11)$	2.0	2.5	1.5	1.1	1.9	1.7	3.7
$\Delta E_{ab}^*(F31)$	1.8	2.5	1.6	1.1	1.9	1.7	3.9
$\Delta E_{94}^*(D50)$	1.2	1.2	1.1	1.0	1.0	1.1	1.1
sRMS	2.0	2.4	1.5	1.1	1.9	1.7	3.7

A first simulation of the printed test chart is performed using the YNSN model. We look at the performance of the spectral printer model for different n values obtained in Table 4.1: average n values for the color differences and spectral difference by colorant are used. The results are shown in Table 4.2.

We tried a second approach to select a suitable n factor value. It follows the same approach as for the n factor and the single colorant ramps: we perform spectral reflectance estimation with the YNSN model for different n values. In Figure 4.4 (a) and Figure 4.4 (b) are displayed the average differences between the measured test chart and the simulated spectral reflectance of the test chart for various n values. We perform this optimization on approximatively 10% of the available patches, since the test chart we have printed is constituted of 4175 we use 400 for the optimization. In Table 4.3 are displayed the color differences and spectral difference between all

Table 4.2: Performance of the YNSN model for the best n factor values obtained by optimization on the single colorant ramps. The first n value tested in this table corresponds to the average n values in the first line of Table 4.1.

		ΔE_{ab}^*					ΔE_{ab}^* D50	sRMS
		A	D65	D50	F11	F31		
n=1.9	Av.	7.6	7.7	7.7	7.4	7.0	6.0	0.034
	Std.	3.8	4.0	4.0	3.9	3.6	3.1	0.026
	Max	29.4	29.2	29.5	30.8	29.6	15.5	0.128
n=2.1	Av.	7.8	7.9	7.9	7.6	7.4	6.3	0.036
	Std.	3.8	4.0	4.0	3.9	3.8	3.3	0.029
	Max	28.2	28.7	28.5	29.8	27.5	15.7	0.137
n=2.1	Av.	7.8	7.9	7.9	7.5	7.3	6.2	0.036
	Std.	3.8	4.0	4.0	3.9	3.8	3.3	0.028
	Max	28.4	28.7	28.6	29.9	27.7	15.6	0.136
n=2.0	Av.	7.8	7.8	7.8	7.5	7.3	6.2	0.036
	Std.	3.8	4.0	4.0	3.9	3.8	3.3	0.028
	Max	28.5	28.8	28.7	30.0	27.9	15.6	0.135
n=2.1	Av.	7.8	7.9	7.9	7.5	7.3	6.2	0.036
	Std.	3.8	4.0	4.0	3.9	3.8	3.3	0.028
	Max	28.4	28.7	28.6	29.9	27.7	15.6	0.136
n=2.1	Av.	7.8	7.9	7.9	7.6	7.4	6.3	0.036
	Std.	3.8	4.0	4.0	3.9	3.8	3.3	0.029
	Max	28.2	28.7	28.5	29.8	27.5	15.7	0.137
n=1.1	Av.	9.9	9.9	10.0	10.0	9.1	6.4	0.034
	Std.	7.0	6.9	6.9	7.2	6.8	4.0	0.030
	Max	45.2	43.8	44.4	47.7	49.1	25.6	0.198
n=2.0	Av.	7.8	7.8	7.8	7.5	7.3	6.2	0.036
	Std.	3.8	4.0	4.0	3.9	3.8	3.3	0.028
	Max	28.5	28.8	28.7	30.0	27.9	15.6	0.135

the measured and estimated spectral reflectances by the YNSN model for the second approach.

By comparing the two approaches for the calculation of the n factor we can see that performing optimization on the measured spectral reflectances of the test chart and their estimated spectral reflectances by the YNSN brings a slight improvement. There is not a big difference in term of ΔE_{ab}^* color differences but the sRMS is better. An explanation can be found in the way the n factor is selected: optimization was performed on various colorant combinations and not only on average best n by single colorant ramps.

The performance of the spectral Neugebauer printer model is poor, but the introduction of an n factor for the YNSN improves the model performance. How to improve the model? We have seen that using the effective colorant values instead of the theoretical values improves the performance, but was also seen that the different colorant do not have exactly the same transformation theoretical to effective value. The simulation of a printed ramp made of two colorants will then carry error due to the new effective values.

The introduction of effective values for the NP should help to model the dot gain. In their works Tzeng (1999) look at the dot gain for the NP as well or Hersch et al. (2004) creates additional LUTs for various inks superposition knowing that the printer is always performing the same order to lay down the inks.

The cellular Neugebauer solves a part of the problem by dividing in smaller pieces the colorant space. We dispose of more NP and this should provide better estimation as it was shown by Rolleston and Balasubramanian (1993) or Wyble and Berns (2000).

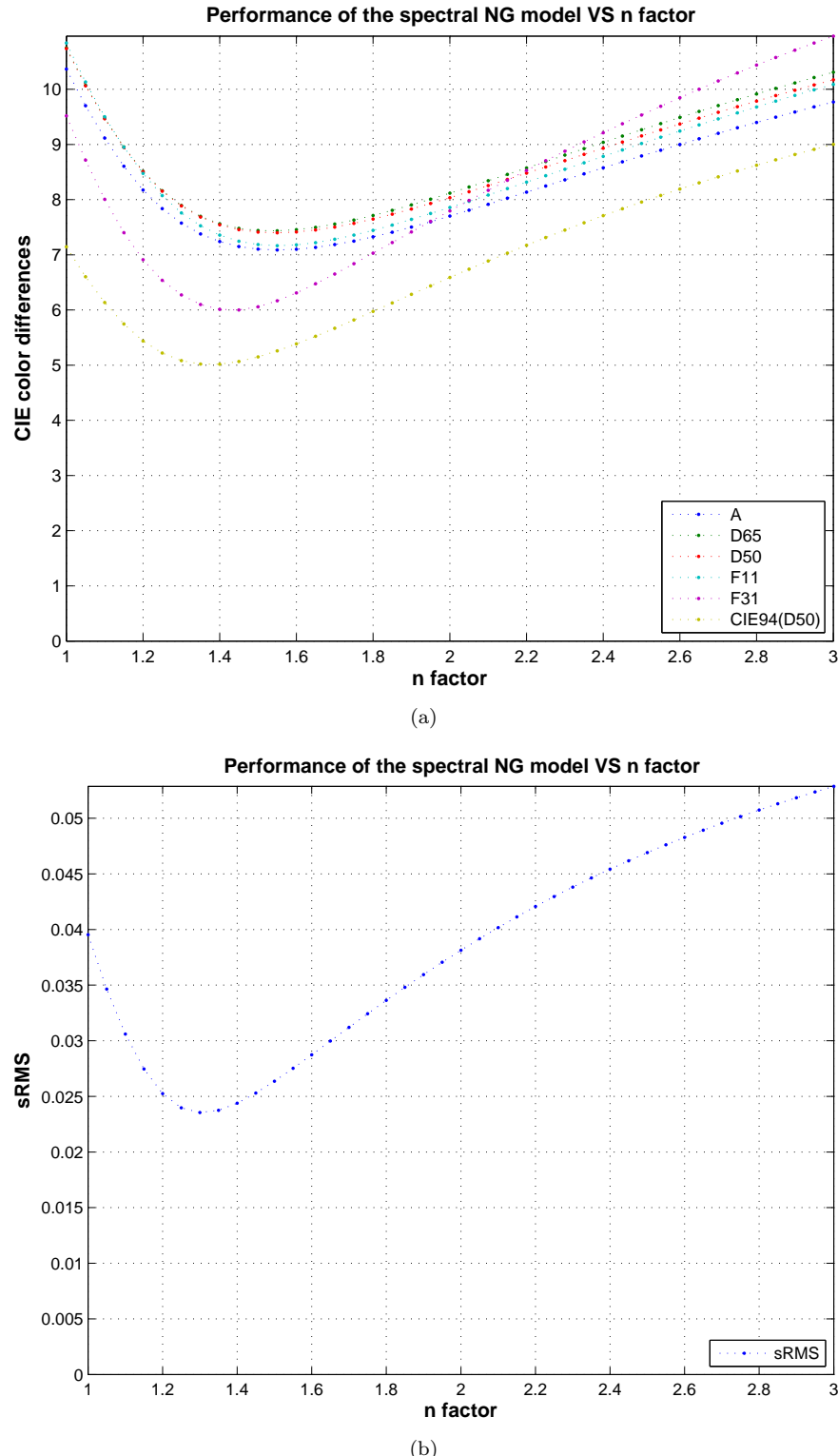


Figure 4.4: *n* factor value versus color differences in (a) and spectral differences in (b) between the measured test chart and its simulation by the YNSN model.

Table 4.3: Performance of the YNSN model for the best n factor values obtained by optimization on approximatively 10% of the printed test chart.

		ΔE_{ab}^*					ΔE_{94}^*	sRMS
		A	D65	D50	F11	F31	D50	
n=1	Av.	11.1	11.1	11.2	11.3	10.5	7.4	0.043
	Std.	7.7	7.6	7.6	8.0	7.7	4.6	0.036
	Max	47.9	46.5	47.1	50.7	52.2	27.8	0.215
n=1.6	Av.	7.6	7.5	7.6	7.3	6.5	5.3	0.028
	Std.	4.4	4.4	4.5	4.5	3.8	2.8	0.021
	Max	33.9	32.5	33.1	35.5	36.2	18.4	0.136
n=1.5	Av.	7.7	7.6	7.7	7.5	6.5	5.2	0.027
	Std.	4.8	4.8	4.8	4.8	4.2	2.8	0.021
	Max	35.9	34.5	35.1	37.7	38.5	19.7	0.146
n=1.5	Av.	7.7	7.6	7.7	7.5	6.5	5.2	0.027
	Std.	4.8	4.8	4.8	4.8	4.2	2.8	0.021
	Max	35.9	34.5	35.1	37.7	38.5	19.7	0.146
n=1.6	Av.	7.6	7.5	7.6	7.3	6.5	5.3	0.028
	Std.	4.4	4.4	4.5	4.5	3.8	2.8	0.021
	Max	33.9	32.5	33.1	35.5	36.2	18.4	0.136
n=1.4	Av.	7.9	7.9	8.0	7.8	6.7	5.2	0.026
	Std.	5.3	5.2	5.2	5.3	4.7	3.0	0.021
	Max	38.0	36.6	37.2	39.9	40.9	21.0	0.157
n=1.4	Av.	7.9	7.9	8.0	7.8	6.7	5.2	0.026
	Std.	5.3	5.2	5.2	5.3	4.7	3.0	0.021
	Max	38.0	36.6	37.2	39.9	40.9	21.0	0.157
n=1.3	Av.	8.4	8.3	8.4	8.3	7.2	5.4	0.027
	Std.	5.8	5.7	5.7	5.9	5.3	3.3	0.023
	Max	40.3	38.8	39.4	42.4	43.5	22.4	0.169

4.3 Conclusion

In this chapter we have presented the spectral characterization of our printing system, system based on a multi-colorant printer with seven inks where all embedded color management has been removed. We can then print any colorant combinations.

The choice of paper was important, a copy paper will should not be used for spectral reproduction. A simple reason is the color gamut is small with such paper. A photo paper or an high quality paper should be chosen. From the previous measured ramps the maximum coverage level should be set for each colorant. Having the limit of coverage we can define more precisely our gamut.

The results we obtained have shown a lake of performance of the spectral NG model, see in Table 4.3 the results for $n = 1$. But with some improvement are noticeable when the YNSN is used and the n factor selected by optimization on part of the printed test chart.

The statistical Demichel model to estimate the weights for the NP of a given colorant combination is assumed to be efficient enough and should not introduce error in the estimation (Chang et al., 1995; Amidror and Hersch, 2000). The main source of error seems to come from the way the dot gain is simulated or characterized for the printer. No distinction is made for the dot gain when an ink level is printed on paper only or on the top of an already printed ink layer. Two approaches should be followed to improve our model: to use the cellular NG or YNSN model, to dispose of intermediate NP values increases the model performance, but there is a trade-off number of intermediate NP to print and accuracy of the model. To characterize the dot gain in

function of the ink superposition should increase as well the performance. Finally a combination of the NG and Clapper-Yule model have show very good results for CMYK printer.

One more time difficulty is to find a easily invertible model which does not loose to much accuracy with its assumption. In the next chapter we will present various method to invert the NG and YNSN model, this to be able to control spectrally our printing system. The inversion of the printer model will provide for each spectral reflectance the colorant combination in order to control the printer and to reproduce the spectral reflectance.

Chapter 5

Inversion of the spectral printer model

5.1 Introduction

The inversion of the spectral printer model (i.e. the spectral Neugebauer equations) answers the question: which colorant combination can reproduce a given spectral reflectance. Multi-colorant systems offer the possibility to create a wider range of spectral reflectance by allowing more combinations between the Neugebauer primaries (NP) than for a smaller set of colorant as a CMY set of colorants for example. But due to printer limitation, such as ink coverage limitation, some parameters in the inversion should be taken in account to obtain feasible colorant combination.

Similar problem in color printing have been met when a colorant combination has to be extracted from a set of m colorants for $m > 3$, see Agar (2001); Tzeng (1999); Jang et al. (2006). In color reproduction the black ink plays an important role and his use can facilitate the inversion of a printer model as proposed by (Ostromoukhov, 1993). The black ink has been used to form sub-groups of 3 to 4 inks in spectral reproduction by Tzeng and Berns (1999) to select first a group of colorant and perform the inversion from the chosen sub set of colorant. In color reproduction a strategy should be chosen first to simplify the inversion of the NG equations: black ink generation, less amount of ink consumption, maximum ink paper coverage and then invert the Neugebauer equation with the selected colorants. These information facilitate the decision which colorant combination to choose by solving a less complex problem such as inverting the Neugebauer equations for a 3 colorants system.

Analytical inversion of the Neugebauer equations in color space are possible for a 3 or 2 colorants printing system without too much complexity, see Mahy and Delabastita (1996). By rewriting the Neugebauer equations in a polynomial form it is possible to calculate the roots of the polynomial and to obtain a colorant combination. But a 3 inks case ends up with resolving a 6th degrees polynomial given multiple solution. A selection of the polynomial roots should be done because not all of them are usable as colorant values. Increasing the number of inks requires to select a feasible solution among a bigger number of solution. Use of look-up table is possible, see Heuberger et al. (1992), but it requires to build enormous grid to have a clear map of the colorant to spectral space or simply to reach enough accuracy. Look-up table in a 3 inks case is possible, it becomes oversized for multi-colorants printing system.

Previous studies have shown the redundancy of colorimetric values for various colorant combination printed by a multi-colorant printer (Rosen et al., 2003). Metamerism can be sufficient enough for color reproduction but becomes a problem for spectral reproduction. The inversion of the spectral Neugebauer equations should bring solution such that the spectral difference between the target and the reproduction is minimized, i.e to reduce the metamerism between the target and the reproduction for a given colorant combination (Tzeng and Berns, 1998, 1999).

The problem of maximum ink coverage should be taken in account in the inversion. Allowing

any colorant combination with limitation of 300% colorant coverage and minimizing the spectral difference (Euclidean distance, spectral RMS or ΔE_{ab}^*) between a target and its simulated reproduction.

In this chapter will be described and discussed various methods for inverting the spectral Neugebauer equations. Method by linear regression iteration (LRI) based on Powel (1964) method presented by Urban and Grigat (2005), by constrained minimization routine (CMR) described by Taplin and Berns (2001), and our method by Alsam et al. (2005) based on the weight inversion (WI).

The choice of inversion method allows to compare a colorimetric and a spectral print. reflectance can be expressed as a weighted summation of the Neugebauer primaries (NP). The final colorant combination obtained after inversion of the spectral printer model is the result of a spectral difference minimization, this operation can be replaced by a colorimetric difference or a combination of spectral and colorimetric differences. A study of color reproduction versus spectral reproduction based on different appropriate metrics will be developed in this chapter (Gerhardt and Hardeberg, 2007a).

Comparison have been studied a bit differently by Zuffi (2004) for a regular cmyk printer. In this work different inversion method have been used for the colorimetric and spectral print. For the colorimetric approach a grid in colorant space is printed, this allowing to get a transformation RGB to CIELAB. Then by interpolation RGB control values are obtained for CIELAB values to reproduce. In case of spectral data to print, the spectral Neugebauer model is inverted by optimization. And in their work spectral reflectance to reproduce are assumed to be in the gamut or out of the printer gamut. Also Tsutsumi et al. (2006) have worked on comparing colorimetric and spectral print with their LabPQR approach.

5.2 Method of inversion for the spectral Neugebauer equations

All the previous proposed methods solve the following problem:

$$\min_{\mathbf{c}} F(\mathbf{c}) \quad (5.1)$$

where the function is defined as follows:

$$F(\mathbf{c}) = \|R_\lambda(\mathbf{c}) - r_\lambda\|_2^2 \quad (5.2)$$

where \mathbf{c} is a colorant combination for m colorants with the following constraints:

$$\mathbf{c} = [c_1 \dots c_m]^T, c_i \in [0, 1] \text{ for } i = 1, \dots, m. \quad (5.3)$$

$R_\lambda(\mathbf{c})$ is the estimated spectral reflectance for a colorant combination \mathbf{c} according to the spectral Neugebauer equations and the Demichel equations, r_λ being the spectral reflectance we wish to reproduce. Ideally we are looking for a solution \mathbf{c} such that:

$$\frac{\delta F(\mathbf{c})}{\delta c_i} = 0 \text{ for } i = 0, \dots, m \quad (5.4)$$

and this is performed by an iterative process.

At each step of the iterative process a new colorant combination is obtained providing a closer estimation of r_λ . This new colorant combination is obtained after the calculation of a descent direction and a step length in the colorant space. The methods differ in the choice of the descent direction and step length calculation.

In all iterative process the search for the best colorant combination stops when the estimated spectral reflectance is close enough to the spectral reflectance to reproduce (i.e. $F(\mathbf{c})$ is minimum in Equation 5.1). Termination criteria should be set to stop the process: conditions to verify

between $F(\mathbf{c}^k)$ and $F(\mathbf{c}^{k+1})$ and between \mathbf{c}^k and \mathbf{c}^{k+1} . A last stop condition is when a maximum number of iteration is reached. We will propose a different approach which does not follow this scheme in Section 5.2.3.

For all the methods described the factor n can be taken in account under the assumption of affine multilinearity in $1/n$ space. All the spectral reflectance are then raised to the power $1/n$ such that:

$$R_\lambda(\mathbf{c}) \rightarrow R_\lambda^{1/n}(\mathbf{c}) \text{ and } r_\lambda \rightarrow r_\lambda^{1/n} \quad (5.5)$$

5.2.1 Inversion by linear regression iteration (LRI)

The LRI method is an iterative method presented by Urban and Grigat (2006) which is based on Powel (1964) method. A loop on the colorant is done where a new colorant value is computed one after the other taking in account the previous new colorant value. A direction search and step length is computed for each colorant in the loop. If we are in a three colorant case, at each iteration the loop will provide three directions and steps.

For each colorant the function in Equation 5.1 is assumed to be single variable dependent, i.e. dependent of one colorant c_j . Assuming that we can see that:

$$R_\lambda(\mathbf{c}) = A_{\lambda,j} c_j + B_{\lambda,j}, \quad (5.6)$$

where $A_{\lambda,j}$ and $B_{\lambda,j}$ hold:

$$\frac{\delta A_{\lambda,j}}{\delta c_j} = \frac{\delta B_{\lambda,j}}{\delta c_j} = 0, \quad (5.7)$$

we then want to solve the following problem:

$$\min_{c_j} \|A_{\lambda,j} c_j + B_{\lambda,j} - r_\lambda\|_2^2, \quad (5.8)$$

where the spectral reflectances put in a discret form allow to calculate the optimal c_j^{\min} by calculating:

$$c_j^{\min} = \frac{\mathbf{A}_j^T(\mathbf{r} - \mathbf{B}_j)}{\mathbf{A}_j^T \mathbf{A}_j} \quad (5.9)$$

The descent direction of the k th iteration step is:

$$p_k := \frac{c_j^{\min} - c_j}{|c_j^{\min} - c_j|} \quad (5.10)$$

and for the optimal step length,

$$\alpha_k := |c_j^{\min} - c_j| \quad (5.11)$$

giving the new colorant value:

$$c^{k+1} = c^k + \alpha_k p_k. \quad (5.12)$$

To start a guess start has to be set for the colorant value $\mathbf{c} = [0.5 \dots 0.5]^T$ for example. The iteration stops when a limit on the number of iterations has been reached or a termination criterion has satisfied. Here also Various criteria can be set to decide if the inversion process should stop before reaching a maximum number of iteration.

5.2.2 Inversion with a constraint minimization routine (CMR)

With the use of Matlab and the function *fmincon* from the optimization toolbox it is easy to implement inversion method with a cost function as Taplin and Berns (2001) did it. This function uses a sequential quadratic programming (SQP) method: the function solves a quadratic programming (QP) subproblem at each iteration (Gill et al., 1981). The cost function returning as output the difference between the spectral reflectance to reproduce and the spectral reflectance

estimated by the Neugebauer equation. The cost function takes as input a colorant combination and integrates the Demichel equations.

This technique allows to set a limit on colorant coverage when we invert the NG equations for more than 3 inks. A cost function, returning here the spectral RMS between a target and its estimation by the NG equations, will be evaluated at each iteration. Each iteration brings new colorant values.

5.2.3 Optimal inversion of the weights (WI)

We introduce here the method we propose. A spectral reflectance resulting from a colorant combination is the weighted summation of all the color the printer can produce, i.e. the spectral reflectance of a colorant combination is the weighted summation of the Neugebauer primaries of the printer. The weights of the Neugebauer primaries being the area they cover on the paper and the statistic Demichel model makes an estimation of the Neugebauer primaries coverage based on the colorant combination. In an ideal and optimal case we could estimate accurately a spectral reflectance if we could control the Neugebauer primaries directly. In this technique we first invert the problem in Equation 5.1 by solving the following problem for the weights:

$$\min_{\mathbf{w}} F(\mathbf{w}) \quad (5.13)$$

where the function is defined as follows:

$$F(\mathbf{w}) = \|\mathbf{P}\mathbf{w} - \mathbf{r}\|_2^2 \quad (5.14)$$

where \mathbf{r} is the spectral reflectance we want to reproduce, \mathbf{P} are the Neugebauer primaries and \mathbf{w} is a set of weights with the following constraints:

$$\sum_{j=0}^{2^m-1} w_j = 1 \text{ and } 0 \leq w_j \leq 1 \quad (5.15)$$

for m colorants. We solve this quadratic problem by optimization technique using the previously introduced constraints. And reminding the Demichel equations (see Section 3.3.1) we can write that the set of weights \mathbf{w} can be obtain by doing for a m colorants combination:

$$\mathbf{w}_{(m)} = \mathbf{M}_{(m)} \mathbf{c}_{(m)}, \quad (5.16)$$

and in a 3 colorants example:

$$\mathbf{w}_{(3)} = \mathbf{M}_{(3)} \mathbf{c}_{(3)}, \quad (5.17)$$

with the weights arranged as follows:

$$\mathbf{w}_{(3)} = [w_0 \ w_1 \ w_2 \ w_3 \ w_{12} \ w_{23} \ w_{13} \ w_{231}]^T, \quad (5.18)$$

where

$$\mathbf{M}_{(3)} = \begin{bmatrix} 1 & -1 & -1 & -1 & 1 & 1 & 1 & -1 \\ 0 & 1 & 0 & 0 & -1 & -1 & 0 & 1 \\ 0 & 0 & 1 & 0 & -1 & 0 & -1 & 1 \\ 0 & 0 & 0 & 1 & 0 & -1 & -1 & 1 \\ 0 & 0 & 0 & 0 & 1 & 0 & 0 & -1 \\ 0 & 0 & 0 & 0 & 0 & 1 & 0 & -1 \\ 0 & 0 & 0 & 0 & 0 & 0 & 1 & -1 \\ 0 & 0 & 0 & 0 & 0 & 0 & 0 & 1 \end{bmatrix} \quad (5.19)$$

and

$$\mathbf{c}_{(3)} = [1 \ c_1 \ c_2 \ c_3 \ c_1c_2 \ c_2c_3 \ c_1c_3 \ c_1c_2c_3]^T. \quad (5.20)$$

and we estimate the values $\mathbf{c}_{(\mathbf{m})}$ in a quadratic form as follows:

$$\mathbf{c}'_{(\mathbf{m})} = \text{pinv}(\mathbf{M}_{(\mathbf{m})})\mathbf{w}_{(\mathbf{m})} \quad (5.21)$$

where $\text{pinv}(\mathbf{M}_{(\mathbf{m})})$ is the pseudo-inverse of $\mathbf{M}_{(\mathbf{m})}$. Finally extracting the elements 2 to $m + 1$ of the vector $\mathbf{c}'_{(\mathbf{m})}$ we should obtain a colorant combination which satisfies the Neugebauer model, e.g. in a 3 colorants example we will extract the elements $c'_{(3),2}$, $c'_{(3),3}$ and $c'_{(3),4}$ of $\mathbf{c}'_{(3)}$.

Put into the Neugebauer model the colorant combination will not always provide a good approximation of the spectral reflectance \mathbf{r} to reproduce since the statistic Demichel model is not completely taken into account. In this inversion it is assumed that Neugebauer model works fine and describes accurately the printer behavior. But the relation between the c_j and the matrix $\mathbf{M}_{(\mathbf{m})}$ is not considered as constraint in the first inversion for the weights (see Equation 5.14), each candidate playing the same role in the quadratic form, in other words the NP are considered to be independent from each other to solve this problem. The experiments in the following sections will reveal drawback and advantage of the this method.

This method could be efficient if we could avoid the pseudo-inverse in the second step of the inversion WI and then use directly NP values to control the printer (i.e. to use the weights as printer control values). This is of course tricky since printing system are controlled by colorant values.

Also this technique can be use as a spectral gamut mapping algorithm. It provides the best spectral decomposition of spectral reflectance for the spectral NP of a printer. This gamut mapping approach will be developed and illustrated in Appendix B.2.

5.3 Comparison of inversion methods

5.3.1 Experiment

We have compared the three methods LRI, CMR and WI we test them on two sets of data: one is in the spectral gamut of the printer and a second from which we do not know if the data are in the spectral gamut. The Neugebauer primaries (NP) of our seven colorants printer have been printed with the Epson 2100 Photo Stylus inkjet printer on Epson photo paper, such printer can produce $2^7 = 128$ NP. In Fig. 5.1 (a) are displayed the spectral reflectances of NP.

A grid in colorant space is created such that $c \in \{0 0.25 0.5 0.75 1\}^7$ and only the patches for which the colorant summation is smaller than 300% are kept, this to take in account the printer ink limitation. The created grid is made of 19980 patches from which a subset of 1000 patches is selected (approximatively one patch every 20 is selected from the our grid). The spectral Neugebauer model is then used to simulate the print of the subset. Inversion is then performed on the printed patches.

We also use the MacBeth ColorChecker test chart to test the inversion methods. Inversion are performed first on the test chart and secondly inversion is performed on gamut mapped ColorChecker. To gamut map the test chart to the spectral printer gamut we inverse the Neugebauer model for the weights only, this given an estimation of the best estimated spectral reflectances the printer can produce. Differences between the original spectral reflectances of the ColorChecker and their gamut mapped version are displayed in Fig. 5.1 (b).

5.3.2 Results and discussion

Once the inversion methods have been tested on the different test charts the calculated colorant combinations are used to simulated the reproduction. You can see in Table 5.1 the results for the grid, in Table 5.2 for the ColorChecker and Table 5.3 for the gamut mapped ColorChecker.

We can observe that all inversion methods give good results for the grid. These good results can be explain by the nature of the created test chart, we know that solution exist since it was simulated by the spectral Neugebauer model and the data are in the spectral gamut of the printer.

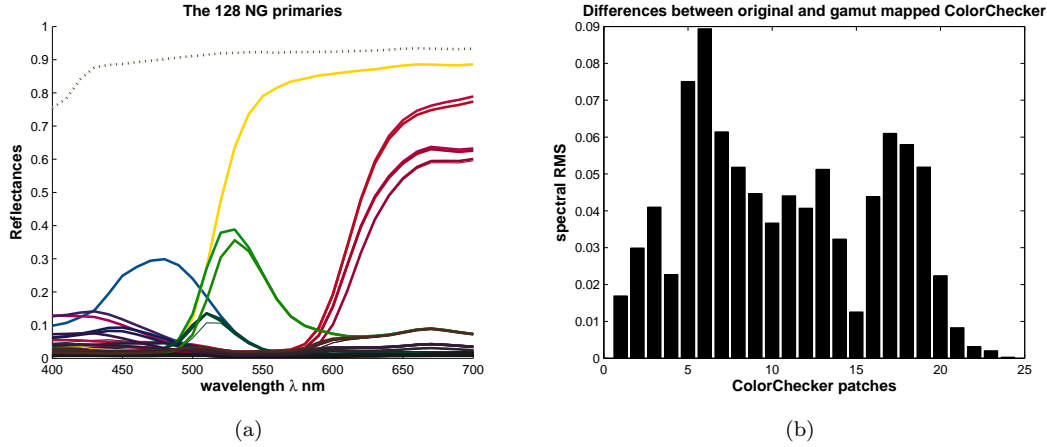


Figure 5.1: Spectral reflectances of the 128 NPs in (a) and spectral differences between the ColorChecker spectral reflectances and its gamut mapped version in (b).

For the ColorChecker test chart the CMR method gives the best performance following by the LRI method and behind the WI method. The CMR method is closer to spectral Neugebauer model than the LRI method maybe due to the added constraint on the total colorant coverage allowed by colorant combination. This can explain the better performance of the CMR method.

We have seen that the WI method works well if the data to invert are following closely what the spectral Neugebauer describes. So in case of random spectral data, data in or out the printer gamut performance of this method are poor but only because it considers an ideal case were we could control directly the NP.

The WI method has been used for performing spectral gamut mapping, only the first step of the inversion given the best weights has been used for this task. We can see that the differences between the gamut mapped data and their reproduction become smaller for the CMR and LRI methods after spectral gamut mapping.

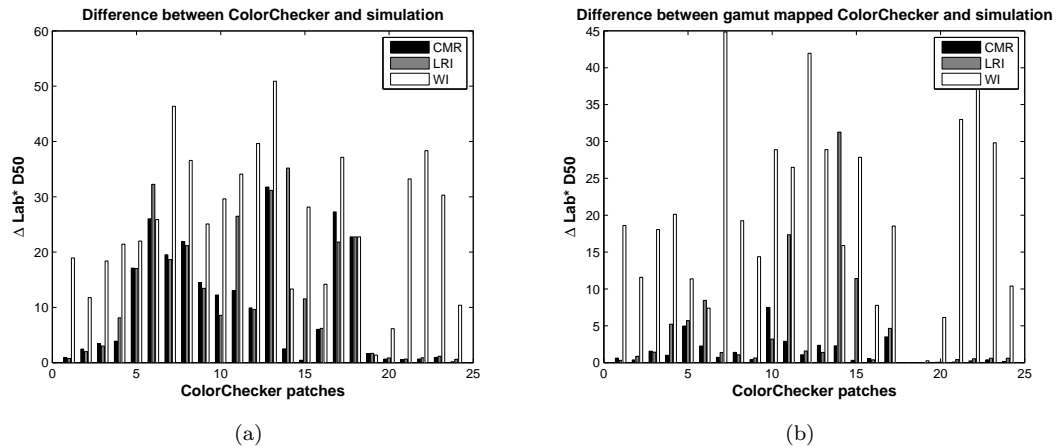


Figure 5.2: ΔE^*_{ab} differences between ColorChecker and inversion by CMR, LRI and W method for illuminant D50 in (a) and difference between gamut mapped ColorChecker and inversion by CMR, LRI and W method for illuminant D50 in (b).

Table 5.1: ΔE_{ab}^* and sRMS differences between the **grid** in colorant space and its reproduction with the colorant combination obtained from the CMR, LRI and WI inversion methods.

		ΔE_{ab}^*				
		A	D65	D50	FL1	sRMS
CMR	Av.	0.43	0.46	0.46	0.54	0.001
	Std	1.29	1.54	1.48	1.53	0.001
	Max	30.14	36.58	34.96	35.71	0.023
LRI	Av.	2.24	2.41	2.39	2.92	0.005
	Std	3.29	3.68	3.62	4.46	0.006
	Max	32.44	36.81	36.14	39.09	0.053
WI	Av.	1.38	1.37	1.38	1.25	0.005
	Std	3.63	3.61	3.64	3.31	0.013
	Max	34.84	35.45	35.27	36.80	0.146

Table 5.2: ΔE_{ab}^* and sRMS differences between the **ColorCecker** and its reproduction with the colorant combinations obtained from the CMR, LRI and WI inversion methods.

		ΔE_{ab}^*				
		A	D65	D50	F11	sRMS
CMR	Av.	8.82	10.49	10.01	10.05	0.040
	Std	8.66	10.97	10.22	10.17	0.025
	Max	24.62	35.44	31.75	32.86	0.097
LRI	Av.	10.77	12.84	12.31	12.03	0.045
	Std	9.85	12.06	11.41	10.85	0.026
	Max	33.09	35.60	35.19	32.18	0.100
WI	Av.	25.07	25.91	25.66	25.88	0.105
	Std	12.35	12.95	12.62	13.47	0.055
	Max	48.68	53.20	50.90	53.46	0.271

Table 5.3: ΔE_{ab}^* and sRMS differences between the **gamut mapped ColorChecker** and its reproduction with the colorant combinations obtained from the CMR, LRI and WI the inversion methods.

		ΔE_{ab}^*				
		A	D65	D50	F11	sRMS
CMR	Av.	1.29	1.51	1.45	1.51	0.005
	Std	1.64	1.91	1.81	1.94	0.004
	Max	6.64	7.94	7.50	8.10	0.016
LRI	Av.	3.55	4.26	4.11	3.91	0.014
	Std	6.27	7.30	7.16	6.44	0.017
	Max	27.85	31.72	31.27	27.66	0.063
WI	Av.	19.93	19.91	19.98	20.28	0.091
	Std	12.49	12.37	12.40	12.90	0.061
	Max	45.65	44.16	44.86	46.75	0.271

5.4 Comparison of color reproduction and spectral color reproduction

In this section we want to evaluate how metamerism is reduced by spectral color reproduction, how better a spectral print is compared to a colorimetric print. The type of reproduction for a spectral data to be printed is defined by the colorant separation process. The colorant separation is based on the inversion of the spectral Neugebauer printer model, it is an optimization process in which a criterion is minimized. The choice of criterion defines the type of print.

We use the CMR method described in Section 5.2.2 to perform the colorant separation. This method allows to set easily different criteria for the optimization. Once inverted the colorant separation provides a colorant combination to control the printer. This colorant combination is used in our experiment to simulate the reproduction of the spectral data.

In the following section are presented the different criteria we have tested: single color difference, average color difference for a set of illuminant, spectral difference and a combination of color difference and spectral difference. All colorant separation start from a spectral reflectance, colorimetric values under given illuminant are calculated only when a criterion requires it.

5.4.1 Color reproduction by single color difference

In order to perform a colorimetric print of a spectral reflectance we minimize the CIE 1976 CIELAB color difference as optimization criterion:

$$\Delta E_{ab}^* = \sqrt{(L_1 - L_2)^2 + (a_1 - a_2)^2 + (b_1 - b_2)^2} \quad (5.22)$$

where L_1 , a_1 , b_1 and L_2 , a_2 , b_2 are respectively the CIELAB values of the desired spectral reflectance and its estimated reproduction at each iteration.

Concretely the estimated spectral reflectance and the desired spectral reflectance are converted to CIELAB values at each iteration and the CIE 1976 CIELAB color difference calculated.

5.4.2 Color reproduction by average color difference

For this colorant separation we use as criterion an average colorimetric difference defines as follows:

$$\overline{\Delta E_{ab}^*(ill)} = \frac{1}{4} \times (\Delta E_{ab}^*(A) + \Delta E_{ab}^*(D65) + \Delta E_{ab}^*(D50) + \Delta E_{ab}^*(FL11)) \quad (5.23)$$

where we use illuminant A, D65, D50 and FL11 for the CIE 1976 CIELAB color difference.

5.4.3 Spectral color reproduction

In order to perform a spectral print of a spectral reflectance we minimize the spectral root mean square difference as optimization criterion:

$$sRMS = \sqrt{\frac{1}{N} \times (\mathbf{r}_1 - \mathbf{r}_2)^T \times (\mathbf{r}_1 - \mathbf{r}_2)} \quad (5.24)$$

where \mathbf{r}_1 and \mathbf{r}_2 are spectral reflectances in a vector column form of the desired spectral reflectance and its estimated reproduction respectively, N being the number of element describing a spectral reflectance. In our experiments spectral reflectances are made of $N = 31$ values from 400nm to 700nm spaced by 10nm.

5.4.4 Combining color reproduction and spectral color reproduction

This criterion combines the CIE 1976 CIELAB color difference for a given illuminant and a spectral difference sRMS as follows:

$$\text{diff} = \alpha \times \Delta E_{ab}^*(ill) + (1 - \alpha) \times \text{sRMS} \quad (5.25)$$

where the parameter α allows to vary the importance on the colorimetric difference or spectral difference. $\alpha = 0$ corresponds to Equation 5.22 (i.e. a colorimetric print) and $\alpha = 1$ to Equation 5.24 (i.e. a spectral print). For this criterion the sRMS difference is scaled such that it varies in the same range of values as for the CIE1976 difference.

5.4.5 Experiment

The prints are simulated for two multi-colorant printers: one with six artificial inks and a second with seven inks printed and measured. In Figure 5.3 (a) are presented the $2^6 = 64$ NP of the six colorants printer and in Figure 5.3 (b) are presented the $2^7 = 128$ NP of our seven colorants printer.

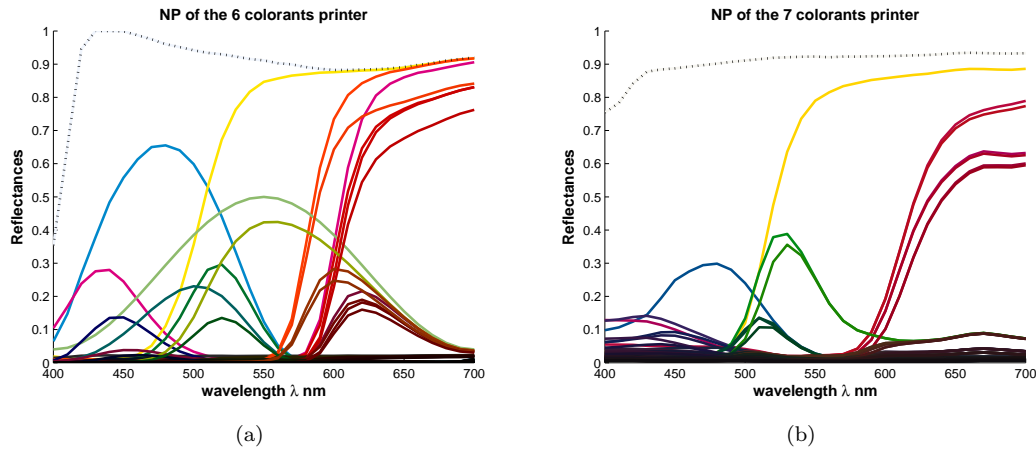


Figure 5.3: Neugebauer primaries spectral reflectances of our printing systems, in (a) for the six colorants printer and in (b) for the seven colorants printer.

To test our approaches of reproduction of spectral data we perform the colorant separation on two kinds of data: spectral reflectance in the printer gamut and spectral data mapped to the printer gamut.

Two grids in the colorant space of both printers are created. Their prints are simulated and Gaussian noise is added with $\sigma = 0.05$ to the obtained spectral reflectances. We keep for our experiments the colorant combinations for a maximum of 300% per patch in the grids. These spectral data are assumed to be in the spectral gamut of their respective printer.

The Esser test chart and the ColorChecker MacBeth test chart are gamut mapped to both spectral printer gamuts. Colorant separation is then tested on these gamut mapped spectral reflectances. These data are assumed to be in the printer gamut or at least on the surface of the gamut.

For all test charts the same series of colorant separations are performed according to the four criteria to minimize presented in the previous sections: colorant separation for color print under one illuminant, colorant separation for color print for more than one illuminant condition, colorant separation for spectral print and colorant separation combining colorimetric and spectral print.

5.4.6 Results and discussion

The results for the colorant separations minimizing a color difference, an average color difference and a spectral difference are shown in Table 5.4, 5.5 and 5.6 for the six colorants printer, in Table 5.7, 5.8 and 5.9 for the seven colorants printer.

The results for the colorant separation combining color print and spectral print with a parameter α are displayed in the Figures 5.4, 5.5 and 5.6 for the six colorants printer, in the Figures 5.7, 5.8 and 5.9 for the seven colorants printer. It has to be noted that for $\alpha = 0$ and $\alpha = 1$ the previously introduced graphs correspond to the results in the firstly introduced Table of results. $\alpha = 0$ is equivalent to a colorimetric print and $\alpha = 1$ is equivalent to a spectral print.

The results we obtain show that a colorimetric print produces a smaller color difference under the used illuminant than for a spectral print, but with the inverse observation for the spectral difference with spectral print comparing to the colorimetric print (for all tested illuminant). For the colorimetric print a peak of performance is reached when we look at the $\Delta E_{ab}^*(ill)$ for the illuminant chosen for the colorant separation. At the opposite the spectral print brings more homogeneous color difference, each illuminant is treated equally.

An interesting result is obtained for the colorant separation using a weighted sum of CIE 1976 CIELAB color difference: here also the color differences are homogeneous in the four tested illuminant and smaller than for a spectral print except for the spectral difference. By adding more than one illuminant in the colorant separation we avoid to emphasize on one illuminant and we reduce the metamerism effect. Adding more illuminant in the colorant separation (in order to take into account various illuminant condition) improves the colorimetric print. Also it is complicated to add all illumination conditions as parameter in the colorant separation except using a spectral difference in the separation. But looking at the two groups of lines in each table of results for $\Delta E_{ab}^*(ill)$ and sRMS we can deduce that it exists a combination of color difference and spectral difference in the colorant separation which reduce both the CIE 1976 CIELAB color difference homogeneously and the sRMS.

The colorant separation involving a weighted sum of ΔE_{ab}^* and sRMS (see Equation 5.25) allows us to investigate for colorant combination minimizing both metrics. The graphs representing the CIE 1976 CIELAB color difference and sRMS versus the weight parameter α shows some areas where both metrics seem to decrease, see Figure 5.4 (a) to (e) and Figure 5.7 (a) to (e) for the simulated grid in the printer colorant space. The results are a bit different for the two other test charts since they are not created by the printers inks. But we can still observe that the sRMS difference is also decreasing when more weight is put on it and this with area of almost constant ΔE_{ab}^* , see Figure 5.5 (a) to (e).

Table 5.4: ΔE_{ab}^* and sRMS differences between the **grid** for the six colorants printer and their simulated prints after colorant separations minimizing $\Delta E_{ab}^*(ill)$ color difference (for illuminant A, D65, D50 and FL11), minimizing $\overline{\Delta E_{ab}^*(ill)}$ (for the previously mentioned illuminants) and colorant separation minimizing the spectral sRMS difference.

Criterion	ΔE_{ab}^*				sRMS	
	A	D65	D50	F11		
$\Delta E_{ab}^*(A)$	Av.	0.08	1.27	0.94	1.60	0.014
	Std	0.84	1.60	1.31	1.64	0.016
	Max	14.02	16.08	15.49	15.93	0.117
$\Delta E_{ab}^*(D65)$	Av.	1.05	0.05	0.34	1.43	0.015
	Std	1.12	0.53	0.55	1.25	0.017
	Max	10.74	12.45	11.88	14.21	0.093
$\Delta E_{ab}^*(D50)$	Av.	0.77	0.36	0.06	1.37	0.014
	Std	0.95	0.77	0.70	1.25	0.015
	Max	11.99	13.44	13.06	14.21	0.112
$\Delta E_{ab}^*(F11)$	Av.	1.59	1.49	1.43	0.04	0.018
	Std	1.33	1.19	1.11	0.36	0.019
	Max	8.14	7.11	6.65	7.52	0.109
$\overline{\Delta E_{ab}^*(ill)}$	Av.	0.19	0.13	0.10	0.46	0.003
	Std	0.85	0.88	0.85	1.01	0.006
	Max	14.02	16.08	15.49	14.79	0.071
sRMS	Av.	0.31	0.34	0.33	0.56	0.001
	Std	0.86	0.97	0.94	0.84	0.001
	Max	19.21	22.68	21.81	15.34	0.011

Table 5.5: ΔE_{ab}^* and sRMS differences between the **mapped Esser test chart** for the six colorants printer and their simulated prints after colorant separations minimizing $\Delta E_{ab}^*(ill)$ color difference (for illuminant A, D65, D50 and FL11), minimizing $\overline{\Delta E_{ab}^*(ill)}$ (for the previously mentioned illuminants) and colorant separation minimizing the spectral sRMS difference.

Criterion	ΔE_{ab}^*				sRMS	
	A	D65	D50	F11		
$\Delta E_{ab}^*(A)$	Av.	0.50	1.90	1.53	1.36	0.018
	Std	1.46	1.87	1.70	1.42	0.013
	Max	9.03	12.76	11.47	8.93	0.085
$\Delta E_{ab}^*(D65)$	Av.	1.64	0.53	0.84	1.46	0.019
	Std	1.49	1.64	1.51	1.47	0.015
	Max	9.04	12.09	11.03	7.34	0.091
$\Delta E_{ab}^*(D50)$	Av.	1.34	0.87	0.53	1.37	0.019
	Std	1.35	1.58	1.59	1.31	0.014
	Max	8.70	12.14	10.98	7.13	0.091
$\Delta E_{ab}^*(F11)$	Av.	1.36	1.68	1.52	0.50	0.020
	Std	1.47	1.92	1.75	1.40	0.015
	Max	9.44	12.28	11.60	8.57	0.096
$\overline{\Delta E_{ab}^*(ill)}$	Av.	0.96	0.80	0.60	0.87	0.012
	Std	1.50	1.74	1.69	1.45	0.013
	Max	9.21	12.20	11.25	8.85	0.090
sRMS	Av.	1.57	1.97	1.85	1.73	0.007
	Std	2.27	2.55	2.46	2.38	0.006
	Max	14.84	16.14	15.84	14.84	0.046

Table 5.6: ΔE_{ab}^* and sRMS differences between the **mapped ColorChecker test chart** for the six colorants printer and their simulated prints after colorant separations minimizing $\Delta E_{ab}^*(ill)$ color difference (for illuminant A, D65, D50 and FL11), minimizing $\overline{\Delta E_{ab}^*(ill)}$ (for the previously mentioned illuminants) and colorant separation minimizing the spectral sRMS difference.

Criterion	ΔE_{ab}^*				sRMS
	A	D65	D50	F11	
$\Delta E_{ab}^*(A)$	Av.	0.18	1.60	1.22	0.94
	Std	0.56	1.14	0.90	0.81
	Max	2.51	3.86	2.83	3.29
$\Delta E_{ab}^*(D65)$	Av.	1.69	0.22	0.65	1.51
	Std	1.00	0.69	0.63	1.18
	Max	4.02	2.50	2.61	4.16
$\Delta E_{ab}^*(D50)$	Av.	1.25	0.66	0.22	1.36
	Std	0.82	0.64	0.70	1.11
	Max	2.78	2.52	2.59	3.93
$\Delta E_{ab}^*(F11)$	Av.	1.08	1.45	1.27	0.17
	Std	0.82	1.19	0.94	0.52
	Max	3.46	3.74	2.86	2.14
$\overline{\Delta E_{ab}^*(ill)}$	Av.	0.65	0.50	0.30	0.57
	Std	0.75	0.72	0.70	0.71
	Max	2.56	2.52	2.60	2.15
sRMS	Av.	1.25	1.58	1.48	1.34
	Std	1.40	1.76	1.63	1.36
	Max	4.71	5.75	5.69	4.47

Table 5.7: ΔE_{ab}^* and sRMS differences between the **grid** for the seven colorants printer and their simulated prints after colorant separations minimizing $\Delta E_{ab}^*(ill)$ color difference (for illuminant A, D65, D50 and FL11), minimizing $\overline{\Delta E_{ab}^*(ill)}$ (for the previously mentioned illuminants) and colorant separation minimizing the spectral sRMS difference.

Criterion	ΔE_{ab}^*				sRMS
	A	D65	D50	F11	
$\Delta E_{ab}^*(A)$	Av.	0.02	0.88	0.64	0.82
	Std	0.31	0.89	0.69	0.67
	Max	8.94	13.94	12.35	9.70
$\Delta E_{ab}^*(D65)$	Av.	0.76	0.00	0.23	0.93
	Std	0.67	0.05	0.19	0.73
	Max	4.15	1.23	1.46	6.66
$\Delta E_{ab}^*(D50)$	Av.	0.53	0.22	0.00	0.81
	Std	0.48	0.19	0.04	0.63
	Max	2.87	1.12	0.77	6.07
$\Delta E_{ab}^*(FL11)$	Av.	0.87	1.09	0.95	0.01
	Std	0.65	0.89	0.79	0.12
	Max	5.30	8.32	7.74	2.23
$\overline{\Delta E_{ab}^*(ill)}$	Av.	0.09	0.05	0.03	0.47
	Std	0.26	0.36	0.32	0.52
	Max	7.01	11.26	9.86	8.17
sRMS	Av.	0.32	0.34	0.34	0.66
	Std	0.37	0.38	0.38	0.59
	Max	4.01	3.60	3.50	4.15

Table 5.8: ΔE_{ab}^* and sRMS differences between the **mapped Esser test chart** for the seven colorants printer and their simulated prints after colorant separations minimizing $\Delta E_{ab}^*(ill)$ color difference (for illuminant A, D65, D50 and FL11), minimizing $\overline{\Delta E_{ab}^*(ill)}$ (for the previously mentioned illuminants) and colorant separation minimizing the spectral sRMS difference.

Criterion	ΔE_{ab}^*				sRMS	
	A	D65	D50	F11		
$\Delta E_{ab}^*(A)$	Av.	0.98	1.61	1.43	1.47	0.012
	Std	2.33	1.88	1.96	2.28	0.012
	Max	13.52	10.28	10.73	14.39	0.089
$\Delta E_{ab}^*(D65)$	Av.	1.64	0.93	1.13	1.47	0.013
	Std	2.26	1.90	1.98	2.17	0.012
	Max	12.41	9.71	10.58	12.68	0.069
$\Delta E_{ab}^*(D50)$	Av.	1.50	1.15	0.98	1.41	0.013
	Std	2.30	1.88	2.08	2.30	0.011
	Max	13.36	10.50	11.36	14.44	0.086
$\Delta E_{ab}^*(FL11)$	Av.	1.65	1.59	1.50	1.00	0.014
	Std	2.57	2.14	2.27	2.30	0.013
	Max	15.05	12.97	13.59	13.28	0.088
$\overline{\Delta E_{ab}^*(ill)}$	Av.	1.22	1.09	1.02	1.22	0.009
	Std	2.33	1.94	2.09	2.25	0.010
	Max	13.37	10.45	11.40	14.09	0.059
sRMS	Av.	1.95	2.11	2.07	2.14	0.006
	Std	3.74	3.34	3.47	3.51	0.012
	Max	41.41	33.06	35.97	30.11	0.174

Table 5.9: ΔE_{ab}^* and sRMS differences between the **mapped ColorCecker test chart** for the seven colorants printer and their simulated prints after colorant separations minimizing $\Delta E_{ab}^*(ill)$ color difference (for illuminant A, D65, D50 and FL11), minimizing $\overline{\Delta E_{ab}^*(ill)}$ (for the previously mentioned illuminants) and colorant separation minimizing the spectral sRMS difference.

Criterion	ΔE_{ab}^*				sRMS	
	A	D65	D50	F11		
$\Delta E_{ab}^*(A)$	Av.	0.41	1.29	1.03	0.85	0.011
	Std	0.86	0.97	0.84	0.76	0.007
	Max	3.29	3.38	2.98	2.95	0.031
$\Delta E_{ab}^*(D65)$	Av.	1.09	0.50	0.65	0.98	0.012
	Std	0.78	0.87	0.79	0.88	0.008
	Max	3.30	2.82	2.98	3.03	0.030
$\Delta E_{ab}^*(D50)$	Av.	0.89	0.68	0.47	0.85	0.012
	Std	0.76	0.79	0.86	0.89	0.008
	Max	3.30	2.83	2.98	2.98	0.030
$\Delta E_{ab}^*(FL11)$	Av.	0.86	1.18	0.99	0.43	0.011
	Std	0.86	1.04	1.00	0.86	0.008
	Max	3.40	3.47	3.12	2.88	0.033
$\overline{\Delta E_{ab}^*(ill)}$	Av.	0.75	0.74	0.65	0.78	0.009
	Std	1.23	1.25	1.27	1.15	0.009
	Max	5.04	5.35	5.22	4.37	0.031
sRMS	Av.	1.32	1.58	1.51	1.50	0.005
	Std	1.61	1.88	1.78	1.73	0.004
	Max	6.65	7.96	7.51	7.13	0.016

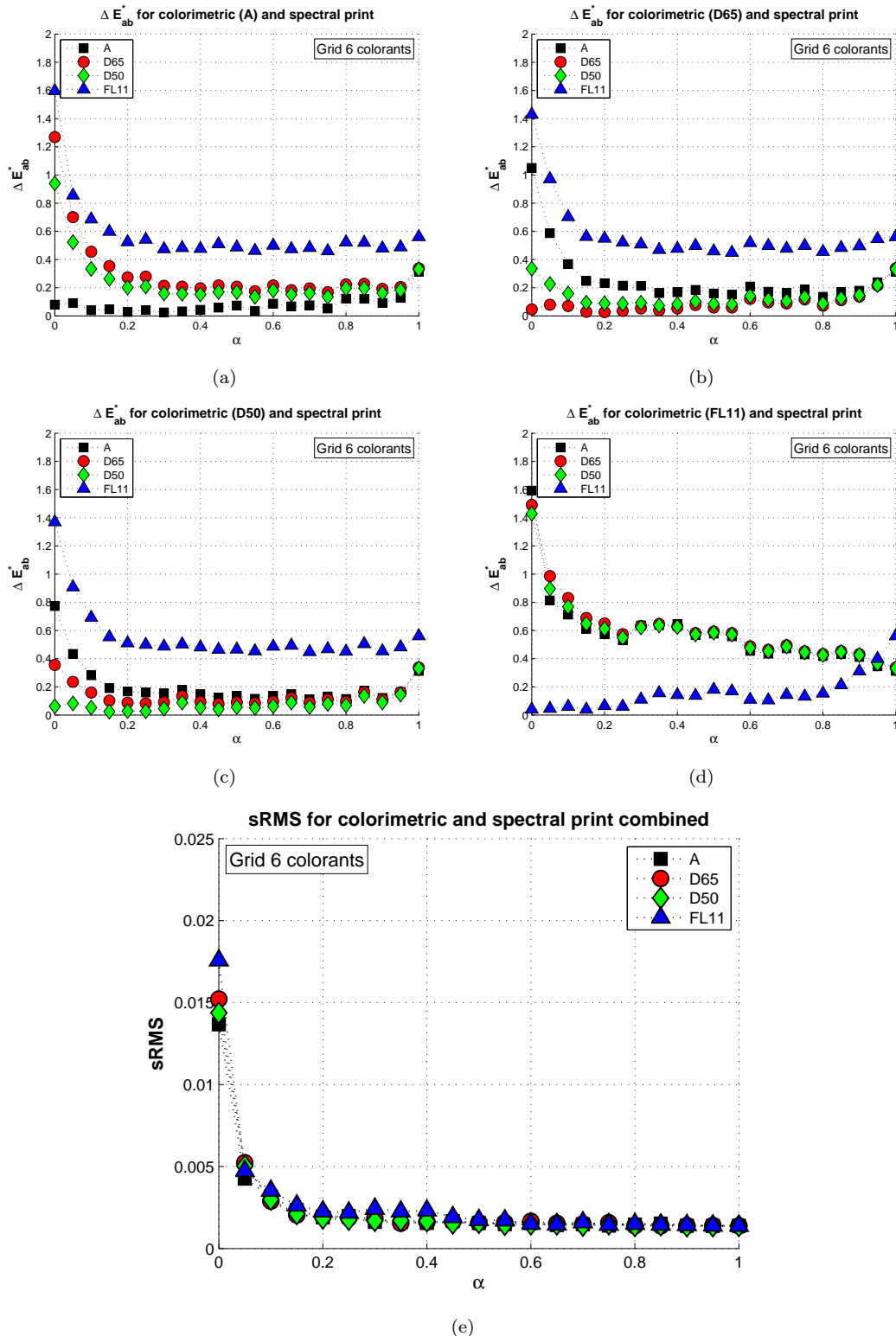


Figure 5.4: Colorimetric differences between the **grid** spectral reflectances and their simulated reproductions for the six colorants printer versus the **α parameter** for colorant separation combining the sRMS difference and one ΔE_{ab}^* color difference for illuminant A in (a), D65 in (b), D50 in (c) and FL11 in (d). In Figure (e) sRMS difference versus the **α parameter** for all four couple sRMS and ΔE_{ab}^* as in Figure (a) to (d).

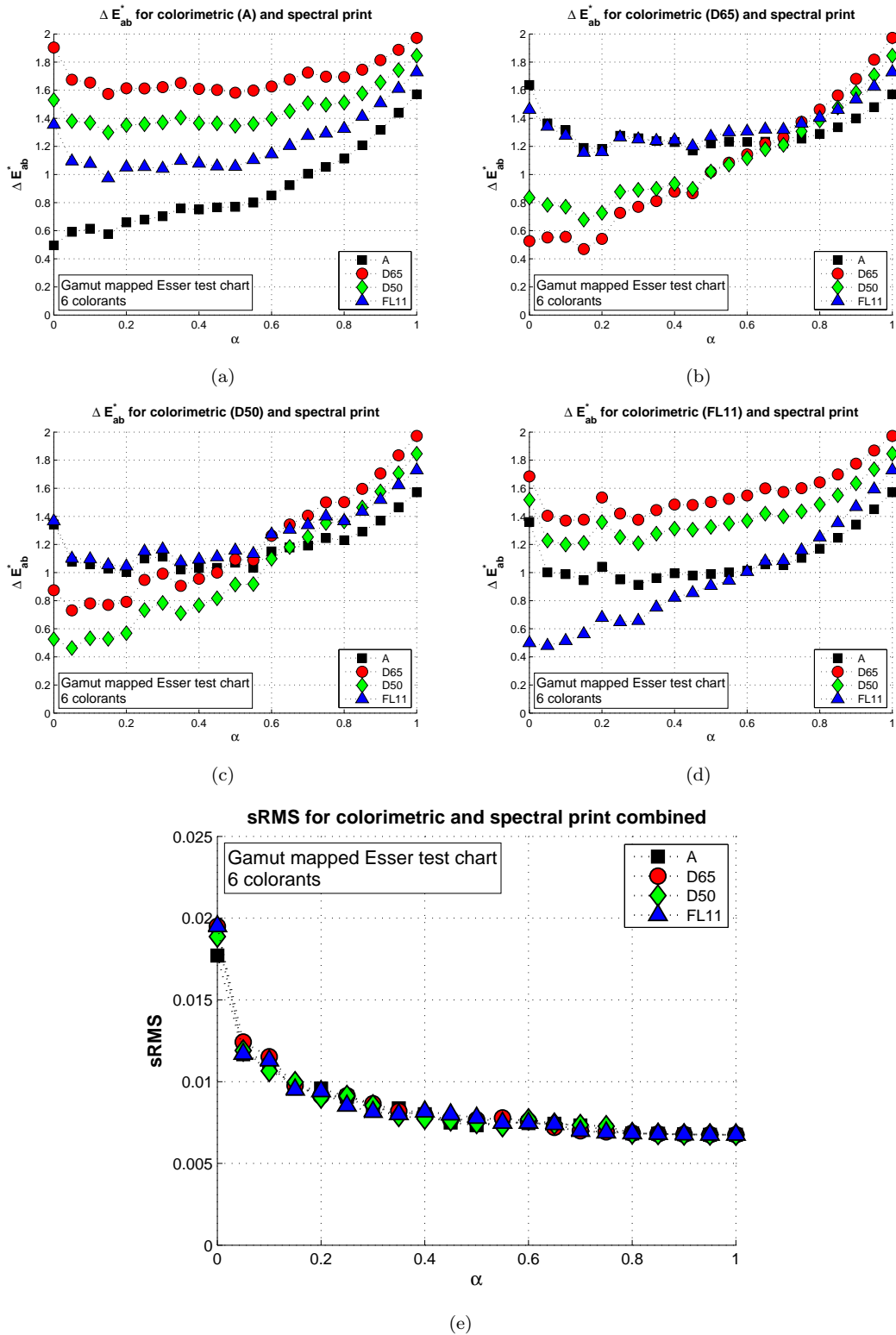


Figure 5.5: Colorimetric differences between the **mapped Esser test chart** spectral reflectances and their simulated reproductions for the six colorants printer versus the α **parameter** for colorant separation combining the sRMS difference and one ΔE_{ab}^* color difference for illuminant A in (a), D65 in (b), D50 in (c) and FL11 in (d). In Figure (e) sRMS difference versus the α **parameter** for all four couple sRMS and ΔE_{ab}^* as in Figure (a) to (d).

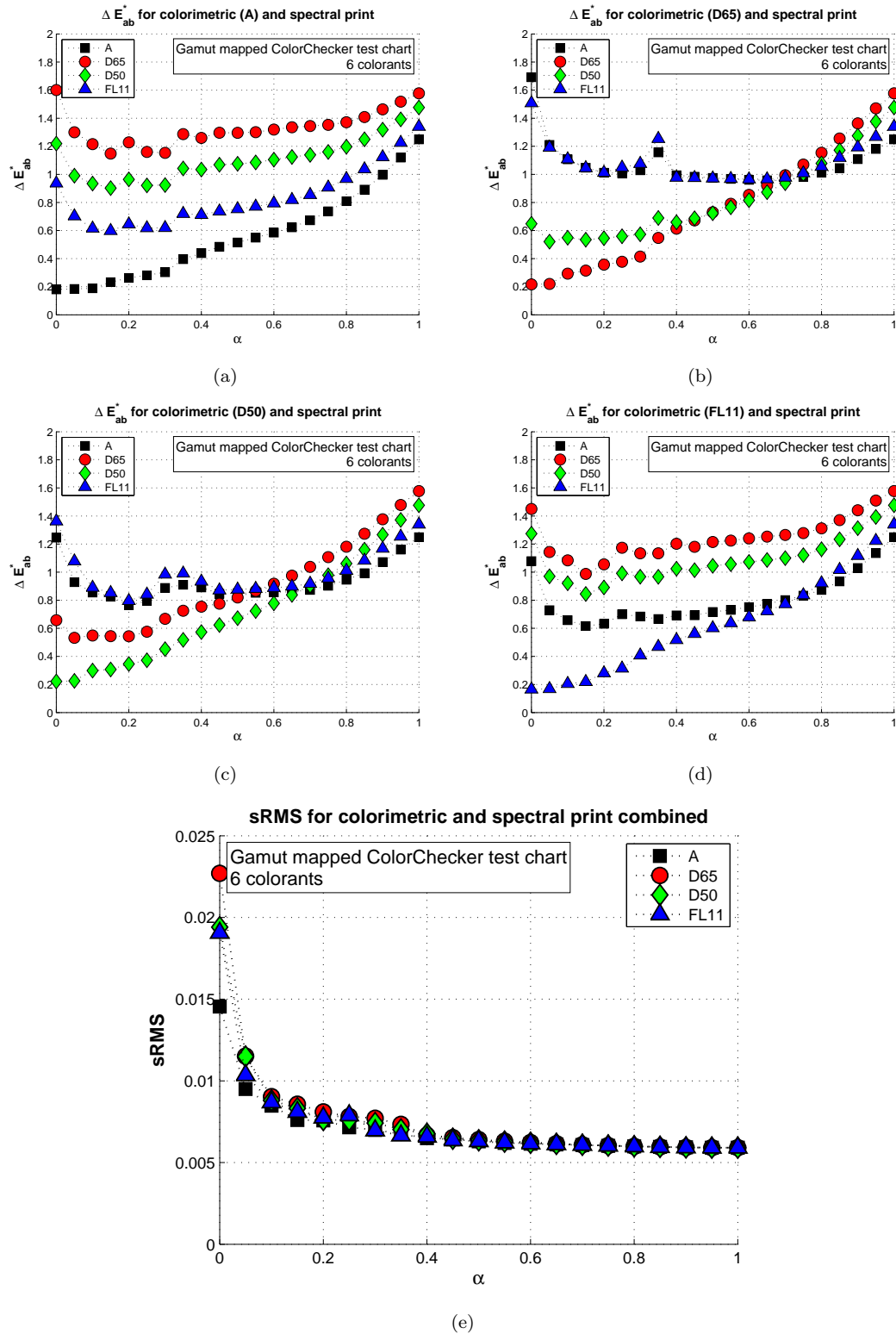


Figure 5.6: Colorimetric differences between the **mapped ColorChecker test chart** spectral reflectances and their simulated reproductions for the six colorants printer versus the α **parameter** for colorant separation combining the sRMS difference and one ΔE_{ab}^* color difference for illuminant A in (a), D65 in (b), D50 in (c) and FL11 in (d). In Figure (e) sRMS difference versus the α **parameter** for all four couple sRMS and ΔE_{ab}^* as in Figure (a) to (d).

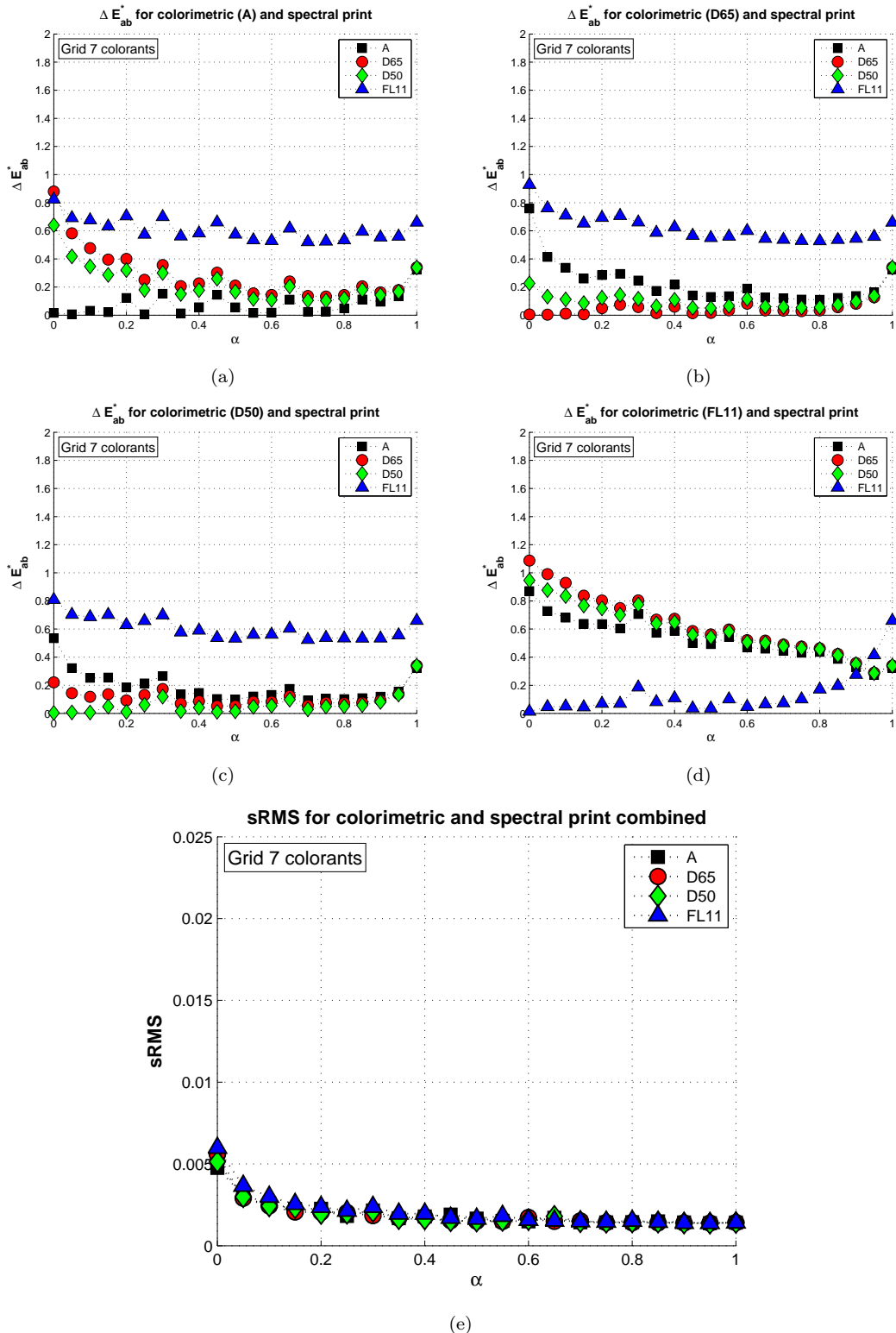


Figure 5.7: Colorimetric differences between the **grid** spectral reflectances and their simulated reproductions for the seven colorants printer versus the α **parameter** for colorant separation combining the sRMS difference and one ΔE_{ab}^* color difference for illuminant A in (a), D65 in (b), D50 in (c) and FL11 in (d). In Figure (e) sRMS difference versus the α **parameter** for all four couple sRMS and ΔE_{ab}^* as in Figure (a) to (d).

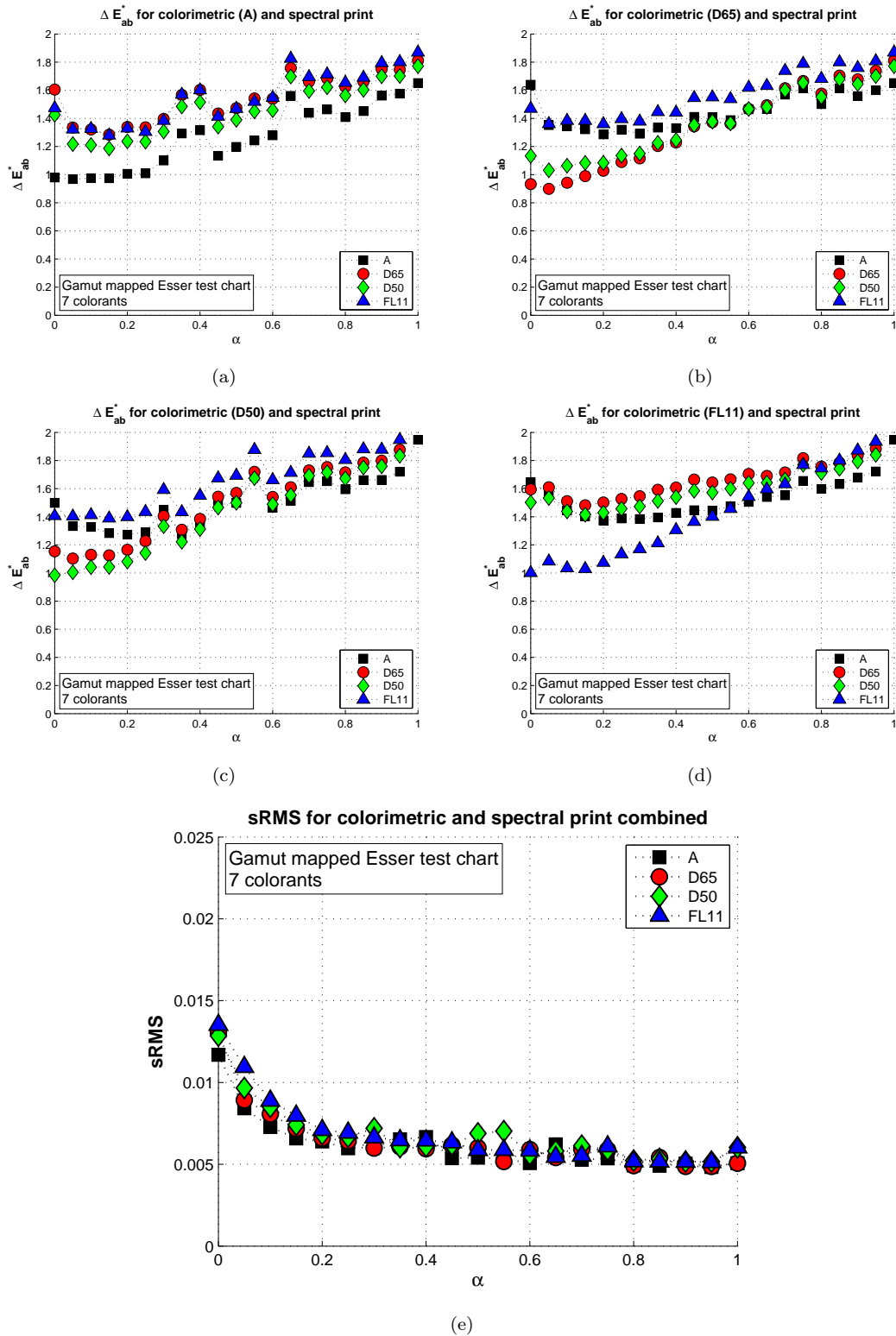


Figure 5.8: Colorimetric differences between the **mapped Esser test chart** spectral reflectances and their simulated reproductions for the seven colorants printer versus the α **parameter** for colorant separation combining the sRMS difference and one ΔE_{ab}^* color difference for illuminant A in (a), D65 in (b), D50 in (c) and FL11 in (d). In Figure (e) sRMS difference versus the α **parameter** for all four couple sRMS and ΔE_{ab}^* as in Figure (a) to (d).

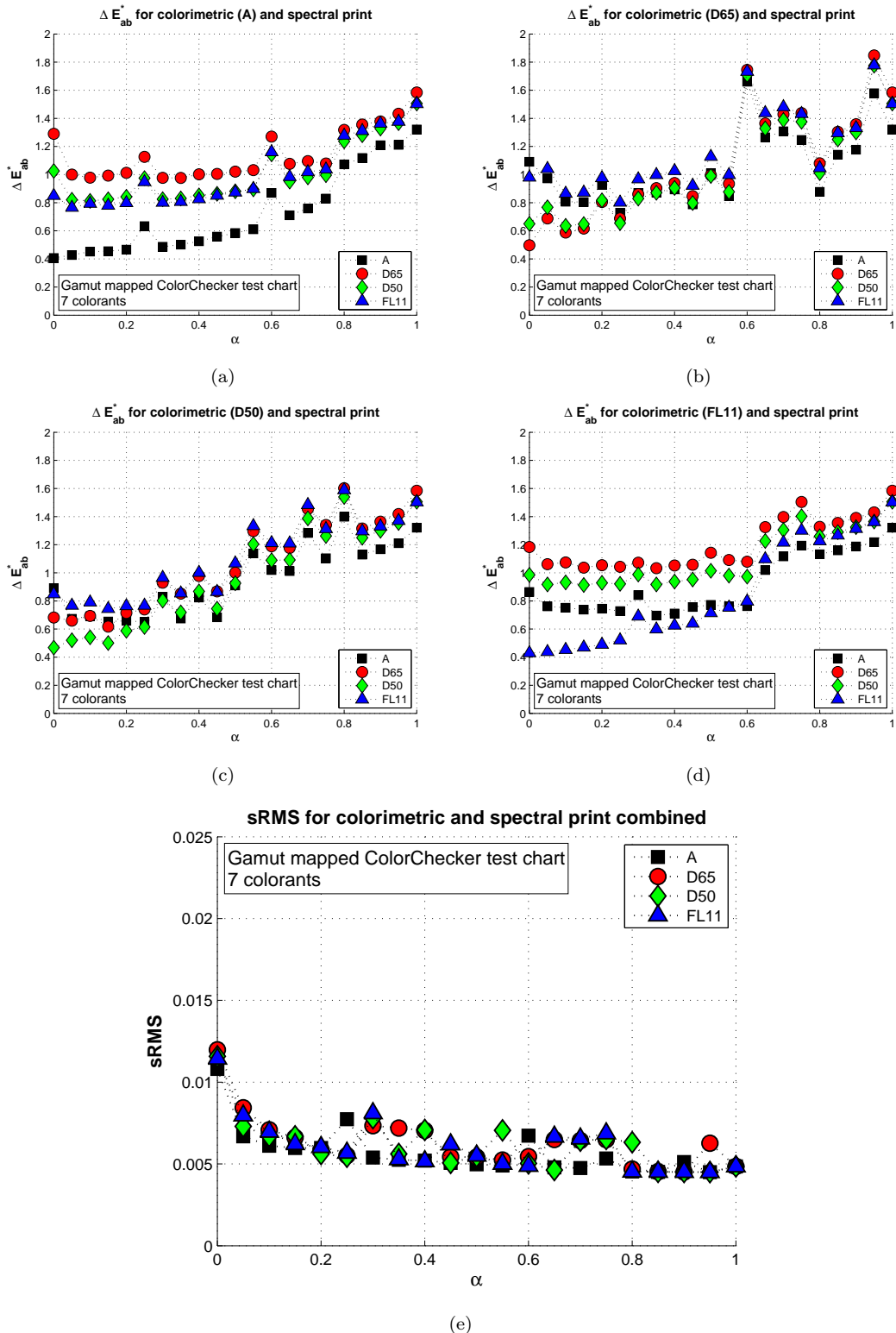


Figure 5.9: Colorimetric differences between the **mapped ColorChecker test chart** spectral reflectances and their simulated reproductions for the seven colorants printer versus the **α parameter** for colorant separation combining the sRMS difference and one ΔE_{ab}^* color difference for illuminant A in (a), D65 in (b), D50 in (c) and FL11 in (d). In Figure (e) sRMS difference versus the **α parameter** for all four couple sRMS and ΔE_{ab}^* as in Figure (a) to (d).

5.5 Conclusion

In this chapter we have presented various methods to invert the spectral Neugebauer equations. The linear regression iteration method (LRI), the constrained minimization routine method (CMR) and the weight inversion method (WI) can provide a colorant combination for given spectral reflectance to reproduce. All presented methods were using optimization techniques to calculate a colorant combination from a set of Neugebauer primaries (NP) and a spectral target, the CMR method allowing to specify easily the ink coverage limitation.

The study of inversion methods has shown that all perform well except for the WI method in case of data out of the printer gamut or data not created by the printer inks. The explanation of this difference of performance comes from the manner the Neugebauer equations are inverted. Both LRI and CMR methods integrate the Demichel equations during the inversion in the same order as for the forward printer model: first a colorant combination is chosen, then the Demichel equations estimate the weights of the NP for this colorant combination and the difference between the spectral target and its estimation is calculated. This order of operation insure that the calculated colorant combination are optimized for the spectral Neugebauer model. The WI method first calculates the weights for a spectral target and a set of NP and then deduces the colorant combination from the weights. Only the second part of this inversion assumes that the weights are following the Demichel model. The WI method inverts the printer model where no specific assumption is made on the interaction between the NP, i.e. the Demichel equations are not completely taken into account and this explain the differences of inversion performance.

In term of spectral color reproduction, a method who could control directly the NP should bring the best results. Such method can calculate a NP combination to reproduce a given spectral reflectance and this is what the WI method does in its first part: solving the Neugebauer equations for the weights. Unfortunately it is not possible to control directly the amount of the NP of a printer. But the inversion of the NP equations for the weights can be used as a pre-processing on the spectral data to print: we can use it as a spectral gamut mapping technique to map the data toward the printer gamut, the printer gamut being defined by their NP spectral reflectances.

Once the spectral data are mapped to the spectral printer gamut they are not anymore the original spectral data, but they are still spectral data. From that point we can compare the color reproduction and the spectral reproduction of these spectral data. We have said that the colorant separation was performed by inverting the spectral Neugebauer equations using optimization techniques. It is an iterative process in which a criterion is minimized: the type of criterion defines the type of print. We can for example minimize at each iteration the CIE 1976 CIELAB color difference under illuminant $D65$ for a colorimetric print instead of a sRMS difference for a spectral print.

The comparison of color reproduction and spectral color reproduction conducted in this chapter have shown better colorimetric or spectral difference regarding of the colorant separation chosen. We also combine these criteria for colorimetric and spectral print in order to gain advantage of both colorant separations and improving the performance in term of colorimetric and spectral differences. Looking at our results with the proposed approaches we can see a trade-off between first adding more ΔE_{ab}^* color differences in the colorant separation in order to include more illuminant conditions and second minimizing a spectral difference and one ΔE_{ab}^* color difference. To include an infinity of lighting condition should decrease both perceptual color difference homogeneously and the spectral difference, but it should also improve the spectral difference in that case for a given observer only. The combination of a ΔE_{ab}^* color difference and a spectral difference tends to be a good compromise for the reproduction of spectral data where the parameter α introduced in this colorant separation can be optimized regarding of the desired spectral data to reproduce.

In the spectral color reproduction workflow the colorant separation is the last step where we have control on the spectral data. For example a spectral image is now expressed as m colorant channels, but to be printed the image has to be halftoned, this operation is performed colorant channel by colorant channel. In order to keep working with spectral data as long as possible

and then to avoid loosing accuracy when computing the colorant combinations, the best will be to drive the printer with NP values directly and this is a complicated task. In the next chapter we will present an halftoning technique which allows to perform the colorant separation and the halftoning of a spectral image (or other spectral data) in one single operation.

Chapter 6

Spectral vector error diffusion

6.1 Introduction

In the previous chapters we have introduced the concept of spectral color reproduction and how to use a multi-colorant system to achieve a spectral color reproduction. Basically the workflow for spectral color reproduction is an adaptation of the workflow for color reproduction but with a change in the dimensionality of the data. The transformation applied to the spectral image for its reproduction will be: colorant separation to convert each pixel of our image in a combination of m colorants and halftoning by colorant channel. The first step involves an inverse printer model such as the spectral Neugebauer model (Wyble and Berns, 2000), this to establish a transformation between spectral reflectance and colorant combinations. In the second operation of halftoning the image is represented by m binary images; this operation is performed channel independently. In this chapter we propose a second approach to reproduce spectral image using the same multi-colorant system: to combine both colorant separation and halftoning in a single operation. We will halftone directly the spectral image in order transform the spectral image into a multi-binary colorant image in one operation called spectral vector error diffusion (sVED). Figure 6.1 presents the two approaches with the transformations applied to a spectral image for its reproduction. We can see that the sVED combines in one operation the colorant separation and halftoning operation.

Vector error diffusion (VED) is based on scalar error diffusion (SED) for the halftoning of color images: an input continuous tone value is set to 0 or 1 as output value by threshold and the difference (i.e. the error) between these two values is diffused into the image. Each pixel of an image is a vector of data expressing a color value in a color image or a spectral reflectance in a spectral image; sVED (Kouzaki et al., 1999; Kawaguchi et al., 1999) is an adaptation for spectral images of VED. In VED the error diffusion is similar to SED and identical filters can be used (Floyd and Steinberg, 1976; Jarvis et al., 1976) to diffuse the error: the output value is set to the binary colorant combination corresponding to a NP of which its spectral reflectance is the closest to the processed pixel spectral reflectance.

The sVED halftoning technique performs directly the transformation from spectral image to multi-binary colorant image. This technique only needs the spectral reflectances of the primaries the printer can produce to halftone the spectral image. Comparing to the full spectral printer characterization described in Chapter 3 it requires less information from the printing system: only the spectral reflectances of the Neugebauer primaries (NP) are necessary.

VED is an improvement upon SED, it brings less color shifts which could occur when image is halftoned channel independently, VED improves the halftone image quality (Hains et al., 2003). But it also brings new issues as Fan (1998) listed them: slowness of error diffusion, poor performance when data are located out of the printer gamut. Also problems already present in SED are still present in VED or sVED, since we are using the same filters, similar limitations are there too.

To evaluate the quality of halftone images after sVED it is common to first look at the dot distribution obtained for single color level or single spectral reflectance (Gerhardt and Hardeberg, 2006). See Ulichney (1987a) and Lau and Arce (2001) for study of dot distribution in error diffusion. This preliminary study is important to know if this algorithm can reproduce a patch with constant level and how long it takes to reach a stable spatial distribution of NP. Then we would like to know how the algorithm behaves in a real case: the halftoning of a spectral image, especially when clear changes of area are in the image knowing that VED is subject to boundary artifacts (Fan, 1998).

In that chapter we will first describe the sVED algorithm, this on spectral patches and spectral images. This will allow us to reveal and illustrate the limitations of such algorithm. Then we will introduce our approaches to correct these limitations: how to take care of out of gamut data by preprocessing the spectral image, how to control the error during the halftoning by thresholding or by designing new filters.

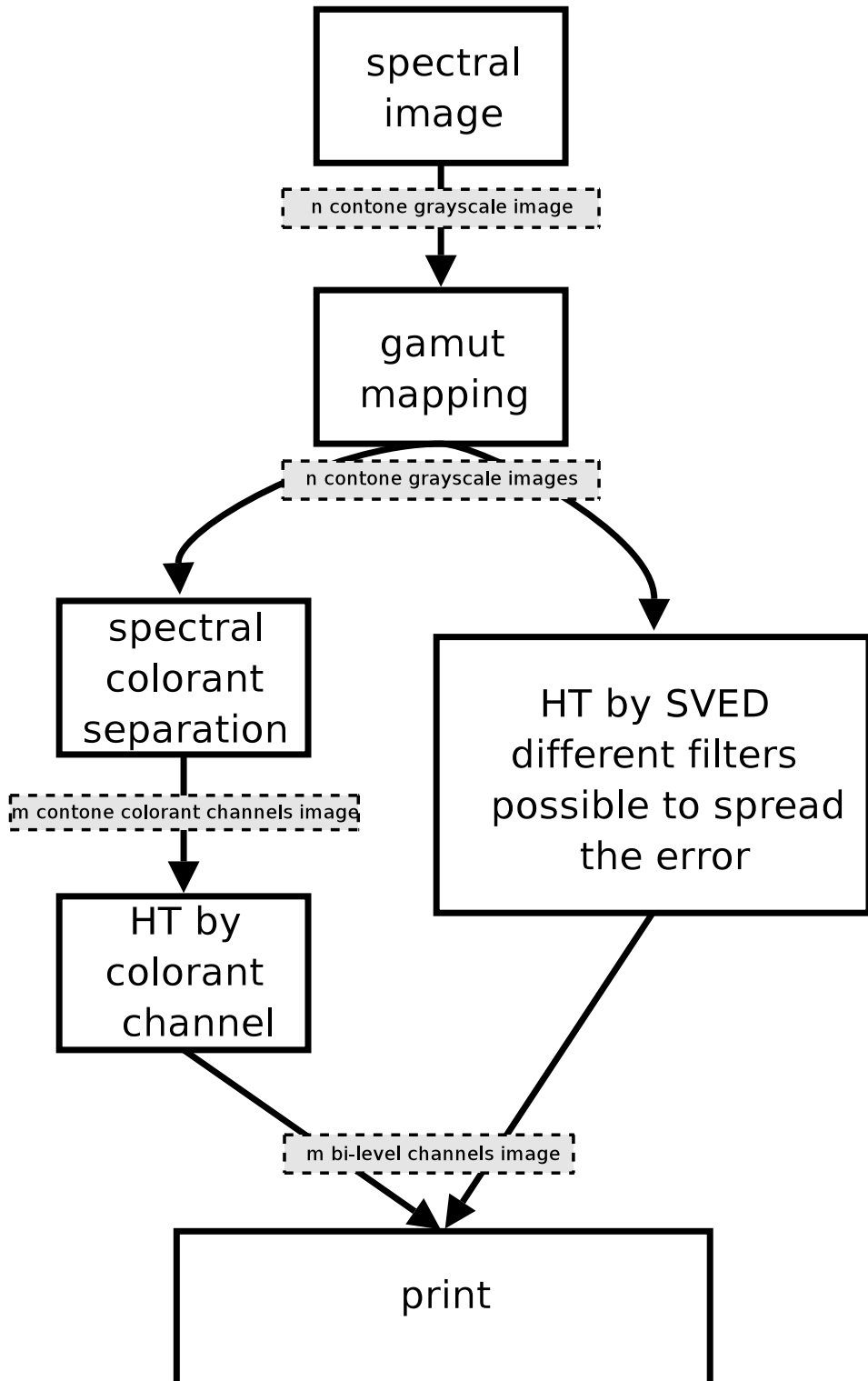


Figure 6.1: Illustration of two possible workflows for the reproduction of spectral data with a m colorant printer. The diagram illustrates how is transformed a spectral image into a multi bi-level colorants image.

6.2 Spectral vector error diffusion

The VED algorithm can be seen as an extension of the conventional error diffusion algorithm (Ulichney, 1987a). As in error diffusion an input pixel is binarised and the difference (i.e. the error) between the input pixel and the output pixel is weighted and diffused to the neighboring pixels. This operation is performed in a raster scan mode, see Figure 2.8. The VED technique halftones a picture taking each pixel value of an image as a vector of data (Sharma, 2003). The VED is performed once for the whole image. The output values in the colorant image is set by the binary colorant combination (i.e. a NP) corresponding to the minimum Euclidean distance in color space between the desired color and the NP colors (Haneishi et al., 1996).

The sVED algorithm is an extension to spectral data of the VED algorithm. Figure 6.2 shows the process of sVED where $in(x, y)$ is the input vector reflectance of the image, $mod(x, y)$ the modified reflectance, $out(x, y)$ the chosen primary and $err(x, y)$ the vector error at position (x, y) in the image.

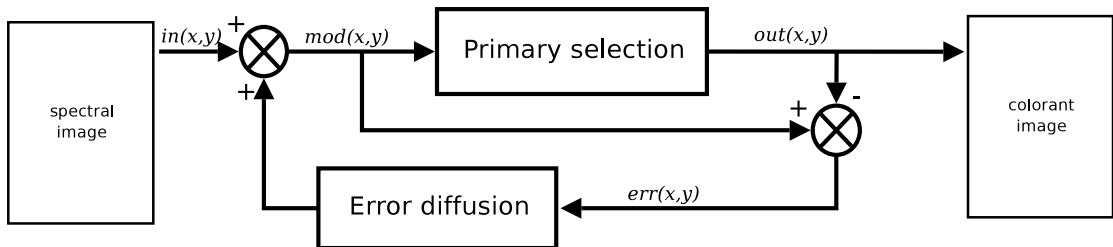


Figure 6.2: The process of spectral vector error diffusion halftoning. $in(x, y)$, $mod(x, y)$, $out(x, y)$ and $err(x, y)$ are vector data representing at the position (x, y) in the image the spectral reflectance of the image, the modified spectral reflectance, the spectral reflectance of the chosen primary and the spectral reflectance error.

The output pixel value in the multi layer binary colorant image is set by the selection of the Neugebauer Primary (NP) for each pixel. The NP are all the possible binary combinations of available colorants. A m colorant printer can produce $k = 2^m$ NP. The calculation of the Euclidean distance in spectral space from the current input pixel $mod(x, y)$ to all the NP are performed. The minimum distance determines the output value, as follows:

$$out(x, y) = \arg \min_{\mathbf{p}_k} \|\mathbf{mod}(x, y) - \mathbf{p}_k\| \quad (6.1)$$

where the vector \mathbf{p}_k is the spectral reflectance of the k th primary in \mathbf{P} , \mathbf{P} being the matrix of NP spectral reflectances, see Equation 3.34 in Section 3.3.2. At this stage of the process $out(x, y)$ can be used as a spectral reflectance value when re-injected in the loop for calculating the error to spread and as the colorant combination corresponding to the selected NP. The colorant combination is a combination of binary values, these binary values are stored to obtain the the halftone image of the spectral image.

Once the output colorant combination is set, the error is calculated as the vector difference between the current pixel and the selected NP spectral reflectance:

$$err(x, y) = mod(x, y) - out(x, y) \quad (6.2)$$

Finally the error is weighted and diffused to the neighboring pixels wavelength by wavelength, see Equation 6.3. Similar filter weights as in conventional error diffusion are used. We use the Jarvis, Judice and Ninke (Jarvis et al., 1976) filter for the examples in this chapter, a property of these filters is the weight summation equal to 1. So the error is spread to the neighboring pixels as follow to the neighboring pixels as follow:

$$mod(x + i, y + j) = mod(x + i, y + j) + w(i, j) \times err(x, y) \quad (6.3)$$

As example of filters used in this experiment, the Floyd and Steinberg (1976) filter of dimension 2×3 pixels:

$$\begin{bmatrix} & \bullet & w_{1,3} \\ w_{2,1} & w_{2,2} & w_{2,3} \end{bmatrix} = \left(\frac{1}{16}\right) \times \begin{bmatrix} & \bullet & 7 \\ 3 & 5 & 1 \end{bmatrix} \quad (6.4)$$

and the Jarvis, Judice, and Ninke (1976) filter of dimension 3×5 pixels:

$$\begin{bmatrix} & \bullet & w_{1,4} & w_{1,5} \\ w_{2,1} & w_{2,2} & w_{2,3} & w_{2,4} & w_{2,5} \\ w_{3,1} & w_{3,2} & w_{3,3} & w_{3,4} & w_{3,5} \end{bmatrix} = \left(\frac{1}{48}\right) \times \begin{bmatrix} & \bullet & 7 & 5 \\ 3 & 5 & 7 & 5 & 3 \\ 1 & 3 & 5 & 3 & 1 \end{bmatrix} \quad (6.5)$$

All previously cited filters have the following property for an n weights filter:

$$\sum_{i,j}^n w_{i,j} = 1. \quad (6.6)$$

Example

In a case of a CMY printer $2^3 = 8$ NPs are available. If for a pixel $mod(x, y)$ spectral reflectance the smallest Euclidean distance is obtained for the NP made of cyan and yellow, then the output values for the CMY channels at this pixel position will be cyan 1, magenta 0 and yellow 1. The spectral difference $mod(x, y) - \mathbf{P}_{101}$ is calculated and diffused.

To illustrate the transformation in the spectral image during the sVED process we perform the sVED halftoning of the ColorChecker spectral image, see Figure 6.3 (a) for the original image and (f) for its halftoned image. This image is 204×291 pixels wide. For this halftoning the NP spectral reflectances of the seven inks printer have been used. From image (b) to (e) we can see how works the algorithm in raster scan mode. The two lines between the processed part and the not yet processed part of the image are the currently modified pixels of the image during the halftoning process as in Equation 6.3. The size of this two pixels band is connected to the size of the filter for spreading the error, here the Jarvis, Judice and Ninke (Jarvis et al., 1976) has been used, this filter is 3×5 pixels wide.

This example illustrates the slowness of error diffusion with sVED while error from one patch in the image is spread to neighbors patches according to the processing path. This is particularly visible in the bottom of the image in Figure 6.3 (f) when error created in the third row is overlapping the last row of patches: the gray and black patches appear partially violet and greenish. These color shifts are due the strong modification of the original spectral reflectances due to error accumulation, the sVED pains to change the direction of error accumulation. To understand how the spectral reflectances in the image are transformed during the sVED process we can see in Figure 6.4 (a) and 6.4 (b) the original spectral reflectance $in(x, y)$, the modified spectral reflectance $mod(x, y)$ and the selected NP for two pixel positions. This example (Figure 6.4 (b)) also reveals that a strongly modified spectral reflectance can still end up by the selection of a close NP spectral reflectance.

6.3 Evaluation of sVED

The evaluation of the sVED algorithm will be conducted for our two available multi-colorant printers, a six colorants printer and a seven colorants printer. Only the NP spectral reflectances of those printer are necessary to perform sVED. In Figure 6.5 are displayed the NP of these printers. After transformation a spectral image or a spectral patch will be represented by a 6 binary colorant channels image for the six colorants printer or 7 binary colorant channels for the seven colorants printer. The first series of evaluation will only halftone spectral patches and the second series will halftone spectral images.

We can observe that both NP spectral reflectances for the six colorants and seven colorants printer are different. The NP spectral reflectances of the six colorants printer correspond to

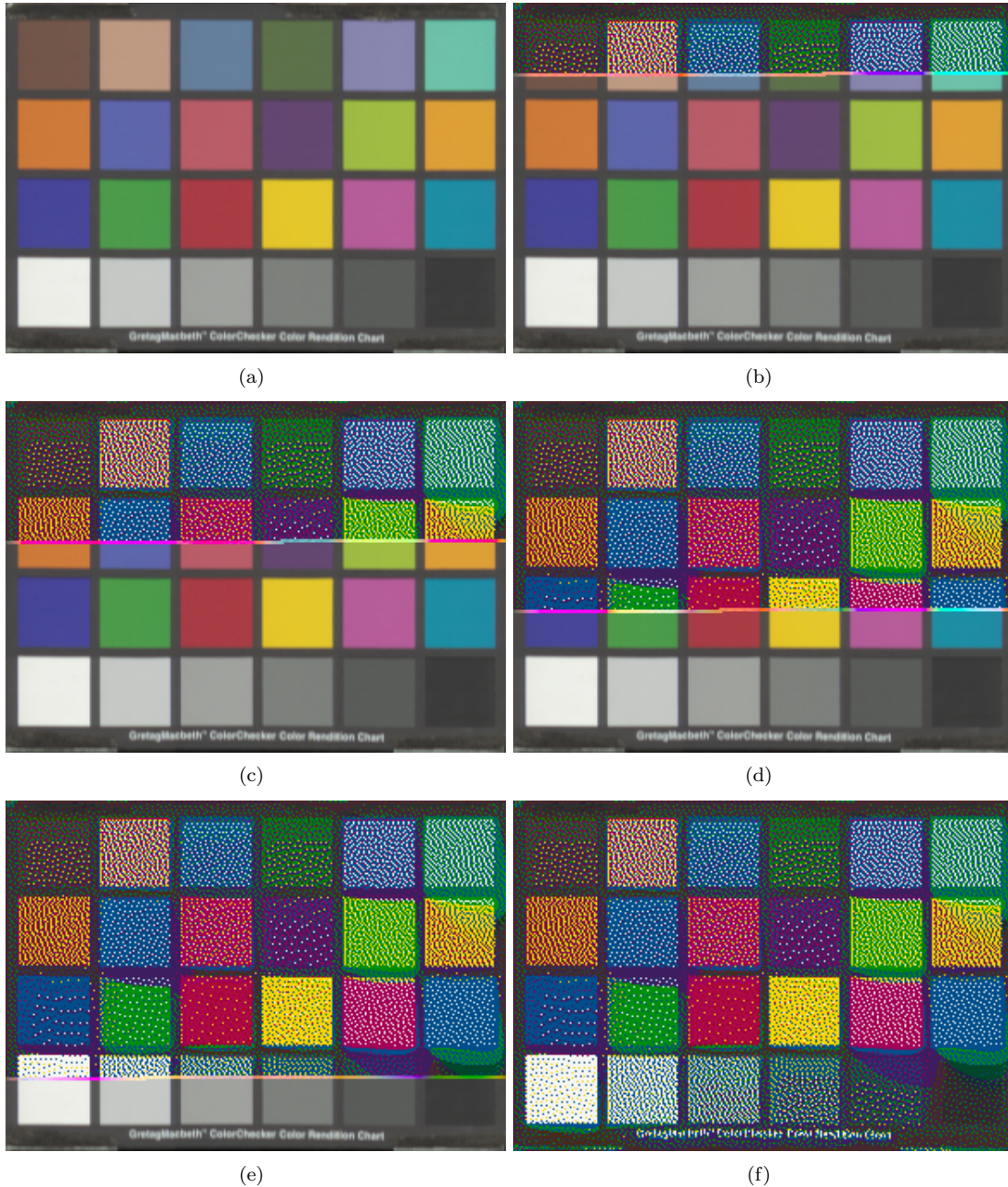


Figure 6.3: The image (a) is the original spectral image, from (b) to (e) are example of the evolution of this image during the sVED process. The last image (f) is the resulting halftoned image where the pixels have been all replaced by their NP according to the sVED algorithm. All the images here are spectral images, the color version have been calculated for illuminant D65 and standard CIE 1931 observer. The color shifts we can observe in different part of the image are the result of error accumulation and slowness to diffuse it, e.g. the two last patches of the last rows appear partially violet and greenish due to the error created in the previous row.

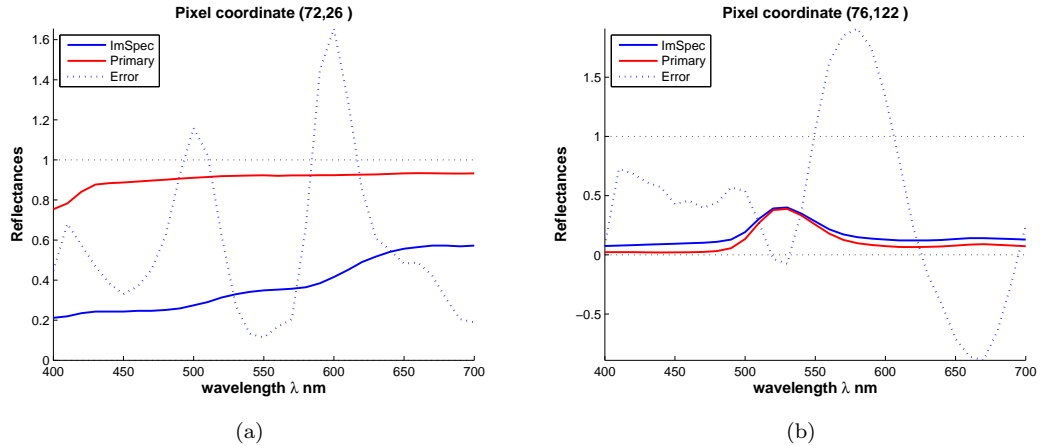


Figure 6.4: Example of spectral reflectances from the spectral image of the ColorChecker test chart where in blue is the original pixel value $i(x, y)$, in dashed blue the current modified pixel $mod(x, y)$ and in red its corresponding NP selected during the sVED. A NP is selected based on the Euclidean distance from the modified pixel to the available NPs. This example shows how the original spectral reflectances are transformed during the sVED process but also that the selected NP can be close to the original, see Figure (b).

synthesized NPs and are brighter than the NP spectral reflectances of the seven colorants printer which correspond to printed and measured NPs.

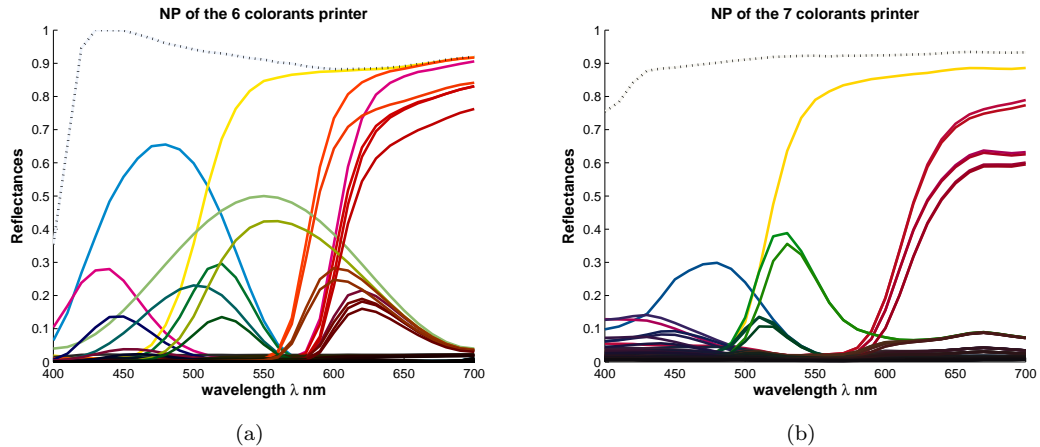


Figure 6.5: NPs spectral reflectances of both six colorants printer (a) and seven colorants printer (b). The six colorants printer provides $2^6 = 64$ NPs and the seven colorants printer provides $2^7 = 128$ NPs.

6.3.1 sVED of spectral patches

The spectral patches are divided in two groups of data: in spectral gamut and outside spectral gamut. The spectral patches representing in spectral gamut data are created randomly: 100 colorants combination are randomly created for both the six colorants and seven colorants printer. The limit of 300% total ink coverage per colorant combination has been set for creating the patches. The spectral reflectances of these colorants combinations are simulated by the spectral Neugebauer model.

Based on the simulated spectral reflectances we create spectral patches, each patch containing a simulated spectral reflectance, each patch is of 256×256 pixels wide. Once created the patches are then halftoned by sVED for the 6 colorants printer and a 7 colorants printer.

A simple printer model is established to estimate the spectral reflectance resulting from each halftoned patch (Kouzaki et al., 1999). Knowing that a spectral halftone image is made of NP spectral reflectances for each pixel we simply sum the NPs weighted by their distribution, this considering a patch having a unitary area. One can see that this approach is similar to the Neugebauer model. Differences between the patches and their reproduction by sVED for both 6 and 7 colorants printer can be seen in Table 6.1 and Table 6.2. The obtained differences are small, both for colorimetric differences and spectral differences.

Table 6.1: Differences between the simulated reflectances of our randomly 100 created patches and their reproduction by sVED for our 6 colorants printer.

Patches	ΔE_{ab}^*				ΔE_{94}^*	sRMS
	A	D65	D50	FL11	D50	
Av.	0.5	0.4	0.4	0.6	0.3	0.005
All	0.3	0.3	0.3	0.4	0.2	0.002
Max	1.9	1.4	1.6	1.9	1.0	0.008

Table 6.2: Differences between the simulated reflectances of our randomly 100 created patches and their reproduction by sVED for our 7 colorants printer.

Patches	ΔE_{ab}^*				ΔE_{94}^*	sRMS
	A	D65	D50	FL11	D50	
Av.	0.7	0.6	0.7	0.7	0.5	0.004
All	0.5	0.4	0.5	0.6	0.4	0.001
Max	2.3	1.9	1.9	3.3	1.7	0.006

The second group of spectral patches tested represents data outside the printer gamut. We choose the spectral reflectances of the MacBeth ColorChecker test chart. Based on each spectral reflectance of this test chart we create 24 spectral patches; they have the same size as the previous patches for the in gamut data experiment. Differences between the ColorChecker patches and their reproduction by sVED for both 6 and 7 colorants printer can be read in Table 6.3. The halftoned patches for the ColorChecker experiment are displayed in Figure 6.6 (a) for the 6 inks printer and in Figure 6.6 (b) for the 7 inks printer. In these illustrations all patches are displayed together but each of them has been halftoned independently.

Comparing both experiment the average colorimetric differences and spectral differences for the ColorChecker patches are much larger than for the in gamut patches, see the results in Table 6.1, 6.2 and 6.3. The better results for the in gamut data are not a surprise. The differences obtained for the ColorChecker patches experiment reveal more the difference of gamut between the data and the printer than a failure of the sVED halftoning.

We can see in the images of the halftoned patches in Figure 6.6 (a) and Figure 6.6 (b) that stable spatial distribution of NP can be obtained for a large difference due to gamut mismatch, e.g. the 5th patch in the first row (i.e. patch number 5 in Table 6.3) or the opposit example in the third patch third row (i.e. the patch number 10 in Table 6.3) with a small difference between data and estimated reproduction for a clear visible unstable spatial distribution of NP on the top of the patch.

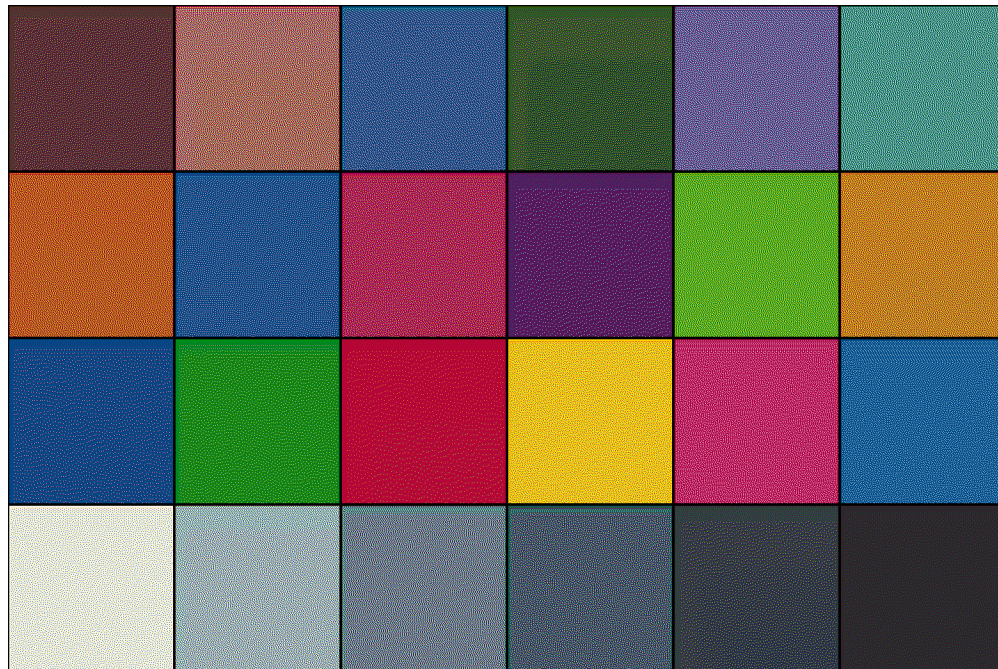
The sVED halftoning technique is a complex algorithm and the following examples in the next section for the haftoning of spectral images will illustrate how behaves the algorithm in

more complex scenes, e.g when the image is not made of one single spectral reflectance. But an observation can be made on the border effect, for each patch the sVED algorithm presents oscillations in the first lines and on the left border due to the path in sVED process, the oscillation will stop when a stable spatial distribution of NPs is reached. The term slowness of error diffusion in the sVED algorithm refers to the length of the oscillation in the halftoned image, the longer the oscillation the slower is the error diffused.

In the reproduction workflow the image will be scaled to match the printer resolution and a direct consequence of this scaling step is the reduction of the visibility of the border effect. Figure 6.7 illustrates the change of resolution by displaying an halftoned patch by sVED for the seven colorants printer for different resolution and identical physical patch size. In that example a spectral patch is created with the first spectral reflectance of the ColorChecker test chart. Then four patches are created with the following size: 64×64 , 128×128 , 256×256 and 512×512 pixels wide, respectively Figure 6.7 (a), (b), (c) and (d). The (c) patch corresponds to the first patch in Figure 6.6. And we can see that the border effect is less visible when the resolution increases.



(a)



(b)

Figure 6.6: Halftoning by **sVED** of the ColorChecker spectral patches for the 6 colorants printer (a) and the 7 colorants printer (b). Each patch has been halftoned independently of the others.

Table 6.3: Differences between the ColorChecker spectral reflectances and their reproduction by sVED for our 6 and 7 colorants printer. For each double column, the left one is for the 6 colorants printer and the right one for the 7 colorants printer.

Patches	ΔE_{ab}^*										sRMS
	A		D65		D50		FL11		FL31		
1	3.7	2.4	2.4	2.1	2.9	2.1	3.9	0.8	3.9	2.7	2.0 1.6 0.023 0.018
2	1.8	1.7	1.9	1.6	1.9	1.7	1.6	5.5	1.4	3.5	1.3 1.0 0.031 0.030
3	2.7	6.6	0.7	3.1	1.2	4.2	2.9	6.4	3.1	4.9	0.9 3.2 0.051 0.041
4	6.8	2.8	5.5	1.6	6.0	1.9	10.6	2.7	5.7	2.5	4.0 1.2 0.028 0.024
5	9.2	14.1	6.1	13.3	7.1	13.2	10.5	14.5	8.4	12.8	5.3 7.7 0.080 0.075
6	11.6	21.5	12.9	22.0	12.7	22.1	15.3	22.1	9.1	14.2	6.0 9.9 0.050 0.089
7	1.2	10.7	4.8	17.3	3.7	15.9	4.6	19.6	4.6	9.5	1.7 7.8 0.042 0.062
8	13.3	16.8	20.4	23.3	18.2	20.8	13.8	17.0	8.5	13.8	9.5 9.7 0.054 0.052
9	1.0	9.8	1.4	12.2	1.3	11.9	1.9	16.6	0.9	11.5	0.8 4.7 0.019 0.045
10	11.5	10.8	9.4	8.0	10.6	9.2	16.9	13.4	13.2	10.9	6.6 6.2 0.053 0.037
11	7.2	8.8	6.5	10.1	6.9	9.6	10.5	9.5	6.2	8.9	3.4 4.1 0.034 0.044
12	1.5	6.0	5.3	9.3	4.2	8.7	4.4	8.9	3.8	3.8	1.7 4.1 0.047 0.041
13	21.8	21.2	32.3	32.7	29.7	29.3	22.7	21.6	12.3	13.7	14.3 12.9 0.051 0.051
14	10.7	5.4	8.0	4.4	9.0	4.4	17.1	5.7	10.3	8.4	4.3 2.9 0.033 0.033
15	3.7	1.0	4.7	1.4	4.5	1.3	9.2	1.8	6.4	1.2	1.3 0.5 0.029 0.013
16	0.1	2.8	0.7	7.2	0.5	5.8	1.2	4.4	1.2	2.9	0.2 1.6 0.020 0.044
17	5.7	19.7	5.4	25.4	5.7	23.6	11.6	22.3	8.2	17.5	2.7 12.1 0.059 0.061
18	3.8	24.5	3.2	21.3	3.4	22.7	5.8	22.8	3.8	17.3	2.0 12.8 0.031 0.058
19	0.5	1.8	0.6	1.6	0.5	1.7	0.6	1.7	0.4	1.1	0.5 1.5 0.023 0.052
20	1.0	0.3	0.9	1.0	0.9	0.7	0.9	0.7	0.7	0.4	0.9 0.7 0.032 0.023
21	1.0	0.9	0.9	0.8	0.9	0.9	1.0	1.0	0.8	1.4	0.9 0.9 0.030 0.010
22	0.9	1.7	0.7	1.5	0.8	1.6	0.8	1.7	0.9	2.3	0.8 1.6 0.020 0.008
23	0.9	2.8	0.5	2.6	0.6	2.7	1.1	2.8	1.1	4.2	0.6 2.7 0.012 0.007
24	1.0	1.6	0.7	1.5	0.8	1.5	1.7	1.2	1.2	3.3	0.8 1.5 0.004 0.004
Av.	5.1	8.1	5.7	9.4	5.6	9.1	7.1	9.4	4.8	7.2	3.0 4.7 0.036 0.038
Std	5.5	7.6	7.4	9.5	6.8	8.9	6.5	8.1	3.9	5.5	3.4 4.1 0.017 0.022
Max	21.8	24.5	32.3	32.7	29.7	29.3	22.7	22.8	13.2	17.5	14.3 12.9 0.080 0.089

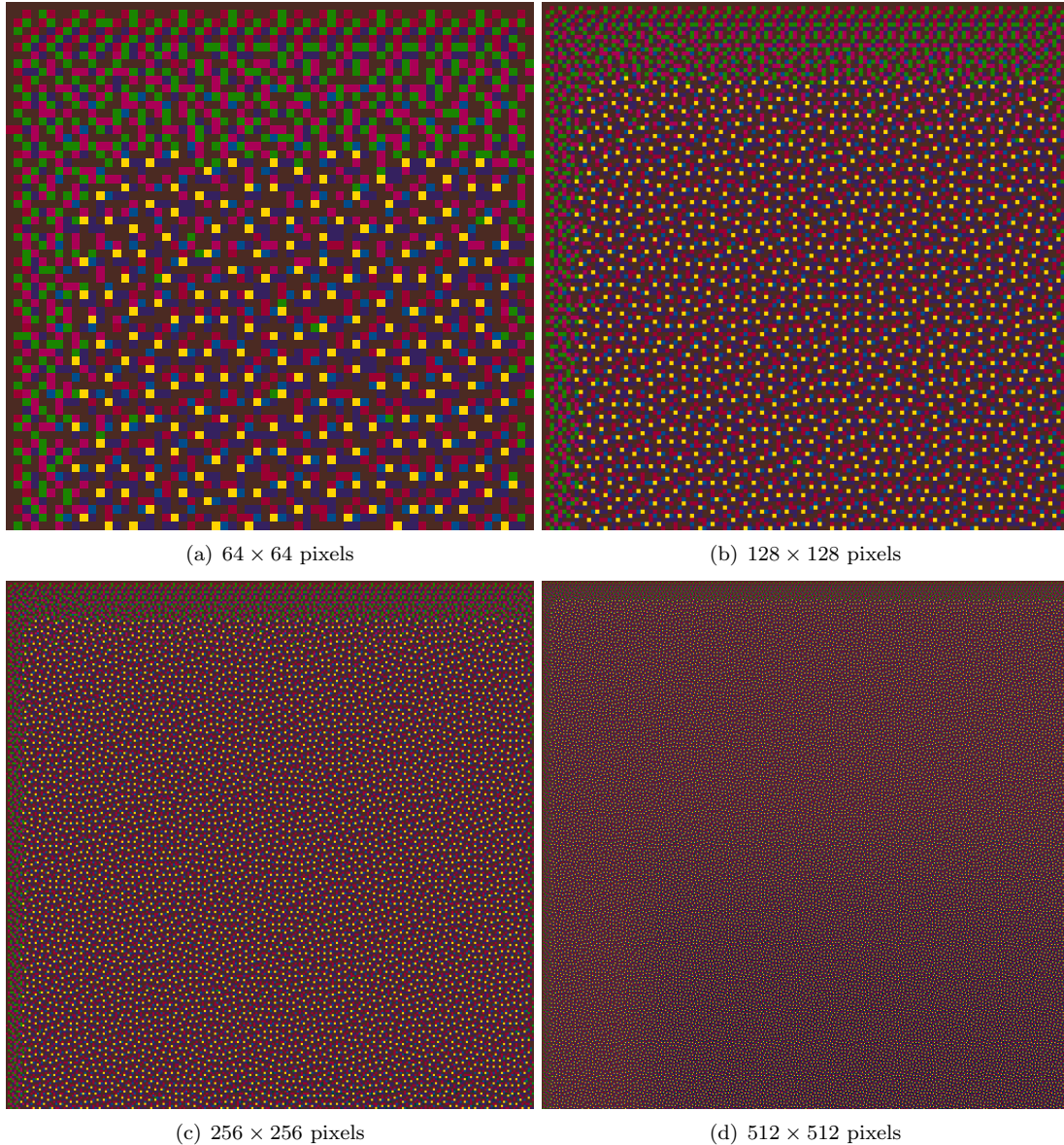


Figure 6.7: To illustrate the visibility of the border effect in sVED halftoning, a spectral patch with the first spectral reflectance value of the ColorChecker test chart is halftoned by sVED for the 7 colorants printer with different patch size: 64 × 64 pixels wide in (a), 128 × 128 pixels wide in (b), 256 × 256 pixels wide in (c) and 512 × 512 pixels wide in (d). All halftoned images of the spectral patches are displayed in the same size to simulate the print at different resolutions.

6.3.2 sVED of spectral images

The previous experiment has shown the possibility in simulation to reproduce spectral data by sVED, especially data in the spectral printer gamut. The algorithm was able to generate stable spatial distribution of NP for a single spectral reflectance value (i.e. for a spectral patch). But most likely in a spectral image, the pixels have different values, representing different areas with more less soft transition from one area to another.

To obtain a color image of an halftoned image after sVED, each pixel of the halftoned image (i.e. a multi-binary colorant image) is replaced by its NP spectral reflectance. Then a color rendering is calculated for the standard observer CIE1934 and CIE D50 illuminant. The same color rendering settings have been used to display the original spectral image called ColorChecker, see Figure 6.8.



Figure 6.8: Color rendering of the original ColorChecker (*CC*) spectral image for standard observer CIE1931 and illuminant CIE D50.

The examples in Figure 6.3 (f) and Figure 6.9 (a) and (b) reveal the difficulties of the sVED algorithm when abrupt changes of area occur in the image. Enormous error are created during the process and a change of area in the image can be crossed during the scan mode before to reach a stable spatial distribution of NP. When the algorithm starts the halftoning of a second region, it is still caring the error accumulated from the first region, this phenomenon is particularly visible on test chart when no soft transition are connecting two regions in the image.

Based on the observation made in the previous section with increasing the resolution of the image before performing the sVED, the spectral image called *CC* will be scaled by a factor of 2. Doing so we decrease the overlapping of error from one region to the following according to the sVED path. In the first example of sVED of spectral image in Figure 6.3 (f) the spectral image *CC* has not been scaled and the same image in Figure 6.9 (a) and (b) has been scaled before performing sVED.

Other spectral images have been used to evaluate the sVED algorithm. These others images are displayed in Appendix C, see Figure C.1 for the *YarnPalette* (*YP*) spectral image and Figure C.2 for the *WomanReading* (*WR*) spectral image in their original version. The *YP*

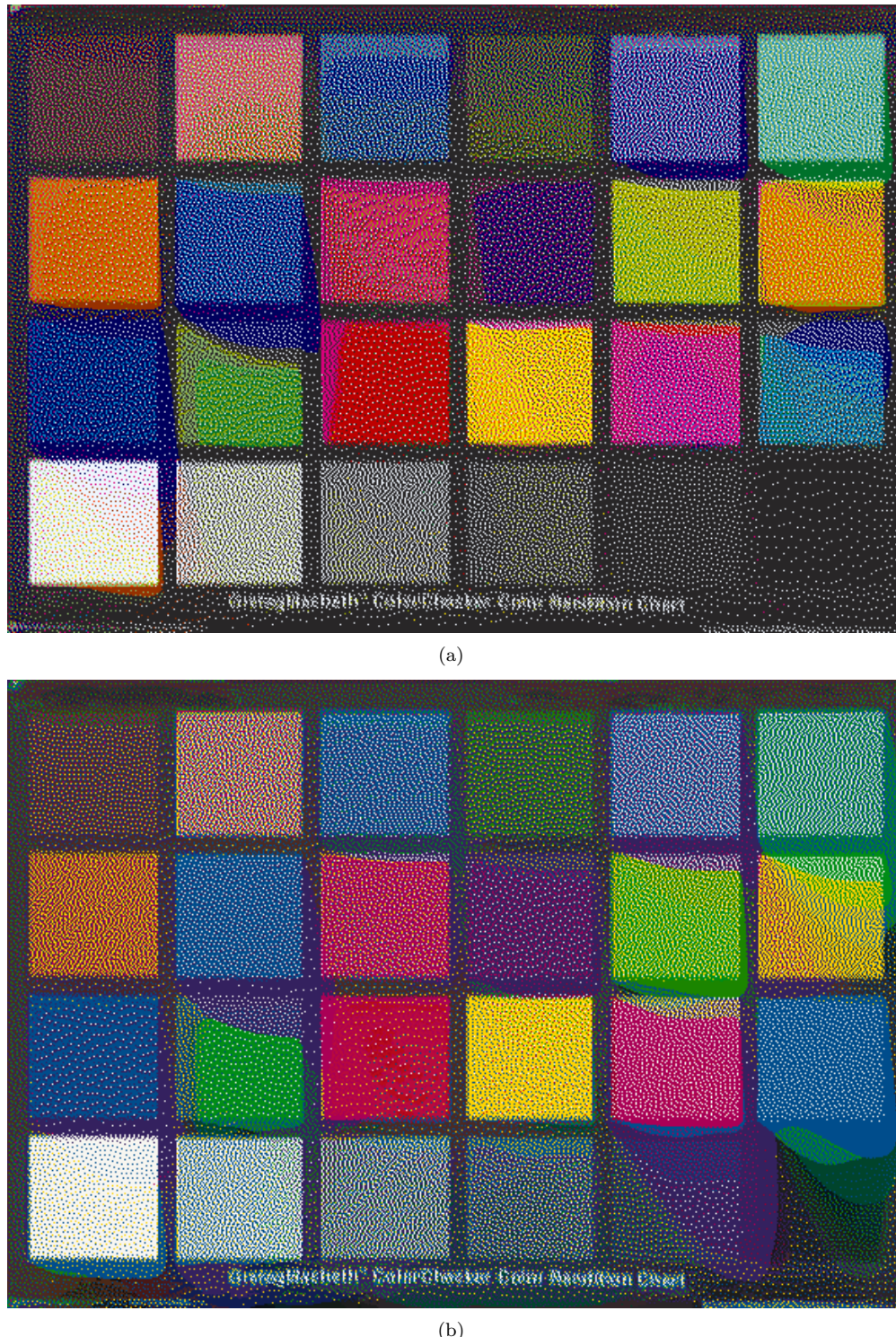


Figure 6.9: sVED of the *CC* spectral image for the 6 and 7 colorants printer in (a) and (b) respectively. The spectral image has been scaled by a factor of 2 before performing the halftoning.

spectral image is displayed in its original size and will be halftoned without scaling when the *WR* spectral image has been scaled by a factor of 2 and will halftoned from its scaled version. All the spectral images used to evaluate the halftoning by sVED come from the Joensuu Spectral Image Database available at <http://www.multispectral.org> (Joensuu).

The two others images in Figure C.3 (a) and Figure C.3 (b) for the *YP* spectral image, Figure C.4 and Figure C.5 for the *WR* spectral image presenting two different scenes are less problematic. The lost of information is due to the degradation of details in the image. But knowing that an image has to be scaled (by a factor > 2) before to be printed, this in order to match its resolution and the printer resolution we may think that this lost will be reduced. Also if the data to be halftoned are not included in the printer gamut it will increase the risk of losing information.

To scale the image before the sVED halftoning does not reduce completely the visibility of the error diffusion; to control the error in the sVED we proposed three operations. One is to pre-process the spectral image before performing the halftoning by sVED, a gamut mapping based on a printer model. A second operation can be performed by clipping or scaling the $mod(x, y)$ pixel spectral reflectance during the sVED halftoning operation pixel by pixel. A third operation is to propagate error using new designed filters. All the proposed operations can be used as a single operation, or combined. The preprocessing by gamut mapping being always performed before the sVED hafltoning.

6.4 Preprocessing by spectral gamut mapping

6.4.1 Spectral gamut mapping by inverting the spectral printer model

Our gamut mapping is based on the inversion of the spectral Neugebauer printer model. This method is explained and illustrated in Appendix B.2. In this appendix are also displayed each spectral reflectance of the ColorChecker test chart and their gamut mapped version for both 6 colorants and 7 colorants printer.

The gamut mapped *CC* spectral image for both 6 and 7 colorants printers are displayed in Figure 6.10 (a) and Figure 6.10.

6.4.2 Experiments

For these experiment we perform similar tests as for the first sVED evaluation but with pre-processing applied to the spectral data: from the spectral patches experiment we keep only the spectral patches created from the ColorChecker spectral reflectances and we use all gamut mapped version of the spectral images *CC*, *YP* and *WR*. The gamut mapped *YP* and *WR* spectral images for both 6 and 7 colorants printers are displayed in Appendix C.2.

In Figure 6.11 (a) and Figure 6.11 (b) are displayed the halftoned images of the gamut mapped spectral patches of the ColorChecker test chart. The gamut mapped spectral reflectances for the 6 colorants printer have been halftoned for this printer and identically for the gamut mapped spectral for the 7 colorants printer. You can see in Table 6.4 the differences between the gamut mapped spectral reflectances patches for both printers and their reproduction by sVED.

In Figure 6.12 (a) and Figure 6.12 (b) are displayed the halftoned image of the gamut mapped *CC* spectral image for the 6 colorants and 7 colorants printer. The two others halftoned images of the gamut mapped *YP* and *WR* spectral images are displayed in Appendix C.2, see Figure C.8 for *YP* and Figure C.9 for *WR*.

We can observe that pre-processing the image with gamut mapping has reduced the visibility of error spreading in all halftoned images. In the following sections all spectral images will first be gamut mapped and then different approaches for controlling the error will be tested.



(a)



(b)

Figure 6.10: Gamut mapped *CC* spectral image for both 6 and 7 colorants printers in (a) and (b) respectively.

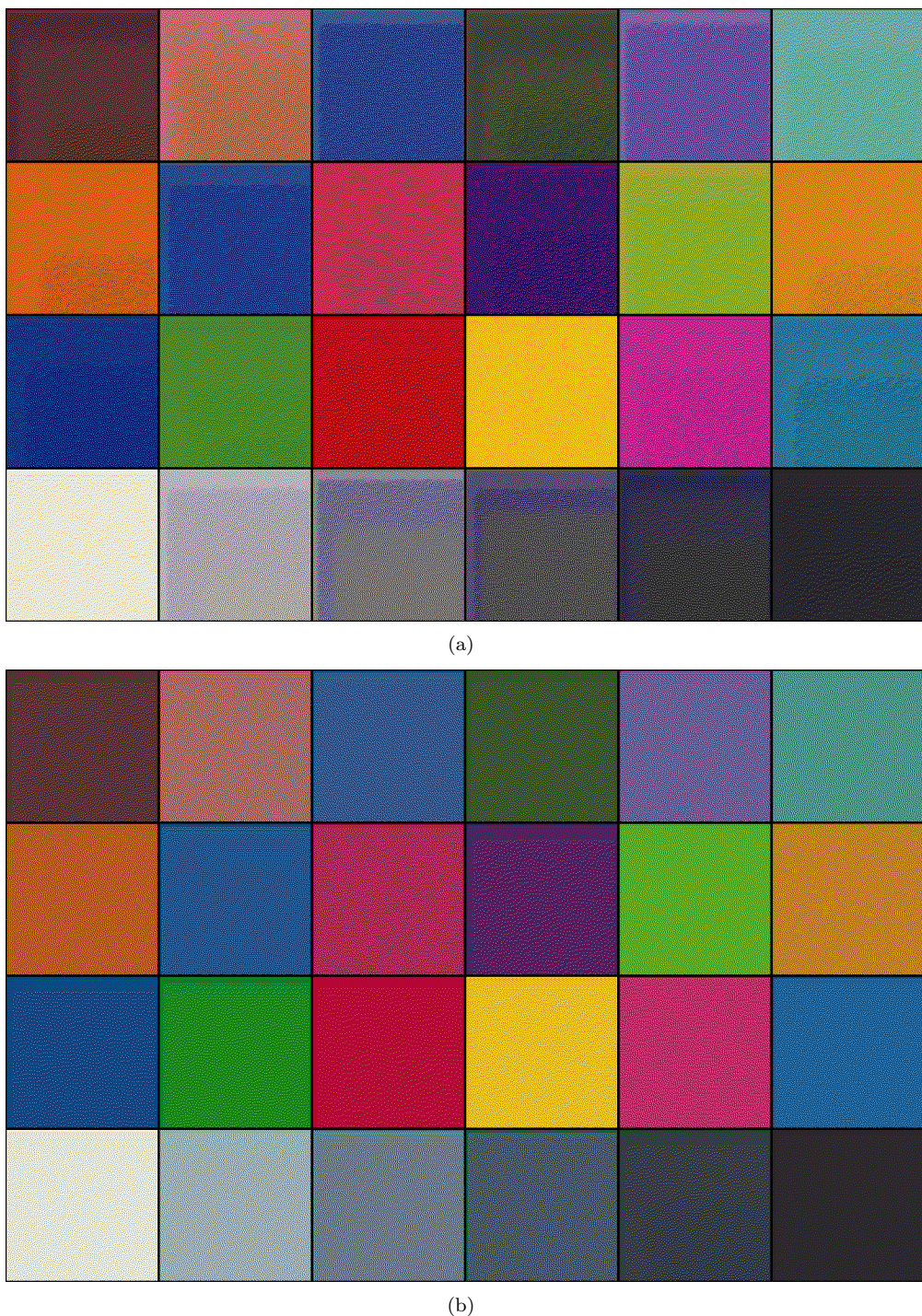


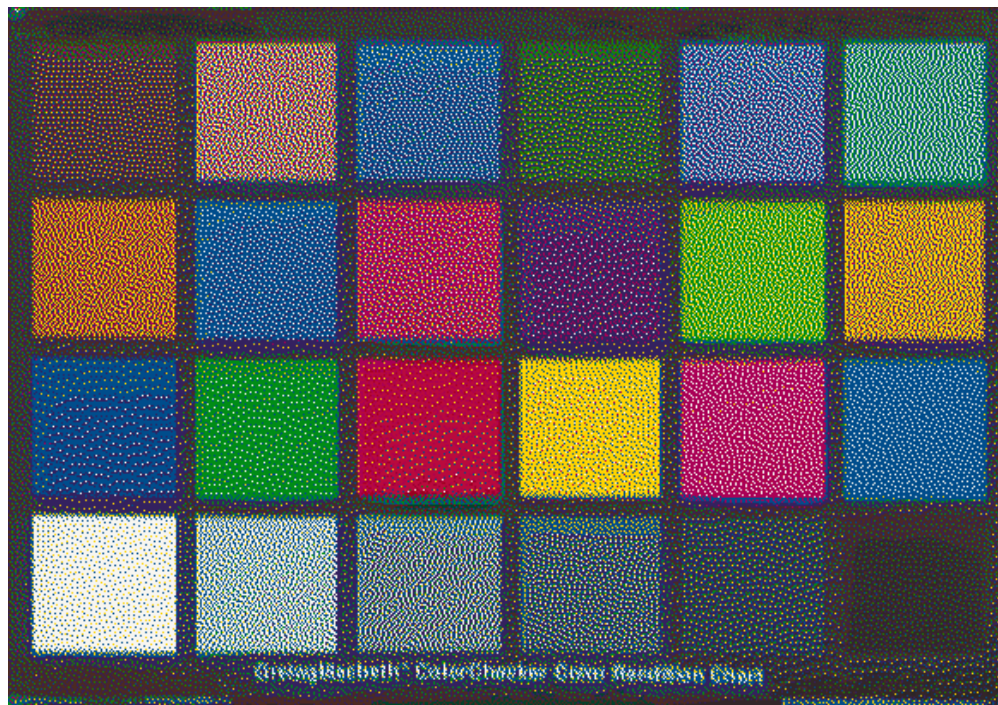
Figure 6.11: Halftoning by **sVED with pre-processing** of ColorChecker spectral patches for the 6 colorants printer (a) and the 7 colorants printer (b). Each patch has been halftoned independently of the others.

Table 6.4: Differences between the gamut mapped ColorChecker spectral reflectances and their reproduction by sVED for our 6 and 7 colorants printer. For each double column, the left one is for the 6 colorants printer and the right one for the 7 colorants printer.

Patches	ΔE_{ab}^*								ΔE_{94}^*		sRMS			
	A		D65		D50		FL11		FL31		D50			
1	1.3	0.8	1.0	0.5	1.1	0.6	1.5	0.5	1.4	1.6	0.7	0.5	0.007	0.004
2	0.7	0.3	0.6	0.4	0.6	0.3	0.8	0.2	0.6	0.1	0.4	0.2	0.008	0.004
3	0.3	0.6	1.1	0.5	0.8	0.5	0.4	0.6	0.5	0.8	0.6	0.4	0.005	0.003
4	1.8	0.6	1.3	0.7	1.5	0.6	2.6	0.4	1.6	1.1	1.1	0.5	0.008	0.004
5	0.3	0.3	0.7	0.3	0.6	0.3	0.4	0.2	0.3	0.3	0.3	0.2	0.005	0.002
6	0.5	0.1	0.6	0.1	0.6	0.1	0.6	0.1	0.4	0.1	0.3	0.1	0.005	0.001
7	1.6	0.4	2.0	0.4	1.9	0.4	2.3	0.4	1.0	0.2	0.5	0.2	0.006	0.003
8	0.4	0.7	1.2	0.6	0.9	0.6	0.4	0.7	0.7	1.0	0.6	0.5	0.005	0.003
9	0.3	0.4	0.2	0.6	0.2	0.6	0.1	0.2	0.3	0.4	0.1	0.4	0.005	0.003
10	1.1	1.0	0.7	0.8	0.8	0.9	1.3	1.0	1.5	1.5	0.4	0.6	0.006	0.003
11	0.6	0.5	0.6	0.6	0.7	0.5	0.8	0.5	0.5	0.3	0.4	0.2	0.006	0.002
12	1.3	0.5	1.7	0.6	1.5	0.6	1.9	0.6	0.8	0.2	0.4	0.2	0.006	0.003
13	0.6	1.2	1.4	0.9	1.2	1.0	0.4	1.1	1.2	1.7	0.8	0.7	0.005	0.003
14	0.9	0.7	0.8	1.1	0.8	0.9	1.2	0.6	0.7	0.4	0.5	0.4	0.006	0.003
15	1.3	0.6	1.4	1.1	1.4	1.0	1.2	0.3	1.1	0.4	0.4	0.5	0.004	0.003
16	0.6	0.9	0.9	0.9	0.8	0.9	0.8	0.8	0.4	0.6	0.2	0.2	0.003	0.003
17	0.5	0.4	0.4	0.3	0.5	0.3	0.6	0.3	0.6	0.2	0.2	0.2	0.004	0.002
18	0.9	0.4	0.5	0.4	0.6	0.4	1.3	0.5	0.9	0.6	0.4	0.3	0.006	0.002
19	0.2	0.1	0.2	0.1	0.2	0.1	0.2	0.1	0.2	0.1	0.2	0.1	0.002	0.002
20	0.1	0.0	0.3	0.2	0.2	0.1	0.3	0.1	0.1	0.1	0.2	0.1	0.007	0.002
21	0.1	0.5	0.3	0.4	0.2	0.4	0.2	0.4	0.2	0.7	0.2	0.4	0.007	0.004
22	0.3	1.2	0.1	1.1	0.1	1.2	0.5	1.1	0.5	1.7	0.1	1.2	0.007	0.006
23	1.1	2.3	0.7	2.1	0.9	2.2	1.5	2.1	1.3	3.5	0.8	2.1	0.007	0.006
24	0.8	1.5	0.6	1.5	0.6	1.5	1.1	1.3	1.0	3.2	0.6	1.5	0.003	0.004
Av.	0.7	0.7	0.8	0.7	0.8	0.7	0.9	0.6	0.7	0.9	0.4	0.5	0.005	0.003
Std	0.5	0.5	0.5	0.5	0.5	0.5	0.7	0.5	0.4	0.9	0.3	0.5	0.002	0.001
Max	1.8	2.3	2.0	2.1	1.9	2.2	2.6	2.1	1.6	3.5	1.1	2.1	0.008	0.006



(a)



(b)

Figure 6.12: Halftoning by **sVED with pre-processing** of the *CC* spectral image for the 6 and 7 colorants printer in (a) and (b) respectively.

6.5 Controlling the error

6.5.1 Reflectance clipping

We have observed that when the error is diffused to the image, the reflectance of pixels can be extremely modified and have values above 1 and below 0, this with or without spectral gamut mapping applied, see Figure 6.4. To decrease the error accumulation and the slowness of the error diffusion we propose to clip the reflectance values to 1 and 0 when those are respectively above or or below these limits. The clipping is performed before the selection of the NP in the sVED process (we set these limits as a reflectance vector of 1 is a perfect white and a reflectance vector of 0 is a perfect black). Figure 6.13 illustrates the diagram of sVED when error control by clipping is used. In Figure 6.14 are two examples of reflectances in the image of the ColorChecker test chart where the clipping has been used during in the sVED process.

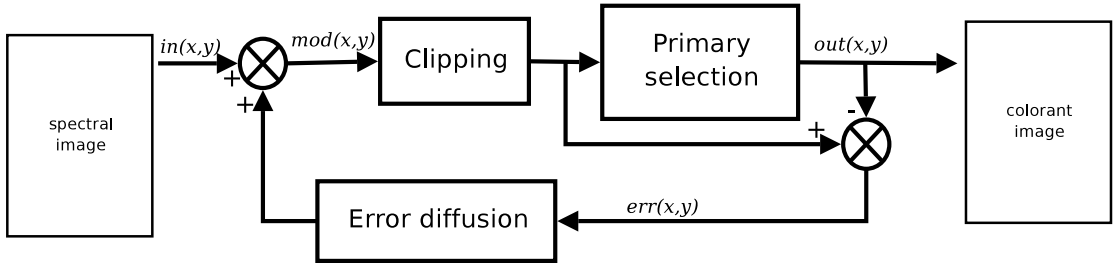


Figure 6.13: The process of spectral vector error diffusion halftoning with clipping to control the error. $in(x, y)$, $mod(x, y)$, $out(x, y)$ and $err(x, y)$ are vector data representing at the position (x, y) in the image the spectral reflectance of the image, the modified spectral reflectance, the spectral reflectance of the chosen primary and the spectral reflectance error. The processed pixel is clipped if necessary before the NP selection.

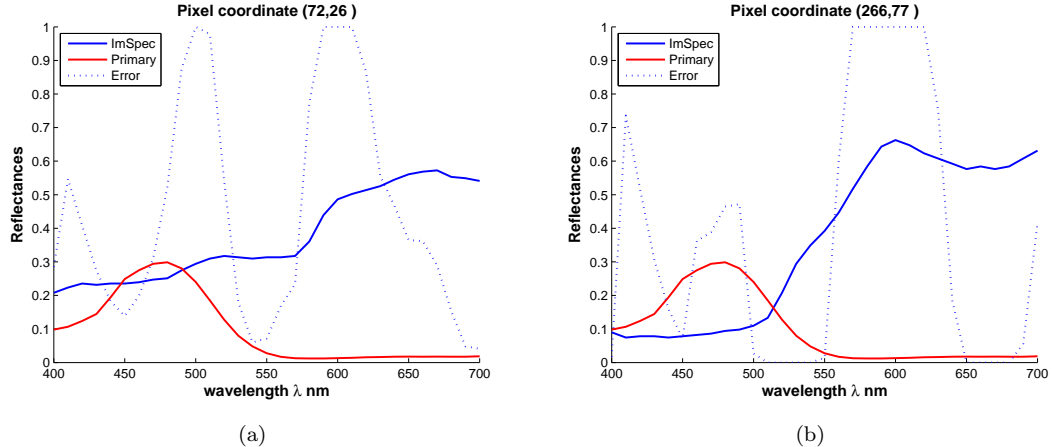


Figure 6.14: Two examples of reflectance where clipping has been applied during the sVED halftoning. Reflectance of the input pixel in blue, modified pixel with clipping in dashed blue and chosen primary in red.

6.5.2 Experiments

For these experiment we perform similar tests as for the first sVED evaluation but with pre-processing applied and then sVED with clipping to the gamut mapped spectral images. We also

run the experiment on the spectral patches using the spectral reflectances of the gamut mapped ColorChecker test chart.

In Figure 6.15 (a) and Figure 6.15 (b) are displayed the halftoned images of the gamut mapped spectral patches of the ColorChecker test chart. The gamut mapped spectral reflectances for the 6 colorants printer have been halftoned for this printer and identically for the gamut mapped spectral reflectances for the 7 colorants printer. You can see in Table 6.5 the differences between the gamut mapped spectral reflectances patches for both printers and their reproduction by sVED.

In Figure 6.16 (a) and Figure 6.16 (b) are displayed the halftoned image by sVED with clipping of the gamut mapped *CC* spectral image for the 6 colorants and 7 colorants printer. The two others halftoned images of the gamut mapped *YP* and *WR* spectral images are displayed in Appendix C.2, see Figure C.8 for *YP* and Figure C.9 for *WR*.

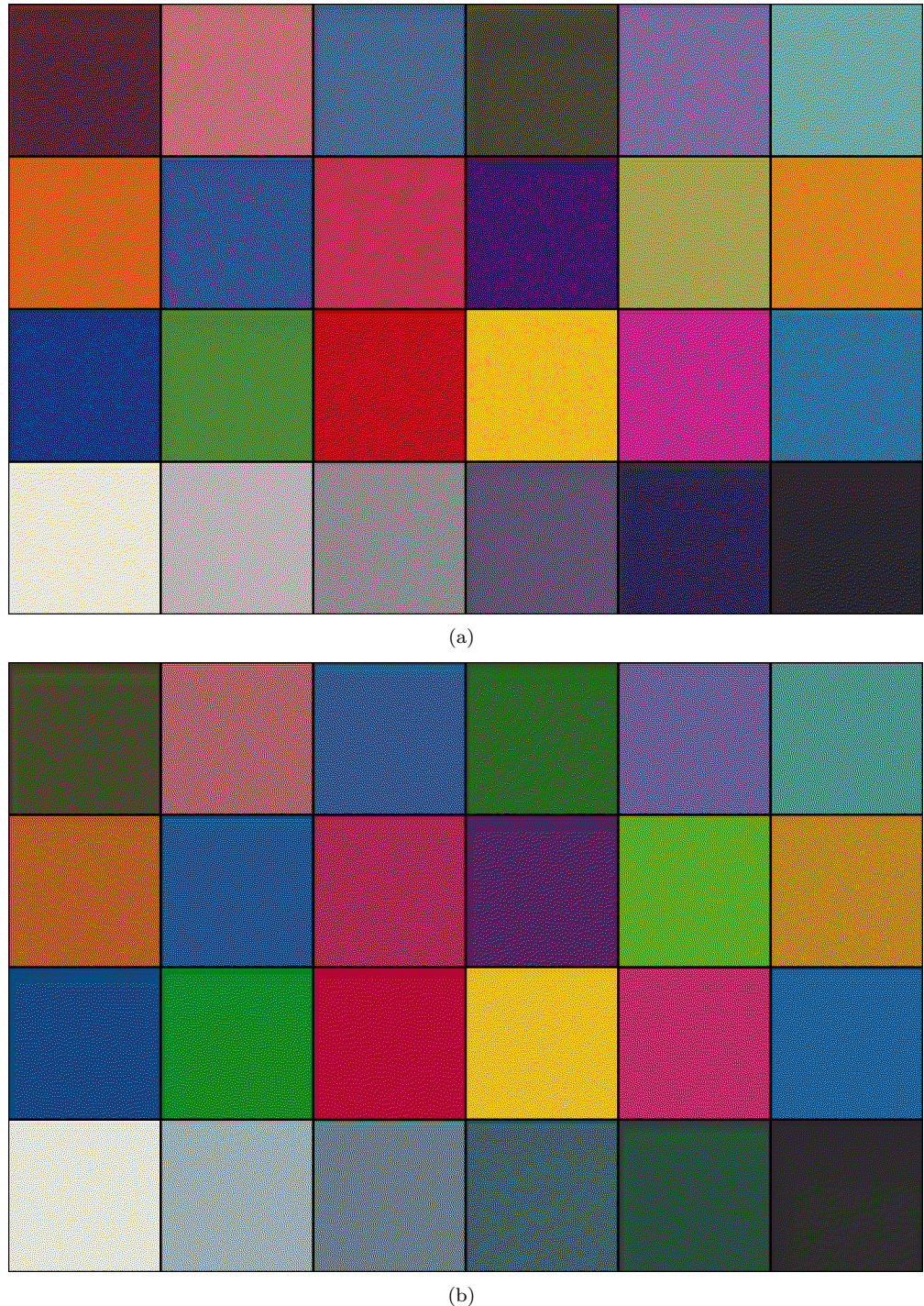


Figure 6.15: Halftoning by **sVED with pre-processing and clipping** of the ColorChecker spectral patches for the 6 colorants printer (a) and the 7 colorants printer (b). Each patch has been halftoned independently of the others.

Table 6.5: Differences between the ColorChecker spectral reflectances and their reproduction by **sVED with pre-processing and clipping** for our 6 and 7 colorants printer. For each double column, the left one is for the 6 colorants printer and the right one for the 7 colorants printer.

Patches	ΔE_{ab}^*								ΔE_{94}^*		sRMS	
	A		D65		D50		FL11		FL31			
1	3.2	12.7	3.5	19.1	3.5	17.9	4.0	18.1	2.9	9.0	2.5 13.7	0.013 0.031
2	0.8	0.9	1.0	1.8	0.9	1.5	1.3	0.5	0.5	0.3	0.6 1.0	0.024 0.014
3	6.1	0.6	11.6	0.5	9.9	0.5	7.9	0.6	3.7	0.8	7.4 0.4	0.040 0.003
4	4.6	11.3	3.7	14.5	4.1	14.0	5.7	14.7	3.7	9.1	3.1 8.7	0.014 0.026
5	5.2	0.3	7.7	0.3	6.7	0.3	6.2	0.2	2.9	0.3	3.4 0.2	0.034 0.002
6	1.9	0.1	2.0	0.1	2.1	0.1	2.1	0.1	1.3	0.1	1.1 0.1	0.012 0.001
7	1.6	2.1	1.0	3.2	1.2	3.0	1.2	3.1	1.2	1.8	0.5 1.5	0.009 0.012
8	4.4	0.7	8.5	0.6	7.2	0.6	5.6	0.7	2.4	1.0	4.9 0.5	0.025 0.003
9	1.8	0.7	2.5	0.9	2.3	0.8	2.5	0.3	1.4	0.3	1.4 0.5	0.009 0.004
10	2.0	1.0	1.9	0.7	1.8	0.8	2.4	0.9	1.7	1.5	1.1 0.6	0.008 0.004
11	11.3	0.5	12.2	0.6	12.2	0.5	10.6	0.5	6.6	0.3	3.4 0.2	0.036 0.002
12	1.4	1.8	0.9	3.0	1.1	2.7	0.9	2.8	1.1	1.3	0.4 1.3	0.009 0.012
13	2.5	1.2	5.0	0.9	4.3	1.0	3.0	1.1	0.8	1.7	2.8 0.7	0.011 0.003
14	1.5	1.4	0.7	2.4	1.0	2.1	1.9	0.6	1.2	0.6	0.5 0.7	0.010 0.007
15	1.3	0.9	1.7	1.7	1.5	1.5	1.2	0.7	1.0	0.5	0.4 0.7	0.007 0.003
16	0.5	0.9	0.8	0.7	0.7	0.8	0.7	0.7	0.3	0.5	0.2 0.2	0.004 0.003
17	1.3	0.4	1.3	0.3	1.3	0.3	1.4	0.3	0.9	0.2	0.7 0.2	0.008 0.002
18	3.6	0.4	1.9	0.4	2.5	0.4	4.0	0.5	3.0	0.6	1.2 0.3	0.012 0.002
19	0.2	0.1	0.2	0.1	0.2	0.1	0.3	0.1	0.2	0.1	0.2 0.1	0.002 0.002
20	2.4	0.0	3.4	0.2	3.0	0.2	3.0	0.1	1.3	0.1	2.9 0.2	0.027 0.002
21	6.2	0.3	8.4	0.6	7.3	0.5	7.5	0.4	3.6	0.6	7.1 0.5	0.049 0.007
22	5.7	0.9	5.6	2.3	5.3	1.8	6.9	1.8	4.4	1.0	5.2 1.7	0.030 0.018
23	4.0	14.2	4.4	17.4	4.5	17.1	4.9	19.0	3.2	11.2	4.3 16.5	0.015 0.025
24	1.1	2.4	0.9	4.2	1.0	3.8	1.6	3.4	1.1	0.7	1.0 3.8	0.003 0.005
Av.	3.1	2.3	3.8	3.2	3.6	3.0	3.6	3.0	2.1	1.8	2.3 2.3	0.017 0.008
Std	2.5	4.1	3.5	5.5	3.1	5.3	2.7	5.6	1.6	3.1	2.1 4.4	0.013 0.009
Max	11.3	14.2	12.2	19.1	12.2	17.9	10.6	19.0	6.6	11.2	7.4 16.5	0.049 0.031

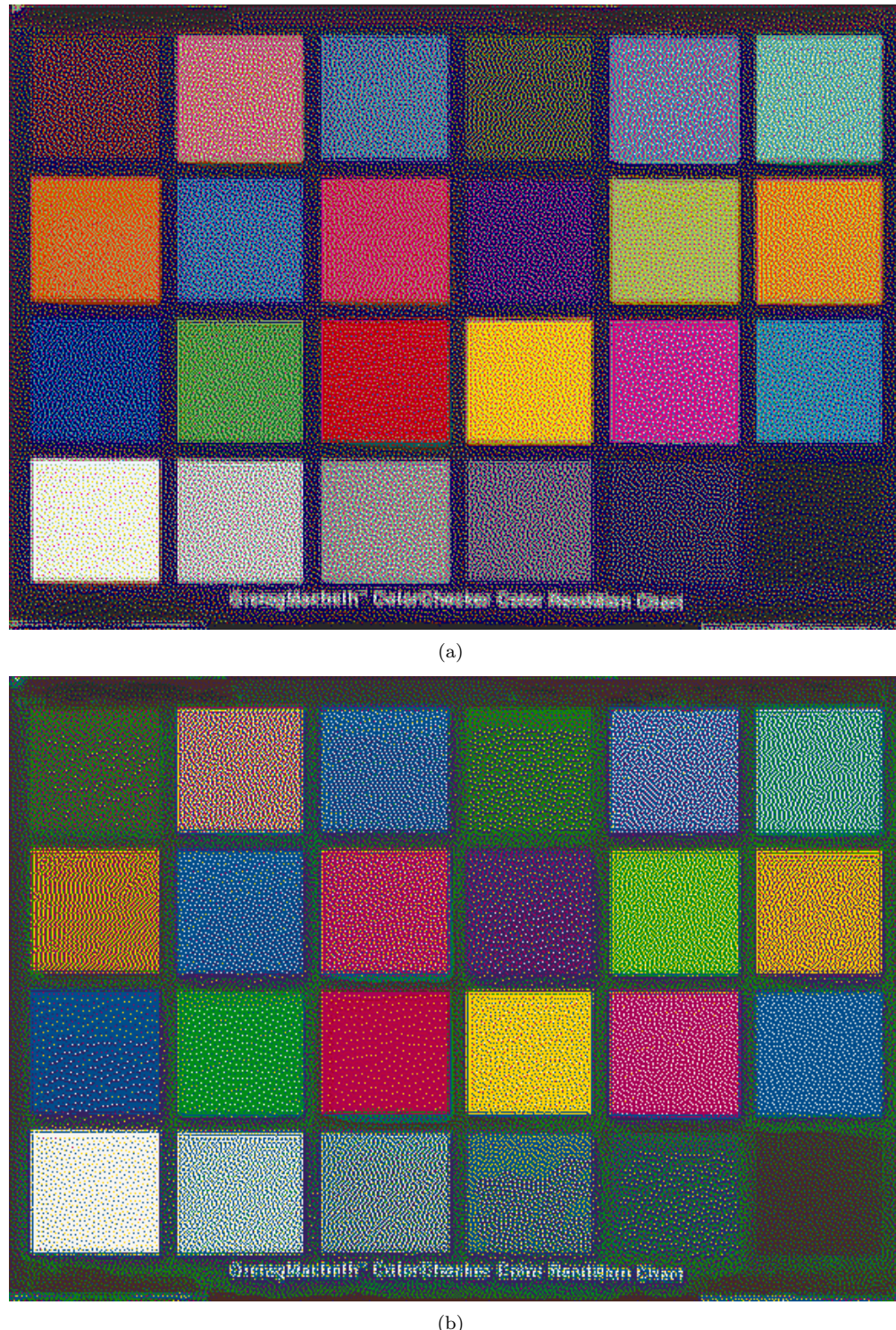


Figure 6.16: sVED with **clipping** of the gamut mapped *CC* spectral image for the 6 and 7 colorants printer in (a) and (b) respectively.

6.5.3 Reflectance scaling

Following the clipping example, we propose an alternative approach in which we scale the modified reflectance during the sVED when its maximum exceeds 1, such that the maximum of this reflectance is 1. The shape of the reflectance is then less broken than with clipping and it reduces the amount of error to spread, but it do not guarantee to part of the modified spectral reflectance below 0. The scaling is performed before the selection of the NP in the sVED process. Figure 6.17 illustrates the diagram of sVED when error control by scaling is used. In Figure 6.18 are two examples of reflectances in the image where the scaling has been performed during the halftoning by sVED.

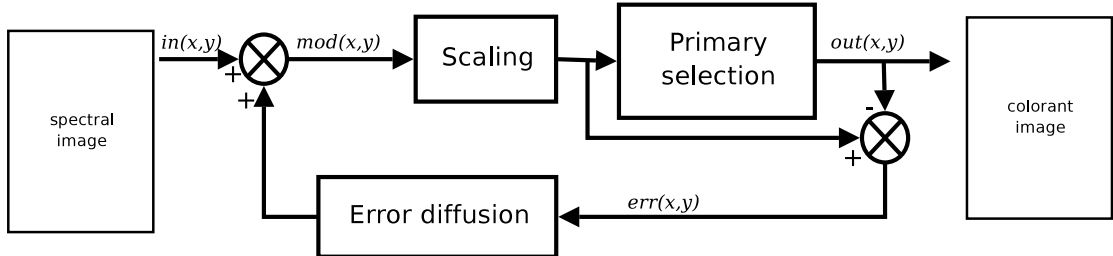


Figure 6.17: The process of spectral vector error diffusion halftoning with scaling to control the error. $in(x,y)$, $mod(x,y)$, $out(x,y)$ and $err(x,y)$ are vector data representing at the position (x,y) in the image the spectral reflectance of the image, the modified spectral reflectance, the spectral reflectance of the chosen primary and the spectral reflectance error. The processed pixel is scaled if necessary before the NP selection.

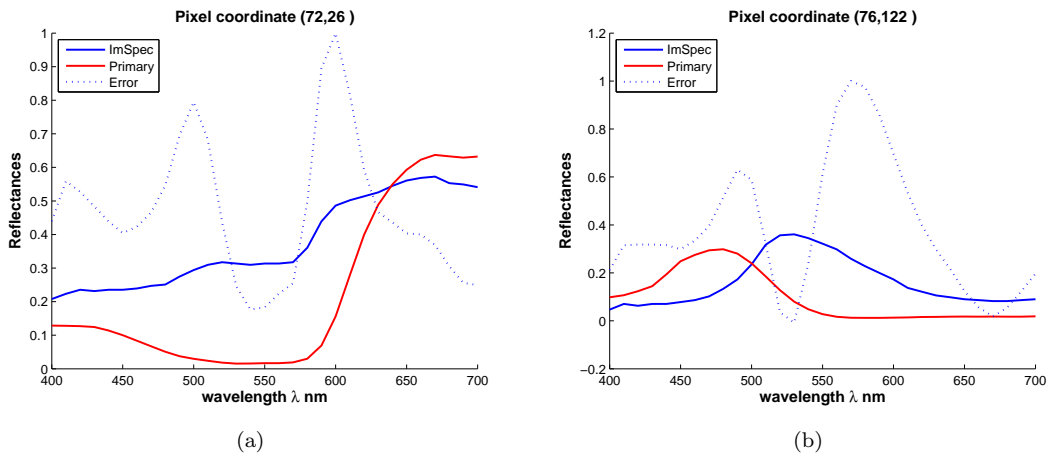


Figure 6.18: Two examples of reflectance where scaling has been applied during the sVED halftoning. Reflectance of the input pixel in blue, modified pixel with clipping in dashed blue and chosen primary in red.

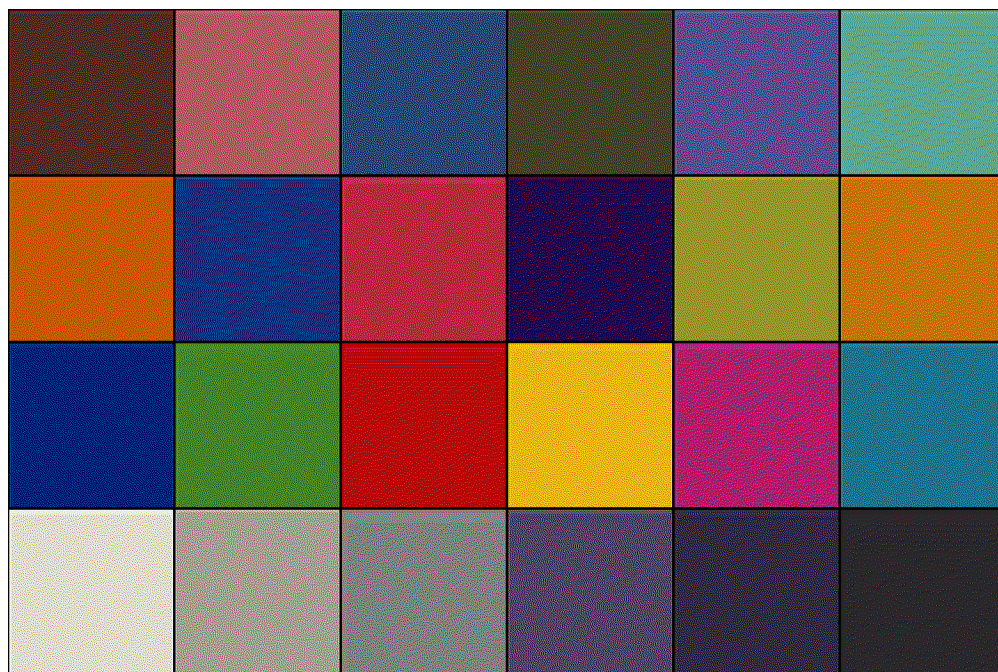
6.5.4 Experiments

For these experiment we perform similar tests as for the first sVED evaluation but with pre-processing applied and then sVED with scaling to the gamut mapped spectral images. We also run the experiment on the spectral patches using the spectral reflectances of the gamut mapped ColorChecker test chart.

In Figure 6.19 (a) and Figure 6.19 (b) are displayed the halftoned images of the gamut mapped spectral patches of the ColorChecker test chart. The gamut mapped spectral reflectances for the

6 colorants printer have been halftoned for this printer and identically for the gamut mapped spectral reflectances for the 7 colorants printer. You can see in Table 6.6 the differences between the gamut mapped spectral reflectances patches for both printers and their reproduction by sVED and scaling.

In Figure 6.20 (a) and Figure 6.20 (b) are displayed the halftoned image by sVED and scaling of the gamut mapped *CC* spectral image for the 6 colorants and 7 colorants printer. The two others halftoned images of the gamut mapped *YP* and *WR* spectral images are displayed in Appendix C.2, see Figure C.8 for *YP* and Figure C.9 for *WR*.



(a)



(b)

Figure 6.19: Halftoning by **sVED with pre-processing and scaling** of the ColorChecker spectral patches for the 6 colorants printer (a) and the 7 colorants printer (b). Each patch has been halftoned independently of the others.

Table 6.6: Differences between the ColorChecker spectral reflectances and their reproduction by **sVED with pre-processing and scaling** for our 6 and 7 colorants printer. For each double column, the left one is for the 6 colorants printer and the right one for the 7 colorants printer.

Patches	ΔE_{ab}^*								ΔE_{94}^*		sRMS			
	A		D65		D50		FL11		FL31					
1	1.9	4.5	1.7	5.2	1.7	4.9	1.8	4.7	1.7	9.6	1.2	4.3	0.013	0.021
2	5.8	3.7	5.8	3.7	5.8	3.7	4.5	2.6	5.7	2.3	5.1	2.9	0.070	0.033
3	5.0	6.6	8.7	6.2	7.5	6.3	4.6	7.0	4.9	10.3	5.8	5.3	0.042	0.035
4	2.0	7.5	1.7	9.3	1.7	9.0	2.7	9.6	1.6	10.7	1.3	6.5	0.014	0.023
5	4.2	0.3	7.7	0.3	6.4	0.3	4.4	0.2	4.2	0.3	3.9	0.2	0.053	0.002
6	2.3	0.1	2.5	0.1	2.4	0.1	2.1	0.1	1.8	0.1	2.2	0.1	0.038	0.001
7	2.5	2.6	3.1	2.8	3.0	2.7	3.4	3.0	1.7	4.7	1.1	2.2	0.012	0.023
8	3.6	4.5	6.0	3.9	5.3	4.1	3.0	4.7	4.3	6.8	3.9	3.3	0.026	0.019
9	1.2	1.7	1.2	1.8	1.2	1.7	1.1	1.1	0.5	1.2	0.7	1.2	0.008	0.009
10	1.6	5.2	1.3	4.3	1.4	4.5	1.6	5.1	1.9	8.3	1.2	3.8	0.011	0.016
11	4.7	0.5	5.7	0.6	5.7	0.5	4.9	0.5	3.4	0.3	3.1	0.2	0.041	0.002
12	1.8	2.4	2.4	3.0	2.2	2.8	2.6	3.1	1.2	4.1	0.8	2.1	0.011	0.026
13	2.9	9.1	3.7	6.8	3.5	7.5	1.9	8.8	3.6	13.9	2.4	5.3	0.012	0.021
14	2.2	0.7	3.1	1.1	2.7	1.0	2.8	0.7	1.6	0.4	1.3	0.4	0.012	0.003
15	4.0	1.4	3.9	2.4	3.9	2.1	3.2	1.3	2.3	1.2	1.5	1.1	0.009	0.005
16	3.2	1.5	4.2	1.4	3.9	1.5	3.5	1.2	1.7	0.8	1.1	0.4	0.015	0.005
17	4.4	0.4	4.1	0.3	4.2	0.3	3.8	0.3	3.7	0.2	3.0	0.2	0.031	0.002
18	1.3	0.4	1.3	0.4	1.2	0.4	0.9	0.5	1.5	0.6	1.0	0.3	0.018	0.002
19	0.7	0.1	0.7	0.1	0.7	0.1	0.9	0.1	0.9	0.1	0.7	0.1	0.011	0.002
20	8.6	0.7	10.5	1.0	9.8	0.9	8.1	0.8	5.9	1.2	9.6	0.8	0.123	0.013
21	7.9	4.3	12.6	4.8	10.9	4.5	8.4	4.7	4.8	6.8	10.5	4.5	0.086	0.047
22	3.7	7.1	4.9	7.8	4.3	7.5	3.5	7.9	2.4	11.6	4.3	7.4	0.039	0.047
23	1.9	8.0	1.8	7.7	1.7	8.0	2.2	9.0	2.9	11.9	1.7	7.8	0.019	0.018
24	0.7	1.7	0.6	1.5	0.6	1.5	0.9	1.5	1.1	3.3	0.6	1.5	0.004	0.004
Av.	3.2	3.1	4.1	3.2	3.8	3.2	3.2	3.3	2.7	4.6	2.8	2.6	0.030	0.016
Std	2.1	2.8	3.2	2.8	2.8	2.8	2.0	3.2	1.6	4.6	2.7	2.5	0.029	0.014
Max	8.6	9.1	12.6	9.3	10.9	9.0	8.4	9.6	5.9	13.9	10.5	7.8	0.123	0.047

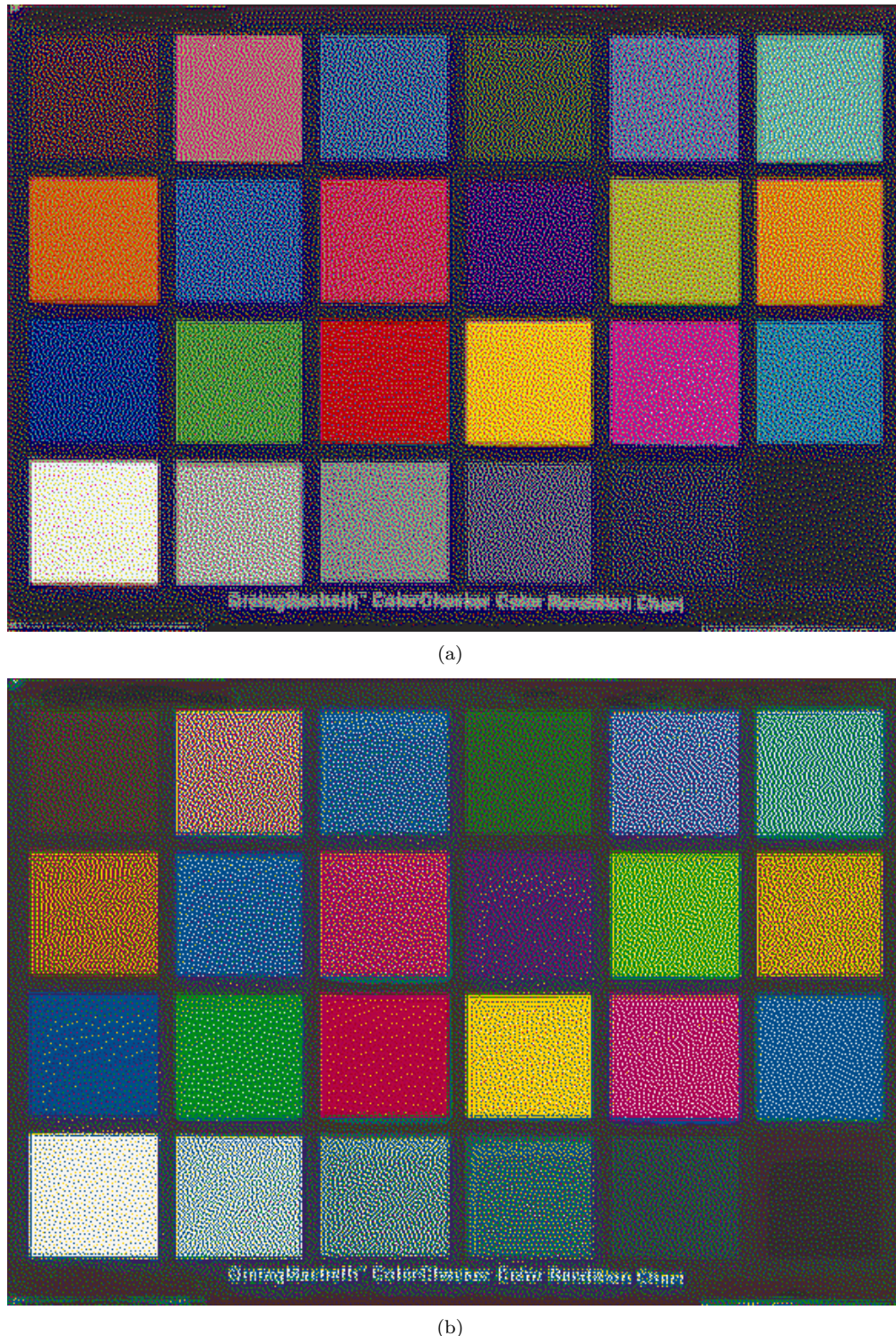


Figure 6.20: Halftoning by **sVED** with **pre-processing and scaling** of the *CC* spectral image for the 6 and 7 colorants printer in (a) and (b) respectively.

6.6 Designing new filters

As we have seen in the previous section the sVED algorithm carries a lot of error during the halftoning process and is slow to diffuse the amount of error accumulated. This phenomenon is increased when data to be halftoned are out of the printer gamut. The preprocessing by spectral gamut mapping allows to reduce concretely this problem, but still a smearing effect is visible when the filter is crossing regions in the image. So even if the image has been mapped, when the path of sVED crosses two different regions the error successively accumulated in region 1 is added to region 2. This is even more visible when the transition is abrupt in the image, see the ColorChecker in Figure 6.3 (f) for example. In case of soft transition the phenomenon of less visible.

The error controls by clipping and scaling introduced in the previous section allows to reduce the amount of error accumulated. Observation of the image transformation have shown that the spectral reflectances are extremely modified during the sVED process and this with or without preprocessing, see in Figure 6.4 the illustration of pixel in the image. Experiences have shown the difficulty of finding a fixed threshold value to cut off the error accumulation without consequences: it can disturb a stable spatial distribution of NP, it is less pleasant visually and it destroys the algorithm.

In this section we will propose new filter design for sVED. Perturbing the weights in a filter or adapting the filter to location in the image is not new (Ulichney, 1987b). Our approach will not threshold the error and will follow the rule of unity for the filter weight sum:

$$\sum_{k=1}^{k=n} w_k = 1. \quad (6.7)$$

Doing so we keep the algorithm of error diffusion, the mean spectral reflectance value of the image is preserved and should be similar as the spectral halftoned image version.

We use standard filter size as Floyd and Steinberg (1976) or Jarvis, Judice, and Ninke (1976) in our experiments. Our goal is to avoid to overload pixel not yet processed when spreading the error by wavelength channel. So for each pixel the regular NP selection is performed, then error is calculated and a new filter is created for each processed pixel taking into account the distance from the selected NP and the neighbors according to the filter size. Figure 6.21 illustrates the sVED diagram when new filter design is added to the halftoning algorithm, both propositions to design new filters use the same diagram, just the filter design changes.

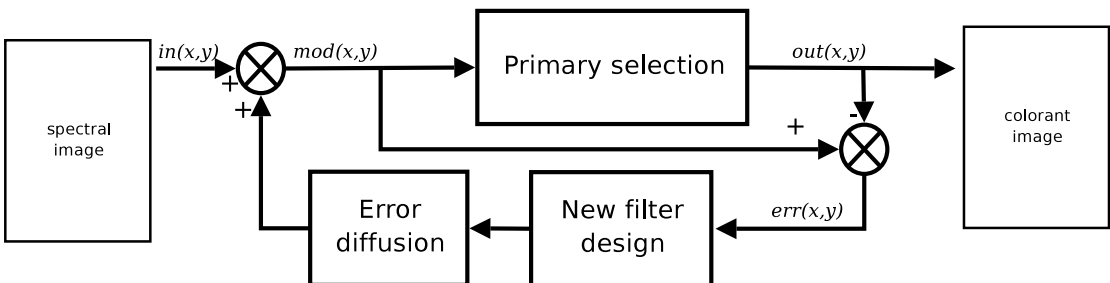


Figure 6.21: The process of spectral vector error diffusion halftoning with new filter designed at for each pixel. $in(x, y)$, $mod(x, y)$, $out(x, y)$ and $err(x, y)$ are vector data representing at the position (x, y) in the image the spectral reflectance of the image, the modified spectral reflectance, the spectral reflectance of the chosen primary and the spectral reflectance error. A new filter is design after the selection of the NP and the calculation of the error to spread.

6.6.1 Design filter by random placement of existing weights

This approach uses existing filters as in Equation 6.4 or Equation 6.5 but with a different placement of the weights in the filter for each processed pixel. This technique keep the properties of the existing filter and avoid to create pattern in the image when a large area is crossed by the filter.

6.6.2 Experiments

For these experiment we perform similar tests as for the first sVED evaluation but with pre-processing applied and then sVED with new filter by random placement of existing weights to the gamut mapped spectral images. We also run the experiment on the spectral patches using the spectral reflectances of the gamut mapped ColorChecker test chart.

In Figure 6.22 (a) and Figure 6.22 (b) are displayed the halftoned images of the gamut mapped spectral patches of the ColorChecker test chart. The gamut mapped spectral reflectances for the 6 colorants printer have been halftoned for this printer and identically for the gamut mapped spectral reflectances for the 7 colorants printer. You can see in Table 6.7 the differences between the gamut mapped spectral reflectances patches for both printers and their reproduction by sVED and new filter by random placement of existing weights.

In Figure 6.23 (a) and Figure 6.23 (b) are displayed the halftoned image by sVED and new filter by random placement of existing weights of the gamut mapped *CC* spectral image for the 6 colorants and 7 colorants printer. The two others halftoned images of the gamut mapped *YP* and *WR* spectral images are displayed in Appendix C.2, see Figure C.8 for *YP* and Figure C.9 for *WR*.

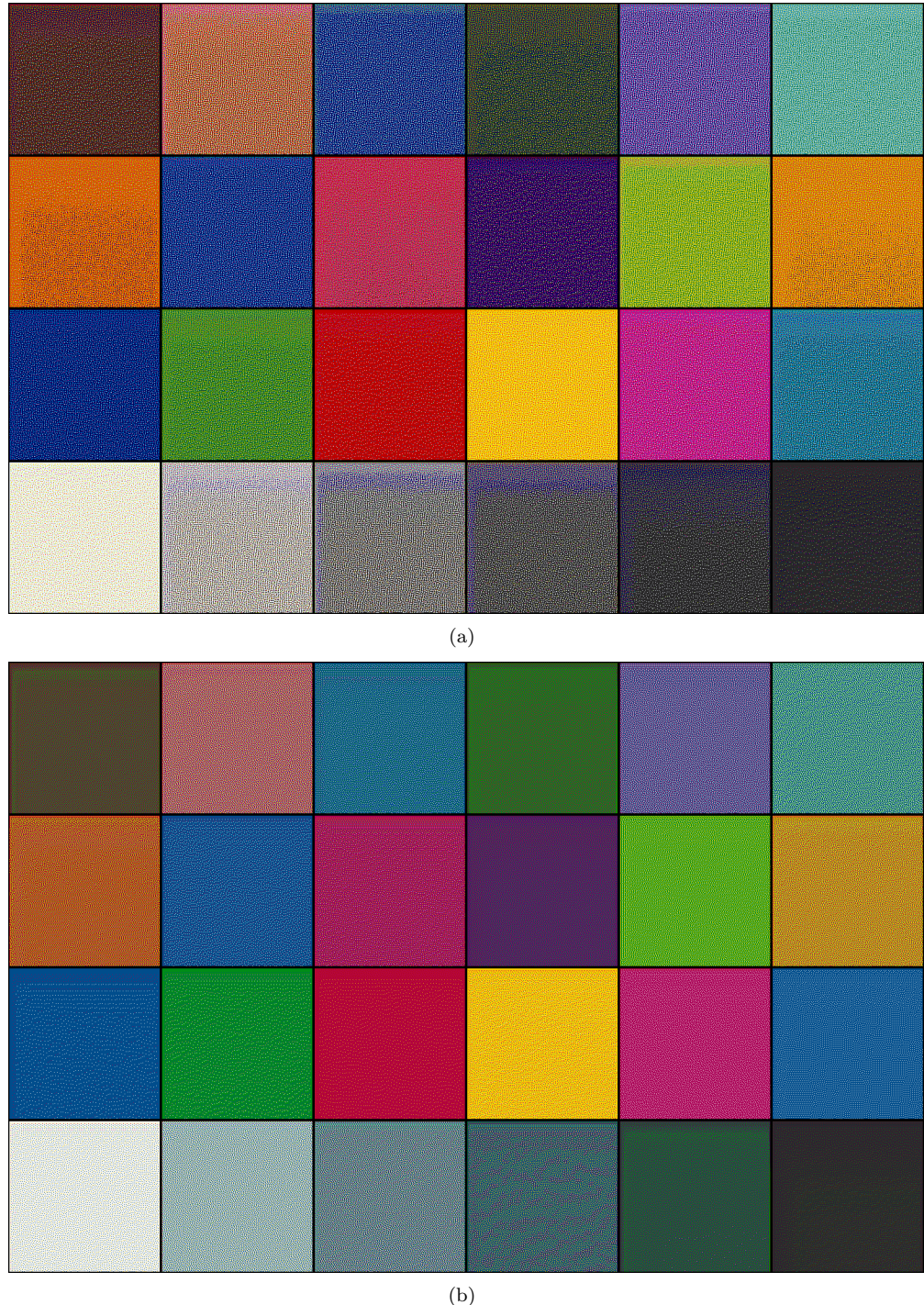


Figure 6.22: Halftoning by sVED with pre-processing and new filter by random placement of existing weights of the ColorChecker spectral patches for the 6 colorants printer (a) and the 7 colorants printer (b). Each patch has been halftoned independently of the others.

Table 6.7: Differences between the ColorChecker spectral reflectances and their reproduction by **sVED with pre-processing and new filter by random placement of existing weights** for our 6 and 7 colorants printer. For each double column, the left one is for the 6 colorants printer and the right one for the 7 colorants printer.

Patches	ΔE_{ab}^*								ΔE_{94}^*		sRMS
	A		D65		D50		FL11		FL31		
1	1.3	0.8	1.0	0.6	1.1	0.6	1.5	0.5	1.4	1.7	0.7 0.5 0.007 0.004
2	0.8	0.4	0.6	0.5	0.7	0.4	0.9	0.2	0.6	0.1	0.4 0.3 0.008 0.004
3	0.4	0.6	1.2	0.5	1.0	0.6	0.5	0.6	0.5	0.9	0.7 0.4 0.006 0.003
4	1.9	0.6	1.3	0.7	1.5	0.7	2.8	0.5	1.7	1.2	1.1 0.6 0.008 0.004
5	0.3	0.3	0.9	0.3	0.7	0.3	0.5	0.3	0.3	0.3	0.3 0.3 0.005 0.002
6	0.5	0.1	0.5	0.1	0.6	0.1	0.6	0.1	0.4	0.2	0.3 0.1 0.005 0.002
7	1.6	0.4	2.0	0.4	1.9	0.4	2.3	0.4	1.0	0.3	0.5 0.2 0.006 0.003
8	0.4	0.8	1.3	0.7	1.0	0.7	0.4	0.8	0.7	1.1	0.7 0.5 0.005 0.003
9	0.4	0.5	0.2	0.7	0.2	0.6	0.2	0.2	0.4	0.4	0.1 0.4 0.005 0.003
10	1.1	1.0	0.8	0.8	0.9	0.9	1.3	1.0	1.5	1.5	0.5 0.6 0.006 0.003
11	0.7	0.6	0.7	0.6	0.7	0.6	0.9	0.5	0.5	0.3	0.4 0.2 0.006 0.002
12	1.3	0.5	1.7	0.6	1.6	0.6	2.0	0.6	0.9	0.2	0.4 0.2 0.006 0.003
13	0.6	1.2	1.4	0.9	1.2	1.0	0.4	1.1	1.2	1.7	0.8 0.7 0.005 0.003
14	0.8	0.7	0.8	1.1	0.8	1.0	1.2	0.7	0.7	0.4	0.5 0.4 0.006 0.003
15	1.4	0.6	1.5	1.1	1.4	1.0	1.3	0.3	1.1	0.4	0.4 0.5 0.004 0.003
16	0.6	1.0	0.9	0.9	0.8	1.0	0.8	0.9	0.4	0.6	0.2 0.2 0.003 0.003
17	0.6	0.4	0.4	0.4	0.5	0.4	0.7	0.3	0.7	0.2	0.2 0.2 0.004 0.002
18	0.9	0.5	0.5	0.4	0.6	0.4	1.3	0.5	1.0	0.6	0.4 0.4 0.007 0.002
19	0.2	0.1	0.2	0.1	0.2	0.1	0.3	0.1	0.2	0.1	0.2 0.1 0.002 0.003
20	0.1	0.0	0.3	0.2	0.2	0.1	0.3	0.1	0.1	0.1	0.2 0.1 0.008 0.003
21	0.1	0.5	0.4	0.4	0.2	0.4	0.3	0.4	0.3	0.8	0.2 0.4 0.009 0.004
22	0.4	1.2	0.1	1.1	0.1	1.2	0.6	1.2	0.6	1.7	0.1 1.2 0.008 0.007
23	1.2	2.3	0.7	2.1	0.9	2.2	1.7	2.1	1.3	3.5	0.9 2.1 0.007 0.006
24	0.8	1.5	0.6	1.5	0.7	1.5	1.1	1.3	1.0	3.2	0.6 1.5 0.003 0.004
Av.	0.8	0.7	0.8	0.7	0.8	0.7	1.0	0.6	0.8	0.9	0.5 0.5 0.006 0.003
Std	0.5	0.5	0.5	0.5	0.5	0.5	0.7	0.5	0.4	0.9	0.3 0.5 0.002 0.001
Max	1.9	2.3	2.0	2.1	1.9	2.2	2.8	2.1	1.7	3.5	1.1 2.1 0.009 0.007

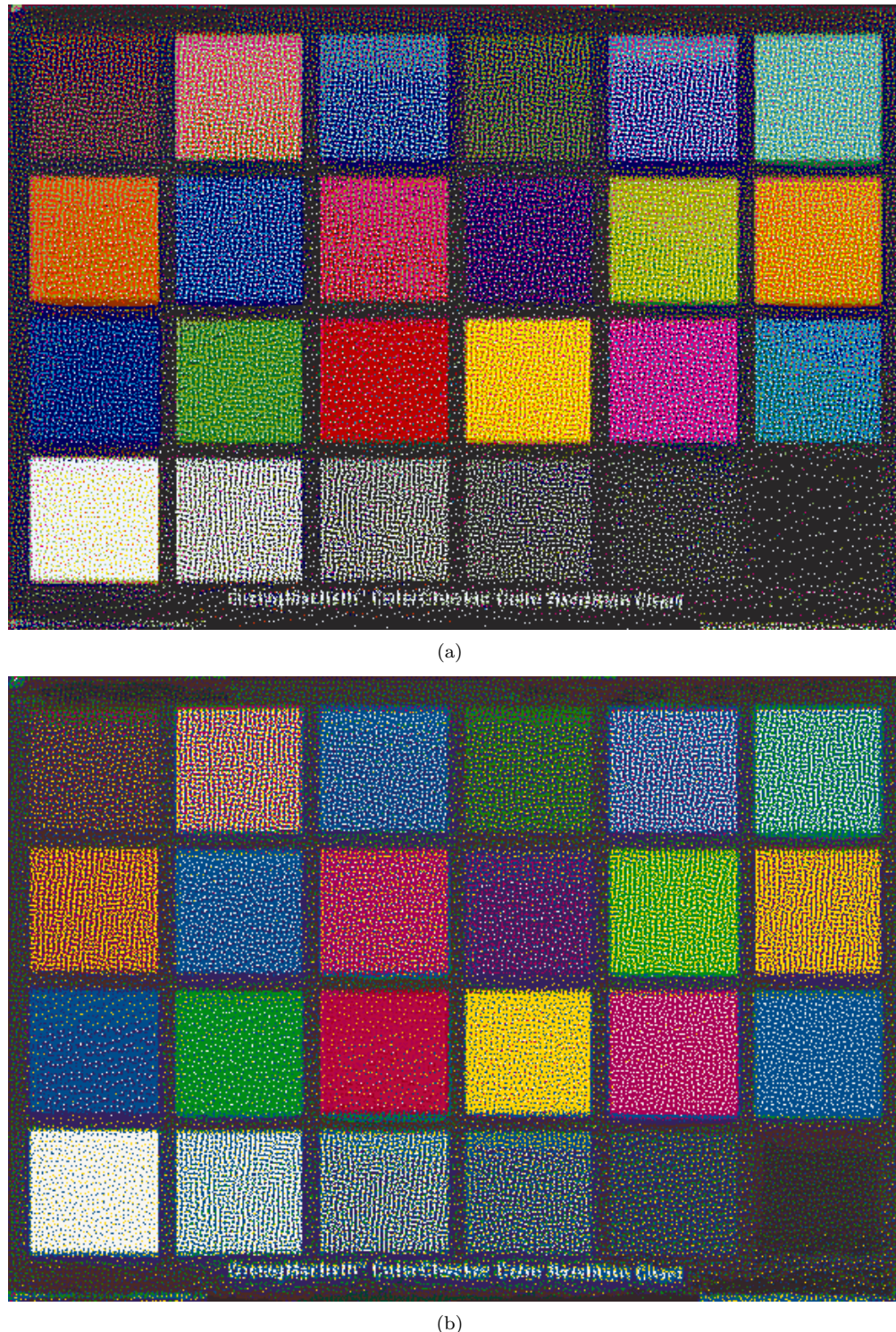


Figure 6.23: Halftoning by sVED with pre-processing and new filter by random placement of existing weights of the CC spectral image for the 6 and 7 colorants printer in (a) and (b) respectively.

6.6.3 Design filter by distance

For each pixel after the NP has been selected and the error calculated the following operation are performed to compute the new filter weights:

$$d_k = \sqrt{(\mathbf{p} - \text{mod}(x+i, y+j))^T \times (\mathbf{p} - \text{mod}(x+i, y+j))} \quad (6.8)$$

where d_k is the Euclidean distance between the selected Neugebauer primary \mathbf{p} and the k th modified spectral reflectance $\text{mod}(x+i, y+j)$ according to the filter shape. For example a Floyd and Steinberg (1976) filter has 4 weights. The set of distance d_i is then normalized by the maximum:

$$d'_k = \frac{d_k}{\max_k(d_k)} \quad (6.9)$$

and doing so we obtain a set weight with values $\in [0, 1]$. We still need to modify our weights since the sum is not equal to one and the maximum = 1 is set to the farthest neighbor and we want the inverse relation. A first solution is to remove the contribution for this pixel by doing:

$$d''_k = 1 - d'_k \quad (6.10)$$

and then most of the error will be spread to the closest neighbor and less to the remaining pixels. A last operation before using the filter is to divide by the sum off them in order to the sum equal to one:

$$w_k = \frac{d''_k}{\sum_k d''_k} \quad (6.11)$$

6.6.4 Experiments

For these experiment we perform similar tests as for the first sVED evaluation but with pre-processing applied and then sVED with new filter by distance to the gamut mapped spectral images. We also run the experiment on the spectral patches using the spectral reflectances of the gamut mapped ColorChecker test chart.

In Figure 6.24 (a) and Figure 6.24 (b) are displayed the halftoned images of the gamut mapped spectral patches of the ColorChecker test chart. The gamut mapped spectral reflectances for the 6 colorants printer have been halftoned for this printer and identically for the gamut mapped spectral reflectances for the 7 colorants printer. You can see in Table 6.8 the differences between the gamut mapped spectral reflectances patches for both printers and their reproduction by sVED and new filter by distance.

In Figure 6.25 (a) and Figure 6.25 (b) are displayed the halftoned image by sVED and new filter by distance of the gamut mapped *CC* spectral image for the 6 colorants and 7 colorants printer. The two others halftoned images of the gamut mapped *YP* and *WR* spectral images are displayed in Appendix C.2, see Figure C.8 for *YP* and Figure C.9 for *WR*.

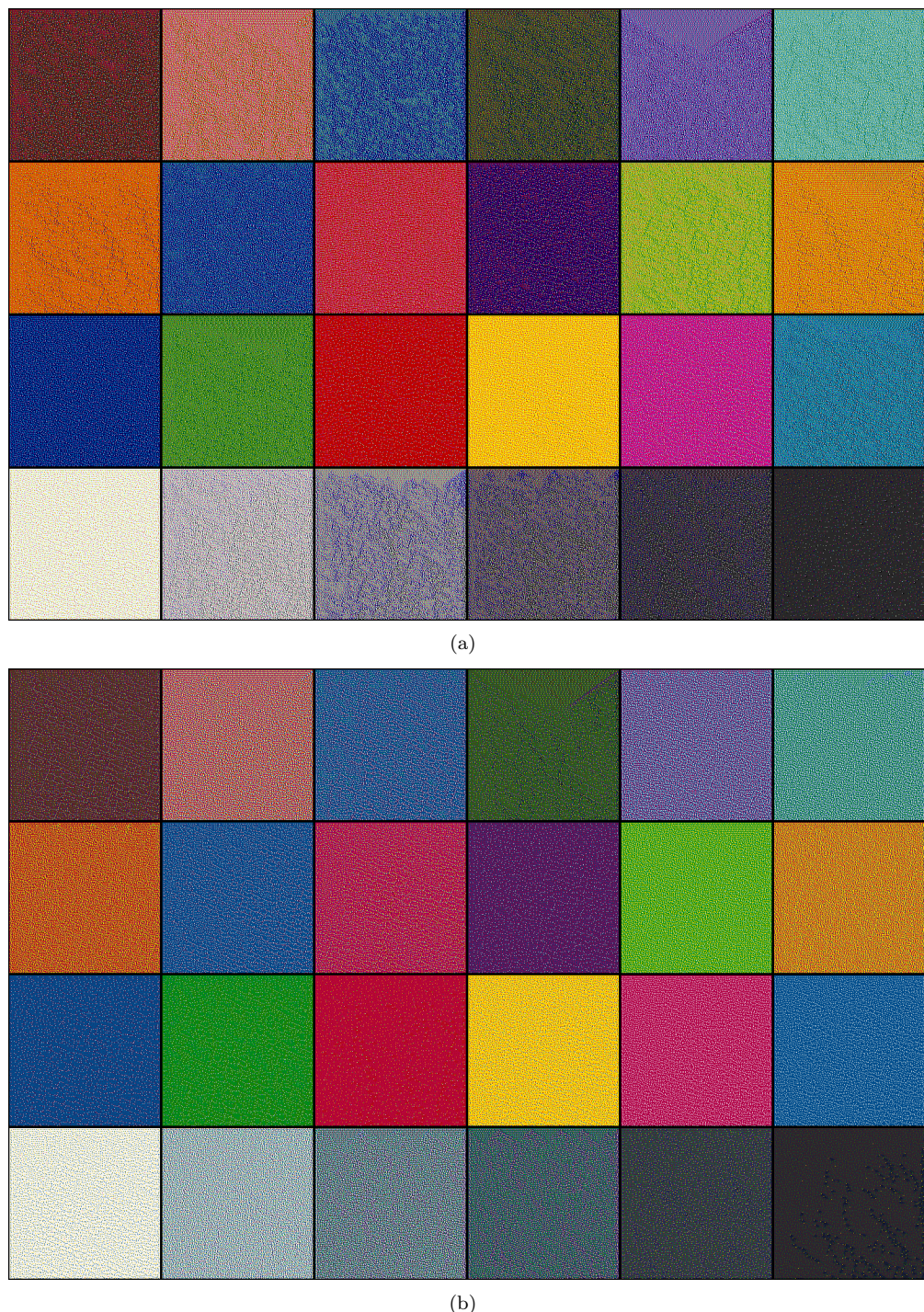


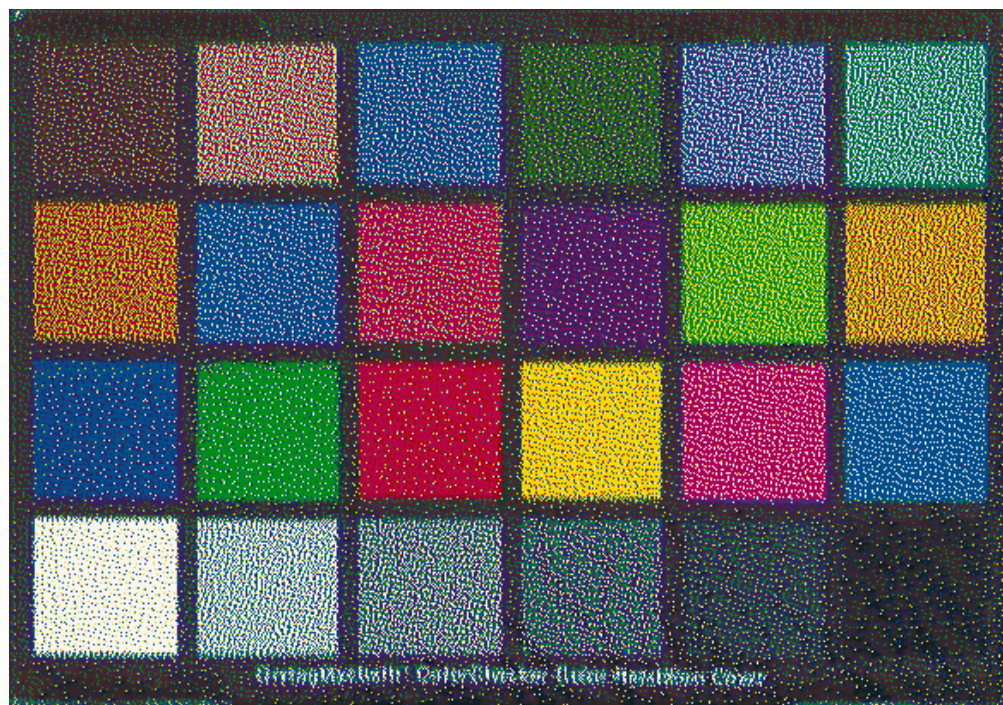
Figure 6.24: Halftoning by **sVED** with pre-processing and new filter by distance of the ColorChecker spectral patches for the 6 colorants printer (a) and the 7 colorants printer (b). Each patch has been halftoned independently of the others.

Table 6.8: Differences between the ColorChecker spectral reflectances and their reproduction by **sVED with pre-processing and new filter by distance** for our 6 and 7 colorants printer. For each double column, the left one is for the 6 colorants printer and the right one for the 7 colorants printer.

Patches	ΔE_{ab}^*								ΔE_{94}^*	sRMS	
	A		D65		D50		FL11		FL31	D50	
1	3.8	0.6	3.0	1.8	3.4	1.5	5.5	1.4	4.3	1.7	2.1 1.1 0.016 0.007
2	1.0	0.6	1.1	1.1	1.1	0.8	1.2	0.2	0.8	0.2	0.7 0.6 0.014 0.011
3	2.4	0.5	5.9	1.2	4.8	0.9	3.2	0.7	0.7	1.3	3.4 0.7 0.020 0.009
4	4.1	0.9	3.1	1.6	3.5	1.4	6.1	1.4	3.9	1.8	2.5 1.0 0.014 0.006
5	2.3	0.2	4.3	0.2	3.6	0.2	3.0	0.2	1.2	0.1	1.9 0.1 0.018 0.001
6	1.4	1.1	1.4	1.0	1.5	1.0	1.5	0.9	1.1	0.7	0.8 0.7 0.008 0.005
7	0.8	0.8	1.4	1.5	1.2	1.3	1.8	1.3	0.6	0.8	0.4 0.6 0.006 0.007
8	3.4	0.4	7.0	1.1	5.9	0.8	4.1	0.6	1.0	1.2	3.9 0.6 0.018 0.007
9	2.3	0.1	4.0	0.1	3.6	0.1	3.4	0.5	1.8	0.3	1.8 0.1 0.010 0.003
10	3.3	0.2	1.8	1.2	2.3	0.8	5.3	0.2	4.7	0.8	1.3 0.4 0.015 0.005
11	2.3	0.9	2.6	1.1	2.7	1.0	2.7	1.0	1.6	0.7	1.2 0.5 0.015 0.004
12	0.6	0.9	1.0	1.7	0.8	1.5	1.4	1.5	0.5	0.7	0.2 0.6 0.006 0.008
13	3.7	0.6	7.4	1.4	6.4	1.2	4.2	0.9	1.7	1.5	4.1 0.8 0.014 0.005
14	1.3	0.6	0.9	0.9	1.1	0.7	1.6	1.1	1.0	0.6	0.5 0.4 0.007 0.006
15	0.9	0.4	1.0	0.5	0.9	0.4	0.9	0.3	0.8	0.3	0.2 0.1 0.004 0.002
16	0.1	0.5	0.2	0.4	0.2	0.5	0.2	0.4	0.1	0.2	0.1 0.1 0.003 0.003
17	0.6	1.1	1.0	1.1	0.8	1.1	0.8	1.1	0.3	1.1	0.4 0.8 0.005 0.003
18	1.8	0.6	0.7	0.5	1.1	0.5	2.2	0.5	1.6	0.4	0.6 0.4 0.009 0.002
19	0.3	0.1	0.3	0.1	0.3	0.1	0.4	0.0	0.2	0.1	0.3 0.1 0.002 0.002
20	0.2	0.4	1.0	0.4	0.7	0.4	0.6	0.4	0.2	0.8	0.7 0.4 0.014 0.007
21	0.8	1.5	2.4	1.6	1.7	1.6	1.8	1.5	0.7	2.8	1.7 1.5 0.025 0.017
22	1.7	2.1	0.6	2.6	0.7	2.5	2.8	2.6	2.1	3.5	0.7 2.5 0.019 0.014
23	2.5	1.9	1.4	2.0	1.8	2.1	3.7	2.4	2.7	3.5	1.7 2.0 0.011 0.008
24	1.3	0.9	0.8	1.2	1.0	1.1	2.0	0.7	1.4	2.4	1.0 1.0 0.003 0.003
Av.	1.8	0.8	2.3	1.1	2.1	1.0	2.5	0.9	1.5	1.1	1.3 0.7 0.012 0.006
Std	1.2	0.5	2.1	0.6	1.7	0.6	1.7	0.7	1.3	1.0	1.2 0.6 0.006 0.004
Max	4.1	2.1	7.4	2.6	6.4	2.5	6.1	2.6	4.7	3.5	4.1 2.5 0.025 0.017



(a)



(b)

Figure 6.25: Halftoning by sVED with pre-processing and new filter by distance of the CC spectral image for the 6 and 7 colorants printer in (a) and (b) respectively.

6.7 Conclusion

In that chapter we have presented an alternative way to print spectral images which combines the different steps of our first spectral color reproduction workflow. The first workflow requires to characterize spectrally our printing system and should transform the spectral image into a multi-colorant binary image. The first operation allows to obtain a colorant combination to reproduce a given spectral reflectance, it is equivalent as the colorant separation in a color reproduction workflow but extended to spectral color reproduction. The transformation of halftoning will finally transform the multi-colorant image into a multi-colorant binary image, this transformation is performed colorant channel by colorant channel independently. The spectral vector error diffusion (sVED) allows to perform all transformations in one step: from a spectral image to a multi-colorant binary image.

sVED is an extension to spectral data of the color VED algorithm where all colorant values of a pixel are halftoned simultaneously. Only a short spectral characterization of our printing system is required for sVED: to measure the Neugebauer primaries (NP) spectral reflectances. The sVED algorithm improves the image quality upon the traditional approach of scalar error diffusion (SED), it provides less noisy dot distribution, decreases the risk of color shift when colorant channel are halftoned independently by SED. However sVED does not come without problems, during the process of error diffusion large amount of error is accumulated and suffer to reach a stable spatial distribution of NP, these two phenomena are referred to the slow response and smear effect. The results is a decreasing of image quality, it is less pleasant visually and we loose details. Also data outside the printer gamut are known to generate large error which slow down the error diffusion. To correct these problems solution have been proposed: pre-processing in lower dimension by gamut mapping of the image before sVED (Kawaguchi et al., 1999) still in lower dimension, threshold the error during the halftoning process (Haneishi et al., 1996) in color VED or combining SED and VED in halftoning of color image (Fan, 1998) to use the advantages of both methods.

We have proposed a method of spectral gamut mapping as pre-processing before the sVED based on an inverse spectral printer model. We invert the spectral Neugebauer printer model, this model says that the spectral reflectance estimation of an area covered by the NP of the printer is the weighted sum of these NP weighted by their coverage on a unitary area. After gamut mapping the spectral reflectances to be halftoned are the closest spectral reflectances the printer model can estimate. The NP used for the pre-processing are identical as those used in the sVED algorithm. In that configuration the data to be reproduced are not anymore the original since they have been mapped to the spectral printer gamut but spectral root mean square difference (sRMS) has been used as optimization criterion in printer model inversion, or in other term no observers or illuminants have been used to perform the mapping. Our approach does not have an heavy computationally cost since it doesn't require to perform PCA or to build a volume (i.e. the gamut) in $n > 3$ dimension (Bakke et al., 2005). Applied before sVED of spectral images have shown improvement of the halftoned images by decreasing of the smear effect or slow response of the algorithm.

Gamut mapping as pre-processing does not solve all the problems. We have shown that even in the gamut, the sVED of spectral image brings large error which results in strong modification of the pixel values (i.e. a spectral reflectance) in the image. To apply threshold on spectral reflectance is complicated: we need to define when a spectral reflectance is too far from the gamut (because of the error accumulated) and we break the error diffusion algorithm. We remind that SED and sVED keep most of the energy in an image after halftoning by quantifying and spreading the difference between the original pixel value and its quantified value. In order to reduce the error accumulated during the sVED process we proposed to modify the processed pixel before the NP selection: clipping or scaling, the first method will clip the processed pixel if their values exceed 1 or is smaller than 0, the second method will normalize the spectral reflectance of the processed pixel when its maximum exceeds 1. These correction have shown interesting results when transition area are halftoned, especially when the transition is abrupt.

Finally a last approach has been tested which attempts to use the local information in the

image to design new filters for spreading the error. The idea is to avoid to spread error to pixel which already far from the processed pixel. Concretely the weights are based on the distance processed pixel to neighboring pixels according to the filter size, we keep the property of unity in the sum of the weights. A second approach combines existing filters as Jarvis, Judice, and Ninke (1976) or Floyd and Steinberg (1976) and a random placement of their weights for each processed pixel. In transition area the new filters (new filter designed at each processed pixel) these approaches have shown a good preservation of the details (i.e. to keep the existing boundaries) but with the side effect of increasing the noise in the image.

Chapter 7

Comparison of the spectral color reproduction workflows

7.1 Introduction

In this chapter we will compare the reproduction of spectral data by two possible workflows presented in Figure 6.1. The first workflow is divided in two steps: colorant separation (CS) and halftoning by colorant channels using scalar error diffusion (SED). The second workflow will halftone directly the spectral image by spectral vector error diffusion (sVED). Both workflows start with a common step of spectral gamut mapping (sGM). It is the reproduction of the gamut mapped spectral data which is compared.

The spectral reflectance targets correspond to spectral reflectance measurements extracted from a paint (Dupraz, Ben Chouikha, and Alquié, 2007). We will first look at the differences between the original measured data and their gamut mapped version. Then spectral patches of size 256×256 pixels will be created and their reproduction simulated for our 7 colorants printer.

7.2 Experiment

The spectral reflectance targets have been obtained by measuring the spectral reflectances of a paint at different locations, see Figure 7.2. Twelve samples have been selected and their spectral reproduction simulated. See in Figure 7.2 the different locations where the measurements were taken in the paint and in Figure 7.2.1 (a) the corresponding spectral reflectances.

7.2.1 Spectral gamut mapping

The sGM operation is performed using the method described in Appendix B for our 7 colorants printer. The gamut mapped spectral reflectances are displayed in Figure 7.2.1 (b). Color and spectral difference between measured spectral reflectances and gamut mapped spectral reflectance are available in Table 7.1.

7.2.2 Colorant separation and halftoning by colorant channel

For the first workflow CS is performed for the 12 gamut mapped spectral reflectances using CMR method as described in Chapter ???. From the 12 colorant combinations obtained we create 12 patches of 7 channels each. The final step is the halftoning operation which is performed channel independently. We use SED halftoning technique with Jarvis, Judice, and Ninke (1976) filter to diffuse the error in the halftoning algorithm.

The spectral reflectance of each patch is estimated by counting the NP pixel's occurrences and then considering a unitary area for each patch. Differences between the gamut mapped



Figure 7.1: Illustration of the spectral measurements location in the paint *La Madeleine*. Spectral acquisition was performed by Dupraz et al. (2007) using a LT2 SAS camera.



Figure 7.2: Paint of *La Madeleine*, the 12 black spots correspond of the location where the spectral reflectances were taken.

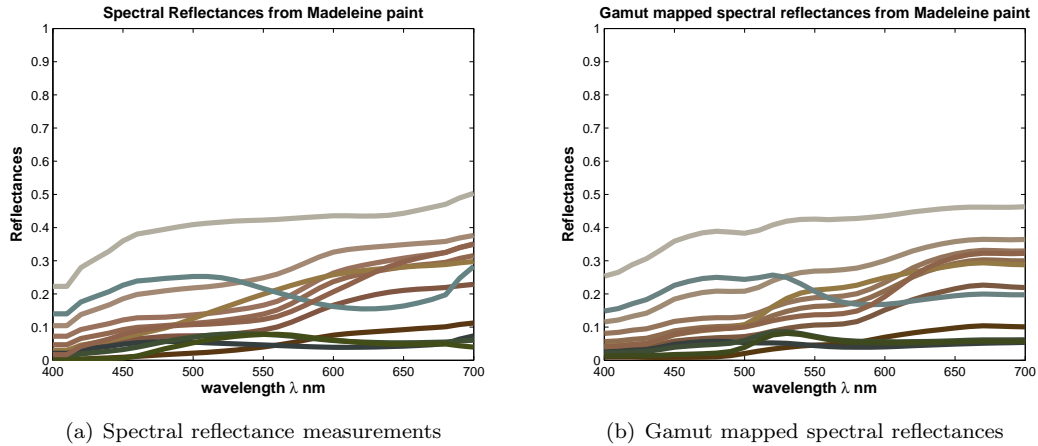


Figure 7.3: Spectral reflectance measurements of the 12 samples in (a) and their gamut mapped version for our 7 colorants printer in (b).

spectral reflectances and their simulated reproduction by CS and SED are presented in all left columns of each pair of column in Table 7.2.

7.2.3 Spectral vector error diffusion

For the second workflow we have created 12 spectral patches of size 256×256 pixels. Each patch is halftoned by sVED using Jarvis, Judice, and Ninke (1976) filter.

The spectral reflectance of each patch is estimated by counting the NP pixel's occurrences and then considering a unitary area for each patch. Differences between the gamut mapped spectral reflectances and their simulated reproduction by sVED are presented in all right columns of each pair of column in Table 7.2.

The comparison of the color differences and spectral differences for the two workflows shows better performances of the second workflow: sGM and halftoning by sVED. But the global difference is not very large between the two workflows except for the spectral differences where average difference, standard deviation and maximum are the smallest for the spectral reproduction by sVED.

7.3 Comparison of the dot distribution

For each halftoned patch we calculate a color rendering for illuminant D50 and standard observer CIE CMFs 1931. Then, we can compare the spatial NPs distribution for the 12 samples, see Figure 7.4 to Figure 7.9. The left side patches are the result of spectral reproduction by CS and SED when the right side patches are the result of the spectral reproduction by sVED.

Table 7.1: Differences between the spectral reflectance measurement and their gamut mapped version to our 7 colorants printer.

Samples	ΔE_{ab}^*				ΔE_{94}^*	sRMS
	A	D65	D50	FL11	D50	
1	3.0	4.5	4.2	6.1	3.1	0.014
2	3.5	5.2	4.9	6.9	3.5	0.014
3	2.4	3.3	3.1	4.8	2.5	0.013
4	2.9	4.4	4.1	5.7	2.9	0.009
5	1.2	1.3	1.3	2.8	0.7	0.009
6	2.1	3.0	2.9	3.8	2.0	0.006
7	1.3	1.4	1.4	0.8	1.2	0.016
8	1.8	1.0	1.3	1.7	1.1	0.005
9	3.5	2.2	2.6	3.3	1.8	0.023
10	2.5	2.9	2.7	2.4	1.7	0.007
11	4.6	6.3	5.7	5.3	2.8	0.011
12	1.1	1.8	1.7	3.2	1.2	0.013
Av.	2.5	3.1	3.0	3.9	2.0	0.012
Std	1.1	1.7	1.5	1.9	0.9	0.005
Max	4.6	6.3	5.7	6.9	3.5	0.023

Table 7.2: Differences between the gamut mapped spectral reflectances and their reproduction by CS and SED (left columns of each double column) and by sVED (right columns of each double column).

Samples	ΔE_{ab}^*				ΔE_{94}^*		sRMS	
	A	D65	D50	FL11	D50	D50		
1	1.2	0.6	1.6	0.6	1.6	0.6	1.2	0.4
2	2.8	0.4	3.0	0.5	3.1	0.5	2.6	0.7
3	1.3	0.3	1.7	0.3	1.7	0.3	0.9	0.6
4	1.9	0.6	2.3	0.9	2.4	0.8	2.2	0.8
5	2.5	0.4	2.5	0.5	2.7	0.5	2.1	0.6
6	1.8	3.5	2.0	3.1	2.0	3.2	2.1	2.9
7	0.5	0.2	0.5	0.2	0.5	0.2	0.1	0.1
8	1.0	1.3	0.7	1.4	0.8	1.3	1.6	1.1
9	0.7	0.4	0.5	0.3	0.6	0.3	2.2	0.5
10	1.1	1.6	0.8	1.9	0.9	1.8	1.5	1.9
11	1.2	1.5	1.0	2.1	1.1	2.0	1.0	2.2
12	2.0	0.4	2.2	0.4	2.3	0.4	1.7	0.7
Av.	1.5	0.9	1.6	1.0	1.6	1.0	1.6	1.1
Std	0.7	1.0	0.9	0.9	0.8	0.9	0.7	0.8
Max	2.8	3.5	3.0	3.1	3.1	3.2	2.6	2.9
							2.0	1.5
							0.010	0.005

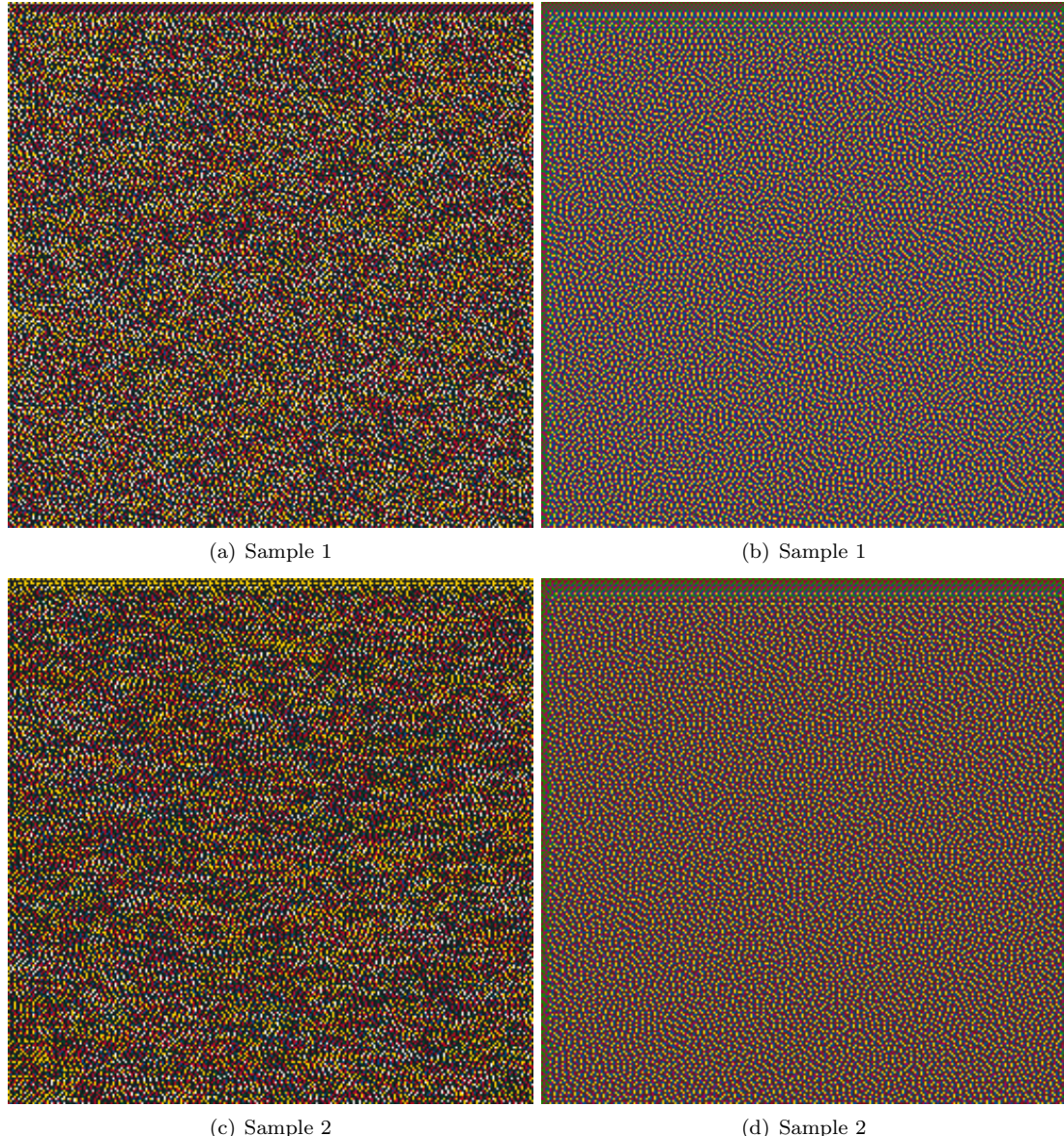


Figure 7.4: Halftoned patches of sample 1 and sample 2 of *La Madeleine* paint. Spatial NPs distribution obtained after the first workflow using CS and SED in (a) and (c) and their corresponding distributions obtained after the second workflow using sVED in (b) and (d).

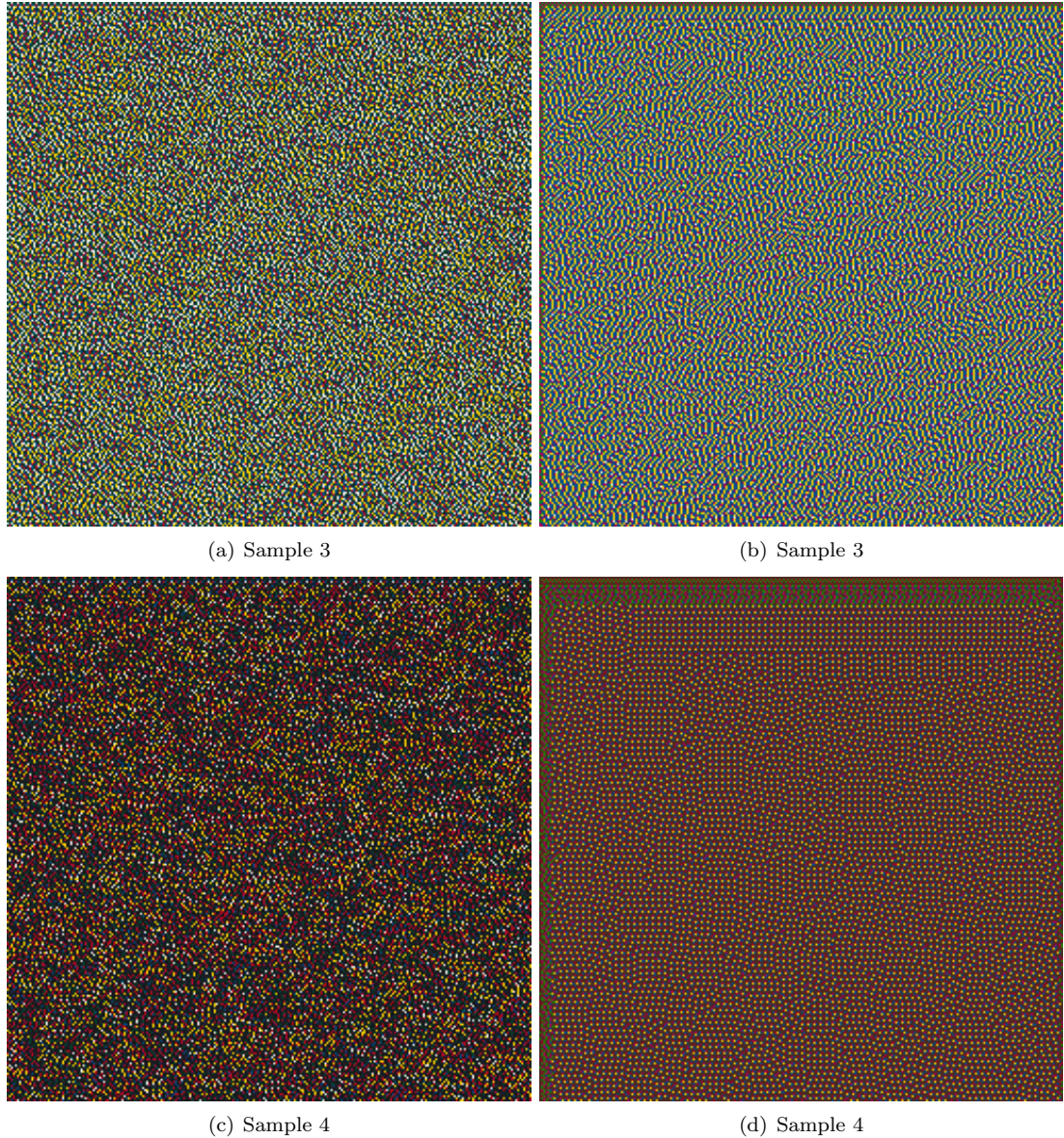


Figure 7.5: Halftoned patches of sample 3 and sample 4 of *La Madeleine* paint. Spatial NPs distribution obtained after the first workflow using CS and SED in (a) and (c) and their corresponding distributions obtained after the second workflow using sVED in (b) and (d).

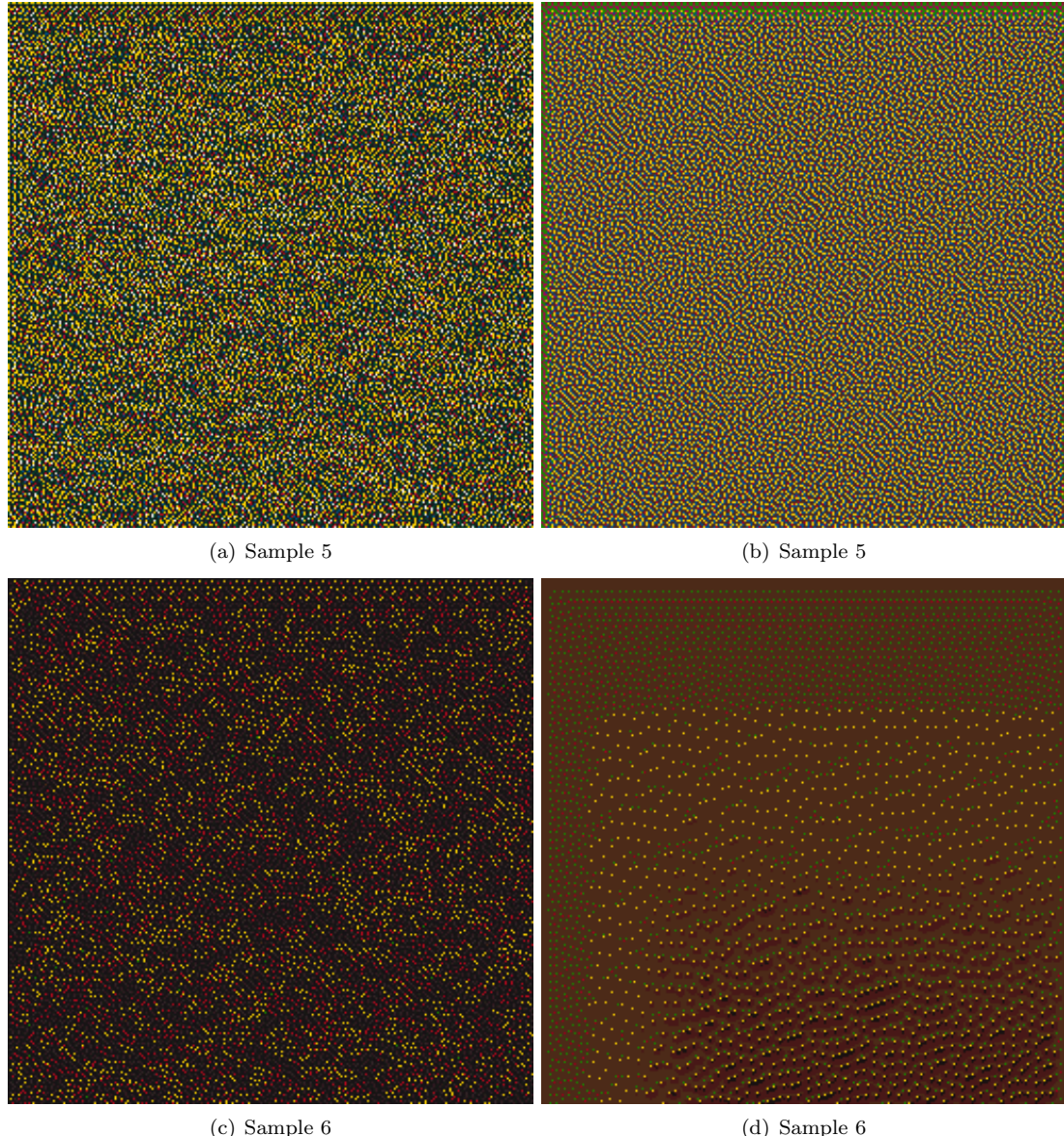


Figure 7.6: Halftoned patches of sample 5 and sample 6 of *La Madeleine* paint. Spatial NPs distribution obtained after the first workflow using CS and SED in (a) and (c) and their corresponding distributions obtained after the second workflow using sVED in (b) and (d).

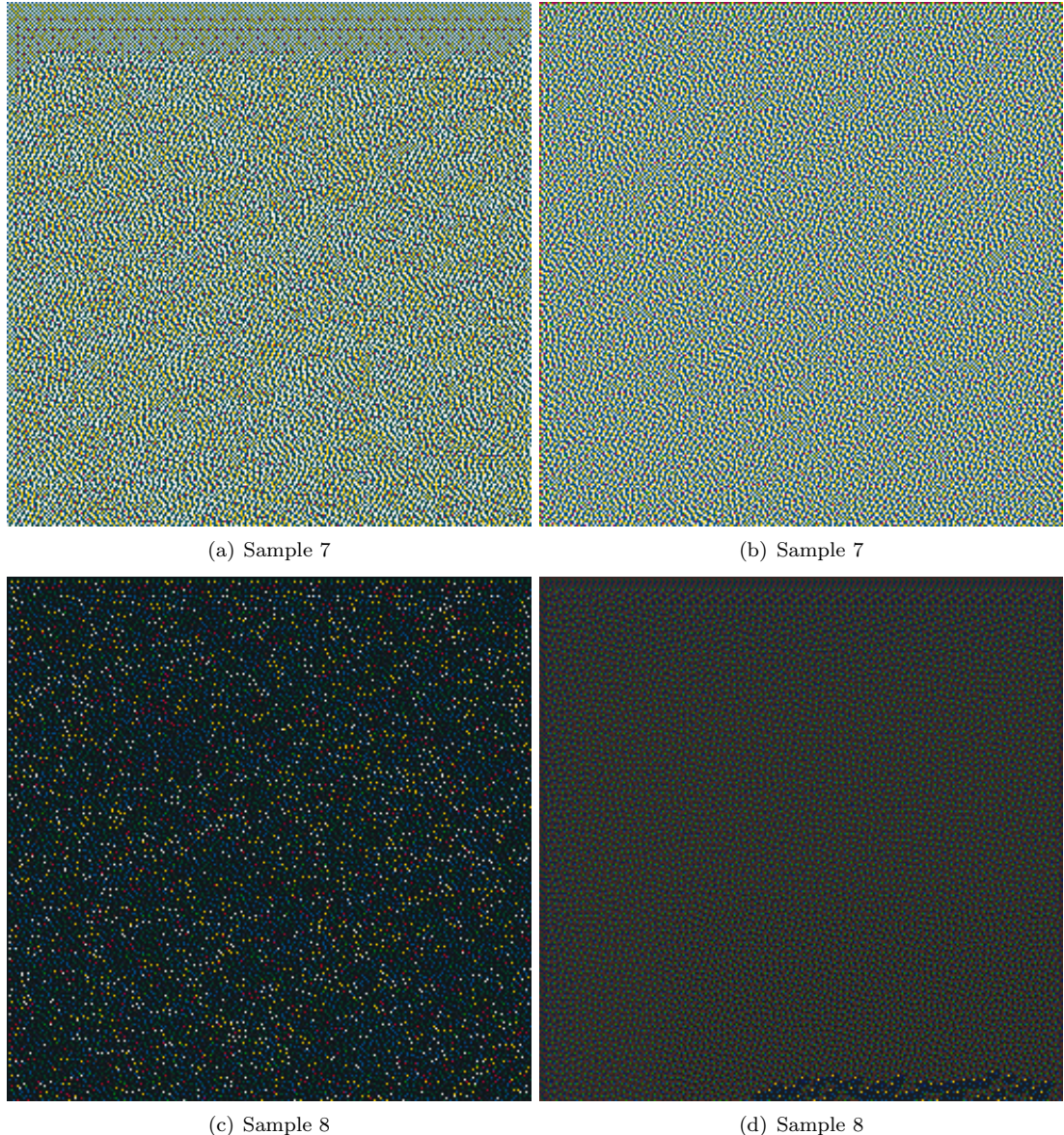


Figure 7.7: Halftoned patches of sample 7 and sample 8 of *La Madeleine* paint. Spatial NPs distribution obtained after the first workflow using CS and SED in (a) and (c) and their corresponding distributions obtained after the second workflow using sVED in (b) and (d).

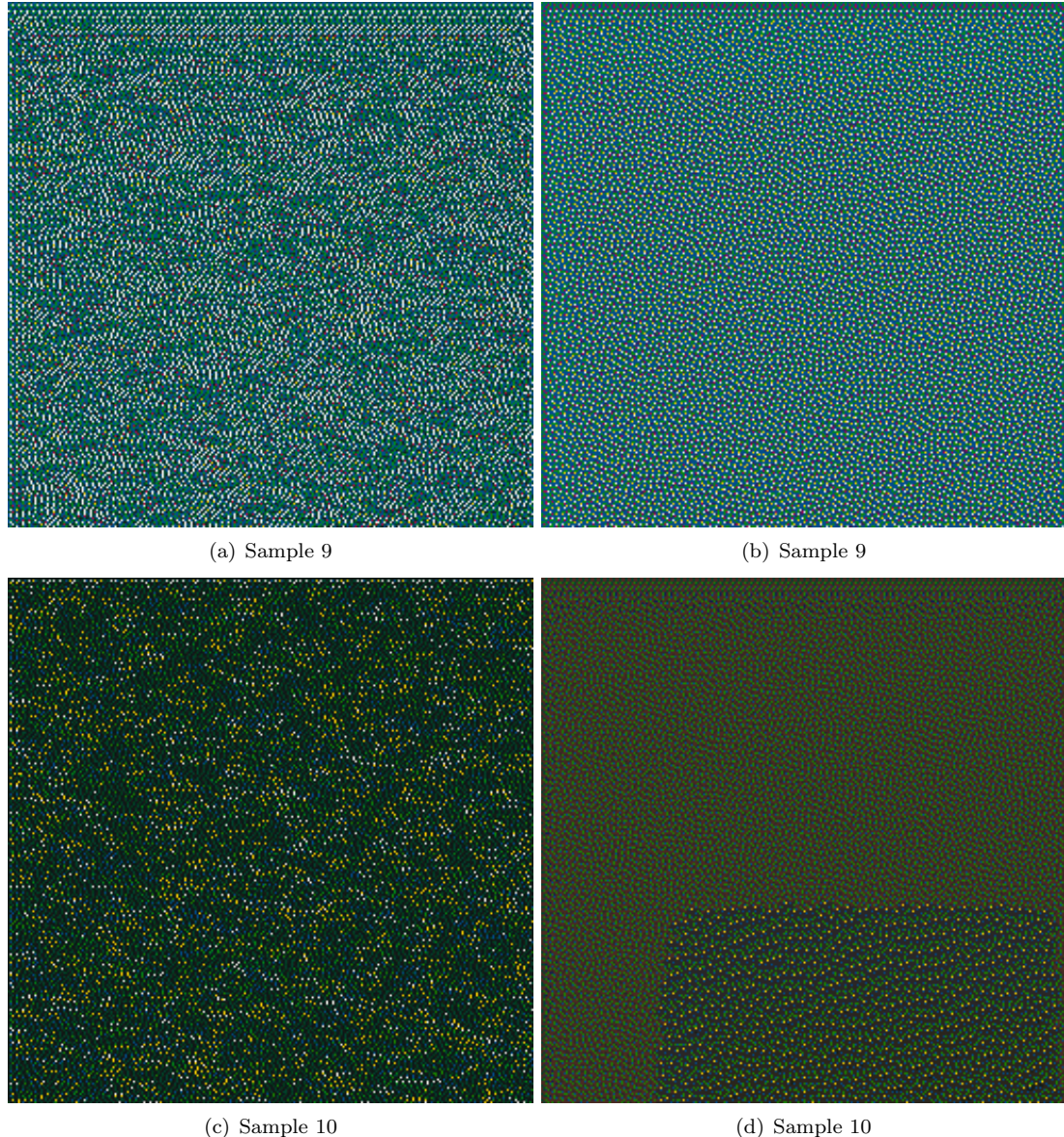


Figure 7.8: Halftoned patches of sample 9 and sample 10 of *La Madeleine* paint. Spatial NPs distribution obtained after the first workflow using CS and SED in (a) and (c) and their corresponding distributions obtained after the second workflow using sVED in (b) and (d).

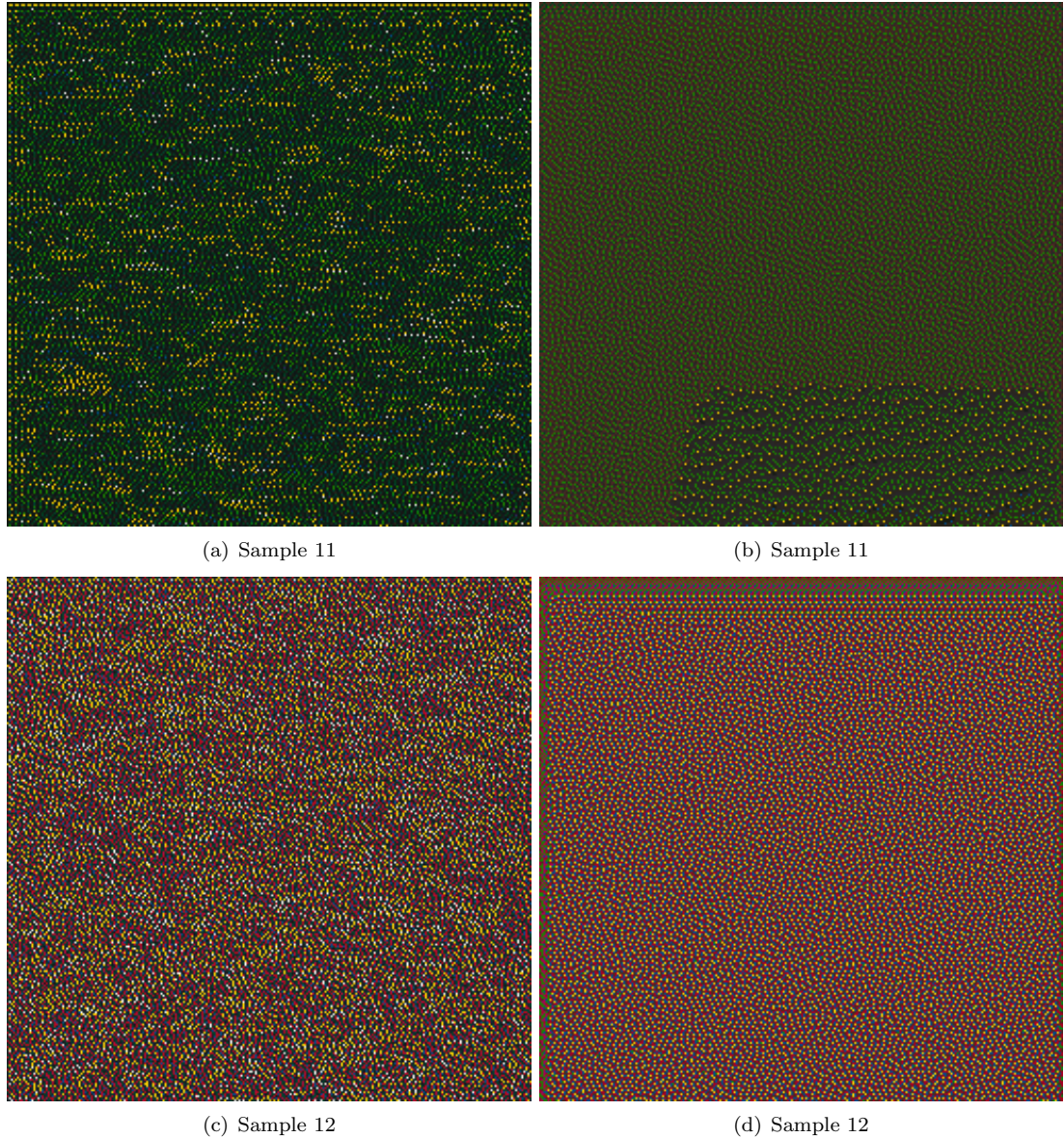


Figure 7.9: Halftoned patches of sample 11 and sample 12 of *La Madeleine* paint. Spatial NPs distribution obtained after the first workflow using CS and SED in (a) and (c) and their corresponding distributions obtained after the second workflow using sVED in (b) and (d).

7.4 Conclusion

The experimentation carried out in this chapter has allowed to compare two spectral color reproduction workflows: one combining a step of spectral colorant separation presented in Chapter 5 and halftoning by error diffusion (see Chapter 2.6.2); a second halftoning directly a spectral patch by sVED as presented in Chapter 6.

The first look at the color and spectral differences gives an advantage to the sVED because of the smaller differences obtained, but the difference of results remaining near between the two workflows. However, the observation of the spatial Neugebauer primaries distribution for both approaches shows that the workflow using sVED bring a much more pleasant and stable spatial NPs distribution for almost all tested samples. The spatial NPs distribution being extremely noisy. Further experiments should be conducted to compare the spectral color reproduction of spectral images by these two workflows.

Chapter 8

Conclusions and Perspective

8.1 Thesis work overview

The spectral color reproduction presented in this thesis is the final step of a chain of operation starting by a spectral acquisition and going by a gamut mapping operation.

The data we aim to reproduce are either measured with spectrophotometer or reconstructed from a spectral acquisition system. In both cases these data are the result of the signal capture of a light falling on a surface and being reflected toward the measuring device. One can see for example that the relief of a paint is considered to be flat with such acquisition system. If spectral reproduction is possible the same orientation as used during the acquisition should be chosen to observe the reproduction which should reminds identical under any illumination condition. Once spectral data are available to the user, he is free to simulate a color rendering of them under every kind of illuminant and observer conditions.

In this thesis work we have tackled the problem of spectral color reproduction. We have considered the following problems: is it possible to reproduce spectral data? How a spectral reproduction can be an improvement upon a color reproduction? The first problem leads us to define the reproduction system to use: printer and inks, the second problem leads us to evaluate the spectral color reproduction with the defined spectral printing system.

The choice of a multi-colorant printer was straightforward, it allows us to use common printing technologies for research purpose. It requires also to understand the color reproduction processes and the transformations applied to an image during the color reproduction workflow: gamut mapping, colorant separation, halftoning and to be aware of the printer limitation and instability.

Color reproduction is often referred to metameric reproduction since a given colorimetric value can be reproduced by different colorant combinations. A colorimetric value is represented by tristimulus values CIEXYZ, by CIELAB values or other color space coordinates.

The spectral reflectance of a surface contains all the color information of this surface, it allows to simulate a color rendering of it for different observers (CIE1931 and CIE1964 for example) and illumination conditions (CIE D50, A, FL11 for example). One can see that we have a dimension issue, a spectral reflectance is described in its most reduced form by 31 narrow bands of 10nm step covering the visible spectrum from 400nm to 700nm when our multi-colorant system is described by m dimensions for m colorants with $4 \leq m \leq 8$ or more. And once the spectral image has been converted into a colorant image (by the colorant separation transformation) it is no longer possible to go back to the original spectral data without loss.

The spectral printer characterization allows us to estimate the spectral accuracy of our printing system. There is a problem of the choice of the metric to evaluate the spectral accuracy: a spectral difference tells us how distant are two spectral reflectances but we know that a human observer does not perceive linearly these differences.

Our approach for the spectral printer characterization have shown the difficulty of spectral

printer modeling, especially in case of multi-colorant printer with wide gamut. To use the spectral Neugebauer model in its initial version, knowing only the gamut limits represented by the Neugebauer primaries (NP) and the single colorant ramp of the available colorants is not accurate enough, see Chapter 3 and Chapter 4. The phenomenon of dot gain and in particularly the optical dot gain (upon the mechanical dot gain) is not easy to model globally (i.e. a single parameter can not count for all the inks and coverage level combination). From that point two solutions are possible: to use a more physical model to intend to estimate accurately the multiple light interaction between the ink layers and paper knowing that halftoning does not produce infinite layer of ink but distribution of dot on the paper, dot being a drop of ink, a color level resulting in areas covered by inks and areas reminded uncovered; or to use the cellular Neugebauer model in order to map completely the spectral printer gamut and to dispose of intermediate NP. In both approaches numerous patches (i.e. colorant combinations) have to be printed and measured and it requires a total control of the printing system, this a technical problem and for sure a tedious task.

However the knowledge of the NP and the limits of the printer gamut are enough to perform the colorant separation in order to decompose a spectral reflectance in a colorant combination. We know that a spectral reflectance in the printer gamut can be decomposed in a convex sum of the NP. This operation called colorant separation can be tested by simulation meaning it does not require to print every time a given colorant combination and to measure its spectral reflectance. It allows us to compare the spectral color reproduction of spectral data with the color reproduction of spectral data. The colorant separation is solved by optimization where a criterion is minimized. The type of criterion defines the type of print. We can then evaluate if metamerism is reduced in a spectral color reproduction. We have shown in Chapter 5 that a colorant separation involving only a spectral difference provides homogeneous color differences for different illumination conditions which can be understood as a reduction of the metamerism (i.e. all illumination conditions have the same importance). Also the combination of the CIE1976 color difference for a set of different illuminants and spectral difference have revealed colorant combinations satisfying both colorimetric and spectral criteria for the colorant separation. These results joined the works aiming to described metamer boundaries in multi-colorant printer.

The work done on the colorant separation were based on the inversion of the spectral NG printer model. This model performs estimation in two steps: an estimation of the surface covered by the NP for a given colorant combination with the Demichel equations and then sum all the NP weighted by their coverage. The inversion for the weights only, developed in chapter 5, have shown the possibility to use this method of inversion as a spectral gamut mapping technique.

The direct use of gamut mapping techniques as those use in color space (3 dimensions) but applied in spectral space (31 dimensions) is possible but requires an enormous computational cost which makes it almost impossible. A reduction of dimension is possible by PCA but further research should be investigated. Our approach does not need to compute volume, or to calculate the gamut boundaries.

All along this research work we have seen that the spectral color reproduction follows the identical steps as the colorant reproduction workflow. We can see that after the color separation transformation the spectral data are no longer spectral, they are colorant combinations which count for spectral reflectance. The halftoning operation sees these data only as colorant values which need to be transformed from continuous-tone value to bi-level value. In order to keep working with spectral data as long as possible (i.e. to stay in spectral space in order to not loose information when going toward lower dimension space) we have adapted an halftoning technique which performs the colorant separation and the halftoning in one operation: this technique is called spectral vector error diffusion (sVED).

8.2 Perspective and future works

We have in Figure 6.1 the comparison of the two workflows used in this thesis work, both using the same multi-colorant printer. The halftoning by sVED offers the great advantage to need

only a few pieces of information about the printing system: the NP spectral reflectances. Of course if the sVED approach solves some of the problems from the first approach it introduces new issues as well. Since sVED is an halftoning technique, the improvement can be made on the algorithm itself. The proposed spectral gamut mapping technique improves the algorithm for the visibility of the error spreading, but a solution adapting the weights to spread the error regarding of the local information should give good results. The correction we proposed based on the distance between the processed pixel and its neighbor is going in this direction.

A research work is never finished and there is always something to improve. The spectral gamut mapping is a very important part of the process to improve, this to be able to simulate or evaluate the possibility of spectral color reproduction for different printing systems.

The colorant separation is performed by inversion of the NG model, inversion based on a more physical model such as the Clapper-Yules model should be tested.

Halftoning by sVED can be improved, work on adapting the filter with the local information in the image to spread the error should be continued. The most interesting point in this technique being to be completely spectral, no color difference is involved. Techniques existing in color for halftoning involving a new path for each image should be tested, spreading then the error in every direction should decrease the smear effect which can appear with vector error diffusion.

We used inkjet printer technology to reproduce spectral data: is this technology good enough for such purpose? Also we should look at the available colorants in a printing system depending on the spectral target to reproduce. The reproduction of a paint with very different colorants compare to the printer colorants may be a serious issue for a true spectral color reproduction. But spectral color reproduction should be seen as an improvement upon the color reproduction in the sens that it reduces the metamerism problem.

Appendix A

Printer characterization

You will find here the study of the monochromatics ramp for the Epson 2100 Photo Stylus inkjet printer for non original inks. For all colorants the ramps are simulated by the spectral Murray Davis (MD) model with various settings:

- with the theoretical colorant values constituting the ramp.
- with the effective colorant values. The LUT was built such that ΔE_{ab}^* for illuminant D50 was minimized.
- with the previous LUT and a n factor minimizing average ΔE_{ab}^* .

A.1 Magenta

Table A.1: Differences between ramp of Magenta measurements and estimated spectral reflectances by MD

		ΔE_{ab}^*						sRMS
		A	D65	C	D50	D55	D75	
MD and theoretical colorant	Av.	34.4	40.7	40.1	39.5	40.0	41.2	0.186
	Std	18.0	21.0	20.7	20.5	20.7	21.3	0.113
	Max	52.7	61.7	60.7	59.9	60.7	62.4	0.322
MD and effective colorant	Av.	16.1	21.5	21.1	20.3	20.8	22.0	0.064
	Std	9.5	12.5	12.3	11.8	12.1	12.8	0.039
	Max	27.9	36.7	36.1	34.8	35.6	37.6	0.111
MD and effective colorant and n factor	Av.	7.0	8.4	8.3	8.0	8.1	8.5	0.075
	Std	4.1	4.9	4.9	4.7	4.8	5.0	0.049
	Max	12.2	14.9	14.8	14.1	14.4	15.2	0.140

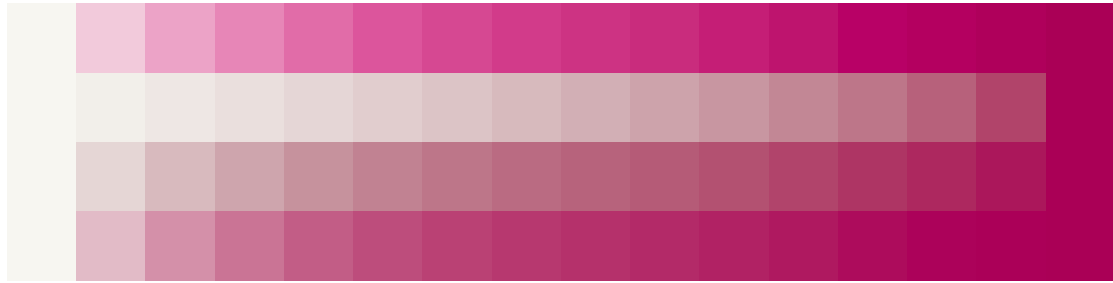


Figure A.1: Measured ramps, MD estimation, MD with effective values, MD with effective values and n factor in sRGB for illuminant D50

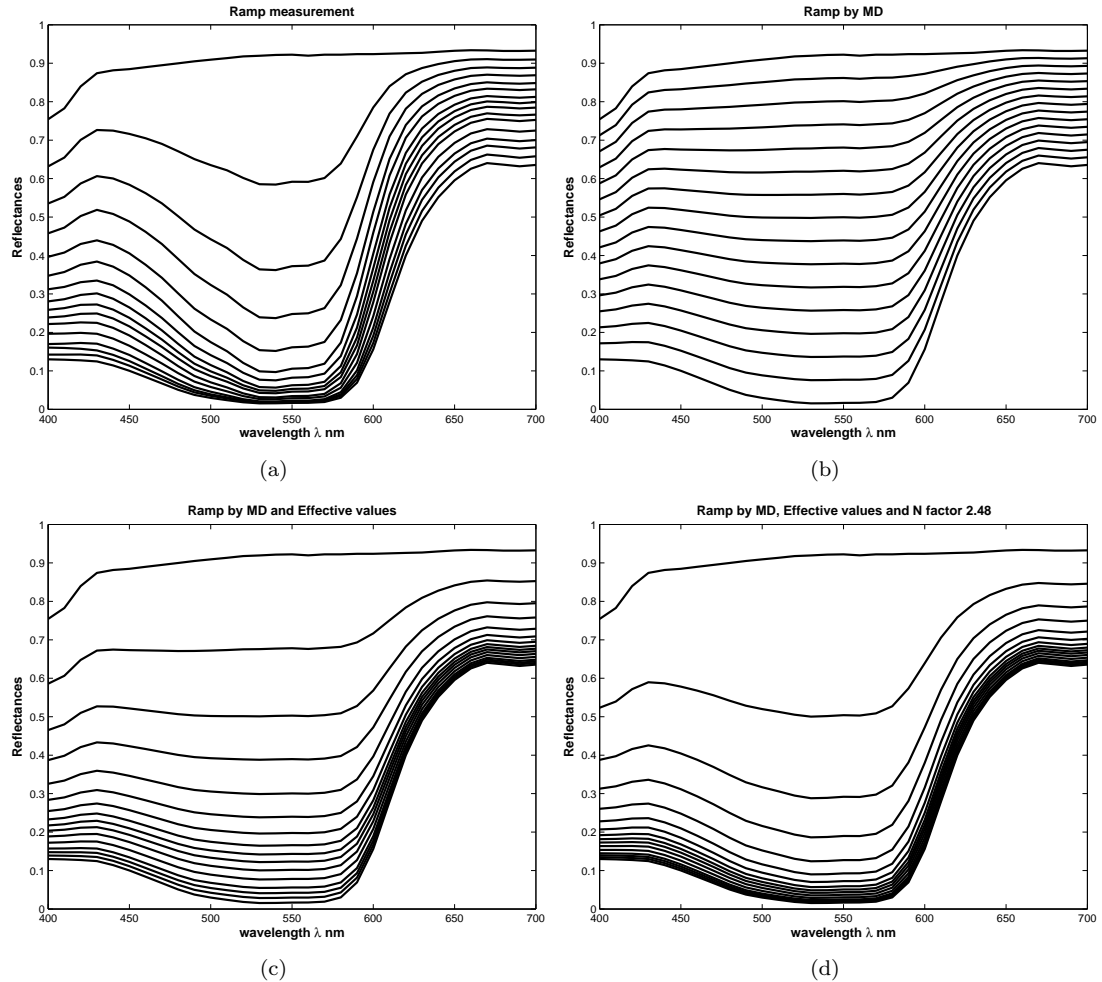


Figure A.2: Measured spectral reflectances (a), estimated spectral reflectances by MD and theoretical ramp values (b), estimated spectral reflectances by MD and effective ramp values (c) and estimated spectral reflectances by MD, effective ramp values and n factor (d).

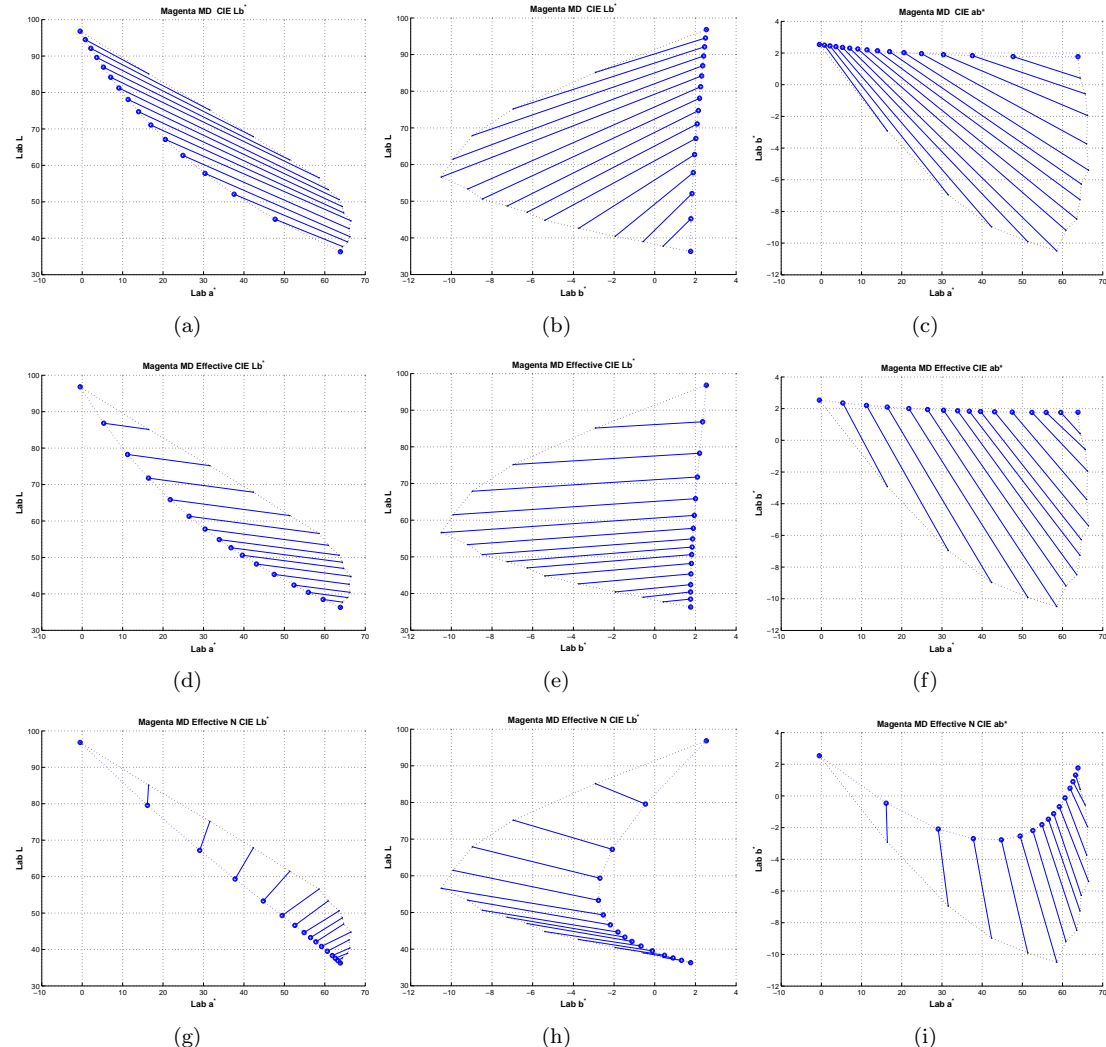


Figure A.3: Comparison in CIELa*, CIELb* and CIEab* plans by column between ramp measurements of Magenta and simulation by MD in the first line (Figure (a), (b) and (c)), by MD and effective values for the second line (Figure (d), (e) and (f)) and MD with effective values and n factor (Figure (g), (h) and (j))

A.2 Yellow

Table A.2: Differences between ramp of Yellow measurements and estimated spectral reflectances by MD

		ΔE_{ab}^*						sRMS
		A	D65	C	D50	D55	D75	
MD and theoretical colorant	Av.	43.1	47.6	48.3	46.5	47.0	48.1	0.169
	Std	22.8	24.9	25.2	24.4	24.6	25.1	0.106
	Max	67.0	73.5	74.4	71.8	72.5	74.1	0.300
MD and effective colorant	Av.	8.6	13.0	13.1	11.9	12.3	13.5	0.046
	Std	5.1	7.7	7.8	7.1	7.3	8.0	0.030
	Max	14.8	22.4	22.5	20.4	21.2	23.3	0.086
MD and effective colorant and n factor	Av.	4.8	7.5	7.3	6.8	7.0	7.8	0.047
	Std	2.9	4.4	4.3	3.9	4.1	4.6	0.031
	Max	8.3	12.7	12.4	11.3	11.8	13.3	0.088

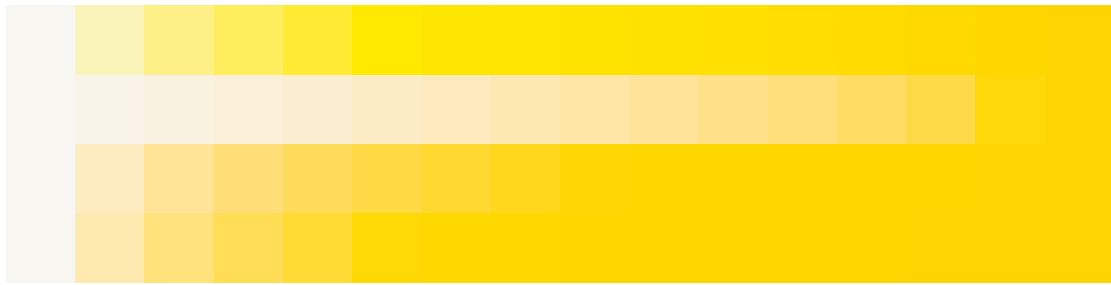


Figure A.4: Measured ramps, MD estimation, MD with effective values, MD with effective values and n factor in sRGB for illuminant D50

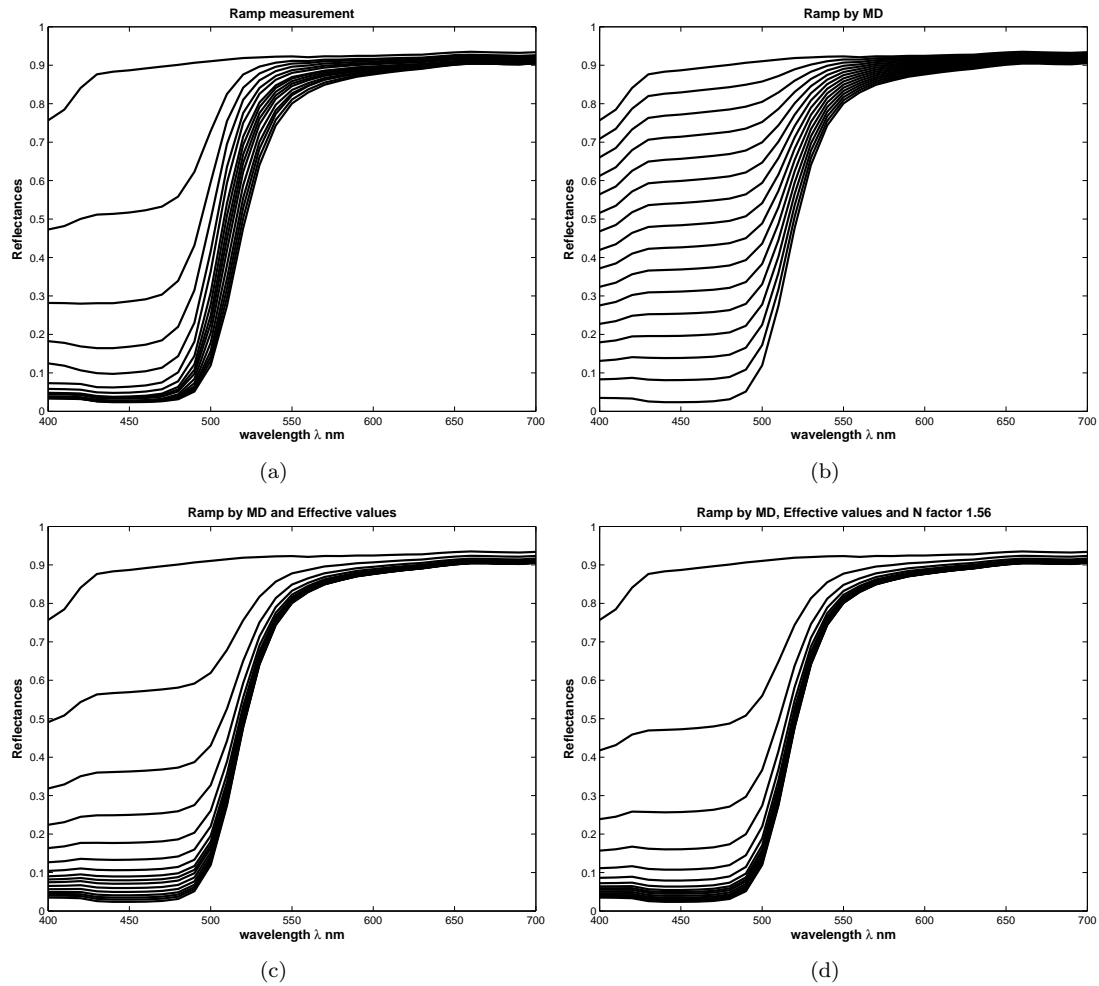


Figure A.5: Measured spectral reflectances (a), estimated spectral reflectances by MD and theoretical ramp values (b), estimated spectral reflectances by MD and effective ramp values (c) and estimated spectral reflectances by MD, effective ramp values and n factor (d).

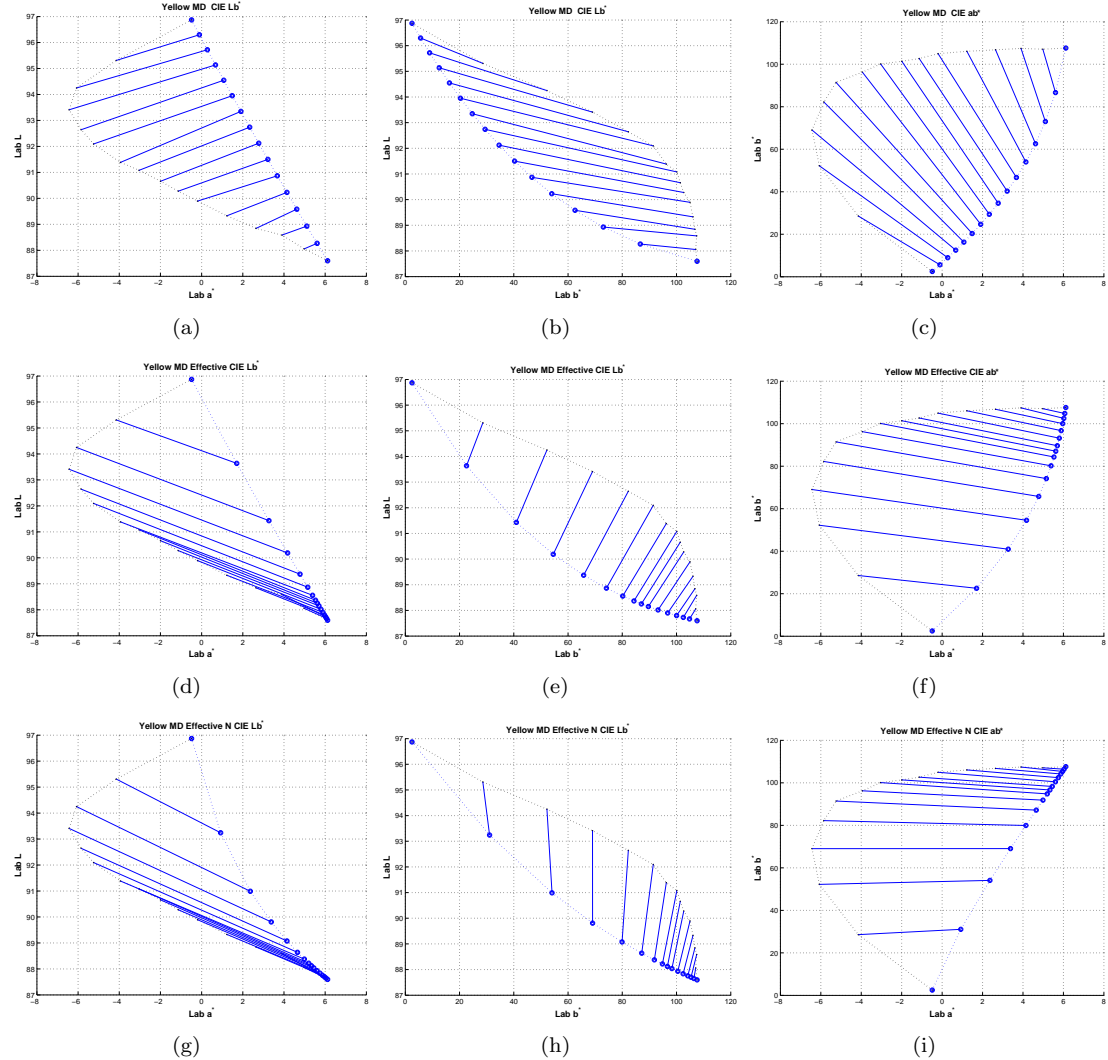


Figure A.6: Comparison in CIELa*, CIELb* and CIEab* plans by column between ramp measurements of Yellow and simulation by MD in the first line (Figure (a), (b) and (c)), by MD and effective values for the second line (Figure (d), (e) and (f)) and MD with effective values and n factor (Figure (g), (h) and (j))

A.3 Black

Table A.3: Differences between ramp of Black measurements and estimated spectral reflectances by MD

		ΔE_{ab}^*						
		A	D65	C	D50	D55	D75	sRMS
MD and theoretical colorant	Av.	43.1	47.6	48.3	46.5	47.0	48.1	0.169
	Std	22.8	24.9	25.2	24.4	24.6	25.1	0.106
	Max	67.0	73.5	74.4	71.8	72.5	74.1	0.300
MD and effective colorant	Av.	8.6	13.0	13.1	11.9	12.3	13.5	0.046
	Std	5.1	7.7	7.8	7.1	7.3	8.0	0.030
	Max	14.8	22.4	22.5	20.4	21.2	23.3	0.086
MD and effective colorant and n factor	Av.	4.8	7.5	7.3	6.8	7.0	7.8	0.047
	Std	2.9	4.4	4.3	3.9	4.1	4.6	0.031
	Max	8.3	12.7	12.4	11.3	11.8	13.3	0.088

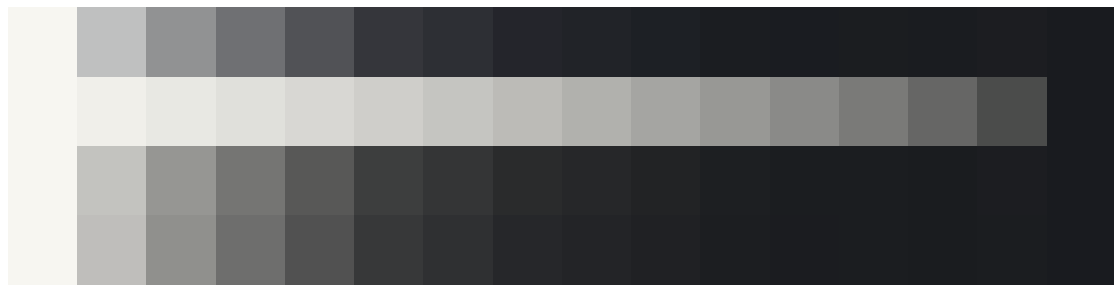


Figure A.7: Measured ramps, MD estimation, MD with effective values, MD with effective values and n factor in sRGB for illuminant D50

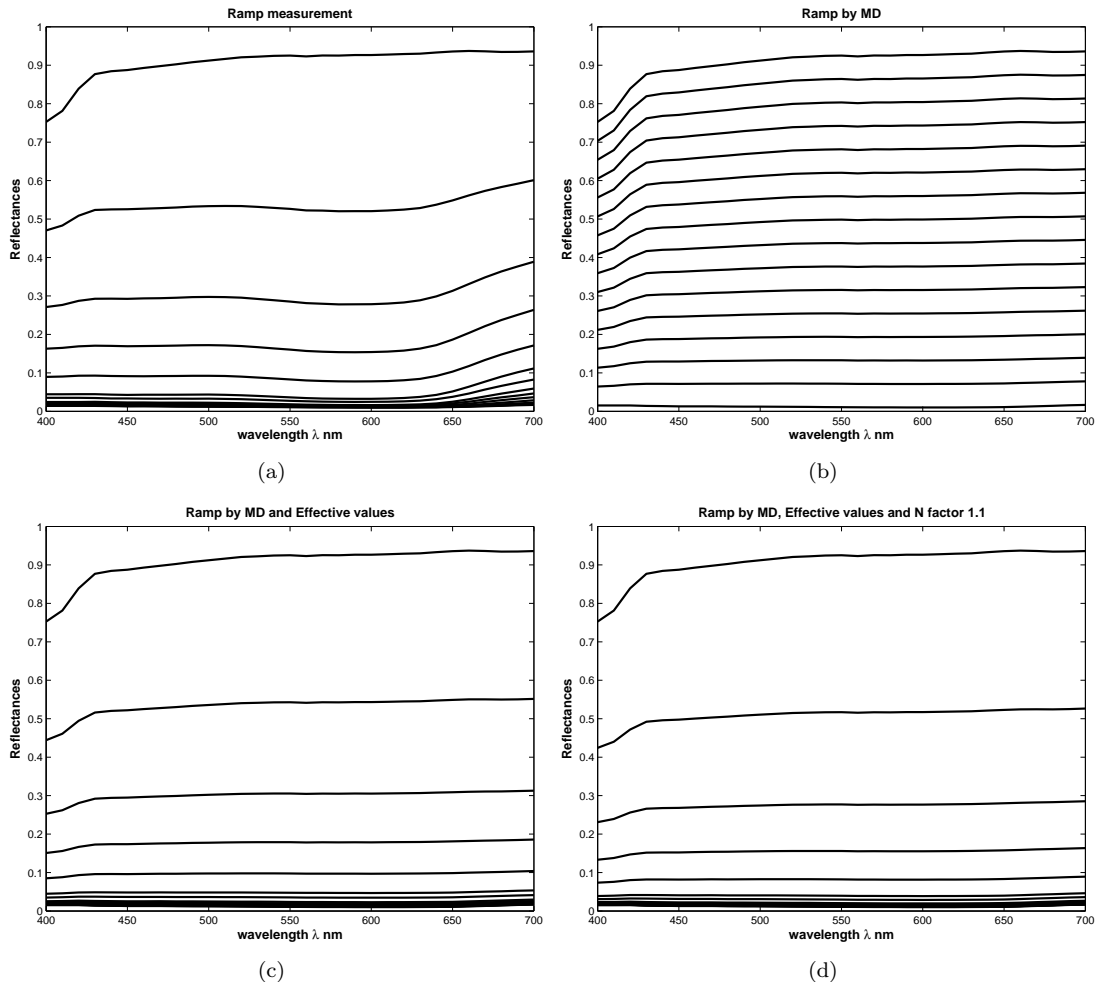


Figure A.8: Measured spectral reflectances (a), estimated spectral reflectances by MD and theoretical ramp values (b), estimated spectral reflectances by MD and effective ramp values (c) and estimated spectral reflectances by MD, effective ramp values and n factor (d).

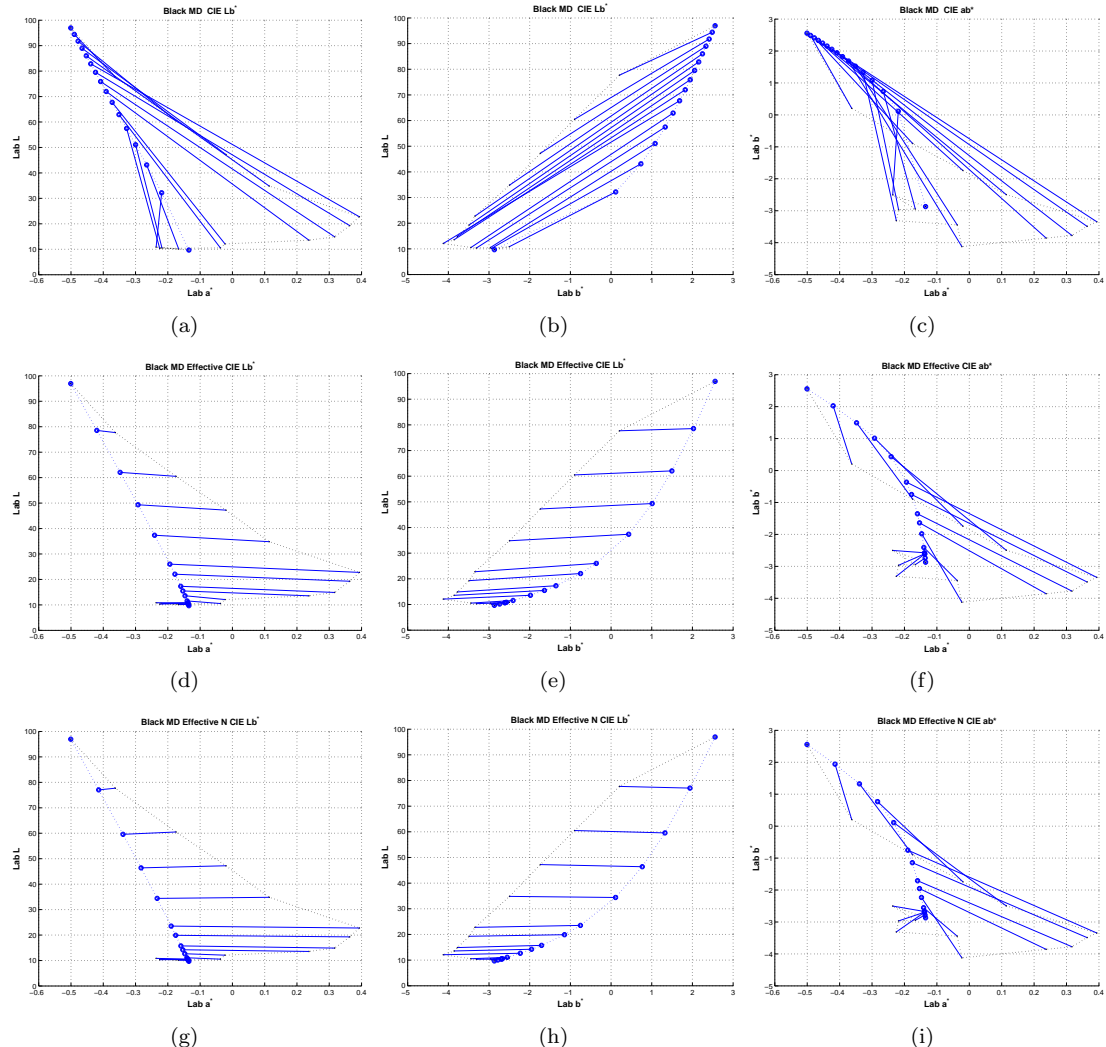


Figure A.9: Comparison in CIELa*, CIELb* and CIEab* plans by column between ramp measurements of Black and simulation by MD in the first line (Figure (a), (b) and (c)), by MD and effective values for the second line (Figure (d), (e) and (f)) and MD with effective values and n factor (Figure (g), (h) and (j))

A.4 Blue

Table A.4: Differences between ramp of Red measurements and estimated spectral reflectances by MD

		ΔE_{ab}^*						sRMS
		A	D65	C	D50	D55	D75	
MD and theoretical colorant	Av.	43.1	47.6	48.3	46.5	47.0	48.1	0.169
	Std	22.8	24.9	25.2	24.4	24.6	25.1	0.106
	Max	67.0	73.5	74.4	71.8	72.5	74.1	0.300
MD and effective colorant	Av.	8.6	13.0	13.1	11.9	12.3	13.5	0.046
	Std	5.1	7.7	7.8	7.1	7.3	8.0	0.030
	Max	14.8	22.4	22.5	20.4	21.2	23.3	0.086
MD and effective colorant and n factor	Av.	4.8	7.5	7.3	6.8	7.0	7.8	0.047
	Std	2.9	4.4	4.3	3.9	4.1	4.6	0.031
	Max	8.3	12.7	12.4	11.3	11.8	13.3	0.088

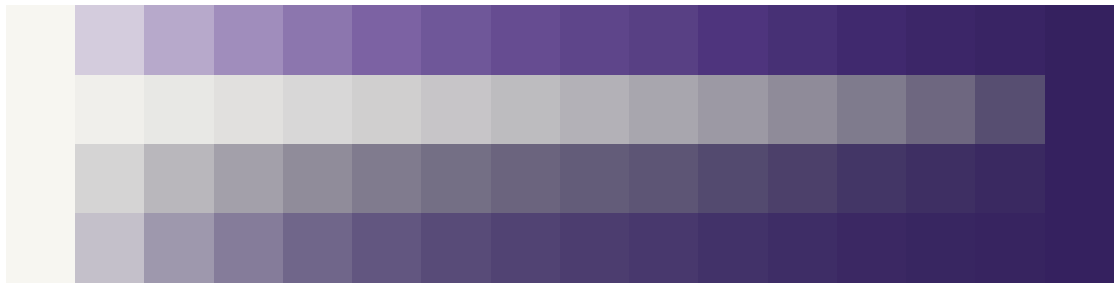


Figure A.10: Measured ramps, MD estimation, MD with effective values, MD with effective values and n factor in sRGB for illuminant D50

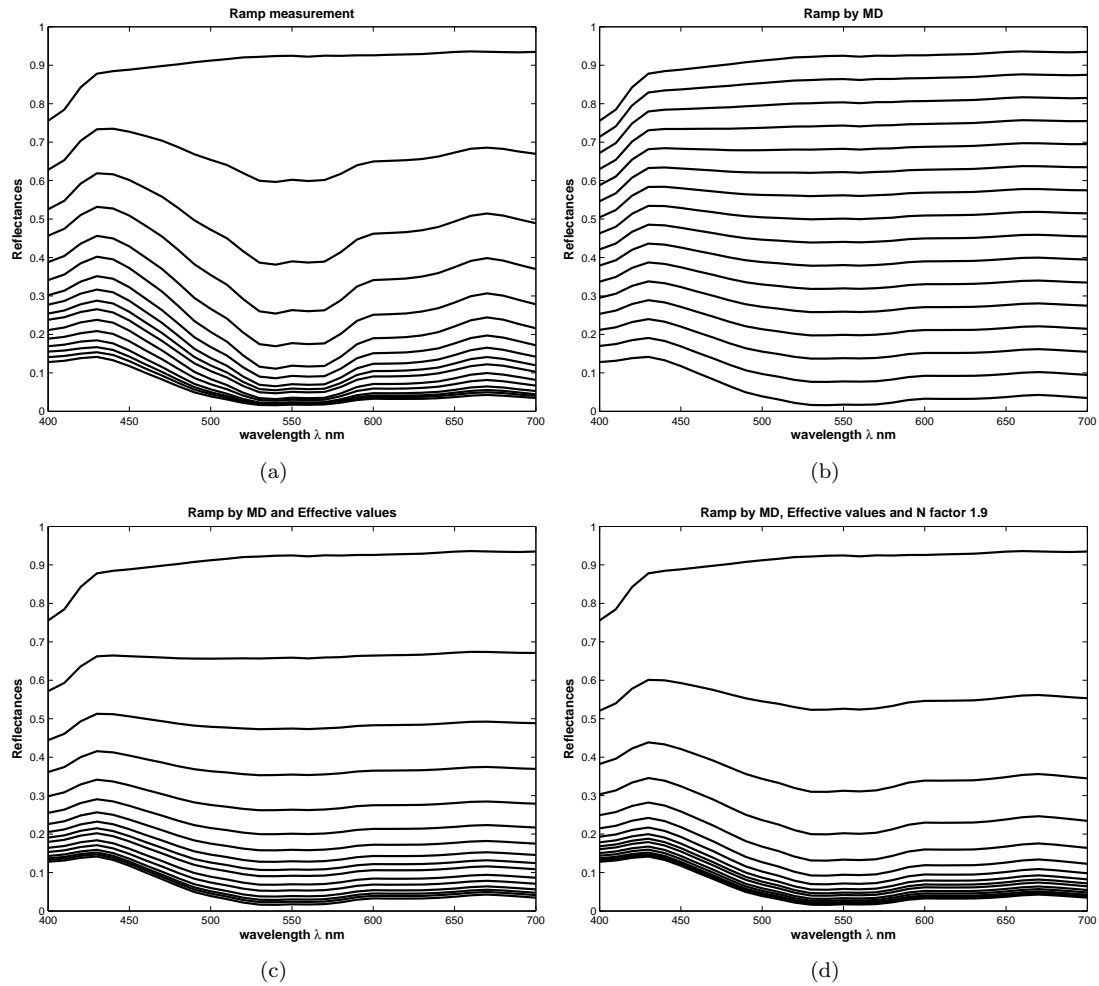


Figure A.11: Measured spectral reflectances (a), estimated spectral reflectances by MD and theoretical ramp values (b), estimated spectral reflectances by MD and effective ramp values (c) and estimated spectral reflectances by MD, effective ramp values and n factor (d).

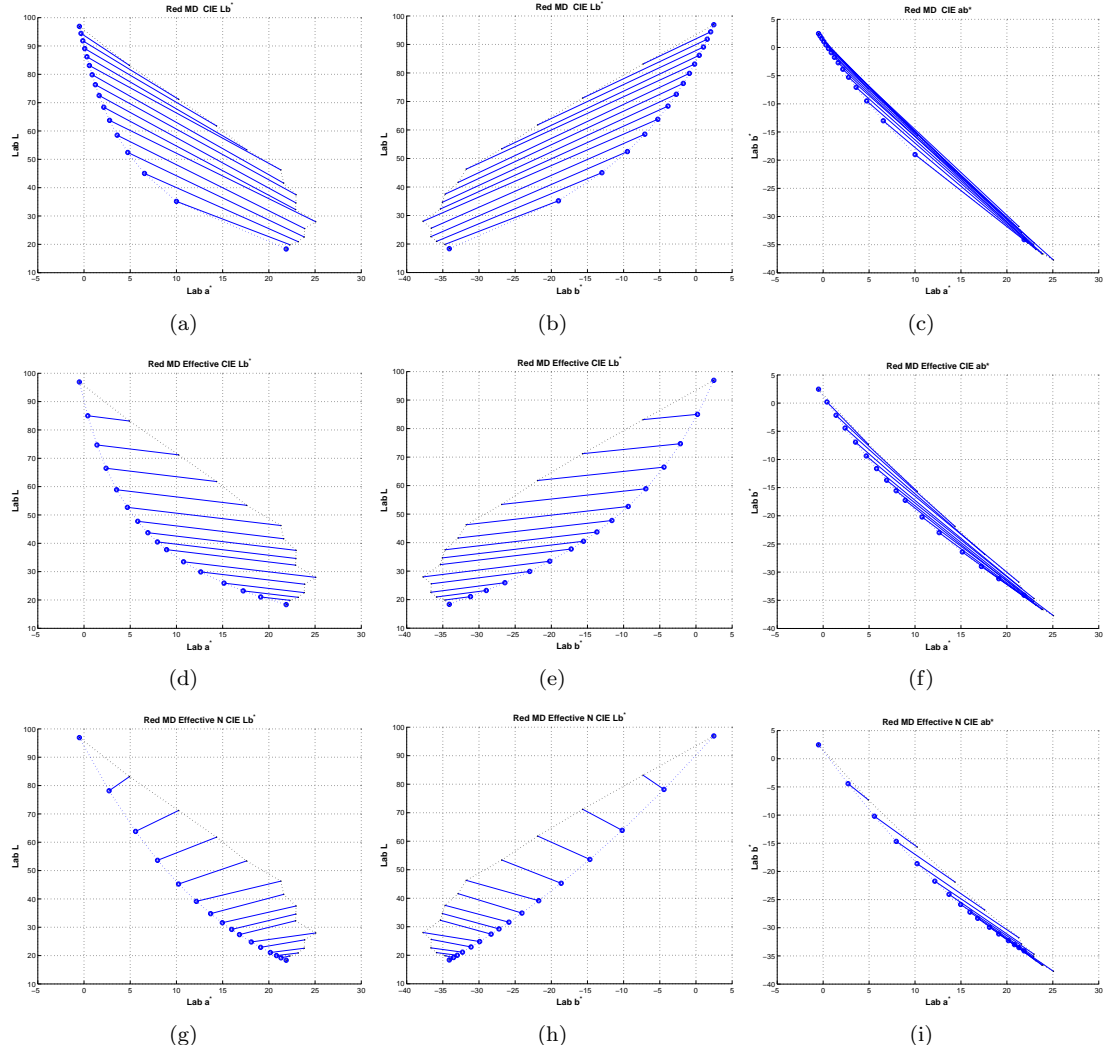


Figure A.12: Comparison in CIELa*, CIELb* and CIEab* plans by column between ramp measurements of Red and simulation by MD in the first line (Figure (a), (b) and (c)), by MD and effective values for the second line (Figure (d), (e) and (f)) and MD with effective values and n factor (Figure (g), (h) and (j))

A.5 Red

Table A.5: Differences between ramp of Green measurements and estimated spectral reflectances by MD

		ΔE_{ab}^*						sRMS
		A	D65	C	D50	D55	D75	
MD and theoretical colorant	Av.	43.1	47.6	48.3	46.5	47.0	48.1	0.169
	Std	22.8	24.9	25.2	24.4	24.6	25.1	0.106
	Max	67.0	73.5	74.4	71.8	72.5	74.1	0.300
MD and effective colorant	Av.	8.6	13.0	13.1	11.9	12.3	13.5	0.046
	Std	5.1	7.7	7.8	7.1	7.3	8.0	0.030
	Max	14.8	22.4	22.5	20.4	21.2	23.3	0.086
MD and effective colorant and n factor	Av.	4.8	7.5	7.3	6.8	7.0	7.8	0.047
	Std	2.9	4.4	4.3	3.9	4.1	4.6	0.031
	Max	8.3	12.7	12.4	11.3	11.8	13.3	0.088

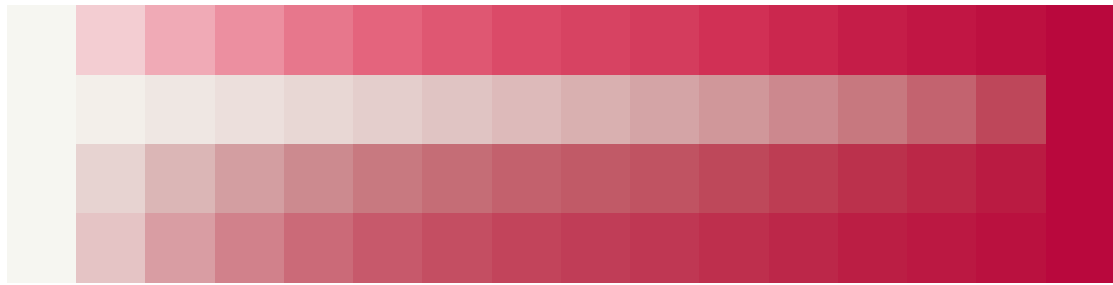


Figure A.13: Measured ramps, MD estimation, MD with effective values, MD with effective values and n factor in sRGB for illuminant D50

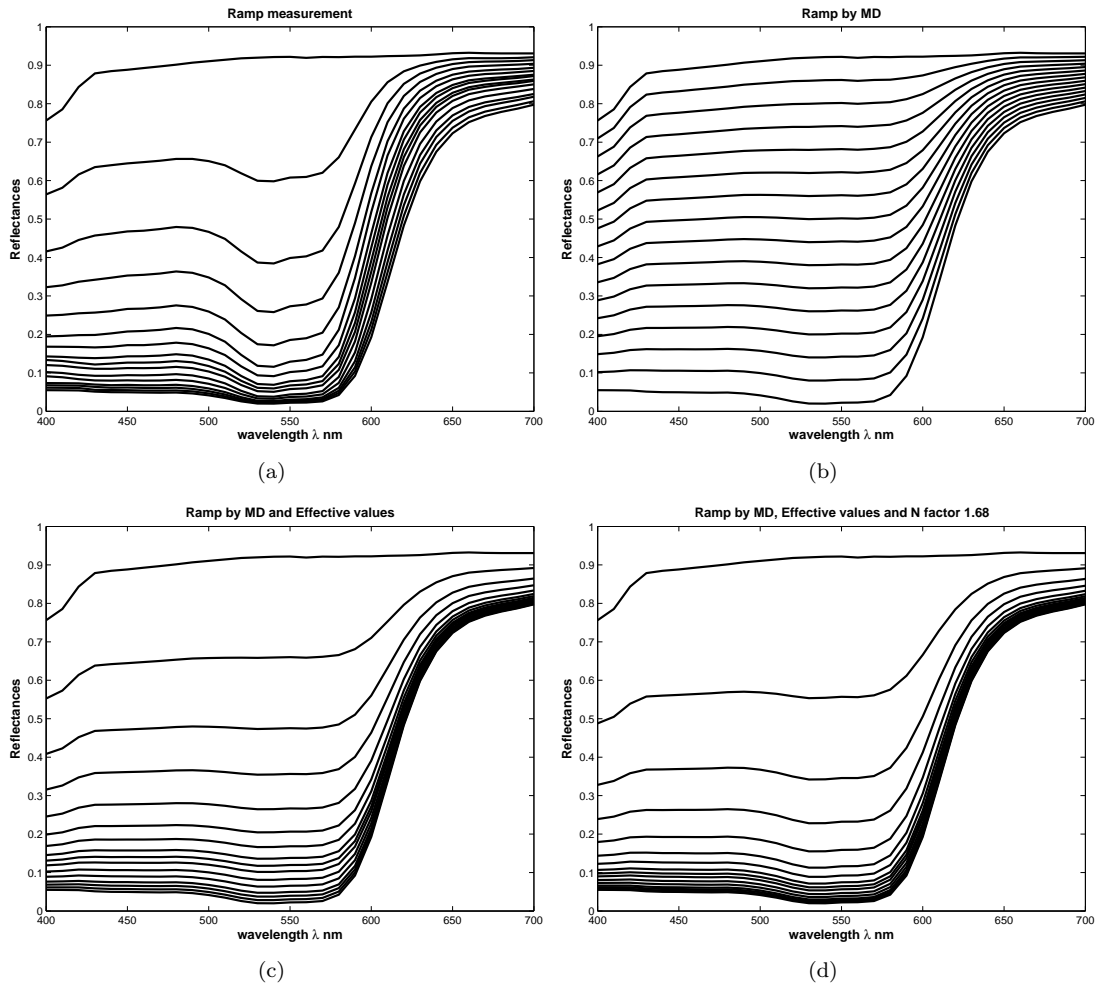


Figure A.14: Measured spectral reflectances (a), estimated spectral reflectances by MD and theoretical ramp values (b), estimated spectral reflectances by MD and effective ramp values (c) and estimated spectral reflectances by MD, effective ramp values and n factor (d).

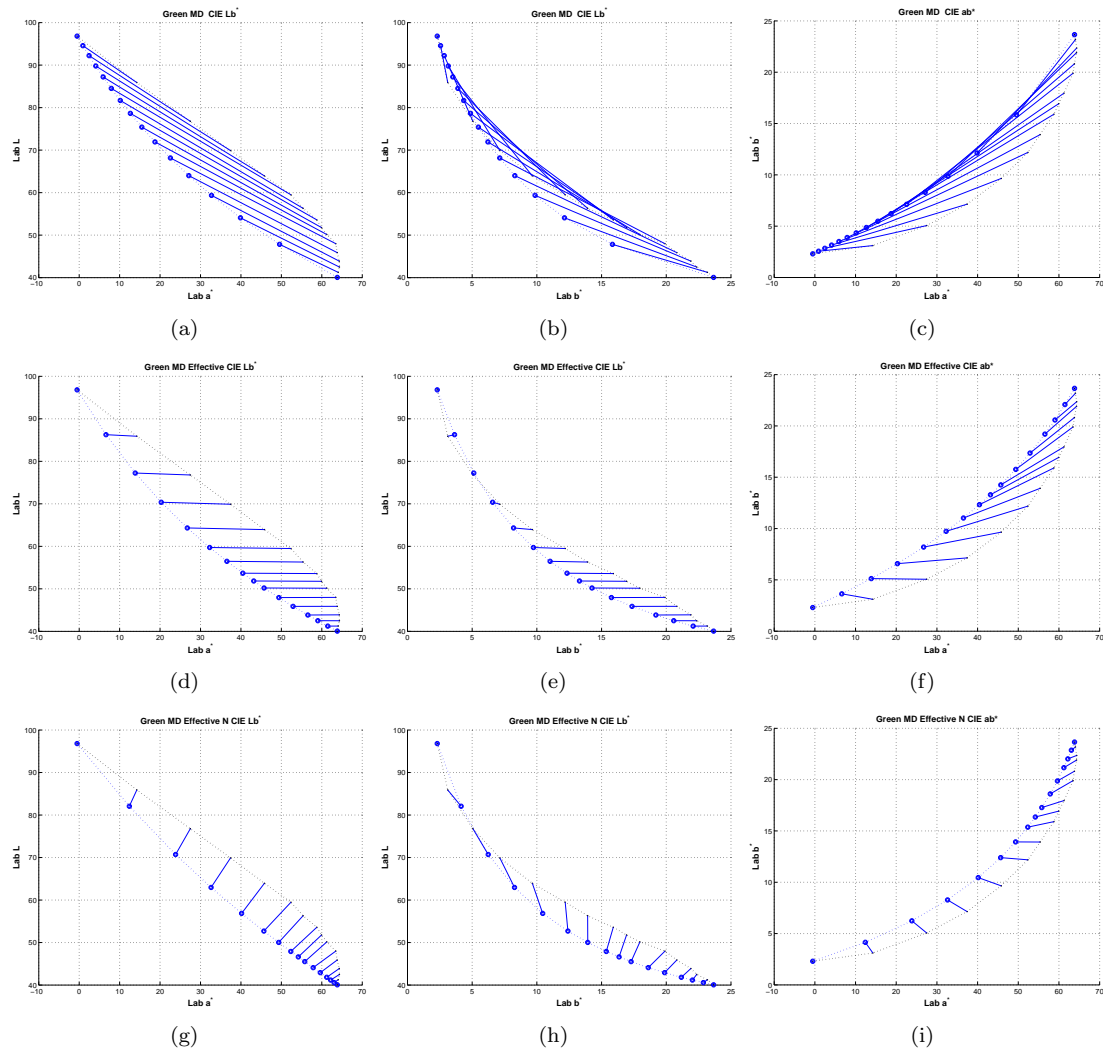


Figure A.15: Comparison in CIELa*, CIELb* and CIEab* plans by column between ramp measurements of Green and simulation by MD in the first line (Figure (a), (b) and (c)), by MD and effective values for the second line (Figure (d), (e) and (f)) and MD with effective values and n factor (Figure (g), (h) and (j))

A.6 Green

Table A.6: Differences between ramp of Blue measurements and estimated spectral reflectances by MD

		ΔE_{ab}^*						sRMS
		A	D65	C	D50	D55	D75	
MD and theoretical colorant	Av.	43.1	47.6	48.3	46.5	47.0	48.1	0.169
	Std	22.8	24.9	25.2	24.4	24.6	25.1	0.106
	Max	67.0	73.5	74.4	71.8	72.5	74.1	0.300
MD and effective colorant	Av.	8.6	13.0	13.1	11.9	12.3	13.5	0.046
	Std	5.1	7.7	7.8	7.1	7.3	8.0	0.030
	Max	14.8	22.4	22.5	20.4	21.2	23.3	0.086
MD and effective colorant and n factor	Av.	4.8	7.5	7.3	6.8	7.0	7.8	0.047
	Std	2.9	4.4	4.3	3.9	4.1	4.6	0.031
	Max	8.3	12.7	12.4	11.3	11.8	13.3	0.088

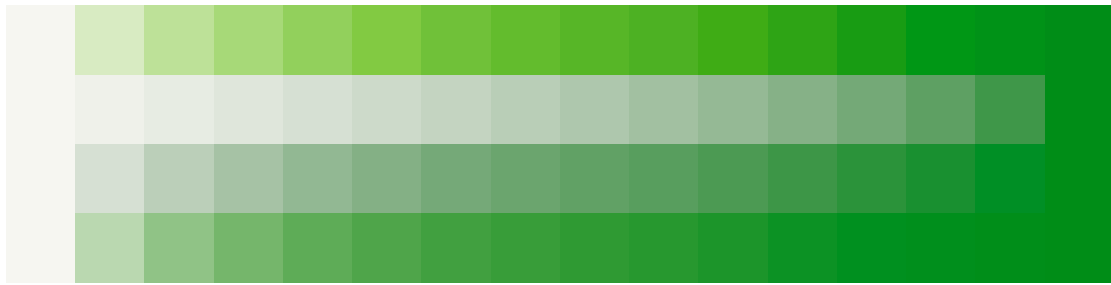


Figure A.16: Measured ramps, MD estimation, MD with effective values, MD with effective values and n factor in sRGB for illuminant D50

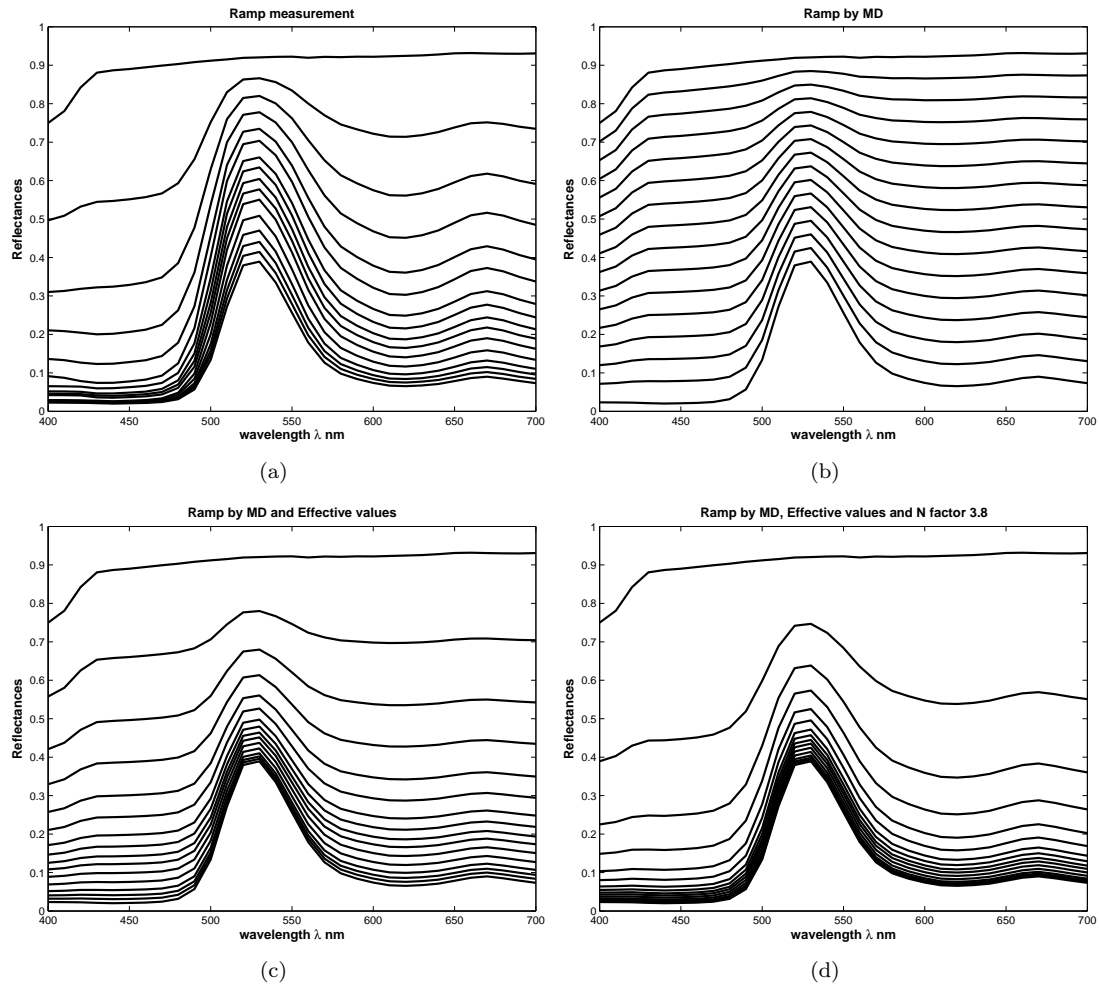


Figure A.17: Measured spectral reflectances (a), estimated spectral reflectances by MD and theoretical ramp values (b), estimated spectral reflectances by MD and effective ramp values (c) and estimated spectral reflectances by MD, effective ramp values and n factor (d).

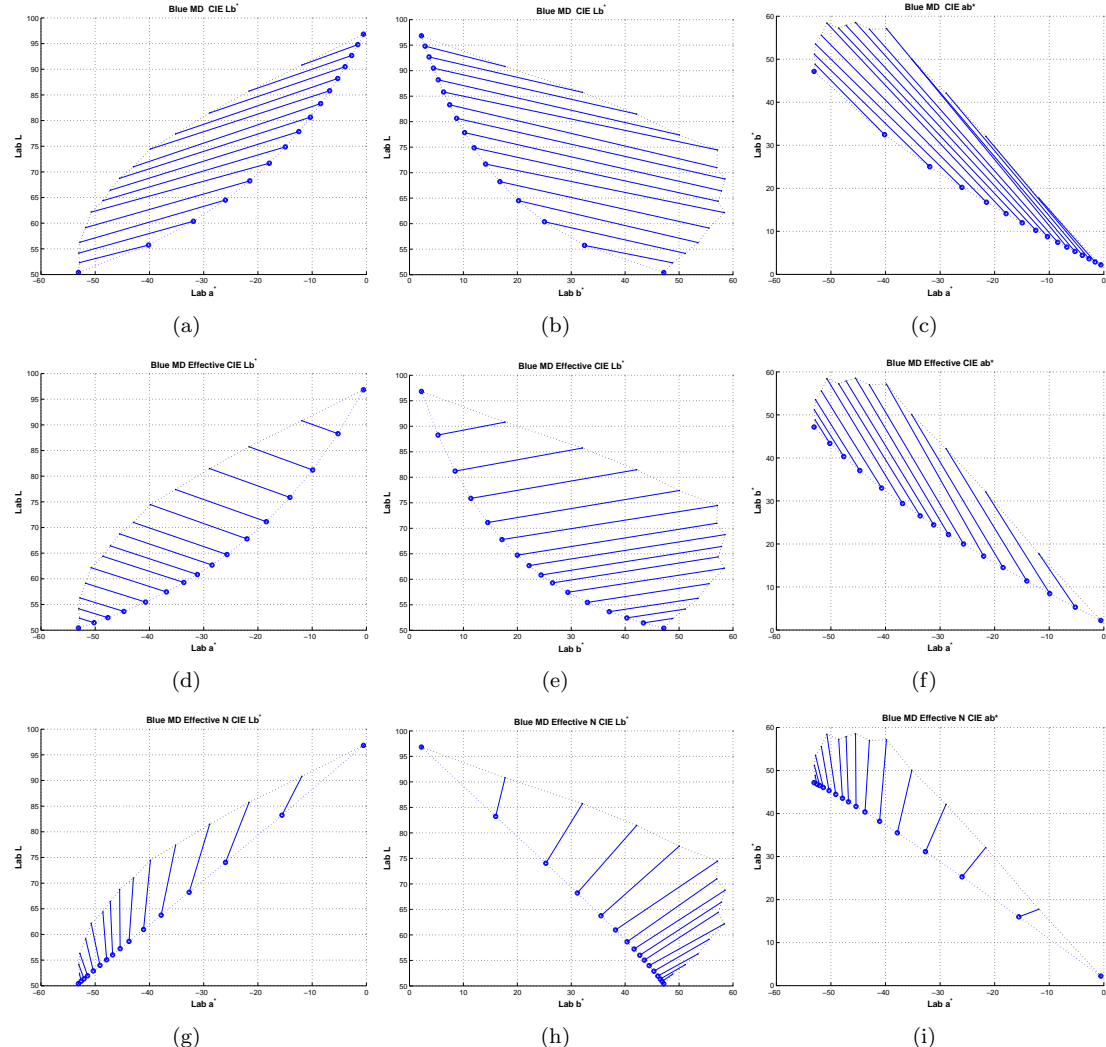


Figure A.18: Comparison in CIELa*, CIELb* and CIEab* plans by column between ramp measurements of Blue and simulation by MD in the first line (Figure (a), (b) and (c)), by MD and effective values for the second line (Figure (d), (e) and (f)) and MD with effective values and n factor (Figure (g), (h) and (j))

Appendix B

Spectral gamut mapping

B.1 Introduction

Gamut mapping algorithm describes the operation of mapping data from one gamut to another gamut (Morovič and Luo, 2001), e.g. an image gamut is mapped toward a printer gamut before its reproduction. Gamut mapping often refers to color gamut mapping techniques. Various techniques exist with the aim of mapping data without the loss of too many information in the original data, e.g. reproduction of an image by a printer knowing that the printer gamut is smaller than the image gamut.

A first solution for gamut mapping of spectral data would be to apply directly color gamut mapping algorithm, but due the spectral problem dimension it is too heavy computationally talking to use this approach. Studies have shown the redundancy of information in spectral data and the possibility to use PCA to reduce the dimension of the problem (Hardeberg, 2002). This approach has been tested for spectral gamut mapping in order to use easily already existing color gamut technique (Bakke et al., 2005). However it requires to characterize our printing system before to compute the PCA basis.

Other research works have investigated the reduction of dimensionality, this combining PCA and CIELAB values (Derhak and Rosen, 2006) to represent spectral data. This last method should at least perform as good as in colorimetric problem. Also the goal is here to develop a similar workflow as with the use of ICC profile in a color workflow but for spectral data, e.g. to allow faster communication between a spectral color acquisition system and a spectral color reproduction system.

Another method for spectral gamut mapping could be to use the properties of the spectral printer model. By inverting the spectral printer model we obtain the closest spectral reflectance the printer can produce according to the spectral printer model performance. This is an optimization problem and comparing to the colorant separation problem (see Chapter 5) it does not require to solve the problem in order to get a colorant combination. The resulting spectral reflectance of a given colorant combination is the summation of the Neugebauer primaries (NP) weighed by their fractional area coverage. By inverting the spectral Neugebauer model we mean to invert the equation for the weights only. After inversion the gamut mapped spectral reflectance is a summation of the NP in the convex space defined by the NP. In the next section we will present our spectral gamut mapping approach based on the inversion of the spectral Neugebauer model for the weights only.

B.2 Spectral gamut mapping by inverting the spectral printer model

Our spectral gamut mapping technique is based on the inversion of the spectral Neugebauer printer model, see Equation 3.32. This model says that the spectral reflectance estimation of a colorant combination is the weighted sum on a unit area of all the primaries (i.e. the NP) of the printer, see Chapter 3.3 for a definition of the NP. For a given colorant combination \mathbf{c} we have the following relation:

$$\mathbf{r} = \mathbf{P}\mathbf{w} \quad (\text{B.1})$$

where \mathbf{r} is the estimated spectral reflectance, \mathbf{w} the corresponding vector of weights for the colorant combination and \mathbf{P} the matrix containing the NP spectral reflectances. The weights are calculated from the Demichel equations (see Chapter 3.3.1) which we do not need here. We are just interested in the weights.

After gamut mapping the original spectral reflectance \mathbf{r} is replaced by its gamut mapped version \mathbf{r}' such that:

$$\mathbf{r}' = \mathbf{P}\mathbf{w}' \quad (\text{B.2})$$

and the vector of weight \mathbf{w}' is obtained while solving the following optimization problem:

$$\min_{\mathbf{w}'} \|\mathbf{r} - \mathbf{P}\mathbf{w}'\|, \quad (\text{B.3})$$

with the constraints set to the weights as:

$$\sum_{i=0}^{k-1} w_i = 1 \text{ and } 0 < w_i < 1. \quad (\text{B.4})$$

where the parameter k is the number of NP of the printing system.

The previous lines described the spectral gamut mapping for a single reflectance. In case of spectral gamut mapping of a spectral image, each pixel of the image is a spectral reflectance. Practically all pixels of the spectral image are stored in a matrix form \mathbf{R} where each column is a spectral reflectance of a pixel. Equation B.3 is then performed for each column vector of \mathbf{R} .

B.3 Experiment

To illustrate the effect of our spectral gamut mapping (sGM) technique we perform the sGM on the ColorChecker test chart and on a spectral image. sGM is then performed for two spectral printer gamuts: a 6 inks printer and a 7 inks printer. Each set of NP is displayed in Figure 6.5.

B.3.1 Spectral gamut mapping on single spectral reflectance

The ColorChecker test chart is made of 24 spectral reflectances. Each spectral reflectance of the test chart is shown in Figure B.1 to Figure B.4 with the corresponding gamut mapped version of the spectral reflectance for each printer.

CIELAB color differences and spectral difference between the original spectral reflectances and their gamut mapped spectral reflectances for both printer are displayed in Table B.1.

Table B.1: Differences between the original ColorChecker spectral reflectances and their spectral gamut mapped version for the six inks printer and the seven inks printer.

Patches	A	ΔE_{ab}^*				ΔE_{94}^*				sRMS	
		D65		D50	FL11	FL31	D50				
1	3.2	0.9	2.0	0.7	2.4	0.7	3.3	2.2	3.3	1.8	0.5
2	1.5	1.9	1.8	1.9	1.7	2.0	1.4	5.6	1.1	3.6	1.2
3	3.3	7.0	1.3	3.4	2.0	4.6	3.5	6.6	3.3	5.0	1.5
4	6.2	3.5	5.0	2.4	5.5	2.7	9.6	3.8	5.1	2.4	3.7
5	9.3	14.1	6.5	13.4	7.4	13.3	10.6	14.6	8.7	13.0	5.5
6	11.9	21.6	13.2	22.1	13.0	22.1	15.5	22.1	9.3	14.3	6.1
7	1.2	11.0	4.1	17.8	2.9	16.3	2.6	20.0	4.9	9.5	1.4
8	14.3	17.5	20.9	23.7	18.8	21.3	14.8	17.7	10.0	14.7	9.8
9	1.7	10.4	2.0	13.3	1.9	12.9	2.4	17.0	1.0	11.7	1.1
10	11.2	10.6	9.2	7.9	10.3	8.9	16.6	13.0	13.2	11.1	6.8
11	7.3	9.1	6.9	10.5	7.1	10.0	10.6	9.9	6.3	9.2	3.4
12	0.7	5.9	4.4	9.2	3.2	8.6	2.8	8.9	3.9	3.9	1.5
13	22.7	21.8	33.0	33.1	30.4	29.7	23.9	22.3	13.8	14.8	14.5
14	10.9	6.0	8.2	5.0	9.2	5.0	17.2	6.2	10.4	8.5	4.3
15	2.8	0.7	3.6	0.7	3.4	0.7	8.3	1.7	5.5	1.0	1.1
16	0.5	3.6	1.0	8.0	0.8	6.7	0.7	5.1	1.4	3.5	0.3
17	5.4	19.8	5.0	25.5	5.3	23.8	11.3	22.4	7.9	17.7	2.8
18	3.9	24.6	3.4	21.3	3.6	22.8	5.7	22.9	3.7	17.5	2.1
19	0.5	1.8	0.6	1.5	0.6	1.6	0.6	1.6	0.4	1.0	0.5
20	1.2	0.3	1.3	0.7	1.3	0.6	1.3	0.6	0.8	0.3	1.3
21	1.4	0.5	1.5	0.4	1.5	0.5	1.5	0.6	1.0	0.8	1.4
22	1.3	0.5	1.3	0.4	1.3	0.5	1.4	0.6	0.9	0.7	1.3
23	0.8	0.7	0.7	0.7	0.7	0.7	0.8	0.8	0.6	1.0	0.7
24	0.7	0.1	0.9	0.1	0.8	0.1	1.0	0.1	0.4	0.1	0.8
Av.	5.2	8.1	5.7	9.3	5.6	9.0	7.0	9.4	4.9	7.0	3.1
Std	5.6	8.0	7.5	9.8	6.9	9.2	6.7	8.4	4.2	6.1	3.4
Max	22.7	24.6	33.0	33.1	30.4	29.7	23.9	22.9	13.8	17.7	14.5
											13.0

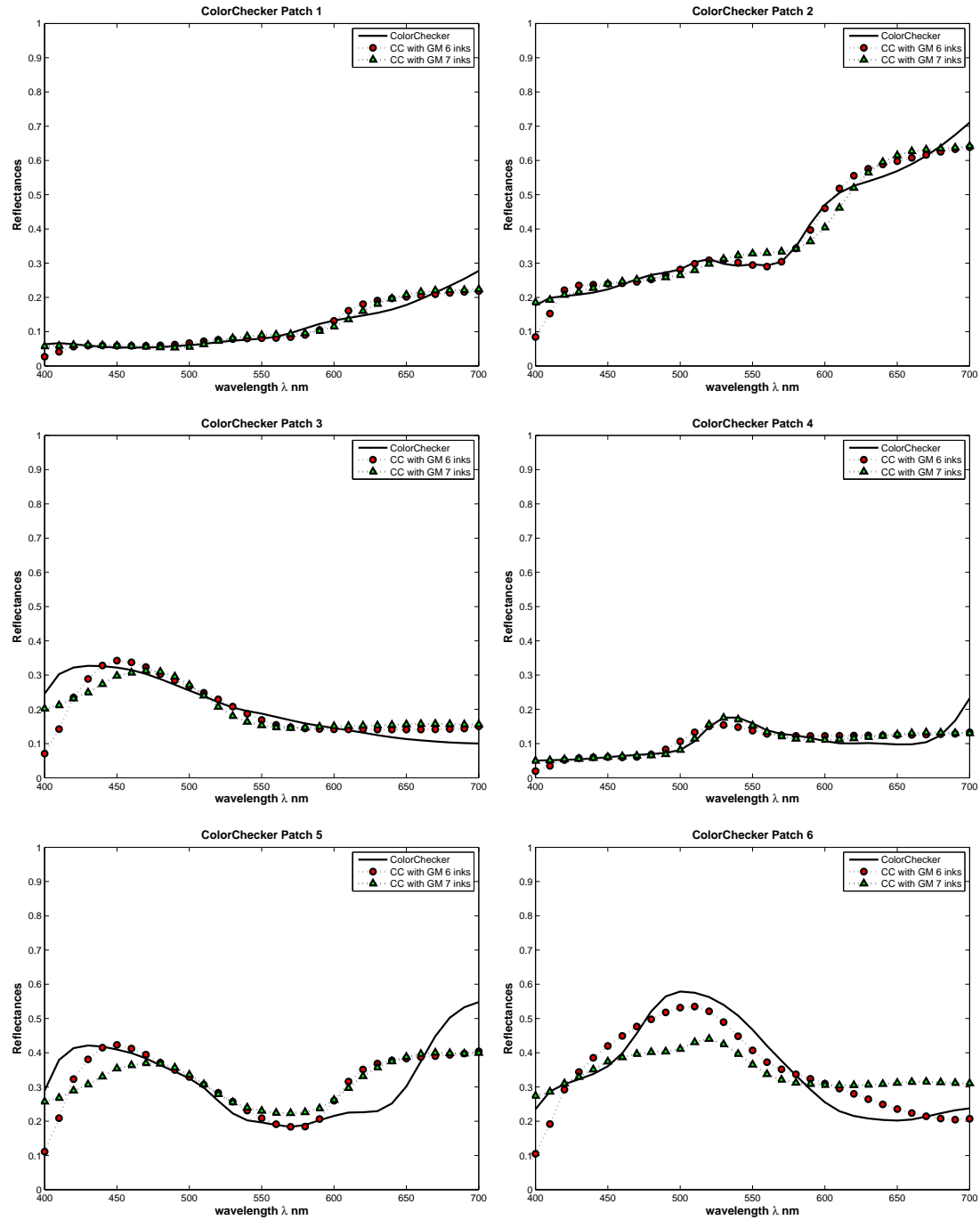


Figure B.1: Spectral reflectance of the ColorChecker patches 1 to 6 and their spectral mapped version for the 6 inks and the 7 inks printer.

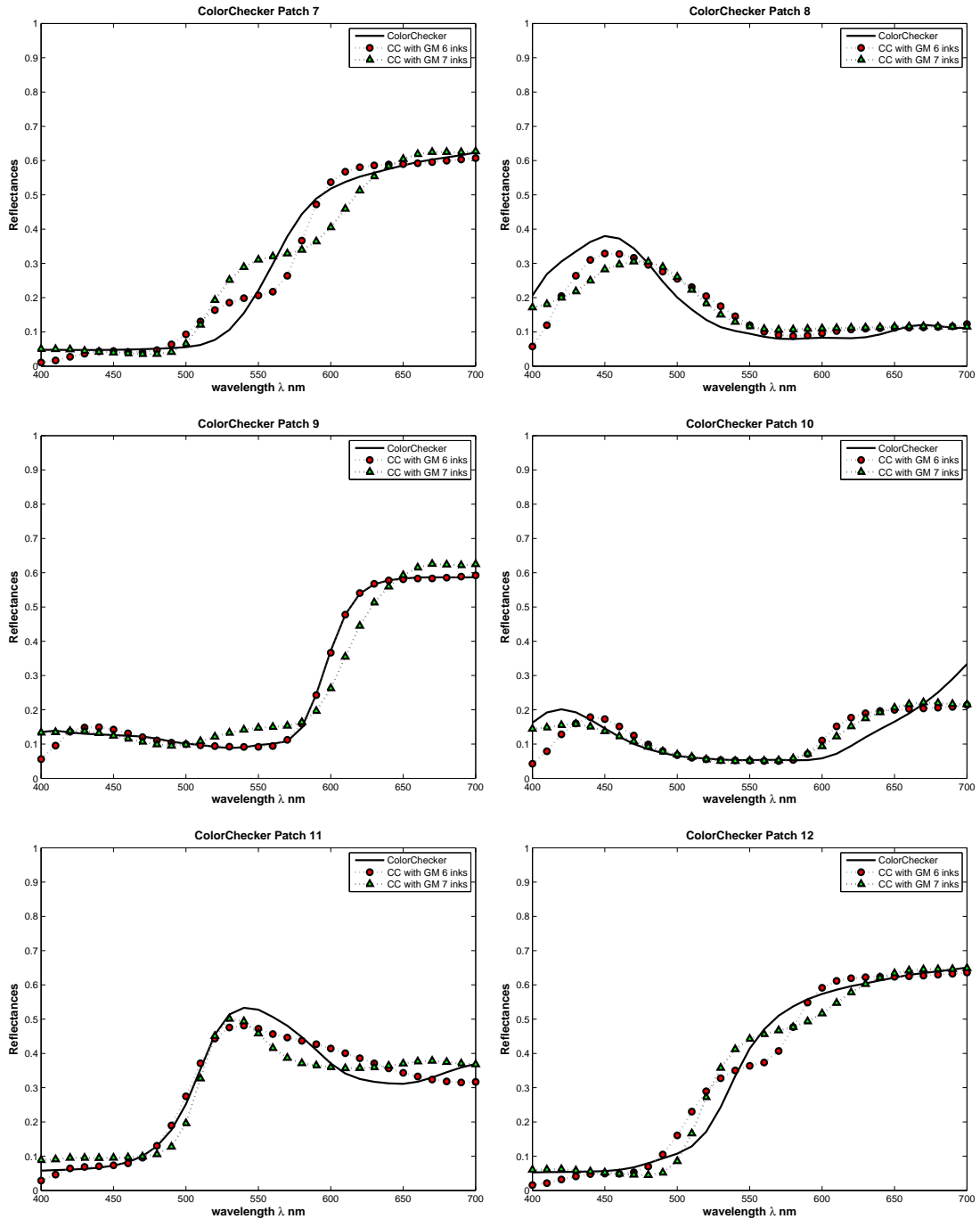


Figure B.2: Spectral reflectance of the ColorChecker patches 7 to 12 and their spectral mapped version for the 6 inks and the 7 inks printer.

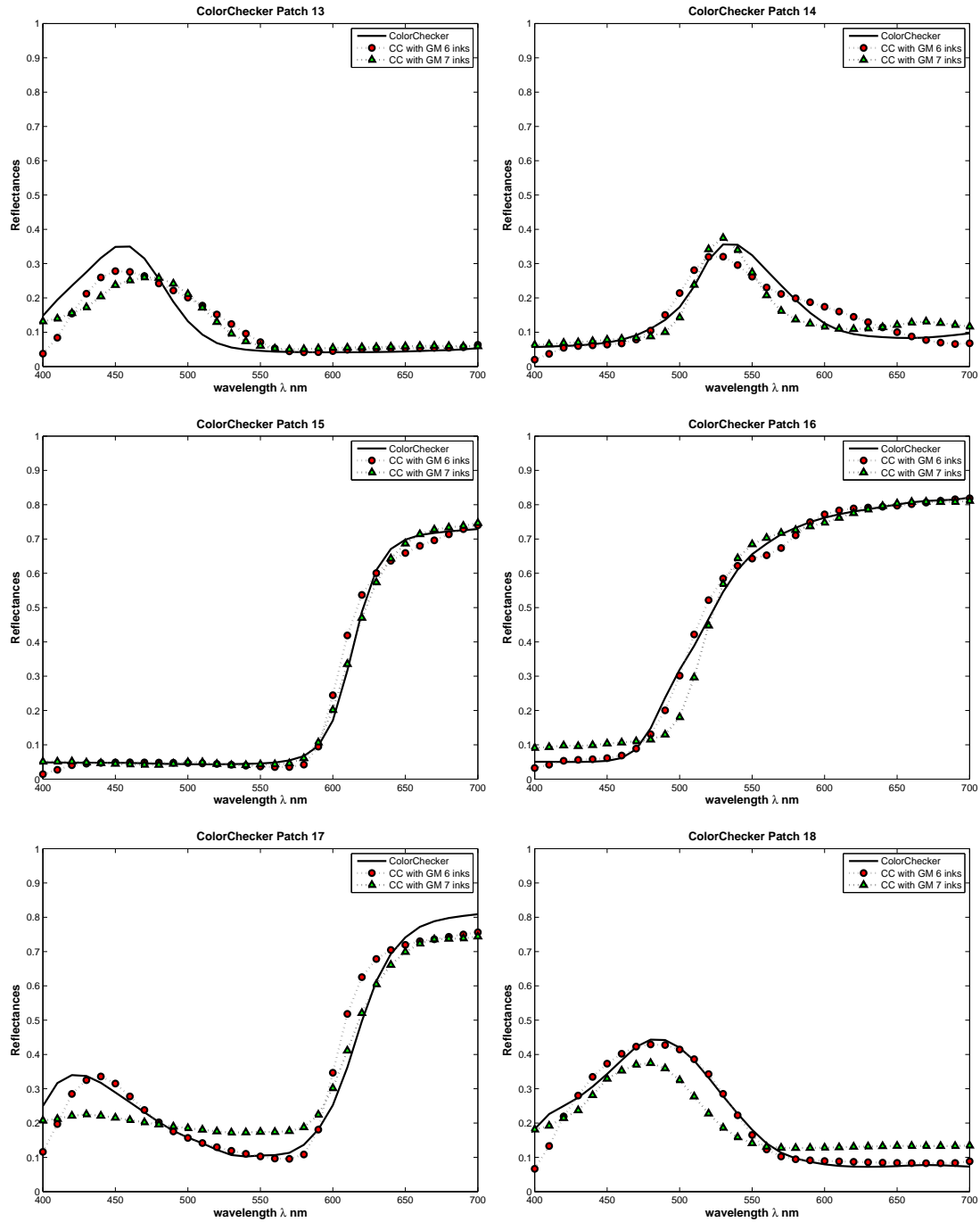


Figure B.3: Spectral reflectance of the ColorChecker patches 13 to 18 and their spectral mapped version for the 6 inks and the 7 inks printer.

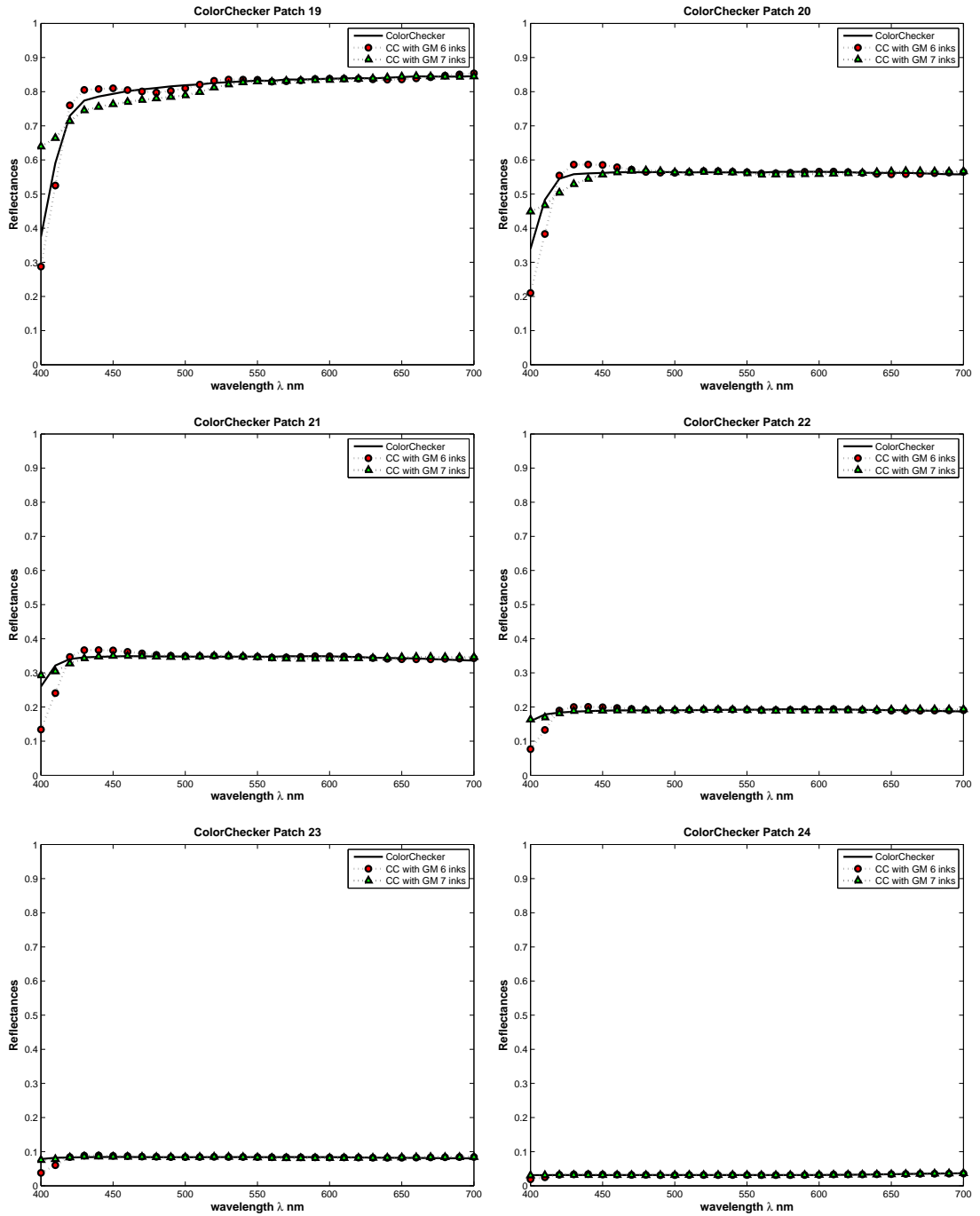


Figure B.4: Spectral reflectance of the ColorChecker patches 19 to 24 and their spectral mapped version for the 6 inks and the 7 inks printer.

B.3.2 Spectral gamut mapping on spectral image

The spectral gamut mapping is performed on the original spectral image (i.e. all the pixels of the image). As we explained it, the inversion of the spectral Neugebauer equations for the weights needs only the NP of the printer. We the spectral image of the ColorChercker test chart.

To illustrate our SGM on spectral image we perform the gamut mapping for two set of NP: one with 7 inks as in Figure 6.5 b and a second with 4 inks. There is $2^4 = 16$ NP for the 4 inks printer and $2^7 = 128$ for the 7 inks printer. The 4 inks printer is made of the CMYK inks of the 7 inks printer.

In Figure B.5 are displayed the original spectral image, the gamut mapped version of it for the 4 inks printer and for the 7 inks printer. We can observe that the spectral gamut mapped image for seven inks printer is less changed than for four inks printer. The grayscale part of the ColorChercker image is the least affected by the gamut mapping.

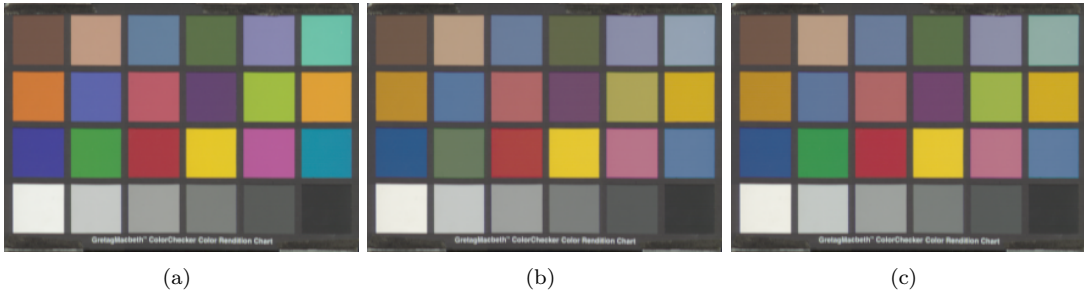


Figure B.5: From left to right the original spectral image, its gamut mapped version with a set of 4 inks CMYK and its gamut mapped version with a set of seven inks including the previous set. The color rendering of both images has been calculated for under illuminant CIE D65 and standard observer CIE1931.

Appendix C

Spectral Vector error diffusion

C.1 Evaluation of sVED

You will find in Figure C.1 and Figure C.2 the original spectral images called *YarnPalette* (*YP*) and *WomanReading* (*WR*).

The halftoning by sVED of the spectral image *YP* for both 6 and 7 colorant printers are displayed in Figure C.3 (a) and Figure C.3 (b), respectively.

The halftoning by sVED of the spectral images *WR* for both 6 and 7 colorant printers are displayed in Figure C.4 and Figure C.5, respectively. This spectral image has been scaled by a factor of 2 before performing the halftoning.



Figure C.1: Original *YarnPalette* (*YP*) spectral image.



Figure C.2: Original *WomanReading* (*WR*) spectral image scaled by a factor of 2.

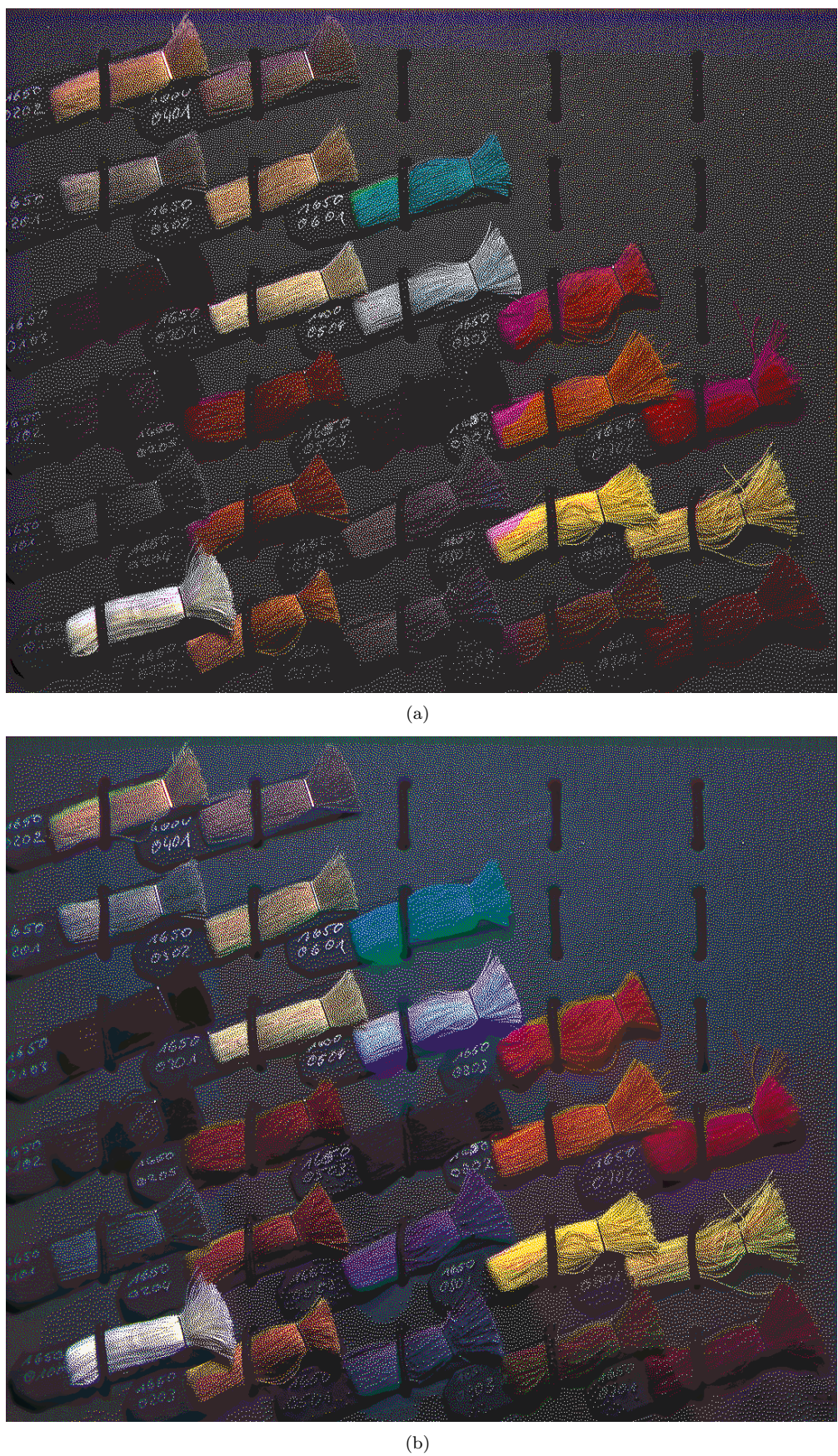


Figure C.3: Halftoning by **sVED** of the *YP* spectral image for the 6 and 7 colorants printer in (a) and (b) respectively.



Figure C.4: Halftoning by **sVED** of the *WR* spectral image for the 6 colorant printers.



Figure C.5: Halftoning by **sVED** of the *WR* spectral image for the 7 colorant printers.

C.2 Preprocessing

In Figure C.6 (a) and Figure C.6 (b) are displayed the gamut mapped YP spectral images (i.e. spectral images after pre-processing) for both 6 and 7 colorant printers; sVED is performed on these images and the halftoned images are displayed in Figure C.8 (a) and Figure C.8 (b) for the 6 and 7 colorant printers respectively.

In Figure C.7 (a) and Figure C.7 (b) are displayed the gamut mapped WR spectral images (i.e. spectral images after pre-processing) for both 6 and 7 colorant printers; sVED is performed on these images and the halftoned images are displayed in Figure C.9 (a) and Figure C.9 (b) for the 6 and 7 colorant printers respectively.



(a)



(b)

Figure C.6: Gamut mapped YP spectral image for the 6 and 7 colorant printers.



Figure C.7: Gamut mapped *WR* spectral image for the 6 and 7 colorant printers.

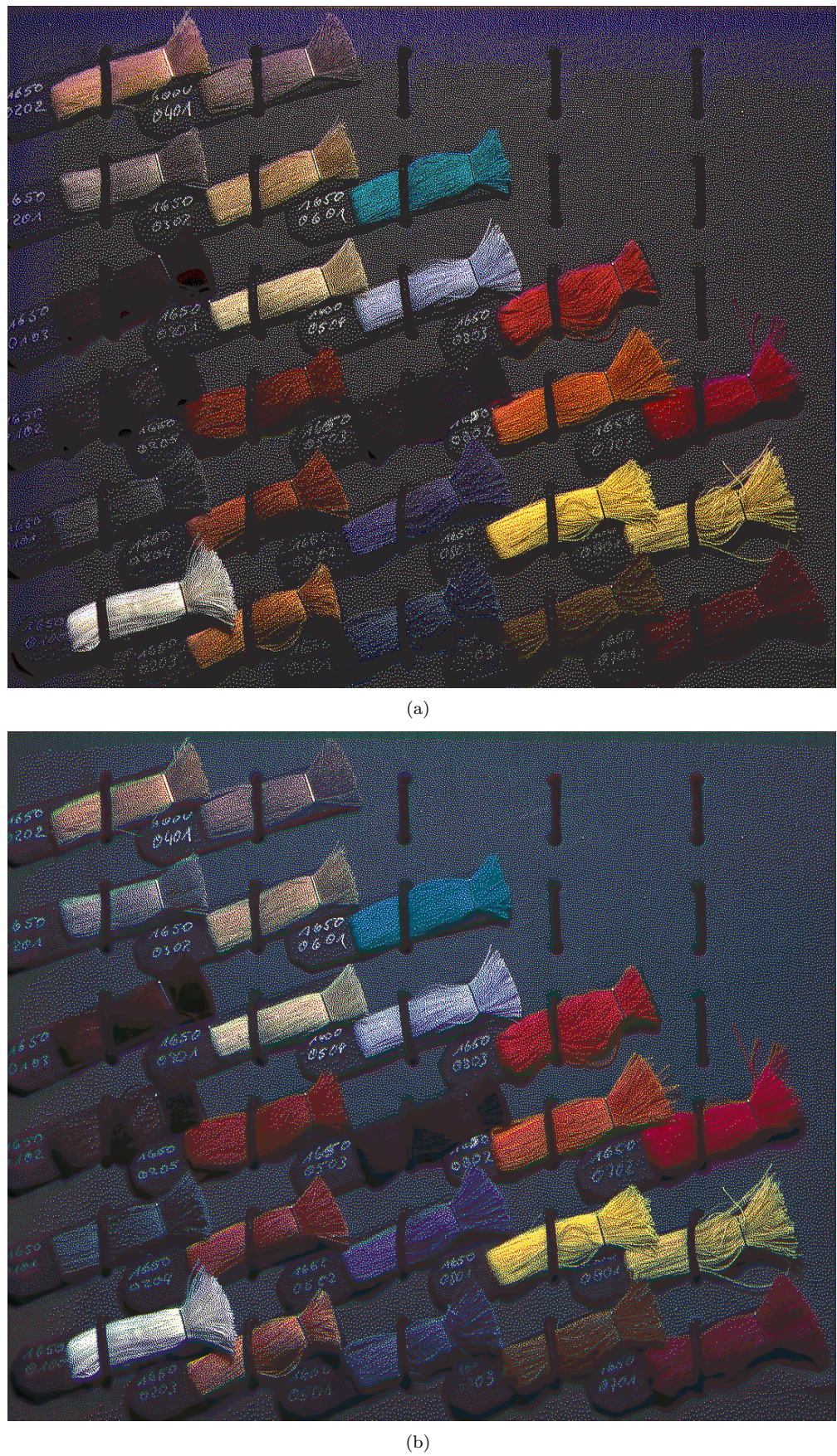


Figure C.8: Halftoning by **sVED** and pre-processing of the *YP* spectral image for the 6 and 7 colorant printers.

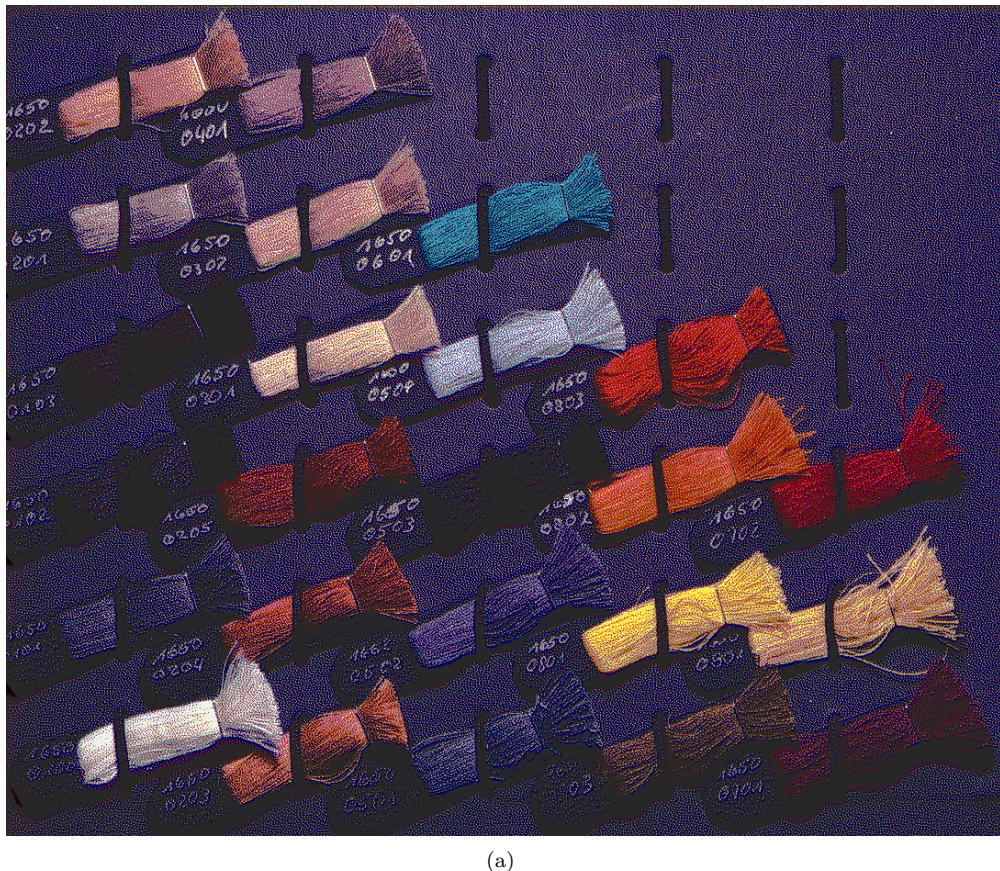


Figure C.9: Halftoning by **sVED with pre-processing** of the *WR* spectral image for the 6 and 7 colorant printers.

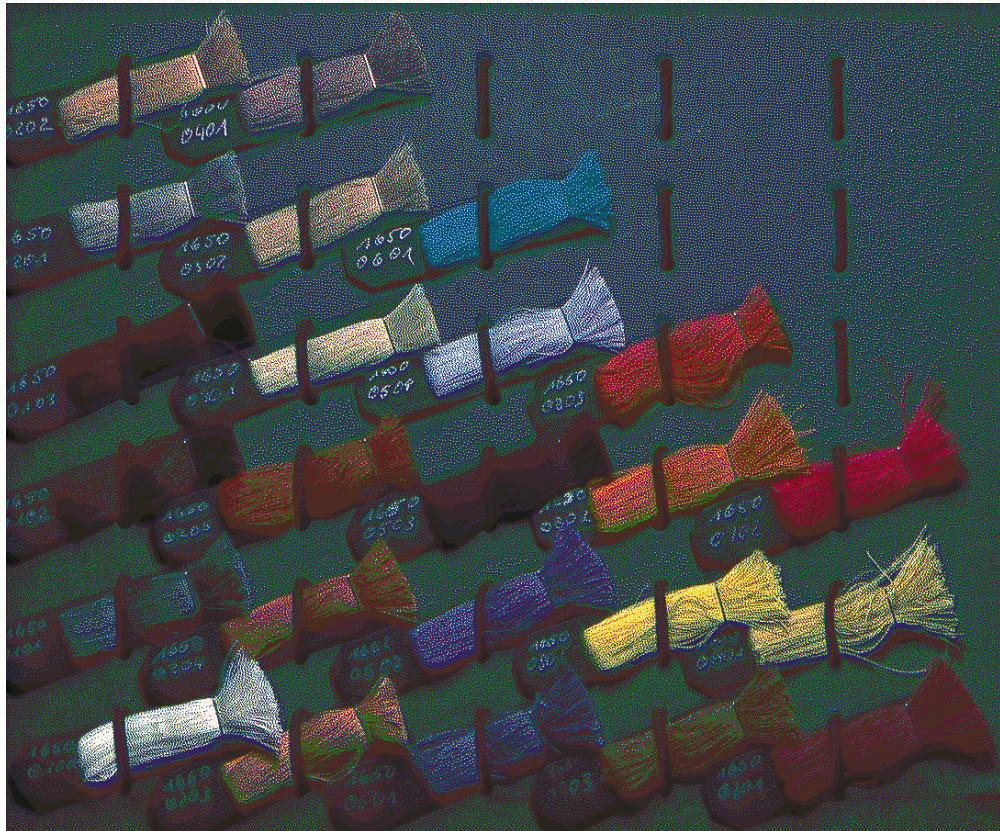
C.3 Evaluation of sVED with clipping

In Figure C.10 (a) and Figure C.10 (b) are displayed the halftoned images by sVED and clipping of the gamut mapped *YP* spectral images for the 6 and 7 colorant printers respectively.

In Figure C.11 (a) and Figure C.11 (b) are displayed the halftoned images by sVED and clipping of the gamut mapped *WR* spectral images for the 6 and 7 colorant printers respectively.



(a)



(b)

Figure C.10: Halftoning by sVED with pre-processing and clipping of the YP spectral image for the 6 and 7 colorant printers in (a) and (b) respectively.

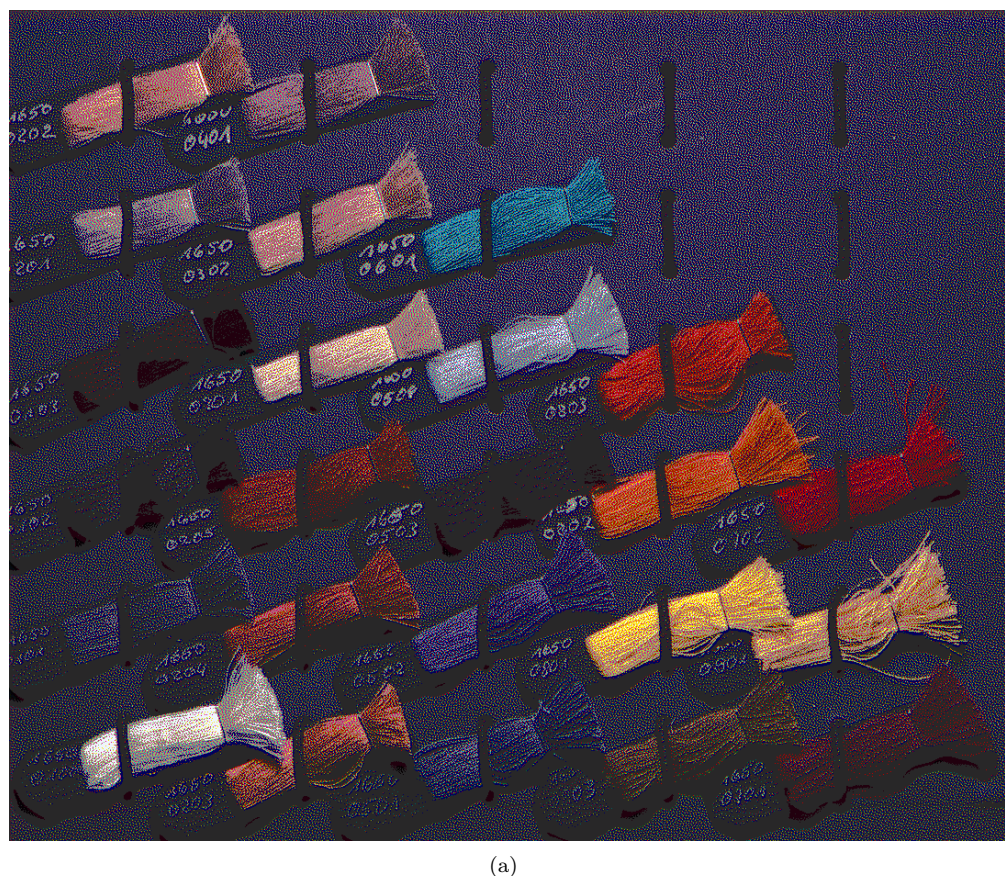


Figure C.11: Halftoning by **sVED with pre-processing and clipping** of the *WR* spectral image for the 6 and 7 colorants printer in (a) and (b) respectively

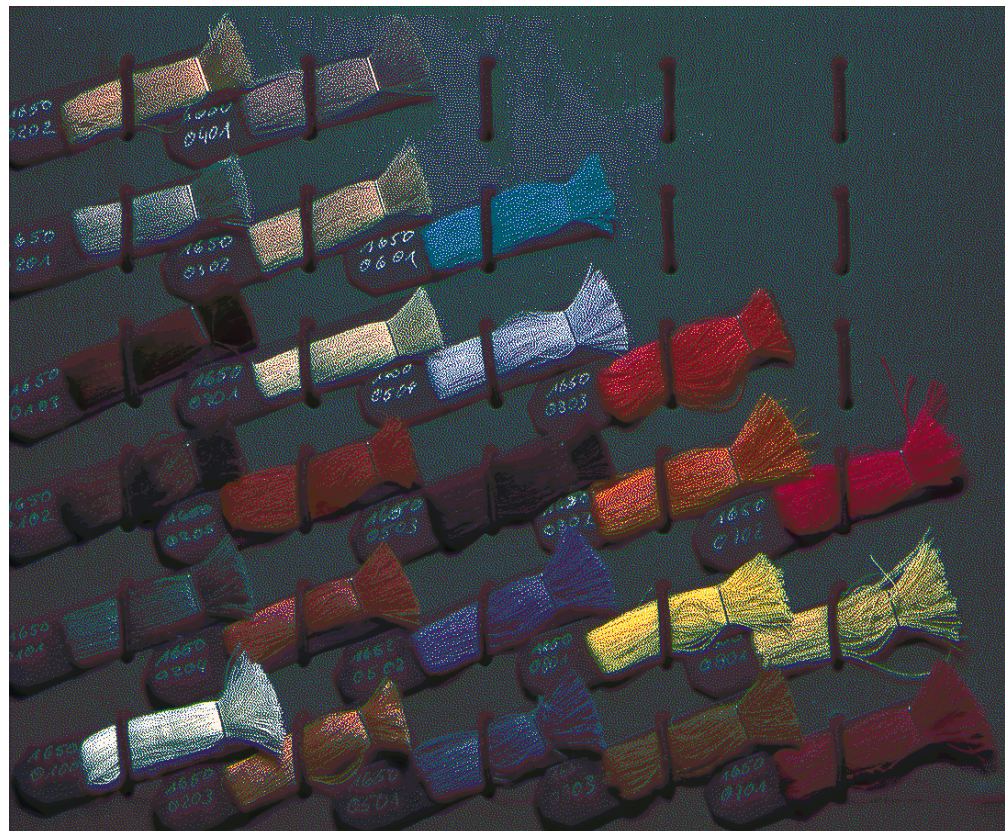
C.4 Evaluation of sVED with scaling

In Figure C.12 (a) and Figure C.12 (b) are displayed the halftoned images by sVED and scaling of the gamut mapped *YP* spectral images for the 6 and 7 colorant printers respectively.

In Figure C.13 (a) and Figure C.13 (b) are displayed the halftoned images by sVED and scaling of the gamut mapped *WR* spectral images for the 6 and 7 colorant printers respectively.



(a)



(b)

Figure C.12: Halftoning by **sVED with pre-processing and scaling** of the *YP* spectral image for the 6 and 7 colorant printers in (a) and (b) respectively.

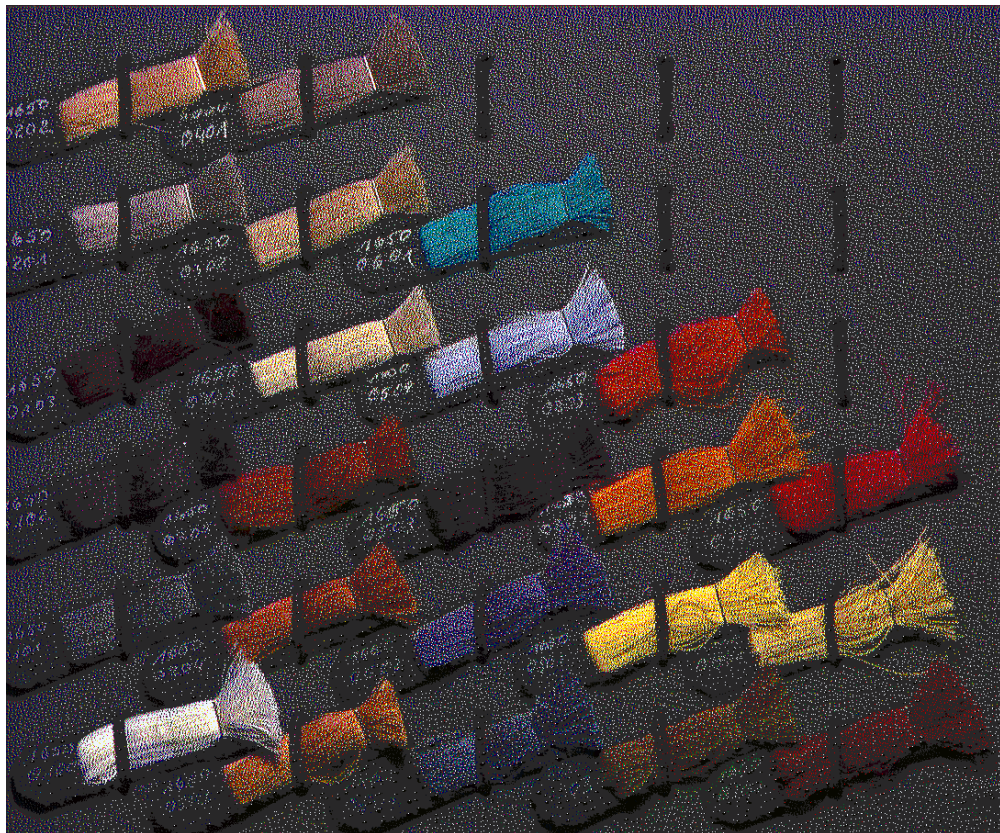


Figure C.13: Halftoning by **sVED with pre-processing and scaling** of the *WR* spectral image for the 6 and 7 colorant printers in (a) and (b) respectively.

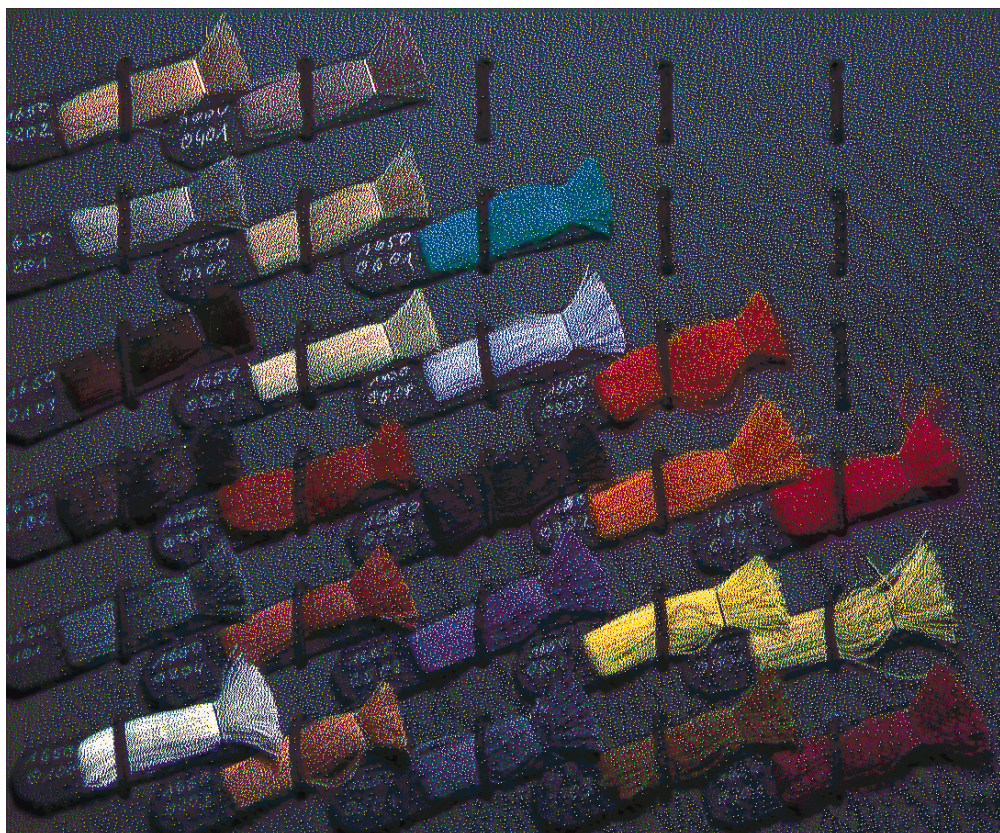
C.5 Evaluation of sVED with new filter design by distance

In Figure C.14 (a) and Figure C.14 (b) are displayed the halftoned images by sVED and new filter design by distance of the gamut mapped *YP* spectral images for the 6 and 7 colorant printers respectively.

In Figure C.15 (a) and Figure C.15 (b) are displayed the halftoned images by sVED and new filter design by distance of the gamut mapped *WR* spectral images for the 6 and 7 colorant printers respectively.



(a)



(b)

Figure C.14: Halftoning by **sVED with pre-processing and filter by distance** of the *YP* spectral image for the 6 and 7 colorant printers in (a) and (b) respectively.

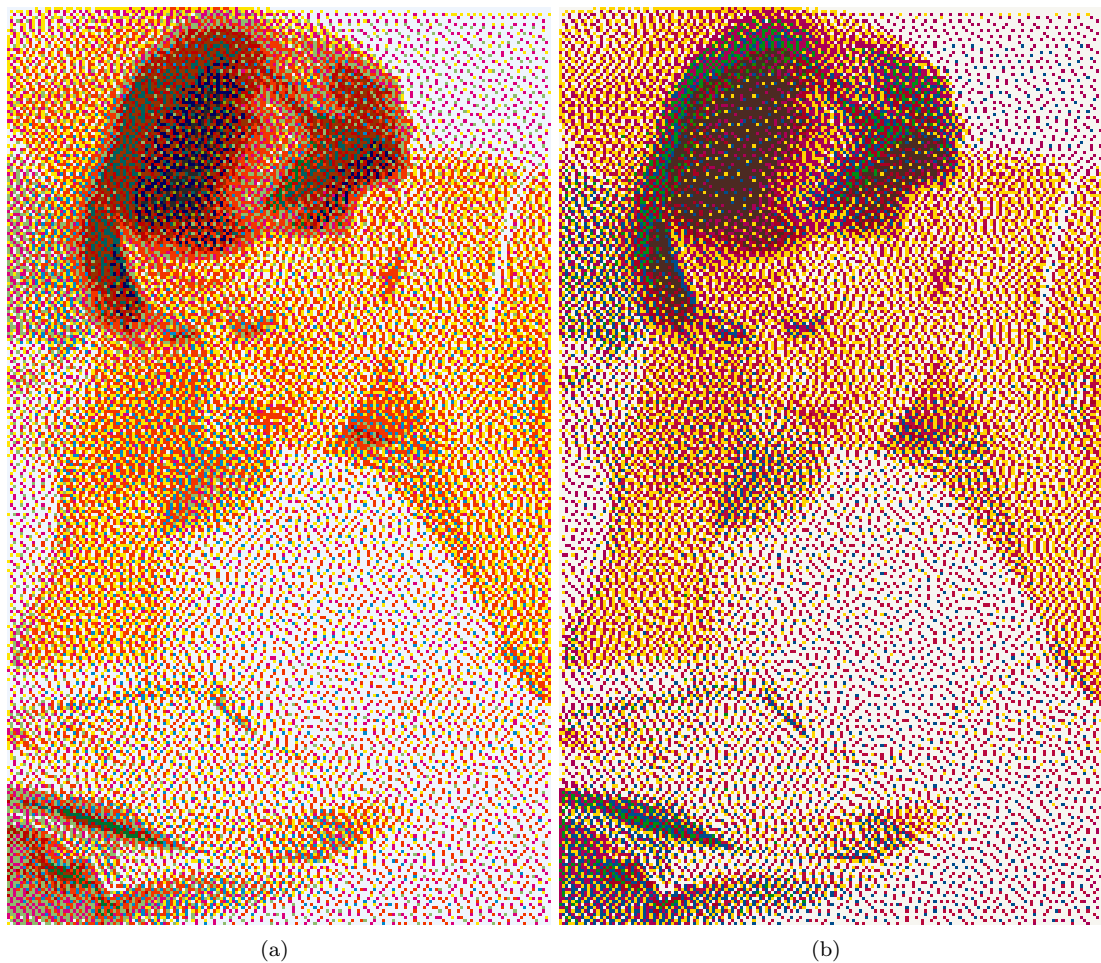


Figure C.15: Halftoning by **sVED with pre-processing and new filter by distance** of the *WR* spectral image for the 6 and 7 colorant printers in (a) and (b) respectively.

C.6 Evaluation of sVED with new filter design by random placement of existing weights

In Figure C.16 (a) and Figure C.16 (b) are displayed the halftoned images by sVED and new filter design by Random placement of existing weights of the gamut mapped *YP* spectral images for the 6 and 7 colorant printers respectively.

In Figure C.17 (a) and Figure C.17 (b) are displayed the halftoned images by sVED and new filter design by Random placement of existing weights of the gamut mapped *WR* spectral images for the 6 and 7 colorant printers respectively.

C.6. EVALUATION OF SVED WITH NEW FILTER DESIGN BY RANDOM PLACEMENT OF EXISTING W

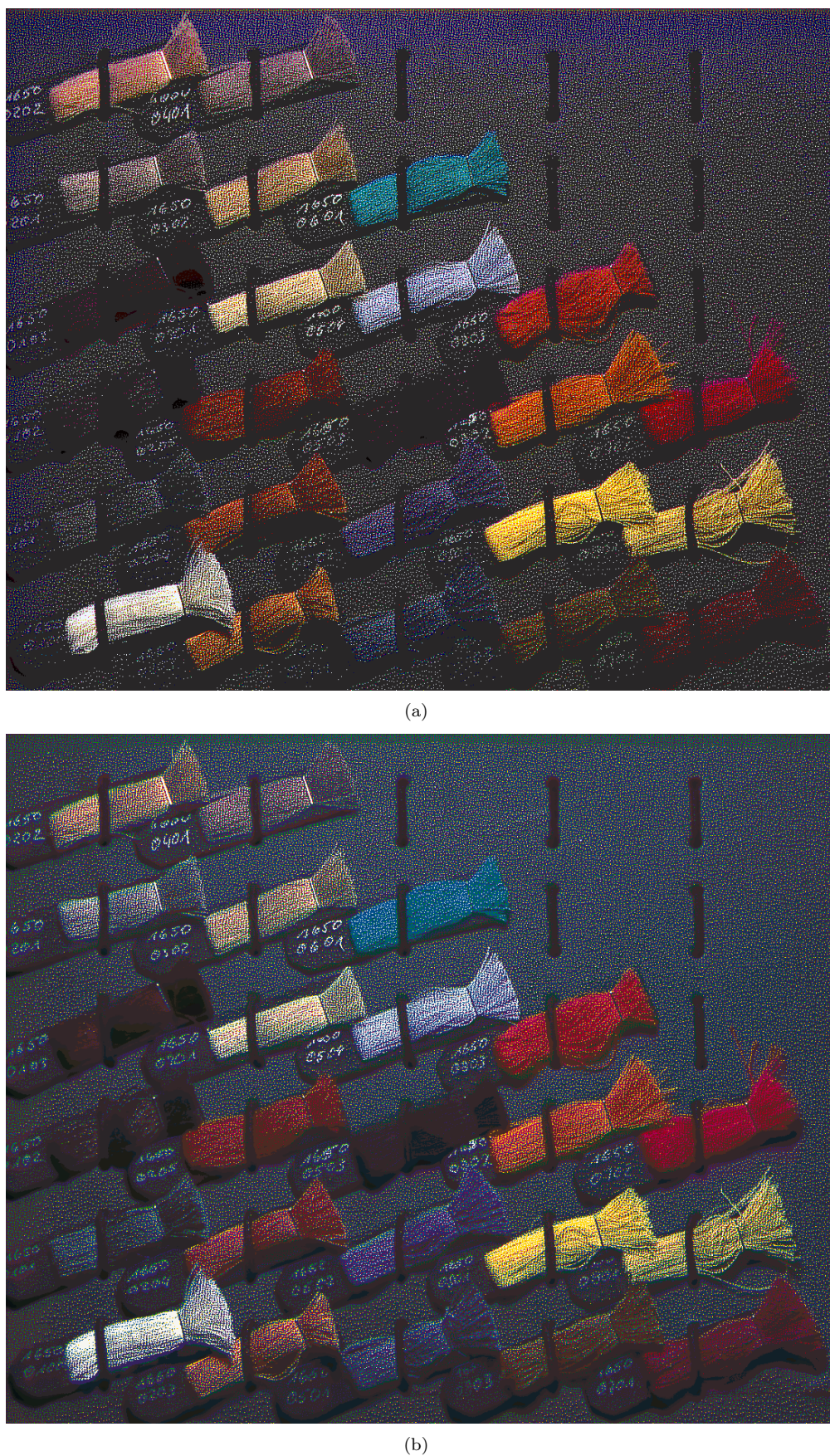


Figure C.16: Halftoning by sVEd with pre-processing and new filter by random placement of existing weights of the YP spectral image for the 6 and 7 colorant printers in (a) and (b) respectively.



Figure C.17: Halftoning by **sVED with pre-processing and new filter by random placement of existing weights** of the *WR* spectral image for the 6 and 7 colorant printers in (a) and (b) respectively.

Bibliography

- A. Ufuk Agar. Model based color separation for cmykcm printing. In *The 9th Color Imaging Conference*, pages 298–302. IS&T - The Society for Imaging Science and Technology, November 2001.
- Ali Alsam, Jérémie Gerhardt, and Jon Y. Hardeberg. Inversion of the Spectral Neugebauer Printer Model. In *AIC Colour 05*, pages 44–62, 2005.
- Isaac Amidror and Roger Hersch. Neugebauer and Demichel: Dependence and Independence in n-screen Superpositions for Colour Paintings. *Color Research and Application*, 25(4):267–277, August 2000.
- Arne M. Bakke, Ivar Farup, and Jon Y. Hardeberg. Multispectral gamut mapping and visualization – a first attempt. In *Color Imaging: Processing, Hardcopy, and Applications X, Electronic Imaging Symposium*, volume 5667 of *SPIE Proceedings*, pages 193–200, San Jose, California, January 2005.
- Raja Balasubramanian. End-to-end color printer calibration by total least squares regression. *Journal of Electronic Imaging*, 8(2):156–166, April 1999.
- Roy S. Berns, Lawrence A. Taplin, and Tony Z. Liang. Spectral color reproduction with six color output. US patent 0098896A1, May 2003.
- Thomas Boosmann and Bernhard Hill. Control algorithms for 6-primary displays. In *PICS 2003: The PICS Conference, An International Technical Conference on The Science and Systems of Digital Photography, including the Fifth International Symposium on Multispectral Color Science*, pages 244–249, Rochester, NY, USA, May 2003. ISBN 0-89208-245-3.
- Shih-Liang Chang, Yuan-Te Liu, and Der-Zong Yeh. A method to estimate fractional areas of neugebauer primary colors. *IS&T SID Color Imaging Conference*, pages 97–100, 1995.
- CIE. CIE 15:2004 COLORIMETRY, 3rd Edition. Technical report, 2004.
- CIE. Colorimetry - Part 4: CIE 1976 L*a*b* Colour Spaces. CIE Draft Standard DS 014-4.2/E:2006, 2006.
- M. E. Demichel. *Le procédé*, Vol. 26:17–21, 1924.
- Maxim W. Derhak and Mitchell R. Rosen. Spectral colorimetry using LabPQR: an interim connection space. *Journal of Imaging Science and Technology*, 50(1):53–63, 2006.
- Damien Dupraz, Mohamed Ben Chouikha, and Georges Alquié. Historic period of fine art painting detection with multispectral data and color coordinates library. In *Proceedings of Ninth International Symposium on Multispectral Colour Science and Application*, 2007.
- Zhigang Fan. Boundary artifacts reduction in vector error diffusion. volume 3648, pages 480–484, December 1998.

- Robert W. Floyd and Louis Steinberg. An adaptive algorithm for spatial greyscale. *Proceedings of the Society for Information Display*, 17(2):75–77, 1976.
- Jérémie Gerhardt and Jon Y. Hardeberg. Spectral colour reproduction by vector error diffusion. In *Proceedings CGIV 2006*, pages 469–473, 2006.
- Jérémie Gerhardt and Jon Y. Hardeberg. Controlling the error in spectral vector error diffusion. In *Color Imaging: Processing, Hardcopy, and Applications XII, Electronic Imaging Symposium*, SPIE Proceedings, San Jose, California, January 2007a.
- Jérémie Gerhardt and Jon Yngve Hardeberg. Spectral color reproduction versus color reproduction. In *Proceedings of the 34th Iarigai Conference*, September 2007b.
- Philip E. Gill, Walter Murray, and Margaret H. Wright. *Practical Optimization*. Academic Press, London, 1981.
- Charles Hains, Shen-Ge Wang, Keith Knox, and Gaurav Sharma. *Digital Color Imaging Handbook*, chapter 6 Digital Color Halftones, pages 385–490. CRC Press, 2003.
- H. Haneishi, T. Suzuki, N. Shimoyama, and Y. Miyake. Color digital halftoning taking colorimetric color reproduction into account. *Journal of Electronic Imaging*, 5(5):95–106, January 1996.
- Jon Y. Hardeberg. On the spectral dimensionality of object colours. In *CGIV'2002*, pages 480–485, 2002.
- Jon Y. Hardeberg and Jérémie Gerhardt. Characterization of an eight colorant inkjet system for spectral color reproduction. pages 263–267, 2004.
- Jon Y. Hardeberg and Jérémie Gerhardt. Exact reproduction of colored images. *Revue Traitement du Signal*, 21(1), 2005.
- Jon Yngve Hardeberg. *Acquisition and reproduction of Color Images: Colorimetric and Multispectral approaches*. PhD thesis, ENST, 1999.
- Jon Yngve Hardeberg and Jérémie Gerhardt. Towards spectral color reproduction. In *Proceedings of Ninth International Symposium on Multispectral Colour Science and Application*, pages 16,22. IS&T, 2007. ISBN 978-0-89208-272-8.
- Roger David Hersch and Frédérique Crêté. Improving the Yule-Nielsen modified spectral Neugebauer model by dot surface coverages depending on the ink superposition conditions. In *Color Imaging: Processing, Hardcopy, and Applications X, Electronic Imaging Symposium*, volume 5667, pages 434–445, January 2005.
- Roger David Hersch, F. Collaud, Frédérique Crêté, and P. Emmel. Spectral prediction and dot surface estimation models for halftone prints. In *Color Imaging: Processing, Hardcopy, and Applications IX, Electronic Imaging Symposium*, volume 5293, pages 356–369, January 2004.
- Roger David Hersch, Patrick Emmel, Fabien Collaud, and Frédérique Crêté. Spectral reflection and dot surface prediction models for color halftone prints. *Journal of Electronic Imaging*, 14(3), Jul-Sep 2005.
- Karl J. Heuberger, Zhou Mo Jing, and Serdar Persiev. Color transformations and lookup tables. *TAGA Proceedings*, 2:863–881, 1992.
- Bernhard Hill. High quality color image reproduction: The multispectral solution. In *Proceedings of Ninth International Symposium on Multispectral Colour Science and Application*, 2007.
- R. W. G. Hunt. *The Reproduction of Colour in Photography, Printing and Television*. Kingston-upon-Thames, England, 3 edition, 1975. (Now in 6th Edition, Wiley, 2004).

- ICC.1:2004-10. Image technology colour management - architecture, profile format, and data structure. The International Color Consortium, 2004.
- In-Su Jang, Chang-Hwan Son, Tae-Yong Park, and Yeong-Ho Ha. Improved Inverse Characterization of Multicolrant Printer Using Colorant Correlation. *JIST*, 51(2):175–184, December 2006.
- John F. Jarvis, C. N. Judice, and W. H. Ninke. A survey of techniques for the display of continuous-tone pictures on bilevel displays. *Computer Graphics and Image Processing*, 5: 13–40, March 1976.
- Joensuu. Joensuu spectral image database. Technical report. <http://www.multispectral.org/>.
- T. Kawaguchi, N. Tsumura, H. Haneishi, M. Kouzaki, and Y. Miyaki. Vector error diffusion method for spectral color reproduction. In *IST&T's PICS Conference*, pages 394–397, 1999.
- Timothy Kohler and Roy S. Berns. Reducing metamerism and increasing gamut using five or more colored inks. *IST&T's Third Technical Symposium On Prepress, Proofing, and Printing*, pages 24–29, 1993.
- M. M. Kouzaki, T. Itoh, T. Kawaguchi, N. Tsumura, H. Haneishi, and Y. Miyake. Evaluation of spectral color reproduction by vector error diffusion method. In R. Eschbach and G. G. Marcu, editors, *Proc. SPIE Vol. 3963, p. 429-436, Color Imaging: Device-Independent Color, Color Hardcopy, and Graphic Arts V, Reiner Eschbach; Gabriel G. Marcu; Eds.*, pages 429–436, December 1999.
- Andreas Kraushaar and Philipp Urban. Spectral redundancy in a 6-ink ink-jet printer. In *IARIGAI Proceedings 33rd International Research Conference*, 2006.
- Carlos Lana, Mario Rotea, and Daniel E. Viassolo. Robust estimation algorithm for the spectral Neugebauer models. *Journal of Electronic Imaging*, 14(1), January–March 2005. Optimization on the NG parameters in order to minimize the max(error).
- Daniel Lau and Gonzalo R. Arce. *Modern Digital Halftoning*. 2001. ISBN 0-8247-0456-8.
- Marc Mahy and Paul Delabastita. Inversion of the Neugebauer Equation. *COLOR research and application*, 21(6):404–411, December 1996.
- Ján Morovič and M. Ronnier Luo. The fundamentals of gamut mapping: A survey. *Journal of Imaging Science and Technology*, 45(3):283–290, 2001.
- A. Murray. Monochrome reproduction in photogravure. *J. Franklin Inst.*, 221:721:744, 1936.
- H. E. J. Neugebauer. Die Theoretischen Grundlagen Des Mehrfarbendruckes. *Zeitschrift für wissenschaftliche Photographie Photophysik und Photochemie*, 36(4), 1937.
- Victor Ostromoukhov. Chromaticity gamut enhancement by heptatone multi-color printing. In *IS&T SPIE*, volume 1990, pages 139–151, 1993.
- Powell. An efficient method for finding the minimum of a function of several variables without calculating derivative. *Computer Journal*, 17:155.162, 1964.
- Geoffrey L. Rogers. Neugebauer Revisited: Random Dots in Halftone Screening. *Color Research and Application*, 23(2):104–113, April 1998.
- Robert Rolleston and Raja Balasubramanian. Accuracy of Various Types of Neugebauer Model. *IS&T and SID Color Imaging Conference: Transforms and Transportability of Color*, pages 32–37, 1993.

- Mitchell R. Rosen, Edward F. Hattenberger, and Noboru Ohta. Spectral redundancy in a 6-ink ink-jet printer. *IS&T 2003 PICS Conference*, pages 236–243, 2003.
- Francis Schmitt. Crisatel multispectral imaging system. In *AIC Colour 05*, 2005.
- Gaurav Sharma. *Digital Color Imaging Handbook*. CRC Press, 2003.
- Lawrence A. Taplin and Roy S. Berns. Spectral Color Reproduction Based on a Six-Color Inkjet Output System. *The Ninth Color Imaging Conference*, pages 209–212, November 2001.
- T Tsutsumi, Mitchell Rosen, and Roy S. Berns. Spectral reproduction using LabPQR: Inverting the Fractional-Area-Coverage-to-Spectra Relationship. In *Proceedings of ICIS*, pages 107–110, 2006.
- Di-Yuan Tzeng. *Spectral-based color separation algorithm development for multiple-ink color reproduction*. PhD thesis, Rochester Institute of Technology, September 1999.
- Di-Yuan Tzeng and Roy S. Berns. Spectral based ink selection for multiple-ink printing I. colorant estimation of original objects. *The IST&SID Sixth Color Imaging Conference: Color Science, Systems, and Applications*, pages 106–111, November 1998.
- Di-Yuan Tzeng and Roy S. Berns. Spectral based ink selection for multiple-ink printing II. optimal ink selection. *The Seventh Color Imaging Conference: Color Science, Systems, and Applications*, pages 182–187, November 1999.
- Di-Yuan Tzeng and Roy S. Berns. Spectral-based six-color separation minimizing metamerism. In *IS&T/SID Eight Color Imaging Conference*, pages 342–347, November 2000.
- Robert Ulichney. *Digital Halftoning*. MIT Press, Cambridge, MA, USA, 1987a. ISBN 0-262-21009-6.
- Robert Ulichney. *Digital Halftoning*, chapter Dithering with Blue Noise, pages 233–319. MIT Press, 1987b.
- Philipp Urban and Rolf-Rainer Grigat. The metamer boundary descriptor method for color correction. *Journal Of Imaging Science And Technology*, 49(4):418–430, July/August 2005.
- Philipp Urban and Rolf-Rainer Grigat. Spectral-based color separation using linear regression iteration. *Color Research & Application*, 31(3):229–238, June 2006.
- J A Stephen Viggiano. The GRL dot gain model. In *TAGA Proceedings*, 1983.
- J. A. Stephen Viggiano. Modeling the color of multi-colored halftones. In *TAGA*, pages 44–62, 1990.
- David R. Wyble and Roy S. Berns. A critical review of spectral models applied to binary color printing. *Color Research Application*, 25(1):4–19, 2000.
- David R. Wyble and Andreas Kraushaar. The theoretical basis of multicolor letterpress printing, Hans E. J. Neugebauer. *Color research and application*, 30(5):322–331, August 2005.
- Günther Wyszecki and W. S. Stiles. *Color Science*. Wiley-Interscience, second edition, 1982a.
- Günther Wyszecki and W. S. Stiles. *Color Science*, chapter 3 Colorimetry, pages 117–243. Wiley-Interscience, 1982b.
- Minghui Xia, Eli Saber, Gaurav Sharma, and A. Murat Tekalp. End-to-end color printer calibration by total least squares regression. *IEEE Transactions on Image Processing*, 8(5):700–716, May 1999.

- J. A. C. Yules and W. J. Nielsen. The penetration of light into paper and its effect on halftone reproductions. *Proc. TAGA*, pages 3–65, 1951.
- Sylvia Zuffi. Colorimetric and spectral-based printing: a simple comparison. In Reiner Eschbach and Gabriel G. Marcu, editors, *Color Imaging X: Processing, Hardcopy, and Applications*, volume 5667 of *Presented at the Society of Photo-Optical Instrumentation Engineers (SPIE) Conference*, pages 178–185, December 2004.